Table of Contents

Overview of our library benzo[b]thiophene based mono(thio)ureas

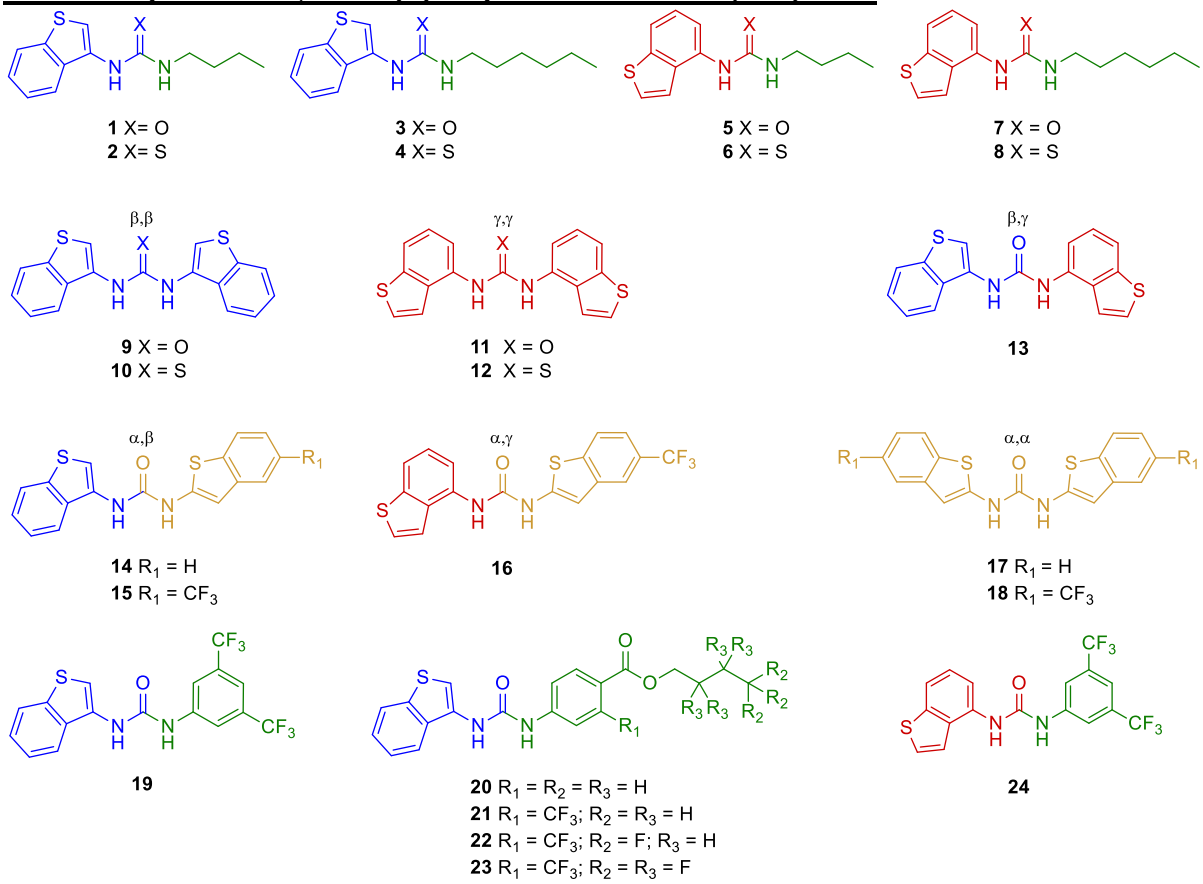

Synthesis

General Remarks

All reagents were used as provided by the chemical suppliers while the solvents were dried according to standard methods before use.[1] Reactions were monitored by TLC using 0.25 mm silica gel 60 F_{254} TLC plates and their spots were visualised under ultraviolet light (254 nm). Melting points were determined with a Stuart SMP30 melting-point apparatus. FTIR spectra were recorded on Thermo Scientific Nicolet™ 6700 FTIR Spectrometer and data were processed with Thermo Scientific™ OMNIC software.

^{1}H and ^{13}C APT NMR spectra were acquired on a Bruker Avance 400 spectrometer equipped with a 5 mm QNP probe operating with a frequency of 400.16 MHz for ^{1}H and 100.61 MHz for ^{13}C at 293 K. Spectra were recorded in suitable deuterated solvents, such as CD_2Cl_2 and CD_6CO for the reaction intermediates and DMSO-d_6 (99.9%) for the twenty-four (thio)urea compounds. ^{1}H and ^{13}C NMR chemical shifts (δ) are reported in parts per million (ppm) downfield to TMS or to the deuterated solvent peaks (CD_6CO, DMSO-d_6, CD_2Cl_2), used as internal references. The unequivocal assignment of ^{1}H and ^{13}C resonances was carried out with resort to Heteronuclear Single Quantum Correlation (HSQC) and Heteronuclear Multiple Bond Correlation (HMBC). Spectral data were processed with the TopSpin software and are presented below following the sequence: chemical shift (δ), multiplicity (*s* = singlet, *d* = doublet, *t* = triplet, *q* = quartet, *m* = multiplet, *br* = broad), coupling constants, relative integral and protons or carbons' assignment.

HR-ESI-MS and ESI-MS spectra were performed on a Bruker Impact II QTOF mass spectrometer with an electrospray ionisation source (ESI). The samples were analysed by direct infusion method through MS/MS scans undertaken in the positive or negative mode. The capillary voltage was set to 4500 V and 3500 V, for the positive and negative modes,

respectively. Signals were recorded with m/z ranging from 50 to 1000. The dry gas was kept at 4.0 L/min, at 200°C. The quadrupole ion energy was set to 5.0 eV, while the collision cell energy was set to 10.0 eV. A flux of 200 μL/h was used. Data were processed with the Data Analysis 4.4 software.

Synthesis

The receptors **1-8** and **19-24** of our library of benzo[*b*]thiophene-based (thio)urea compounds were prepared in one-stepwise synthesis by the reaction between aliphatic or aromatic amines with β- or γ-iso(thio)cyanates as depicted in Scheme S1. The bis-benzo[*b*]thiophene (thio)urea derivatives, except **17** and **18**, were obtained by the coupling of α-, β- or γ- benzo[*b*]thiophene iso(thio)cyanates with β- or γ- benzo[*b*]thiophene amines, akin to a Lego approach, as depicted in Scheme S2. The symmetrical α,α-benzo[*b*]thiophene-based ureas **17** and **18** were obtained as side products of the syntheses of highly reactive benzo[*b*]thiophen-2-yl isocyanate and its 5-trifluoromethyl derivative, as detailed below.

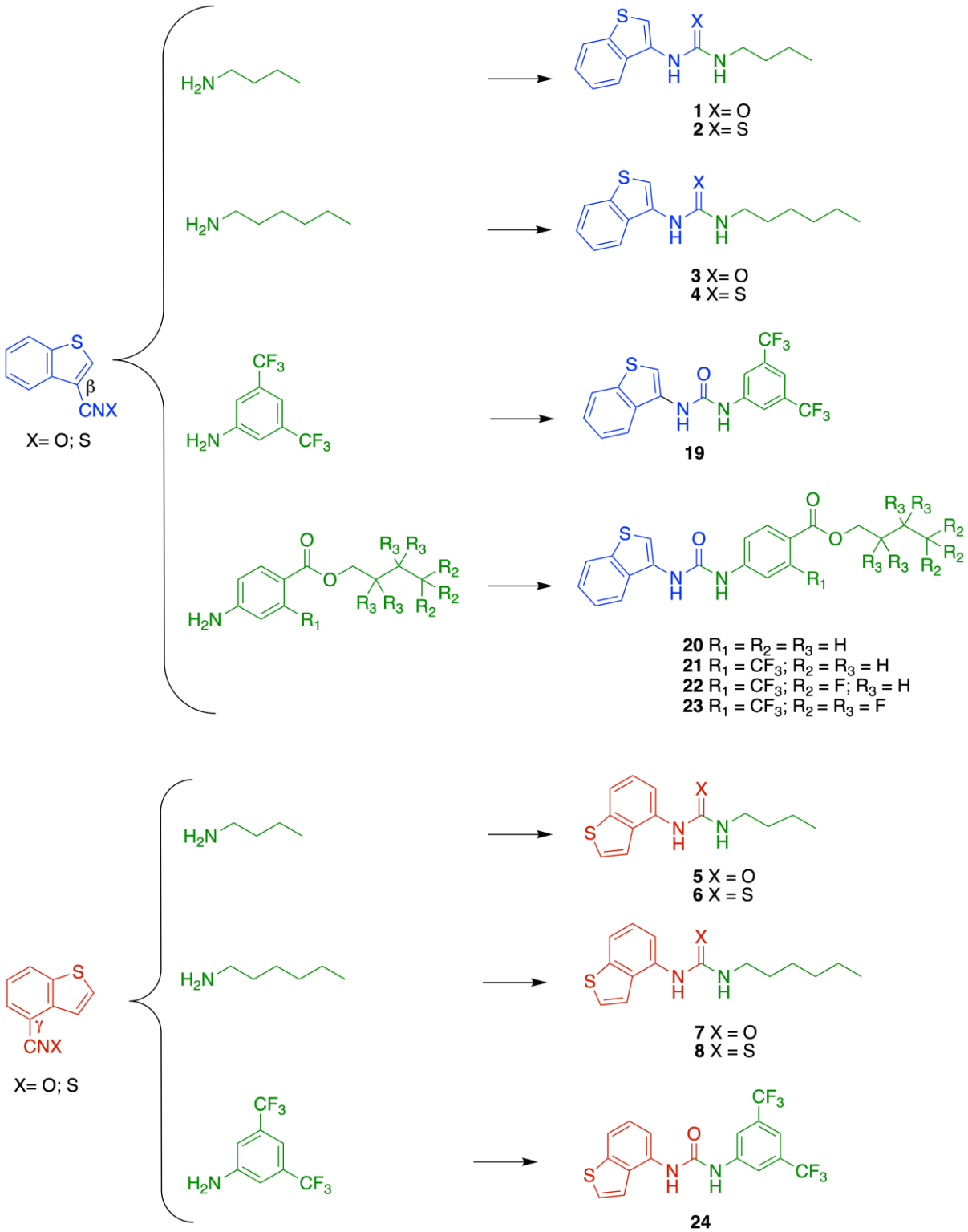

Scheme S1. Asymmetrical benzo[*b*]thiophene (thio)urea derivatives obtained by coupling of isomeric β- and γ-benzo[*b*]thiophene iso(thio)cyanates with aliphatic or aryl amines.

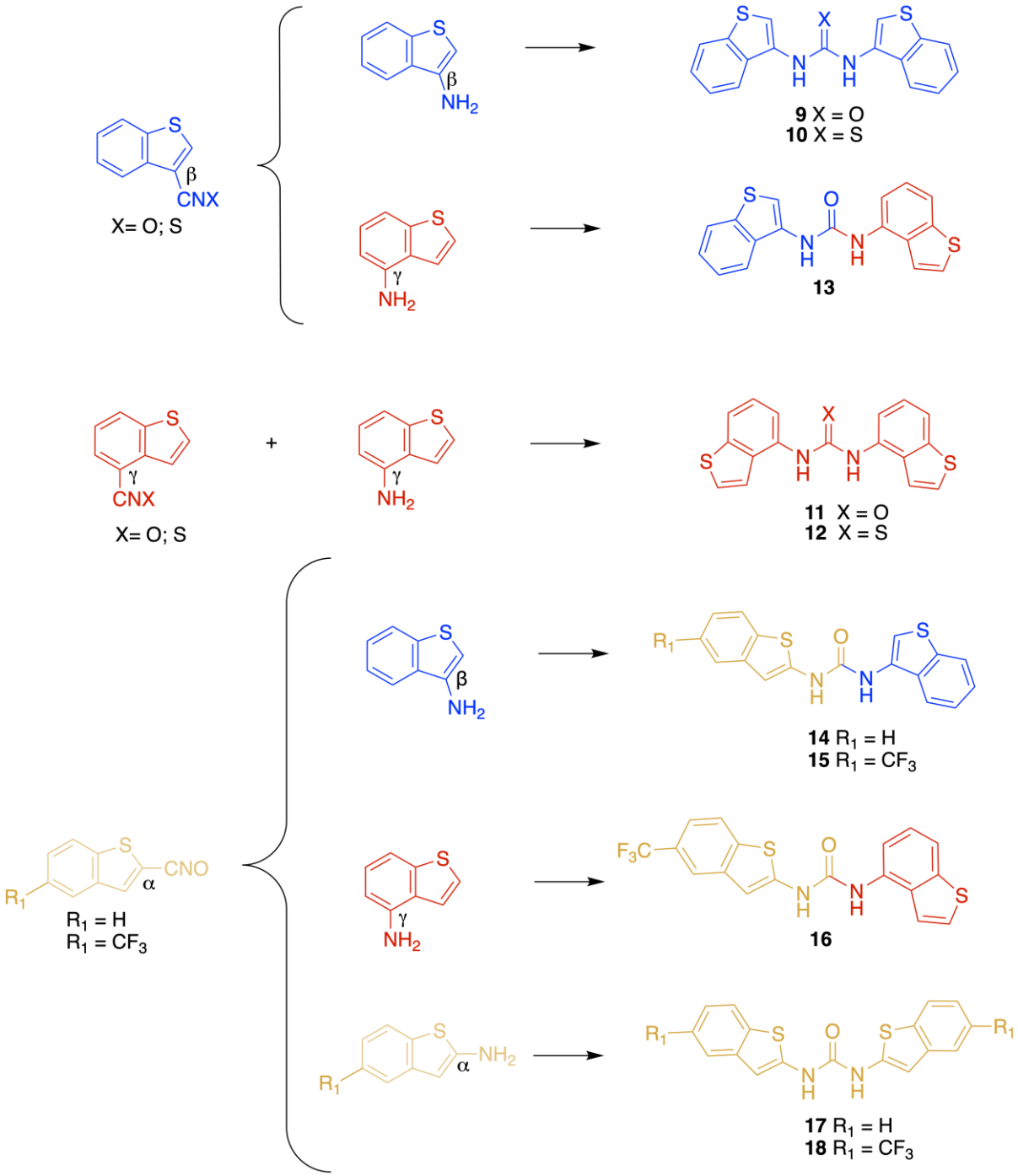

Scheme S2. Asymmetrical and symmetrical bis-benzo[*b*]thiophene (thio)urea derivatives afforded by coupling of α-, β- or γ-iso(thio)cyanates with β- or γ-benzo[*b*]thiophene amines.

Synthesis of starting building blocks

The α-, β- and γ-benzo[*b*]thiophene isocyanate derivatives were synthetised from α-, β- and γ-benzo[*b*]thiophene carboxylic acids following the synthetic route previously reported by us and depicted in Scheme S3.[2] On the other hand, the β- and γ-benzo[*b*]thiophene isothiocyanates, required to afford the β- and γ-benzo[*b*]thiophene-based thioureas (**2**, **4**, **6**, **8** and **10**), were obtained through the oxidation of benzo[*b*]thiophen-3-amine hydrochloride and benzo[*b*]thiophen-4-amine, respectively with TCP, as detailed below.

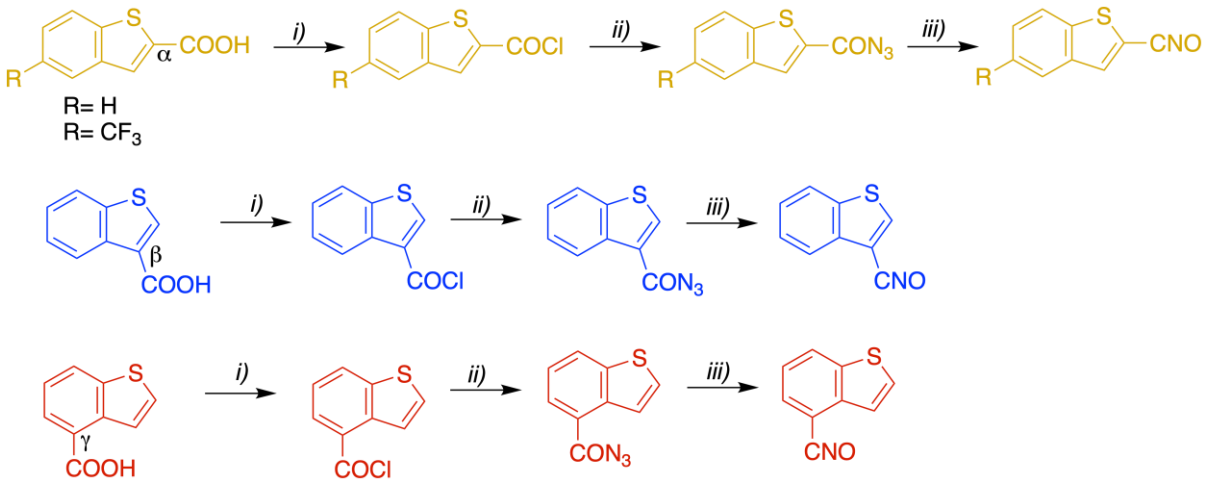

Scheme S3. Synthetic route to obtain the β-, γ- and α-benzo[*b*]thiophene-based isocyanates. Reaction conditions: *i*) $SOCl_2$, THF, reflux, *ii*) NaN_3, 0°C, *iii*) Toluene, reflux.

The syntheses of the β-benzo[*b*]thiophene urea derivatives **20-23** were accomplished with the previous esterification of 4-nitrobenzoic and 4-nitro-2-(trifluoromethyl)benzoic acids through the *Steglich* reaction,[3] followed by the reduction of the nitro group by catalytic hydrogenation with Pd/C, in ethanol (see Scheme S4) leading to aminobenzoate derivatives, which were further used without purification. The remaining synthetic details are given below with the syntheses of the intermediates **C1**-**C4**.

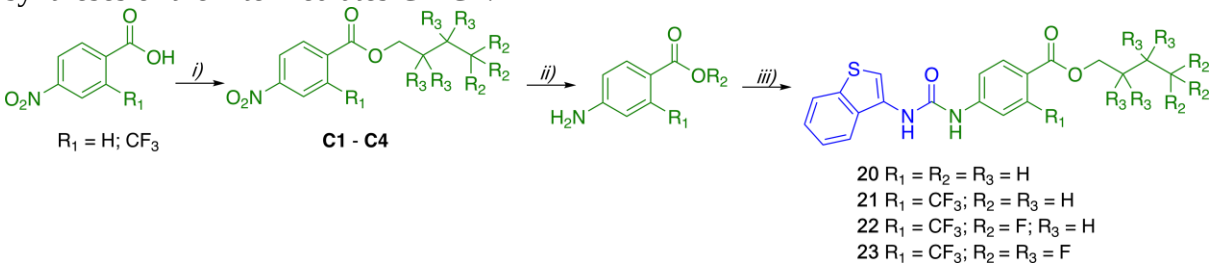

Scheme S4. Synthetic route followed to yield the aromatic amine building blocks **C1** (R_1 = R_2 = R_3= H), **C2** (R_1 = CF_3; R_2 = R_3 = H); **C3** (R_1 = CF_3; R_2 =F; R_3 = H) and **C4** (R_1 = CF_3; R_2 = R_3 = F) of **20-23**. Reaction conditions: *i*) EDCI (1.5 eq), DMAP (0.33 eq.), corresponding alcohol, THF, 24 h, r.t.; ii) H_2, Pd/C, EtOH, 1 h, 40 Psi, r.t.; *iii*) β-isocyanate benzo[*b*]thiophene, THF, 1 h, r.t.

Butyl 4-nitrobenzoate C1

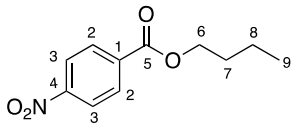

Intermediate **C1** was synthetised by addition of butanol (0.106 g, 1.43 mmol) to a mixture of 4-nitrobenzoic acid (0.200 g, 1.19 mmol), EDCI (0.246 g, 1.58 mmol), DMAP (0.048 g, 0.39 mmol) in THF. The reaction was stirred for 24 h at r.t., under nitrogen atmosphere. The crude ester was purified by flash chromatography with CH_2Cl_2 affording **C1** as yellow powder with 71% of yield (0.190 g). ^{1}H NMR (400 MHz, CD_2Cl_2, δ = ppm): 8.26 (d, $^3J_{H\text{-}H}$ = 7.9 Hz, 2H, H_3), 8.19 (d, $^3J_{H\text{-}H}$ = 7.9 Hz, 2H, H_2), 4.35 (t, $^3J_{H\text{-}H}$ = 6.6 Hz, 2H, H_8), 1.76 (quintet, $^3J_{H\text{-}H}$ = 7.0 Hz,2H, H_9), 1.48 (sextet, $^3J_{H\text{-}H}$ = 7.2 Hz, 2H, H_{10}), 0.98 (t, $^3J_{H\text{-}H}$ = 7.4 Hz, 2H, H_{11}). ^{13}C NMR (101 MHz, CD_2Cl_2, δ = ppm): 165.2 (C_5), 151.0 (C_4), 136.5 (C_1), 131.2 (C_2), 124.0 (C_3), 66.3 (C_6), 31.2 (C_7), 19.8 (C_8), 14.0 (C_9).

Butyl 4-nitro-2-(trifluoromethyl)benzoate C2

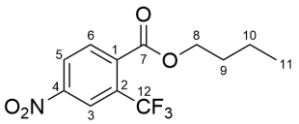

Intermediate **C2** was prepared from 4-nitro-2-(trifluoromethyl)benzoic acid (0.200 g, 0.85 mmol), EDCI (0.180 g, 1.16 mmol), DMAP (0.035 g, 0.28 mmol) and butanol (0.063 g, 0.85 mmol). The reaction was stirred for 24 h at r.t., under nitrogen atmosphere. The ester intermediate was purified by flash chromatography with CH_2Cl_2, and **C2** was obtained as a yellow powder in 40% yield (0.135 g). ^{1}H NMR (400 MHz, CD_2Cl_2, δ = ppm): 8.60 (s, 1H, H_3), 8.47 (d, $^3J_{H\text{-}H}$ = 8.5 Hz, 1H, H_5), 7.98 (d, $^3J_{H\text{-}H}$ = 8.5 Hz, 1H, H_6), 4.38 (t, $^3J_{H\text{-}H}$ = 6.6 Hz, 2H, H_8), 1.75 (quintet, $^3J_{H\text{-}H}$ = 7.2 Hz, 2H, H_9), 1.45 (sextet, $^3J_{H\text{-}H}$ = 7.3 Hz, 2H, H_{10}), 0.96 (t, $^3J_{H\text{-}H}$ = 7.4 Hz, 3H, H_{11}). ^{13}C NMR (101 MHz, CD_2Cl_2, δ = ppm): 165.6 (C_7), 149.3 (C_4), 137.7 (q, $^3J_{C\text{-}F}$ = 1.8 Hz, C_1), 132.3 (C_6), 130.6 (q, $^2J_{C\text{-}F}$ = 34.1 Hz, C_2), 127.3 (C_5), 122.9 (q, $^1J_{C\text{-}F}$ = 274.1 Hz, C_{12}), 122.8 (q, $^3J_{C\text{-}F}$ = 5.5 Hz, C_3), 67.4 (C_8), 30.9 (C_9), 19.6 (C_{10}), 14.0 (C_{11}).

4,4,4-Trifluorobutyl 4-nitro-2-(trifluoromethyl)benzoate C3

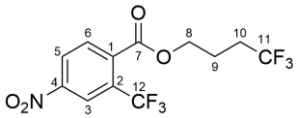

Intermediate **C3** was prepared using 4-nitro-2-(trifluoromethyl)benzoic acid (0.200 g, 0.85 mmol), EDCI (0.180, 1.16 mmol), DMAP (0.035 g, 0.28 mmol) and 4,4,4-trifluorobutanol (0.109 g, 0.85 mmol). The reaction was stirred for 24 h at r.t., under nitrogen atmosphere and **C3** was obtained through flash chromatography with CH_2Cl_2 as a yellow powder in 32% yield (0.130 g). ^{1}H NMR (400 MHz, CD_2Cl_2, δ = ppm): 8.60 (s, 1H, H_3), 8.48 (d, $^3J_{H\text{-}H}$ = 8.4 Hz, 1H, H_5), 7.99 (d, $^3J_{H\text{-}H}$ = 8.4 Hz, 1H, H_6), 4.44 (t, $^3J_{H\text{-}H}$ = 6.2 Hz, 2H, H_8), 2.27 (sextet, $^3J_{H\text{-}H}$ = 10.1 Hz, 2H, H_{10}), 2.05 (quintet, $^3J_{H\text{-}H}$ = 7.2 Hz, 2H, H_9). ^{13}C NMR (101 MHz, CD_2Cl_2, δ = ppm): 165.5 (C_7), 149.5 (C_4), 137.0 (q, $^3J_{C\text{-}F}$ = 1.6 Hz, C_1), 132.5 (C_6), 130.6 (q, $^2J_{C\text{-}F}$ = 34.2 Hz, C_2), 127.6 (q, $^1J_{C\text{-}F}$ = 276.0 Hz, C_{11}), 127.4 (C_5), 122.9 (q, $^1J_{C\text{-}F}$ = 274.0 Hz, C_{12}), 122.9 (q, $^3J_{C\text{-}F}$ = 5.6 Hz, C_3), 65.7 (C_8), 31.0 (q, $^2J_{C\text{-}F}$ = 29.3 Hz, C_{10}), 21.9 (q, $^3J_{C\text{-}F}$ = 3.1 Hz, C_9).

2,2,3,3,4,4,4-Heptafluorobutyl 4-nitro-2-(trifluoromethyl)benzoate C4

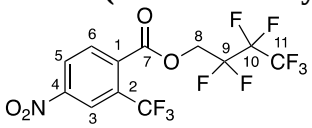

Intermediate **C4** was prepared from 4-nitro-2-(trifluoromethyl)benzoic acid (0.200 g, 0.85 mmol), EDCI (0.180 g, 1.16 mmol), DMAP (0.035 g, 0.28 mmol) and 2,2,3,3,4,4,4-heptafluorobutanol (large excess). The reaction was stirred for 24 h at r.t., under nitrogen atmosphere. The crude ester was purified by flash chromatography with CH_2Cl_2 affording **C4** as a yellow powder in 49% yield (0.176 g). ^{1}H NMR (400 MHz, CD_6CO, δ = ppm): 8.66 (d, $^3J_{H\text{-}H}$ = 8.3 Hz, 1H, H_5), 8.62 (s, 1H, H_3), 8.22 (d, $^3J_{H\text{-}H}$ = 8.3 Hz, 1H, H_6), 5.11 (t, $^3J_{H\text{-}F}$ = 13.9 Hz, 2H, H_8). ^{13}C NMR (101 MHz, CD_6CO, δ = ppm): 164.2 (C_7), 150.7 (C_4), 135.3 (C_1), 133.5 (C_6), 130.8 (q, $^2J_{C\text{-}F}$ = 34.2 Hz, C_2), 127.6 (C_5), 122.3 (q, $^3J_{C\text{-}F}$ = 5.6 Hz, C_3), 119.1 (q, $^1J_{C\text{-}F}$ = 273.4 Hz, C_{12}), 119.3-112.1 (m, C_{10}, C_{11}), 110.2-108.8 (m, C_9), 61.6 (t, $^2J_{C\text{-}F}$ = 26.7 Hz, C_8).

Synthesis of benzo[b]thiophene-based (thio)ureas

Compound 1

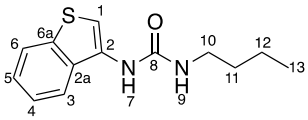

The β-benzo[*b*]thiophene isocyanate was prepared accordingly to Scheme S3 from benzo[*b*]thiophene-3-carboxylic acid (0.1 g, 0.56 mmol), thionyl chloride (0.819 g, 6.9 mmol) and sodium azide (0.05 g, 0.76 mmol). Subsequently it was added dropwise (without purification) to THF solution of butylamine (0.074 g, 1.0 mmol), stirred during 1 h at r.t., under nitrogen atmosphere. The urea **1** was yielded as white powder with 52% of yield (0.072 g). Mp: 128.6-130.0°C. FTIR (KBr) ν_{max} cm^{-1}: 3360 (NH, stretch), 3290 (CH, stretch, Ar), 2960, 2930, 2860, 1640 (C=O, urea), 1555, 1460, 1430, 1240, 752, 731, 669. ^{1}H NMR (400 MHz, DMSO-*d*$_6$, δ = ppm): 8.76 (s, 1H, H_7), 7.93 (d, $^3J_{H\text{-}H}$ = 7.8 Hz, 1H, H_6), 7.83 (d, $^3J_{H\text{-}H}$ = 7.9 Hz, 1H, H_3), 7.59 (s, 1H, H_1), 7.44 (t, $^3J_{H\text{-}H}$ = 7.4 Hz, 1H, H_4), 7.39 (t, $^3J_{H\text{-}H}$ = 7.4 Hz, 1H, H_5), 6.34 (t, $^3J_{H\text{-}H}$ = 5.2 Hz, 1H, H_9), 3.14 (q, $^3J_{H\text{-}H}$ = 6.1 Hz, 2H, H_{10}), 1.45 (quintet, $^3J_{H\text{-}H}$ = 7.1 Hz, 2H, H_{11}), 1.34 (sextet, $^3J_{H\text{-}H}$ = 7.1 Hz, 2H, H_{12}), 0.91 (t, $^3J_{H\text{-}H}$ = 7.1 Hz, 3H, H_{13}). ^{13}C APT NMR (101 MHz, DMSO-*d*$_6$, δ = ppm): 155.2 (C_8), 137.1 (C_{6a}), 132.7 (C_{2a}), 131.1 (C_2), 124.7 (C_5), 123.8 (C_4), 123.1 (C_6), 119.8 (C_3), 105.3 (C_1), 38.8 (C_{10}), 31.9 (C_{11}), 19.6 (C_{12}), 13.7 (C_{13}). HRMS [ESI$^+$] m/z: [M+H]$^+$ calcd for $C_{13}H_{16}N_2OS$ 249.1056, found 249.1059.

Compound 2

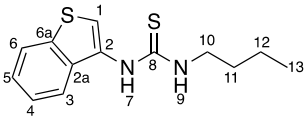

The β-benzo[*b*]thiophene isothiocyanate was prepared from a solution of benzo[*b*]thiophen-3-amine hydrochloride (0.100 g, 0.54 mmol) and DIPEA (0.074 g, 0.57 mmol), in CH_2Cl_2 (15 mL), which was added dropwise to TCP (0.160 g, 0.68 mmol). After the stirring the reaction mixture for 1 h, the solvent was removed, and the β-benzo[*b*]thiophene isothiocyanate was isolated by flash chromatography with CH_2Cl_2 as a yellow oil in a quantitative yield. Subsequently, a solution of butylamine (0.037 g, 0.50 mmol) in THF (5 mL) was added dropwise to the isothiocyanate, and the reaction mixture was stirred at r.t. for 24 h, under nitrogen atmosphere. The solvent was removed and **2** precipitated with CH_2Cl_2 as a yellow powder in 74% yield (0.100 g). Mp: 118.7-120.9°C. FTIR (KBr) ν_{max} cm^{-1}: 3200 (NH, stretch), 3140 (CH, stretch, Ar), 2950, 2930, 2860, 1540 (C=S, thiourea), 1520, 1550, 1280, 1240, 1210, 1080, 764, 750, 648. ^{1}H NMR (400 MHz, DMSO-*d*$_6$, δ = ppm): 9.53 (s, 1H, H_7), 8.03-7.94 (m, 2H, H_1 and H_6), 7.88 (brs, 1H, H_9), 7.73 (d, $^3J_{H\text{-}H}$ = 7.0 Hz, 1H, H_3), 7.46-7.37 (m, 2H, H_4 and H_5), 3.46 (brs, 2H, H_{10}), 1.52 (quintet, $^3J_{H\text{-}H}$ = 7.0 Hz, 2H, H_{11}), 1.31 (sextet, $^3J_{H\text{-}H}$ = 7.0 Hz, 2H, H_{12}), 0.90 (t, $^3J_{H\text{-}H}$ = 7.4 Hz, 3H, H_{13}). ^{13}C APT RMN (101 MHz, DMSO-*d*$_6$, δ = ppm):

180.8 (C_8), 137.4 (C_{6a}), 136.2 (C_{2a}), 134.5 (C_2), 124.8 (C_5), 124.0 (C_4), 123.1 (C_6), 120.7 (C_3), 116.5 (C_1)*, 43.7 (C_{10}), 30.6 (C_{11}), 19.6 (C_{12}), 13.7 (C_{13}). HRMS [ESI$^+$] m/z: $[M+H]^+$ calcd for $C_{13}H_{16}N_2S_2$ 265.0828, found 265.0836.
*assigned with HMQC

Compound 3

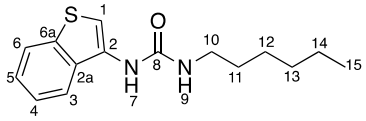

The β-benzo[*b*]thiophene isocyanate, prepared as described for **1**, was added dropwise to a THF solution of hexylamine (0.077 g, 0.77 mmol), and the mixture was stirred for 1 h at r.t., under nitrogen atmosphere. **3** was obtained as white powder with 52% of yield (0,070 g). Mp: 127.4-129.0°C. FTIR (KBr) ν_{max} cm^{-1}: 3310 (NH, stretch), 3100 (CH, stretch, Ar), 2930, 2860, 1640 (C=O, urea), 1570, 1520, 1270, 1200, 756, 729, 652. ^{1}H NMR (400 MHz, DMSO-*d*$_6$, δ = ppm): 8.74 (s, 1H, H_7), 7.93 (d, $^3J_{H\text{-}H}$ = 7.8 Hz, 1H, H_6), 7.83 (d, $^3J_{H\text{-}H}$ = 7.9 Hz, 1H, H_3), 7.59 (s, 1H, H_1), 7.44 (t, $^3J_{H\text{-}H}$ = 7.4 Hz, 1H, H_4) , 7.39 (t, $^3J_{H\text{-}H}$ = 7.3 Hz, 1H, H_5), 6.34 (t, $^3J_{H\text{-}H}$ = 5.1 Hz, 1H, H_9), 3.13 (q, $^3J_{H\text{-}H}$ = 6.2 Hz, 2H, H_{10}), 1.46 (quintet, $^3J_{H\text{-}H}$ = 6.2 Hz, 2H, H_{11}), 1.29 (brs, 6H, H_{12}-H_{14}), 0.87 (t, $^3J_{H\text{-}H}$ = 5.8 Hz, 3H, H_{15}). ^{13}C APT RMN (101 MHz, DMSO-*d*$_6$, δ = ppm): 155.1 (C_8), 137.0 (C_{6a}), 132.5 (C_{2a}), 130.9 (C_2), 124.5 (C_5), 123.6 (C_4), 123.0 (C_6), 119.7 (C_3), 105.2 (C_1), 39.2 (C_{10}), 30.9 (C_{11}), 29.6 (C_{12}), 26.0 (C_{13}), 22.0 (C_{14}), 13.9 (C_{15}). HRMS [ESI$^+$] m/z: $[M+H]^+$ calcd for $C_{15}H_{20}N_2OS$ 277.1369, found 277.1374.

Compound 4

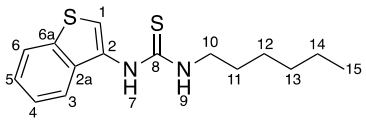

To the β-benzo[*b*]thiophene isothiocyanate, prepared as described for **2**, a solution of hexylamine (0.071 g, 0.70 mmol) in THF (5 mL) was added dropwise, and the reaction mixture was stirred at r.t. for 24 h, under nitrogen atmosphere. The solvent was removed and **4** was precipitated in CH_2Cl_2 as yellow powder with 16.5% yield (0.028 g). Mp: 72.7-74.1°C. FTIR (KBr) ν_{max} cm^{-1}: 3240 (NH, stretch), 3090, 3040 (CH, stretch, Ar), 2960, 2930, 2850, 1560 (C=S, thiourea), 1540, 1430, 1390, 1250, 1060, 758, 723, 457. ^{1}H NMR (400 MHz, DMSO-*d*$_6$, δ = ppm): 9.50 (s, 1H, H_7), 8.00-7.94 (m, 2H, H_1, H_6), 7.84 (brs, 1H, H_9), 7.72 (d, $^3J_{H\text{-}H}$ = 7.1 Hz, 1H, H_3), 7.46-7.37 (m, 2H, H_4, H_5), 3.50-3.40 (m, 2H, H_{10}), 1.52 (brs, 2H, H_{11}), 1.27 (brs, 6H, H_{12}-H_{14}), 0.87 (t, $^3J_{H\text{-}H}$ = 5.7 Hz, 3H, H_{15}). ^{13}C APT NMR (101 MHz, DMSO-*d*$_6$, δ = ppm): 180.8 (C_8), 137.4 (C_{6a}), 134.5 (C_{2a}), 130.8 (C_2), 124.8 (C_5), 124.0 (C_4), 123.1 (C_6), 120.7 (C_3), 116.6 (C_1), 44.0 (C_{10}), 31.0 (C_{11}), 28.4 (C_{12}), 26.1 (C_{13}), 22.1 (C_{14}), 13.9 (C_{15}). HRMS [ESI$^+$] m/z: $[M+H]^+$ calcd for $C_{15}H_{20}N_2S_2$ 293.1141, found 293.1154.

Compound 5

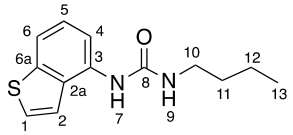

Butyl isocyanate (0.07 g, 0.7 mmol) was added dropwise to a THF solution of benzo[*b*]thiophen-4-amine (0.100 g, 0.67 mmol). The mixture was stirred during 1 h at r.t., under nitrogen atmosphere, and **5** was yielded as grey white powder with 7% of yield (0.012 g). Mp: 156.5-158.3°C. FTIR (KBr) ν_{max} cm^{-1}: 3350 (NH, stretch), 3250, 3090(CH, stretch, Ar), 2950, 2860 (CH, stretch), 1630 (C=O, urea), 1600, 1570, 1450, 1410, 1260, 754, 698. ^{1}H

NMR (400 MHz, DMSO-d_6, δ = ppm): 8.46 (s, 1H, H_7), 7.96 (d, $^3J_{H\text{-}H}$ = 7.9 Hz, 1H, H_4), 7.72 (d, $^3J_{H\text{-}H}$ = 5.4 Hz, 1H, H_1), 7.59-7.51 (m, 2H, H_2, H_6), 7.25 (t, $^3J_{H\text{-}H}$ = 7.9 Hz, 1H, H_5), 6.45 (t, $^3J_{H\text{-}H}$ = 4.9 Hz, 1H, H_9), 3.13 (q, $^3J_{H\text{-}H}$ = 6.3 Hz, 2H, H_{10}), 1.45 (quintet, $^3J_{H\text{-}H}$ = 6.7 Hz, 2H, H_{11}), 1.34 (sextet, $^3J_{H\text{-}H}$ = 6.9 Hz, 2H, H_{12}), 0.91 (t, $^3J_{H\text{-}H}$ = 7.2 Hz, 3H, H_{13}). ^{13}C APT NMR (101 MHz, DMSO-d_6, δ = ppm): 155.0 (C_8), 139.7 (C_{6a}), 135.1 (C_3), 129.6 (C_{2a}), 125.6 (C_1), 124.9 (C_5), 120.1 (C_2), 115.4 (C_6), 112.7 (C_4), 38.6 (C_{10}), 31.7 (C_{11}), 19.5 (C_{12}), 13.6 (C_{13}). HRMS [ESI$^+$] m/z: $[M+H]^+$ calcd for $C_{13}H_{16}N_2OS$ 249.1056, found 249.1062.

Compound 6

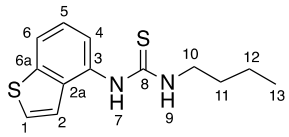

The γ-benzo[*b*]thiophene isothiocyanate was prepared by dropwise addition of a solution of benzo[*b*]thiophen-4-amine (0.100 g, 0.67 mml) in CH_2Cl_2 (15 mL), to TCP (0.230 g, 0.99 mmol). After stirring the reaction mixture for 1 h, the γ-benzo[*b*]thiophene isothiocyanate was isolated as yellow oil in quantitative yield, following the procedure adopted for the isomeric β-benzo[*b*]thiophene isothiocyanate (*vide supra*). Subsequently, a solution of butylamine (0.074 g, 1.0 mmol) in THF (5 mL) was added dropwise to the γ-benzo[*b*]thiophene isothiocyanate. The reaction mixture was stirred at at r.t. for 24 h, under nitrogen atmosphere, the solvent was removed and **6** was precipitated in CH_2Cl_2 as pink-white powder with 76% of yield (0.147 g). Mp: 80.7-82.2°C. FTIR (KBr) ν_{max} cm^{-1}: 3390 (NH, stretch), 3150, 3060 (CH, stretch, Ar), 2930, 2870 (CH, stretch), 1540 (C=S, thiourea), 1500, 1450, 1340, 1320, 1280, 1250, 758, 688, 542. ^{1}H NMR (400 MHz, DMSO-d_6, δ = ppm): 9.59 (s, 1H, H_7), 7.85 (d, $^3J_{H\text{-}H}$ = 8.0 Hz, 1H, H_6), 7.75 (d, $^3J_{H\text{-}H}$ = 5,4 Hz, 1H, H_1), 7.69 (m, 1H, H_9), 7.46 (d, $^3J_{H\text{-}H}$ = 7.2 Hz, 1H, H_4), 7.39-7.30 (m, 2H, H_2, H_5), 3.50-3.40 (m, 2H, H_{10}), 1.50 (quintet, $^3J_{H\text{-}H}$ = 7.2 Hz, 2H, H_{11}), 1.29 (sextet, $^3J_{H\text{-}H}$ = 7.2 Hz, 2H, H_{12}), 0.89 (t, $^3J_{H\text{-}H}$ = 7.3 Hz, 3H, H_{13}). ^{13}C APT NMR (101 MHz, DMSO-d_6, δ = ppm): 180.9 (C_8), 140.2 (C_{6a}), 135.4 (C_{2a}), 133.6 (C_3), 127.1 (C_1), 124.6 (C_5), 121.4 (C_2), 121.2 (C_4), 120.0 (C_6), 43.9 (C_{10}), 30.7 (C_{11}), 19.7 (C_{12}), 13.8 (C_{13}). HRMS [ESI$^+$] m/z: $[M+H]^+$ calcd for $C_{13}H_{16}N_2S_2$ 265.0828, found 265.0832.

Compound 7

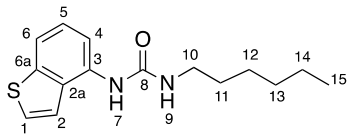

Hexyl isocyanate (0.087 g, 0.67 mml) was added dropwise to a THF solution of benzo[*b*]thiophen-4-amine (0.100 g, 0.67 mmol), and the mixture stirred during 1 h at r.t., under nitrogen atmosphere. **7** was isolated as white grey powder with 73% of yield (0.136 g). Mp: 141.9-143.2 °C. FTIR (KBr) ν_{max} cm^{-1}: 3330 (NH, stretch), 3270 (CH, stretch, Ar), 3100, 2960, 2940, 2850, 1630 (C=O, urea), 1570, 1460, 1450, 1410, 1320, 1250, 922, 756, 700, 675. ^{1}H NMR (400 MHz, DMSO-d_6, δ = ppm): 8.46 (s, 1H, H_7), 7.96 (d, $^3J_{H\text{-}H}$ = 7.9 Hz, 1H, H_4), 7.72 (d, $^3J_{H\text{-}H}$ = 5.5 Hz, 1H, H_1), 7.57-7.53 (m, 2H, H_2, H_6), 7.25 (t, $^3J_{H\text{-}H}$ = 7.9 Hz, 1H, H_5) , 6.46 (t, $^3J_{H\text{-}H}$ = 5.3 Hz, 1H, H_9), 3.12 (q, $^3J_{H\text{-}H}$ = 6.2 Hz, 2H, H_{10}), 1.46 (quintet, $^3J_{H\text{-}H}$ = 6.2 Hz, 2H, H_{11}), 1.29 (brs, 6H, H_{12}, H_{13}, H_{14}), 0.88 (t, $^3J_{H\text{-}H}$ = 6.0 Hz, 3H, H_{15}). ^{13}C APT NMR (101 MHz, DMSO-d_6, δ = ppm): 155.2 (C_8), 139.8 (C_{6a}), 135.2 (C_3), 129.8 (C_{2a}), 125.8 (C_1), 125.0 (C_5), 120.3 (C_2), 115.5 (C_6), 112.9 (C_4), 39.1 (C_{10}), 31.1 (C_{11}), 29.7 (C_{12}), 26.2 (C_{13}), 22.2 (C_{14}), 14.0 (C_{15}). HRMS [ESI$^+$] m/z: $[M+H]^+$ calcd for $C_{15}H_{20}N_2OS$ 277.1369, found 277.1365.

Compound 8

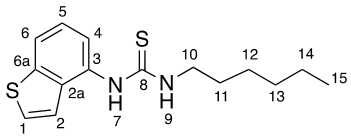

The γ-benzo[*b*]thiophene isothiocyanate was obtained by dropwise addition of a solution of benzo[*b*]thiophen-4-amine (0.10 g, 0.67 mmol) to TCP (0.187 g, 0.80 mmol) as reported for the compound **6**. Afterwards, a solution of hexylamine (0.077 g, 0.76 mmol) in THF (5 mL) was added dropwise to the isothiocyanate, and the mixture was stirred at r.t. for 24 h, under nitrogen atmosphere. **8** was precipitated in CH_2Cl_2 as white powder with 84% of yield (0.152 g). Mp: 85.9-86.7°C. FTIR (KBr) ν_{max} cm^{-1}: 3220 (NH, stretch), 3060 (CH, stretch, Ar), 2950, 2940, 2860, 1600, 1560 (C=S, thiourea), 1450, 1410, 1350, 1320, 930, 758, 690. ^{1}H NMR (400 MHz, DMSO-*d*$_6$, δ = ppm): 9.60 (s, 1H, H_7), 7.85 (d, $^3J_{H\text{-}H}$ = 7.8 Hz, 1H, H_6), 7.75 (d, $^3J_{H\text{-}H}$ = 5.1 Hz, 1H, H_1), 7.69 (brs, 1H, H_9), 7.49-7.41 (m, 1H, H_4), 7.39-7.29 (m, 2H, H_2, H_5), 3.43 (brs, 2H, H_{10}), 1.51 (brs, 2H, H_{11}), 1.27 (brs, 6H, H_{12}, H_{13}, H_{14}), 0.87 (brs, 3H, H_{15}). ^{13}C APT NMR (101 MHz, DMSO-*d*$_6$, δ = ppm): 180.8 (C_8), 140.1 (C_{6a}), 135.4 (C_{2a}), 133.5 (C_3), 127.1 (C_1), 124.6 (C_5), 121.4 (C_2), 121.2 (C_4), 120.0 (C_6), 44.2 (C_{10}), 31.1 (C_{11}), 28.5 (C_{12}), 26.1 (C_{13}), 22.1 (C_{14}), 14.0 (C_{15}). HRMS [ESI^+] m/z: $[M+H]^+$ calcd for $C_{15}H_{20}N_2S_2$ 293.1141, found 293.1145.

Compound 9

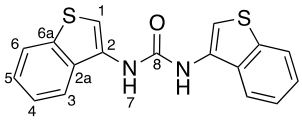

The β,β-bis(benzo[*b*]thiophene) urea **9** was obtained by coupling of β-benzo[*b*]thiophene isothiocyanate with β-benzo[*b*]thiophene amine. The isocyanate, prepared from benzo[*b*]thiophene-3-carboxylic accordingly to Scheme S3, was added dropwise to THF solution of benzo[*b*]thiophene-3-amine hydrochloride (0.050 g, 0.27 mmol), and DIPEA (0.074 g, 0.57 mmol) in THF (10 mL). The reaction mixture was stirred for 1 h at r.t., under nitrogen atmosphere, and **9** was isolated as white powder from a THF solution with 56% of yield (0.050 g). Mp: 255.4-257.5°C. FTIR (KBr) FTIR (KBr) ν_{max} cm^{-1}: 3270 (NH, stretch), 3090 (CH, stretch, Ar), 1630 (C=O, urea), 1580, 1555, 1430, 1360, 1260, 854, 793, 756, 731, 696, 654. ^{1}H NMR (400 MHz, DMSO-*d*$_6$, δ = ppm): 9.27 (s, 2H, H_7), 8.00 (d, $^3J_{H\text{-}H}$ = 8.0 Hz, 2H, H_6), 7.89 (d, $^3J_{H\text{-}H}$ = 8.0 Hz, 2H, H_3), 7.77 (s, 2H, H_1), 7.53 (t, $^3J_{H\text{-}H}$ = 7.5 Hz, 2H, H_4), 7.45 (t, $^3J_{H\text{-}H}$ = 7.5 Hz, 2H, H_5). ^{13}C APT NMR (101 MHz, DMSO-*d*$_6$, δ = ppm): 152.3 (C_8), 137.3 (C_{6a}), 132.7 (C_{2a}), 130.1 (C_2), 125.1 (C_5), 124.2 (C_4), 123.4 (C_6), 119.8 (C_3), 107.3 (C_1). HRMS [ESI^+] m/z: $[M+H]^+$ calcd for $C_{17}H_{12}N_2OS_2$ 325.0464, found 325.0446.

Compound 10

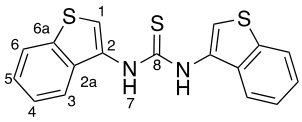

The β,β-bis(benzo[*b*]thiophene) thiourea **10** was obtained by coupling of β-benzo[*b*]thiophene isothiocyanate with β-benzo[*b*]thiophene amine. The isothiocyanate was prepared from a solution of benzo[*b*]thiophene-3-amine hydrochloride (0.097 g, 0.52 mmol) and DIPEA (0.074 g, 0.57 mmol) in CH_2Cl_2 (15 mL) added dropwise to TCP (0.190 g, 0.81 mmol), as reported for the compound **2**. Subsequently, a solution of benzo[*b*]thiophene-3-amine hydrochloride (0.094 g, 0,5 mmol) and DIPEA (0.066 g, 0.51 mmol) in THF (5 mL) was added dropwise to the isothiocyanate. After the stirring the reaction mixture at r.t. for 24 h, under nitrogen atmosphere, the solvent was removed and **10** precipitated in CH_2Cl_2 as yellow powder with 53% of yield (0.081 g). Mp: 176.2-178.8°C. FTIR (KBr) ν_{max} cm^{-1}: 3330 (NH, stretch), 3150 (CH, stretch, Ar), 3070, 2940, 1560, 1530 (C=O, thiourea), 1550, 1430, 1360, 1340, 1230, 852, 762, 733. ^{1}H NMR (400 MHz, DMSO-*d*$_6$, δ = ppm): 10.02 (s, 2H, H_7), 8.12 (s, 2H, H_1), 8.00 (d, $^3J_{H\text{-}H}$ = 7.8 Hz, 2H, H_6), 7.87 (d, $^3J_{H\text{-}H}$ = 7.8 Hz, 2H, H_3), 7.48 (t, $^3J_{H\text{-}H}$ = 7.4 Hz, 2H, H_4), 7.43 (t, $^3J_{H\text{-}H}$ = 7.4 Hz, 2H, H_5). ^{13}C APT NMR (101 MHz, DMSO-*d*$_6$, δ = ppm): 180.2 (C_8), 137.4 (C_{6a}), 134.7 (C_{2a}), 131.0 (C_2), 124.9 (C_5), 124.1 (C_4), 123.2 (C_6), 121.1 (C_3), 117.9 (C_1). HRMS [ESI$^+$] m/z: $[M+H]^+$ calcd for $C_{17}H_{12}N_2S_3$ 341.0235, found 341.0227.

Compound 11

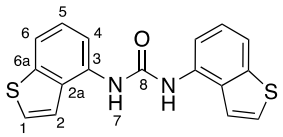

The γ,γ-bis(benzo[*b*]thiophene) urea **11** was obtained by coupling of γ-benzo[*b*]thiophene isocyanate with γ-benzo[*b*]thiophene amine. The isocyanate was prepared following Scheme S3 from benzo[*b*]thiophene-4-carboxylic acid (0.1 g, 0.56 mmol), thionyl chloride (0.819 g, 6.9 mmol) and sodium azide (0.05 g, 0.76 mmol). Then, it was added dropwise to a solution of benzo[*b*]thiophen-4-amine (0.060 g, 0.40 mmol) in THF. The reaction mixture was stirred for 1 h at r.t., under nitrogen atmosphere, and **11** was obtained as grey powder with 34% of yield (0.075 g). Mp: 300.2-302.1°C. FTIR (KBr) ν_{max} cm^{-1}: 3280 (NH, stretch), 3080 (CH, stretch, Ar), 1630 (C=O, urea), 1560, 1450, 1410, 1320, 1250, 924, 864, 793, 756, 692, 648. ^{1}H NMR (400 MHz, DMSO-*d*$_6$, δ = ppm): 9.06 (s, 2H, H_7), 8.02 (d, $^3J_{H\text{-}H}$ = 7.8 Hz, 2H, H_4), 7.83 (d, $^3J_{H\text{-}H}$ = 5.5 Hz, 2H, H_1), 7.71-7.64 (m, 4H, H_2, H_6), 7.35 (t, $^3J_{H\text{-}H}$ = 7.8 Hz, 2H, H_5). ^{13}C APT NMR (101 MHz, DMSO-*d*$_6$, δ = ppm): 152.5 (C_8), 140.0 (C_{6a}), 134.1 (C_3), 130.6 (C_{2a}), 126.6 (C_1), 125.1 (C_5), 120.2 (C_2), 116.8 (C_6), 114.1 (C_4). HRMS [ESI$^+$] m/z: $[M+H]^+$ calcd for $C_{17}H_{12}N_2OS_2$ 325.0464, found 325.0451.

Compound 12

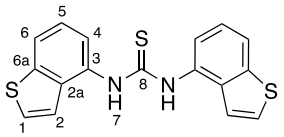

The γ,γ-bis(benzo[*b*]thiophene) thiourea **12** was obtained by coupling of γ-benzo[*b*]thiophene isothiocyanate with the corresponding γ-benzo[*b*]thiophene amine. The isothiocyanate was prepared from benzo[*b*]thiophen-4-amine (0.100 g, 0.67 mml) in DCM (15 mL) as a yellow oil with quantitative yield following the experimental procedure reported for **6**. A solution of benzo[*b*]thiophen-4-amine (0.100 g, 0.67 mmol) in THF (5 mL) was added dropwise to the isothiocyanate. After stirring the reaction mixture for 24 h at r.t., under nitrogen atmosphere, **12** was precipitated in CH_2Cl_2 as grey powder with 41% of yield (0.085 g). Mp: 189.9-191.1°C. FTIR (KBr) ν_{max} cm^{-1}: 3180 (NH, stretch), 3010 (CH, stretch, Ar), 1540 (C=O, thiourea), 1560, 1460, 1410, 1320, 1080, 985, 862, 793, 756, 683, 663. ^{1}H NMR (400 MHz, DMSO-d_6, δ = ppm): 9.94 (s, 2H, H_7), 7.86 (d, $^3J_{H\text{-}H}$ = 7.8 Hz, 2H, H_6), 7.77 (d, $^3J_{H\text{-}H}$ = 5.3 Hz, 2H, H_1), 7.51 (d, $^3J_{H\text{-}H}$ = 7.7 Hz, 2H, H_4), 7.47 (d, $^3J_{H\text{-}H}$ = 5.4 Hz, 2H, H_2), 7.36 (t, $^3J_{H\text{-}H}$ = 7,8 Hz, 2H, H_5). ^{13}C APT NMR (101 MHz, DMSO-d_6, δ = ppm): 181.2 (C_8), 139.9 (C_{6a}), 136.0 (C_{2a}),134.0 (C_3), 127.0 (C_1), 124.4 (C_5), 122.1 (C_2), 121.7 (C_4), 120.4 (C_6). HRMS [ESI$^+$] m/z: $[M+H]^+$ calcd for $C_{17}H_{12}N_2S_3$ 341.0235, found 341.0218.

Compound 13

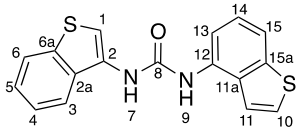

The β,γ-bis(benzo[*b*]thiophene) urea **13** was produced by coupling of β-benzo[*b*]thiophene isocyanate with γ-benzo[*b*]thiophene amine. The isocyanate, prepared as described for **1**, was added dropwise to THF solution of benzo[*b*]thiophen-4-amine (0.050 g, 0.33 mmol) in THF (10 mL). After stirring the reaction mixture for 1 h at r.t., under nitrogen atmosphere, **13** was obtained as grey powder with 21% of yield (0.040 g). Mp: 268.2-269.7°C. FTIR (KBr) ν_{max} cm^{-1}: 3270 (NH, stretch), 3280 (CH, stretch, Ar), 1630 (C=O, urea), 1580, 1550, 1460, 1360, 1320, 1260, 1050, 949, 866, 754, 727, 692, 652. ^{1}H NMR (400 MHz, DMSO-d_6, δ = ppm): 9.30 (s, 1H, H_7), 9.00 (s, 1H, H_9), 8.05 (d, $^3J_{H\text{-}H}$ = 8.0 Hz, 1H, H_{13}), 8.01 (d, $^3J_{H\text{-}H}$ = 8.0 Hz, 1H, H_6), 7.92 (d, $^3J_{H\text{-}H}$ = 8.1 Hz, 1H, H_3), 7.84 (d, $^3J_{H\text{-}H}$ = 5.5 Hz, 1H, H_{10}), 7.77 (s, 1H, H_1), 7.68 (d, $^3J_{H\text{-}H}$ = 8.0 Hz, 1H, H_{15}), 7.64 (d, $^3J_{H\text{-}H}$ = 5.5 Hz, 1H, H_{11}), 7.54 (t, $^3J_{H\text{-}H}$ = 7.5 Hz, 1H, H_4), 7.45 (t, $^3J_{H\text{-}H}$ = 7.5 Hz, 1H, H_5), 7.35 (t, $^3J_{H\text{-}H}$ = 7.9 Hz, 1H, H_{14}). ^{13}C APT NMR (101 MHz, DMSO-d_6, δ = ppm): 152.5 (C_8), 140.0 (C_{15a}), 137.2 (C_{6a}), 134.1 (C_{12}), 132.7 (C_{2a}), 130.4 (C_{11a}), 130.1 (C_2), 126.6 (C_{10}), 125.1 (C_5), 125.0 (C_{14}), 124.0 (C_4), 123.3 (C_6), 120.0 (C_{11}), 119.8 (C_3), 116.7 (C_{15}), 113.7 (C_{13}), 107.3 (C_1). HRMS [ESI$^+$] m/z: $[M+H]^+$ calcd for $C_{17}H_{12}N_2OS_2$ 325.0464, found 325.0448.

Compound 14

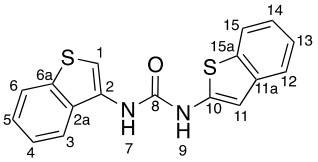

The α,β-bis(benzo[*b*]thiophene) urea **14** was produced by addition of α-benzo[*b*]thiophene isocyanate to a β-benzo[*b*]thiophene amine. The isocyanate was prepared following Scheme S3 from benzo[*b*]thiophene-2-carboxylic acid (0.1 g, 0.67 mmol), thionyl chloride (0.819 g, 6.9 mmol) and sodium azide (0.058 g, 0.89 mmol). This intermediate, obtained as a yellow oil in quantitative yield, was added dropwise to THF solution of the benzo[*b*]thiophen-3-amine hydrochloride (0.060 g, 0.32 mmol) and DIPEA (0.074 g, 0.57 mmol) in THF (5 mL). The reaction mixture was stirred at r.t. for 1 h, under nitrogen atmosphere, and **14** was yielded as white powder with 19% of yield (0.020 g). Mp 219.3-220.5°C. FTIR (KBr) ν_{max} cm^{-1}: 3280 (NH, stretch), 3060 (CH, stretch, Ar), 2960 (CH, stretch), 1720, 1630 (C=O, urea), 1580, 1550, 1220, 1020, 994, 806, 754, 723. ^{1}H NMR (400 MHz, DMSO-*d*$_6$, δ = ppm): 10.11 (s, 1H, H_9), 9.31 (s, 1H, H_7), 7.99 (d, $^{3}J_{H\text{-}H}$ = 7.9 Hz, 1H, H_6), 7.87 (d, $^{3}J_{H\text{-}H}$ = 7.9 Hz, 1H, H_3), 7.80 (d, $^{3}J_{H\text{-}H}$ = 7.9 Hz, 1H, H_{15}), 7.76 (s, 1H, H_1), 7.62 (d, $^{3}J_{H\text{-}H}$ = 7.8 Hz, 1H, H_{12}), 7.50 (t, $^{3}J_{H\text{-}H}$ = 7.4 Hz, 1H, H_4), 7.44 (t, $^{3}J_{H\text{-}H}$ = 7.4 Hz, 1H, H_5), 7.28 (t, $^{3}J_{H\text{-}H}$ = 7.5 Hz, 1H, H_{13}), 7.17 (t, $^{3}J_{H\text{-}H}$ = 7.5 Hz, 1H, H_{14}), 6.89 (s, 1H, H_{11}). ^{13}C APT NMR (101 MHz, DMSO-*d*$_6$, δ = ppm): 151.8 (C_8), 141.2 (C_{10}), 137.7 (C_{11a}), 137.3 (C_{6a}), 134.2 (C_{15a}), 132.7 (C_{2a}), 129.7 (C_2), 125.0 (C_5), 124.4 (C_{13}), 124.1 (C_4), 123.3 (C_6), 122.1 (C_{14}), 121.7 (C_{15}), 121.3 (C_{12}), 119.9 (C_3), 108.4 (C_1), 103.9 (C_{11}). HRMS [ESI^+] m/z: $[M+H]^+$ calcd for $C_{17}H_{12}N_2OS_2$ 325.0464, found 325.0464.

Compound 15

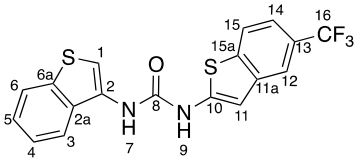

The α,β-bis(benzo[*b*]thiophene) urea **15** was produced by coupling of fluorinated α-benzo[*b*]thiophene isocyanate to a β-benzo[*b*]thiophene amine. The isocyanate was prepared from (5-trifluoromethyl)benzo[*b*]thiophene-2-carboxylic acid (0.100 g, 0.4 mmol), thionyl chloride (0.819 g, 6.9 mmol) and sodium azide (0.035 g, 0.53 mmol) following the experimental procedure reported for **14**. The isocyanate, obtained as yellow oil in quantitative yield, was added dropwise to THF solution of the benzo[*b*]thiophen-3-amine hydrochloride (0.100 g, 0.54 mmol) and DIPEA (0.074 g, 0.57 mmol) in THF (5 mL). After stirring the reaction mixture at r.t. for 1 h, under nitrogen atmosphere, **15** was isolated as a white powder with 17% of yield (0.037 g). Mp: 222.5-224.1°C. FTIR (KBr) ν_{max} cm^{-1}: 3310 (NH, stretch), 3260 (NH, stretch), 3090 (CH, stretch, Ar), 1640 (C=O, urea), 1580, 1550, 1480, 1430, 1340, 1270, 1110 (CF, stretch), 1080 (CF, stretch), 918, 897, 812, 789, 754, 725, 708, 629. ^{1}H NMR (400 MHz, DMSO-*d*$_6$, δ = ppm): 10.32 (s, 1H, H_9), 9.33 (s, 1H, H_7), 8.06 (d, $^{3}J_{H\text{-}H}$ = 8.3 Hz, 1H, H_6), 8.03-7.98 (m, 2H, H_{12}, H_{15}), 7.86 (d, $^{3}J_{H\text{-}H}$ = 7.7 Hz, 1H, H_3), 7.78 (s, 1H, H_1), 7.51 (t, $^{3}J_{H\text{-}H}$ = 7.6 Hz, 1H, H_4), 7.48-7.41 (m, 2H, H_5, H_{14}), 7.04 (s, 1H, H_{11}). ^{13}C APT NMR (101 MHz, DMSO-*d*$_6$, δ = ppm): 151.7 (C_8), 143.4 (C_{10}), 137.6 (C_{15a}, C_{6a}), 137.1 (C_{11a}), 132.6 (C_{2a}), 129.4 (C_2), 124.9 (q, $^{2}J_{C\text{-}F}$ = 31.6 Hz, C_{13}), 124.8 (C_5), 124.7 (q, $^{1}J_{C\text{-}F}$ = 272.1 Hz, C_{16}), 124.0 (C_4), 123.1 (C_{15}), 122.7 (C_6), 119.9 (C_3), 117.8 (q, $^{3}J_{C\text{-}F}$ = 4.1 Hz, C_{12}), 117.6 (q, $^{3}J_{C\text{-}F}$ = 3.5 Hz, C_{14}), 108.8 (C_1), 103.5 (C_{11}). HRMS [ESI^+] m/z: $[M+H]^+$ calcd for $C_{18}H_{11}F_3N_2OS_2$ 393.0338, found 393.0330.

Compound 16

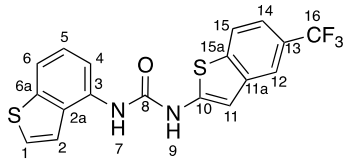

The α,γ-bis(benzo[*b*]thiophene) urea **16** was obtained by coupling of fluorinated α-benzo[*b*]thiophene isocyanate to a γ-benzo[*b*]thiophene amine. The isocyanate, prepared through the synthetic procedure followed for **15**, was added dropwise to a solution of the benzo[*b*]thiophene-4-amine (0.060 g, 0.40 mmol) in THF. The reaction mixture was stirred at r.t. for 1 h, under nitrogen atmosphere, and **16** precipitated as grey powder with 19% of yield (0.030 g). Mp: 230.5-231.6°C. FTIR (KBr) ν_{max} cm^{-1}: 3290 (NH, stretch), 3080 (CH, stretch, Ar), 1640 (C=O, urea), 1580, 1560, 1460, 1430, 1410, 1340, 1280, 1240, 1140, 1110 (CF, stretch), 1080 (CF, stretch), 916, 897, 818, 752, 729, 625. ^{1}H NMR (400 MHz, DMSO-d_6, δ = ppm): 10.38 (s, 1H, H_9), 9.05 (s, 1H, H_7), 8.05 (d, $^3J_{H\text{-}H}$ = 8.3 Hz, 1H, H_{15}), 8.02 (s, 1H, H_{12}), 7.92 (d, $^3J_{H\text{-}H}$ = 7.8 Hz, 1H, H_4), 7.81 (d, $^3J_{H\text{-}H}$ = 5.4 Hz, 1H, H_1), 7.73 (d, $^3J_{H\text{-}H}$ = 8.0 Hz, 1H, H_6), 7.57 (d, $^3J_{H\text{-}H}$ = 5.4 Hz, 1H, H_2), 7.44 (d, $^3J_{H\text{-}H}$ = 8.3 Hz, 1H, H_{14}), 7.36 (t, $^3J_{H\text{-}H}$ = 7.9 Hz, 1H, H_5), 7.03 (s, 1H, H_{11}). ^{13}C APT NMR (101 MHz, DMSO-d_6, δ = ppm): 151.8 (C_8), 143.6 (C_{10}), 140.1 (C_{6a}), 138.0 (C_{15a}), 137.7 (C_{11a}), 133.3 (C_3), 131.0 (C_{2a}), 126.9 (C_1), 125.3 (q, $^2J_{C\text{-}F}$ = 32.2 Hz, C_{13}), 125.0 (C_5), 124.9 (q, $^1J_{C\text{-}F}$ = 270.8 Hz, C_{16}), 122.8 (C_{15}), 114.6 (C_6), 120.2 (C_2), 118.0 (q, $^3J_{C\text{-}F}$ = 4.0 Hz, C_{12}), 117.8 (q, $^3J_{C\text{-}F}$ = 3.8 Hz, C_{14}), 117.5 (C_4), 103.6 (C_{11}). HRMS [ESI$^+$] m/z: [M+H]$^+$ calcd for $C_{18}H_{11}F_3N_2OS_2$ 393.0338, found 393.0324.

Compound 17

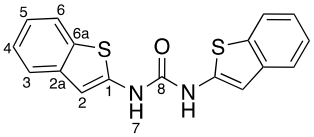

The α,α-bis(benzo[*b*]thiophene) urea **17** was directly obtained through the hydrolysis of α-benzo[*b*]thiophene isocyanate carried out overnight at r.t. The isocyanate was prepared from benzo[*b*]thiophene-2-carboxylic acid (0.1 g, 0.4 mmol), thionyl chloride (0.819 g, 6.9 mmol), and sodium azide (0.040 g, 0.61 mmol) following the synthetic pathway presented in Scheme S3. **17** precipitated in THF as a pink powder with 5.5% of yield (0.01 g). Mp: 252.3-253.7°C. FTIR (KBr) ν_{max} cm^{-1}: 3300 (NH, stretch), 3050 (CH, stretch, Ar), 1650 (C=O, urea), 1600, 1580, 1470, 1460, 1430, 1270, 1240, 1010, 935, 810, 741, 725, 669, 565. ^{1}H NMR (400 MHz, DMSO-d_6, δ = ppm): 10.24 (s, 2H, H_7), 7.81 (d, $^3J_{H\text{-}H}$ = 7.7 Hz, 2H, H_6), 7.63 (d, $^3J_{H\text{-}H}$ = 7.7 Hz, 2H, H_3), 7.29 (t, $^3J_{H\text{-}H}$ = 7.2 Hz, 2H, H_4), 7.18 (t, $^3J_{H\text{-}H}$ = 7.2 Hz, 2H, H_5), 6.91 (s, 2H, H_2). ^{13}C APT NMR (101 MHz, DMSO-d_6, δ = ppm): 150.9 (C_8), 141.0 (C_1), 137.7 (C_{2a}), 134.3 (C_{6a}), 124.4 (C_4), 122.3 (C_5), 121.8 (C_6), 121.5 (C_3), 105.0 (C_2). HRMS [ESI$^+$] m/z: [M+H]$^+$ calcd for $C_{17}H_{12}N_2OS_2$ 325.0464, found 325.0443.

Compound 18

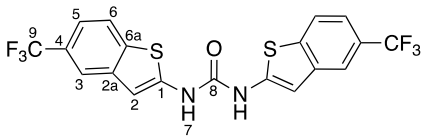

Likewise compound **17**, the symmetrical fluorinated analogue **18** was produced by coupling of 5-(trifluoromethyl)-benzo[*b*]thiophene-2-isocyanate and its corresponding amine generated *in situ* through the hydrolysis of the isocyanate. This highly reactive intermediate was prepared from (5-trifluoromethyl) benzo[*b*]thiophene-2-carboxylic acid (0.1 g, 0.4 mmol), thionyl chloride (0.819 g, 6.9 mmol), and sodium azide (0.040 g, 0.61 mmol) following Scheme S3.

18 was yielded as a pink powder in 5% yield (0.006 g). Mp: 242.9-244.0°C. FTIR (KBr) ν_{max} cm^{-1}: 3356 (NH, stretch), 3083 (CH, stretch, Ar), 1660 (C=O, urea), 1575, 1552, 1433, 1335, 1265, 1242, 1148, 1122 (CF, stretch), 1074 (CF, stretch), 918, 889, 818, 729. ^{1}H NMR (400 MHz, DMSO-*d*$_6$, δ = ppm): 10.62 (s, 2H, H_7), 8.16 - 8.00 (m, 4H, H_3 and H_6), 7.47 (d, $^3J_{H\text{-}H}$ = 8.4 Hz, 2H, H_5), 7.10 (s, 2H, H_2). ^{13}C APT NMR (101 MHz, DMSO-*d*$_6$, δ = ppm): 151.0 (C_8), 143.3 (C_1), 138.0 (C_{6a}), 137.6 (C_{2a}), 125.5 (q, $^2J_{C\text{-}F}$ = 31.4 HZ, C_4), 124.9 (q, $^1J_{C\text{-}F}$ = 271.9 HZ, C_9), 122.9 (C_6), 118.4 (q, $^3J_{C\text{-}F}$ = 4.1 HZ, C_3), 118.1 (q, $^3J_{C\text{-}F}$ = 3.2 HZ, C_5), 105.01 (C_2). HRMS [ESI$^+$] m/z: $[M+H]^+$ calcd for $C_{19}H_{10}F_6N_2OS_2$ 461.0212, found 461.019419.

Compound 19

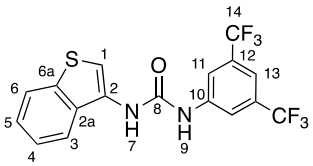

The β-benzo[*b*]thiophene isocyanate was prepared from benzo[*b*]thiophene-3-carboxylic following the synthetic pathway presented in Scheme S3 in the experimental conditions described for **1**. Subsequently, it was added dropwise a solution of 3,5-bis(trifluoromethyl)aniline (0.146 g, 0.63 mmol) in THF. The reaction mixture was stirred during 1 h at r.t., under nitrogen atmosphere. **19** was yielded as white powder in 64% yield (0.148 g). Mp: 238.4-239.7°C. FTIR (KBr) ν_{max} cm^{-1}: 3310 (NH, stretch), 3100 (CH, stretch, Ar), 1640 (C=O, urea), 1560, 1390, 1370, 1290, 1180 (CF, Strech) 1130 (CF, Strech), 893, 758, 725, 687, 619. ^{1}H NMR (400 MHz, DMSO-*d*$_6$, δ = ppm): 9.54 (s, 1H, H_9), 9.33 (s, 1H, H_7), 8.18 (s, 2H, H_{11}), 8.00 (d, $^3J_{H\text{-}H}$ = 7.8 Hz, 1H, H_6), 7.89 (d, $^3J_{H\text{-}H}$ = 7.7 Hz, 1H, H_3), 7.78 (s, 1H, H_{13}), 7.69 (s, 1H, H_1), 7.51 (t, $^3J_{H\text{-}H}$ = 7.2 Hz, 1H, H_4), 7.44 (t, $^3J_{H\text{-}H}$ = 7.2 Hz, 1H, H_5). ^{13}C APT RMN (101 MHz, DMSO-*d*$_6$, δ = ppm): 152.6 (C_8), 141.7 (C_{10}), 137.3 (C_{6a}), 132.9 (C_{2a}), 130.8 (q, $^2J_{C\text{-}F}$ = 32.8 Hz, C_{12}), 129.7 (C_2), 125.0 (C_5), 124.2 (C_4), 123.4 (q, $^1J_{C\text{-}F}$ = 273.9 Hz, C_{14}), 123.3 (C_6), 120.1 (C_3), 117.9 (C_{11}), 114.6 (C_{13}), 109.3 (C_1). HRMS [ESI$^+$] m/z: $[M+H]^+$ calcd for $C_{17}H_{10}F_6N_2OS$ 405.0491, found 405.0500.

Compound 20

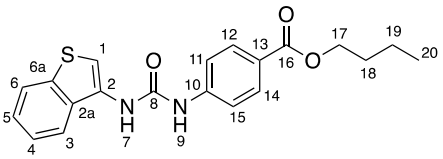

The β-benzo[*b*]thiophene isocyanate, prepared as described for **1**, was added dropwise to a solution of butyl 4-aminobenzoate in THF, previously yielded by quantitative catalytic hydrogenation of **C1** (0.080 g, 0.35 mmol) in ethanol with Pd/C (0.025 g). The reaction mixture was stirred for 1 h at r.t. and **20** was obtained as a white powder in 39% yield (0.067 g). Mp: 156.1-157.6°C. FTIR (KBr) ν_{max} cm^{-1}: 3381 (NH, stretch), 3354 (NH, stretch), 3134 (CH, stretch, Ar), 3068 (CH, stretch, Ar), 2960 (CH, stretch), 2872 (CH, stretch), 1714 (C=O, ester), 1668 (C=O, urea), 1601, 1533, 1514, 1458, 1385, 1298, 1292, 1261, 1205, 1184, 1143, 1122, 966, 852, 771, 752, 727, 642. ^{1}H NMR (400 MHz, DMSO-*d*$_6$, δ = ppm): 9.30 (s, 1H, H_9), 9.19 (s, 1H, H_7), 7.98 (d, $^3J_{H\text{-}H}$ =7.9 Hz, 1H, H_6), 7.95 - 7.88 (m, 3H, H_3, H_{12}, H_{14}), 7.75 (s, 1H, H_1), 7.66 (d, $^3J_{H\text{-}H}$ = 8.7 Hz, 2H, H_{11}, H_{15}), 7.49 (t, $^3J_{H\text{-}H}$ = 7.5 Hz, 1H, H_4), 7.42 (t, $^3J_{H\text{-}H}$ = 7.5 Hz, 1H, H_5), 4.24 (t, $^3J_{H\text{-}H}$ = 6.4 Hz, 2H, H_{17}), 1.68 (quintet, $^3J_{H\text{-}H}$ = 6.9 Hz, 2H, H_{18}), 1.42 (sextet, $^3J_{H\text{-}H}$ = 7.4 Hz, 2H, H_{19}), 0.94 (t, $^3J_{H\text{-}H}$ = 7.2 Hz, 3H, H_{20}). ^{13}C APT NMR (101 MHz, DMSO-*d*$_6$, δ = ppm): 165.5 (C_{16}), 152.4 (C_8), 144.4 (C_{10}), 137.2 (C_{6a}), 132.8 (C_{2a}), 130.5 (C_{12}, C_{14}), 130.1 (C_2), 124.9 (C_5), 124.1 (C_4), 123.2 (C_6), 122.8 (C_{13}), 120.1 (C_3), 117.3 (C_{11}, C_{15}), 107.8

(C_1), 64.0 (C_{17}), 30.4 (C_{18}), 18.8 (C_{19}), 13.7 (C_{20}). HRMS [ESI$^+$] m/z: [M+H]$^+$ calcd for $C_{20}H_{20}N_2O_3S$ 369.1267, found 369.1269.

Compound 21

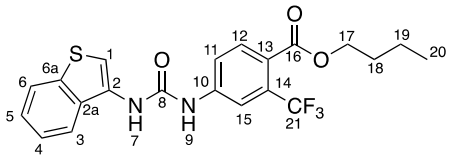

The β-benzo[*b*]thiophene isocyanate (*vide supra*), was added dropwise to a solution of butyl 4-amino-2-(trifluoromethyl)benzoate in THF, previously produced by quantitative catalytic hydrogenation of **C2** (0.050 g, 0.17 mmol) in ethanol with Pd/C (0.030 g). The reaction mixture was stirred for 1 h at r.t. and **21** was obtained as a white powder in 48% yield (0.100 g). Mp: 145.6-146.5°C. FTIR (KBr) ν_{max} cm^{-1}: 3404 (NH, stretch), 3354 (NH, stretch), 3305 (CH, stretch, Ar), 3132 (CH, stretch, Ar), 2958 (CH, stretch), 2872 (CH, stretch), 1726 (C=O, ester), 1674 (C=O, urea), 1595 1549, 1460, 1429, 1394, 1356, 1323, 1248, 1215, 1148, 1128 (CF, stretch), 1043 (CF, stretch), 895, 752, 727, 685. ^{1}H NMR (400 MHz, DMSO-d_6, δ = ppm): 9.51 (s, 1H, H_9), 9.25 (s, 1H, H_7), 8.19 (s, 1H, H_{15}), 7.99 (d, $^3J_{H\text{-}H}$ = 7.9 Hz, 1H, H_6), 7.87 (d, $^3J_{H\text{-}H}$ = 8.4 Hz, 2H, H_3, H_{12}), 7.77 (s, 1H, H_1), 7.73 (d, $^3J_{H\text{-}H}$ = 8.6 Hz, 1H, H_{11}), 7.50 (t, $^3J_{H\text{-}H}$ = 7.4 Hz, 1H, H_4), 7.43 (t, $^3J_{H\text{-}H}$ = 7.4 Hz, 1H, H_5), 4.26 (t, $^3J_{H\text{-}H}$ = 6.4 Hz, 2H, H_{17}), 1.67 (quintet, $^3J_{H\text{-}H}$ = 7.0 Hz, 2H, H_{18}), 1.40 (sextet, $^3J_{H\text{-}H}$ = 7.4 Hz, 2H, H_{19}), 0.92 (t, $^3J_{H\text{-}H}$ = 7.2 Hz, 3H, H_{20}). ^{13}C APT NMR (101 MHz, DMSO-d_6, δ = ppm): 165.5 (C_{16}), 152.3 (C_8), 143.0 (C_{10}), 137.3 (C_{6a}), 132.8 (C_{2a}), 132.2 (C_{12}), 129.7 (C_2), 128.4 (q, $^2J_{C\text{-}F}$ = 31.5 Hz, C_{14}), 125.0 (C_5), 124.2 (C_4), 123.4 (q, $^1J_{C\text{-}F}$ = 273.8 Hz, C_{21}), 123.3 (C_6), 122.9 (C_{13}), 120.5 (C_{11}), 120.0 (C_3), 115.3 (q, $^3J_{C\text{-}F}$ = 5.4 Hz, C_{15}), 108.7 (C_1), 65.1 (C_{17}), 30.1 (C_{18}), 18.7(C_{19}), 13.6 (C_{20}). HRMS [ESI$^+$] m/z: [M+H]$^+$ calcd for $C_{21}H_{19}F_3N_2O_3S$ 437.1141, found 437.1141.

Compound 22

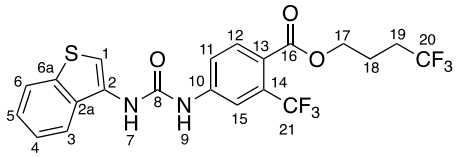

The β-benzo[*b*]thiophene isocyanate (*vide supra*), was added dropwise to a solution of 4,4,4-trifluorobutyl 4-amino-2-(trifluoromethyl)benzoate in THF, previously produced by quantitative catalytic hydrogenation of **C3** (0.130 g, 0.14 mmol) in ethanol with Pd/C (0.030 g). The reaction mixture was stirred for 1 h at r.t. and **22** was obtained as a white powder in 21% yield (0.060 g). Mp: 208.4-209.9°C. FTIR (KBr) ν_{max} cm^{-1}: 3402 (NH, stretch), 3350 (NH, stretch), 3305 (CH, stretch, Ar), 3128 (CH, stretch, Ar), 2964 (CH, stretch), 2895 (CH, stretch), 1726 (C=O, ester), 1682 (C=O, urea), 1595, 1545, 1462, 1427, 1389, 1340, 1311, 1261, 1215, 1175, 1128 (CF, stretch), 1043 (CF, stretch), 1005 (CF, stretch), 893, 756, 731, 663. ^{1}H NMR (400 MHz, DMSO-d_6, δ = ppm): 9.56 (s, 1H, H_9), 9.28 (s, 1H, H_7), 8.21 (s, 1H, H_{15}), 8.00 (d, $^3J_{H\text{-}H}$ = 7.9 Hz, 1H, H_6), 7.93 (d, $^3J_{H\text{-}H}$ = 8.5 Hz, 1H, H_{12}), 7.88 (d, $^3J_{H\text{-}H}$ = 8.0 Hz, 1H, H_3), 7.79 (s, 1H, H_1), 7.75 (d, $^3J_{H\text{-}H}$ = 8.5 Hz, 1H, H_{11}), 7.51 (t, $^3J_{H\text{-}H}$ = 7.5 Hz, 1H, H_4), 7.44 (t, $^3J_{H\text{-}H}$ = 7.4 Hz, 1H, H_5), 4.33 (t, $^3J_{H\text{-}H}$ = 6.2 Hz, 2H, H_{17}), 2.45 - 2.35 (m, 2H, H_{19}), 1.94 (quintet, $^3J_{H\text{-}H}$ = 6.7 Hz, 2H, H_{18}). ^{13}C APT NMR (101 MHz, DMSO-d_6, δ = ppm): 165.1 (C_{16}), 152.2 (C_8), 143.1 (C_{10}), 137.1 (C_{6a}), 132.6 (C_{2a}), 132.4 (C_{12}), 129.5 (C_2), 128.3 (q, $^2J_{C\text{-}F}$ = 31.6 Hz, C_{14}), 127.4 (q, $^1J_{C\text{-}F}$ = 278 Hz, C_{20}), 124.8 (C_5), 124.0 (C_4), 123.2 (q, $^1J_{C\text{-}F}$ = 273.3 Hz, C_{21}), 123.1 (C_6), 122.2 (C_{13}), 120.4 (C_{11}), 119.8 (C_3), 115.2 (q, $^3J_{C\text{-}F}$ = 6.0 Hz, C_{15}), 108.6 (C_1), 63.7 (C_{17}), 29.3 (q, $^2J_{C\text{-}F}$ 28.4 Hz, C_{19}), 20.9 (q, $^3J_{C\text{-}F}$ = 3.2 Hz, C_{18}). HRMS [ESI$^+$] m/z: [M+H]$^+$ calcd for $C_{21}H_{16}F_6N_2O_3S$ 491.0859, found 491.0842.

Compound 23

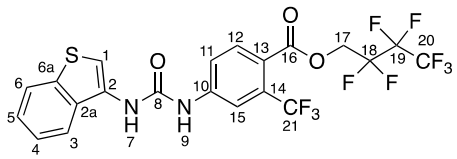

The β-benzo[*b*]thiophene isocyanate (*vide supra*), was added dropwise to a solution of 2,2,3,3,4,4,4-heptafluorobutyl 4-amino-2-(trifluoromethyl)benzoate in THF, previously produced by quantitative catalytic hydrogenation of **C4** (0.176 g, 0.42 mmol) in ethanol with Pd/C (0.030 g). The reaction mixture was stirred for 1 h at r.t. and **23** was obtained as a white powder in 29% yield (0.093 g). Mp: 110.5-112.1°C. FTIR (KBr) υ_{max} cm^{-1}: 3570 (NH, stretch), 3490 (NH, stretch), 3350 (CH, stretch, Ar), 2980 (CH, stretch), 1730 (C=O, ester), 1700 (C=O, urea), 1600, 1560, 1460, 1430, 1400, 1330, 1300, 1270, 1230, 1170 (CF, stretch), 1140 (CF, stretch), 1120 (CF, stretch), 910, 877, 754, 727. ^{1}H NMR (400 MHz, DMSO-*d*$_6$, δ = ppm): 9.64 (s, 1H, H$_9$), 9.31 (s, 1H, H$_7$), 8.28 (s, 1H, H$_{15}$), 8.00 (d, $^{3}J_{H\text{-}H}$ = 7.9 Hz, 1H, H$_6$), 7.96 (d, $^{3}J_{H\text{-}H}$ = 8.6 Hz, 1H, H$_{12}$), 7.88 (d, $^{3}J_{H\text{-}H}$ = 7.8 Hz, 1H, H$_3$), 7.83 - 7.74 (m, 2H, H$_1$, H$_{11}$), 7.51 (t, $^{3}J_{H\text{-}H}$ = 7.4 Hz, 1H, H$_4$), 7.44 (t, $^{3}J_{H\text{-}H}$ = 7.4 Hz, 1H, H$_5$), 5.13 (t, $^{3}J_{H\text{-}H}$ = 14.2 Hz, 2H, H$_{17}$). ^{13}C APT NMR (101 MHz, DMSO-*d*$_6$, δ = ppm): 163.1 (C$_{16}$), 152.1 (C$_8$), 144.0 (C$_{10}$), 137.1 (C$_{6a}$), 132.8 (C$_{12}$), 132.6 (C$_{2a}$), 129.4 (C$_2$), 129.1 (q, $^{2}J_{C\text{-}F}$ = 35.5 Hz, C$_{14}$), 124.9 (C$_5$), 124.0 (C$_4$), 123.5 (C$_{13}$), 123.1 (C$_6$), 123.0 (q, $^{1}J_{C\text{-}F}$ = 272.8 Hz, C$_{21}$), 120.3 (C$_{11}$), 119.8 (C$_3$), 115.6 (q, $^{3}J_{C\text{-}F}$ = 6.3 Hz, C$_{15}$), 108.8 (C$_1$), 59.6 (t, $^{2}J_{C\text{-}F}$ = 26.6 Hz, C$_{17}$). HRMS [ESI$^+$] m/z: [M+H]$^+$ calcd for $C_{21}H_{12}F_{10}N_2O_3S$ 563.0482, found 563.0494.

Compound 24

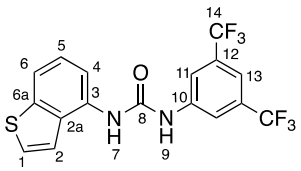

The γ-benzo[*b*]thiophene isocyanate was prepared from benzo[*b*]thiophene-4-carboxylic accordingly the synthetic pathway presented in Scheme S3 and using the experimental conditions described for **11**. Then, it was added dropwise a solution of 3,5-bis(trifluoromethyl)aniline (0.146 g, 0.63 mmol) in THF. The reaction mixture was stirred during 1 h at r.t., under nitrogen atmosphere and **24** was produced as white powder in 4% yield (0.012 g). Mp: 212.7-213.8°C. FTIR (KBr) υ_{max} cm^{-1}: 3300 (NH, stretch), 3008 (CH, stretch, Ar), 1650 (C=O, urea), 1560, 1380, 1280, 1180 (CF, stretch), 1130 (CF, stretch), 899, 758, 685. ^{1}H NMR (400 MHz, DMSO-*d*$_6$, δ = ppm): 9.62 (s, 1H, H$_9$), 9.06 (s, 1H, H$_7$), 8.16 (s, 2H, H$_{11}$), 7.87 (d, $^{3}J_{H\text{-}H}$ = 7.8 Hz, 1H, H$_4$), 7.81 (d, $^{3}J_{H\text{-}H}$ = 5.4 Hz, 1H, H$_1$), 7.73 (d, $^{3}J_{H\text{-}H}$ = 7.8 Hz, 1H, H$_6$), 7.68 (brs, 1H, H$_{13}$), 7.58 (d, $^{3}J_{H\text{-}H}$ = 5.3 Hz, 1H, H$_2$), 7.35 (t, $^{3}J_{H\text{-}H}$ = 7.8 Hz, 1H, H$_5$).^{13}C APT NMR (101 MHz, DMSO-*d*$_6$, δ = ppm): 152.6 (C$_8$), 141.8 (C$_{10}$), 140.0 (C$_{6a}$), 133.4 (C$_3$), 131.5 (C$_{2a}$), 130.9 (q, $^{2}J_{C\text{-}F}$ = 30.4 Hz, C$_{12}$), 126.8 (C$_1$), 124.9 (C$_5$), 123.4 (q, $^{1}J_{C\text{-}F}$ = 273.58 Hz, C$_{14}$), 121.4 (C$_2$), 117.9 (q, $^{3}J_{C\text{-}F}$ = 3.9 Hz, C$_{11}$), 117.6 (C$_6$), 114.3 (q, $^{3}J_{C\text{-}F}$ = 3.4 Hz, C$_{13}$), 114.0 (C$_4$). HRMS [ESI$^+$] m/z: [M+H]$^+$ calcd for $C_{17}H_{10}F_6N_2OS$ 405.0491, found 405.0491.

^{1}H and ^{13}C NMR spectra

Alkyl aryl ester intermediates

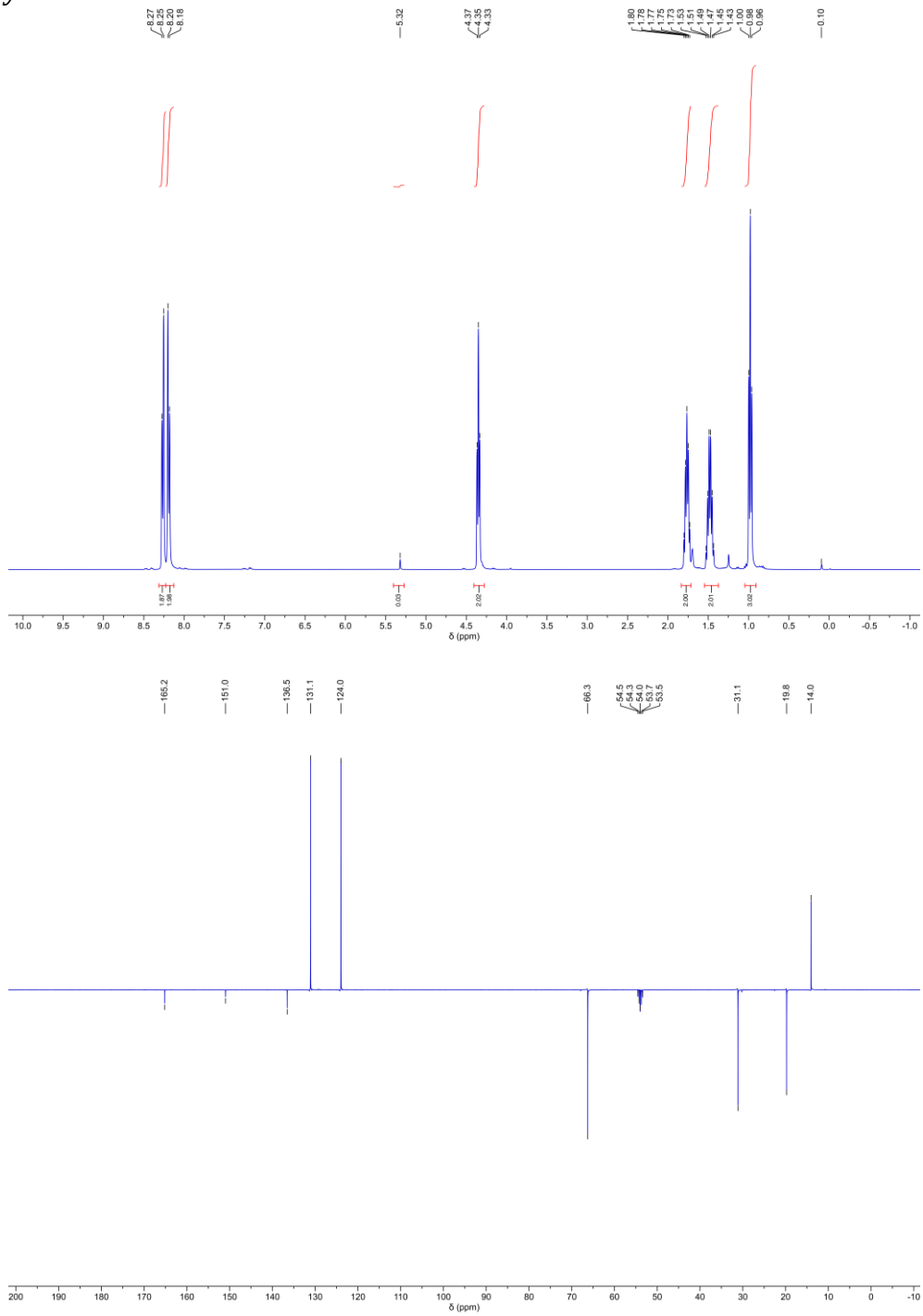

Figure S1. ^{1}H NMR (top) and ^{13}C APT NMR (bottom) spectra of **C1** in CD_2Cl_2 at 293 K.

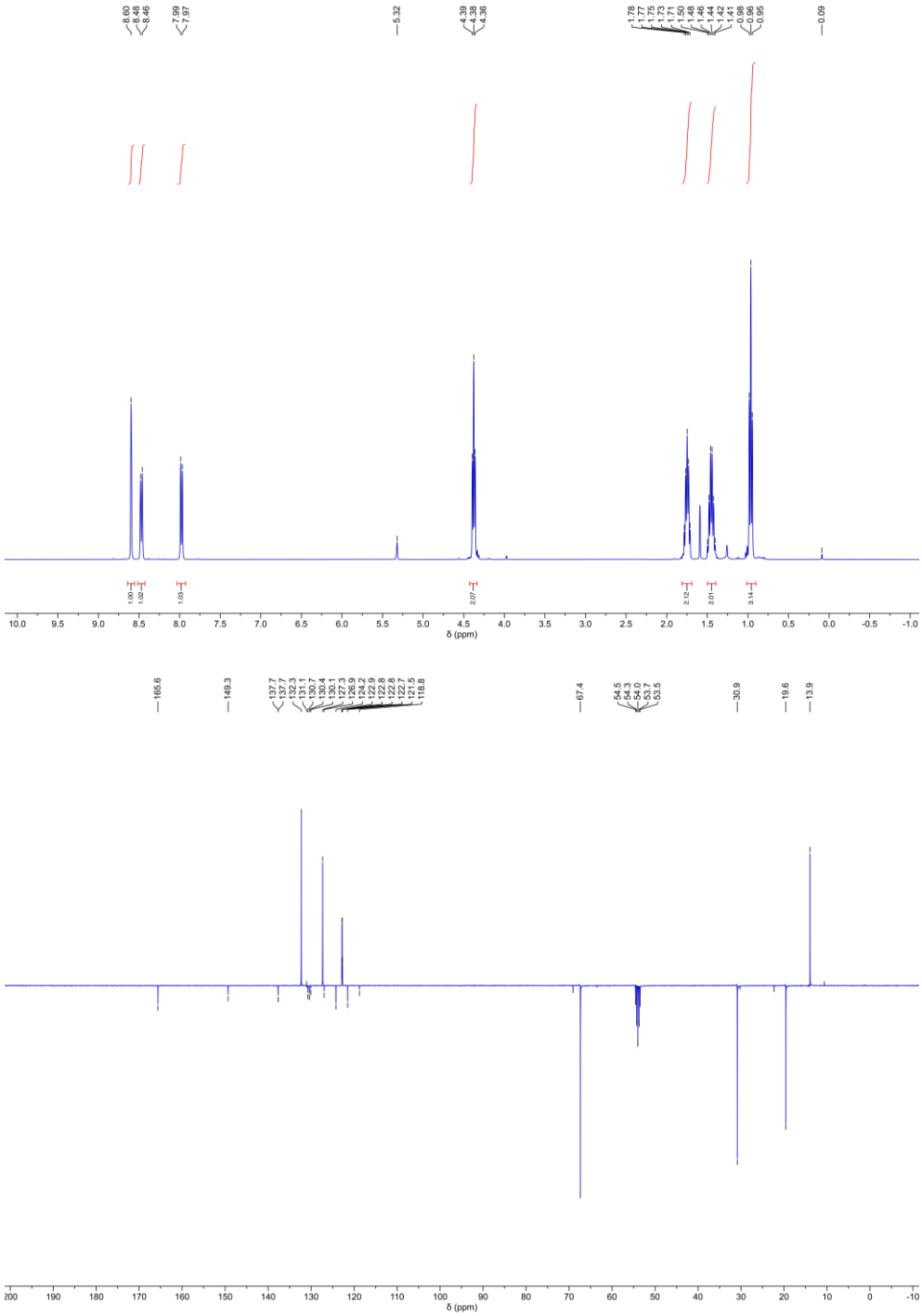

Figure S2. ^{1}H NMR (top) and ^{13}C APT NMR (bottom) spectra of **C2** in CD_2Cl_2 at 293 K.

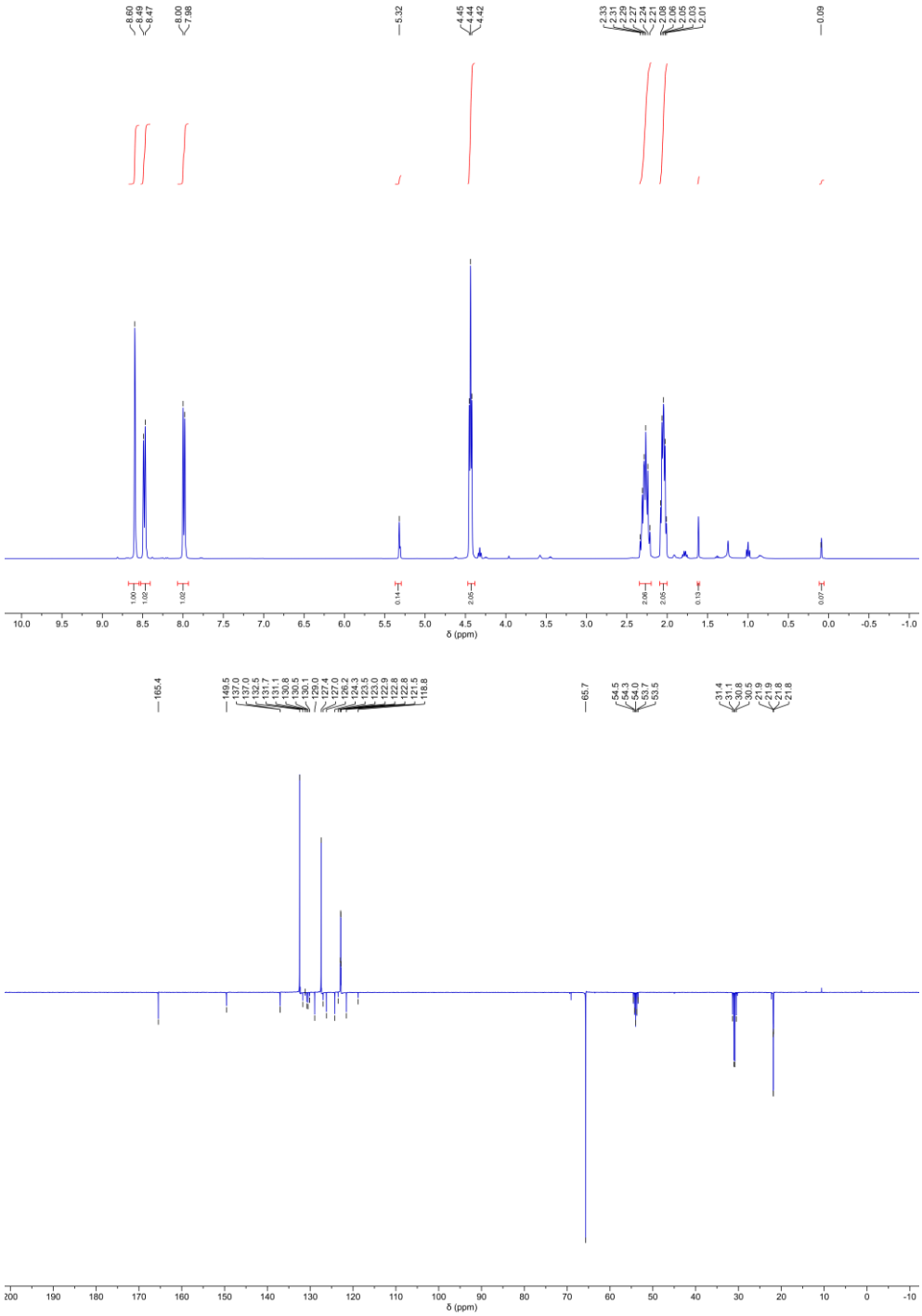

Figure S3. ^{1}H NMR (top) and ^{13}C APT NMR (bottom) spectra of **C3** in CD_2Cl_2 at 293 K.

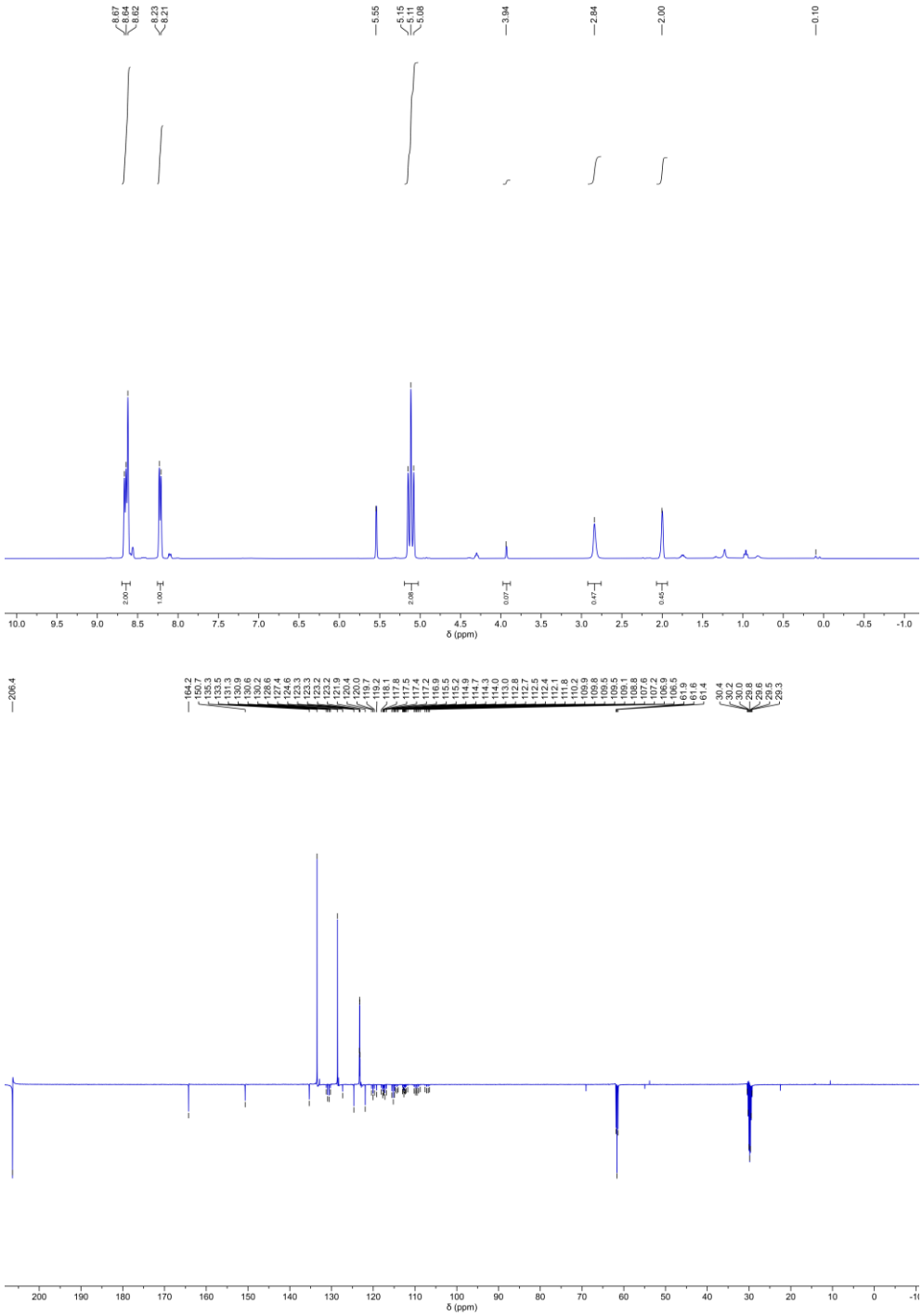

Figure S4. ^{1}H NMR (top) and ^{13}C APT NMR (bottom) spectra of **C4** in CD_6CO at 293 K.

Benzo[b]thiophene based (thio)ureas

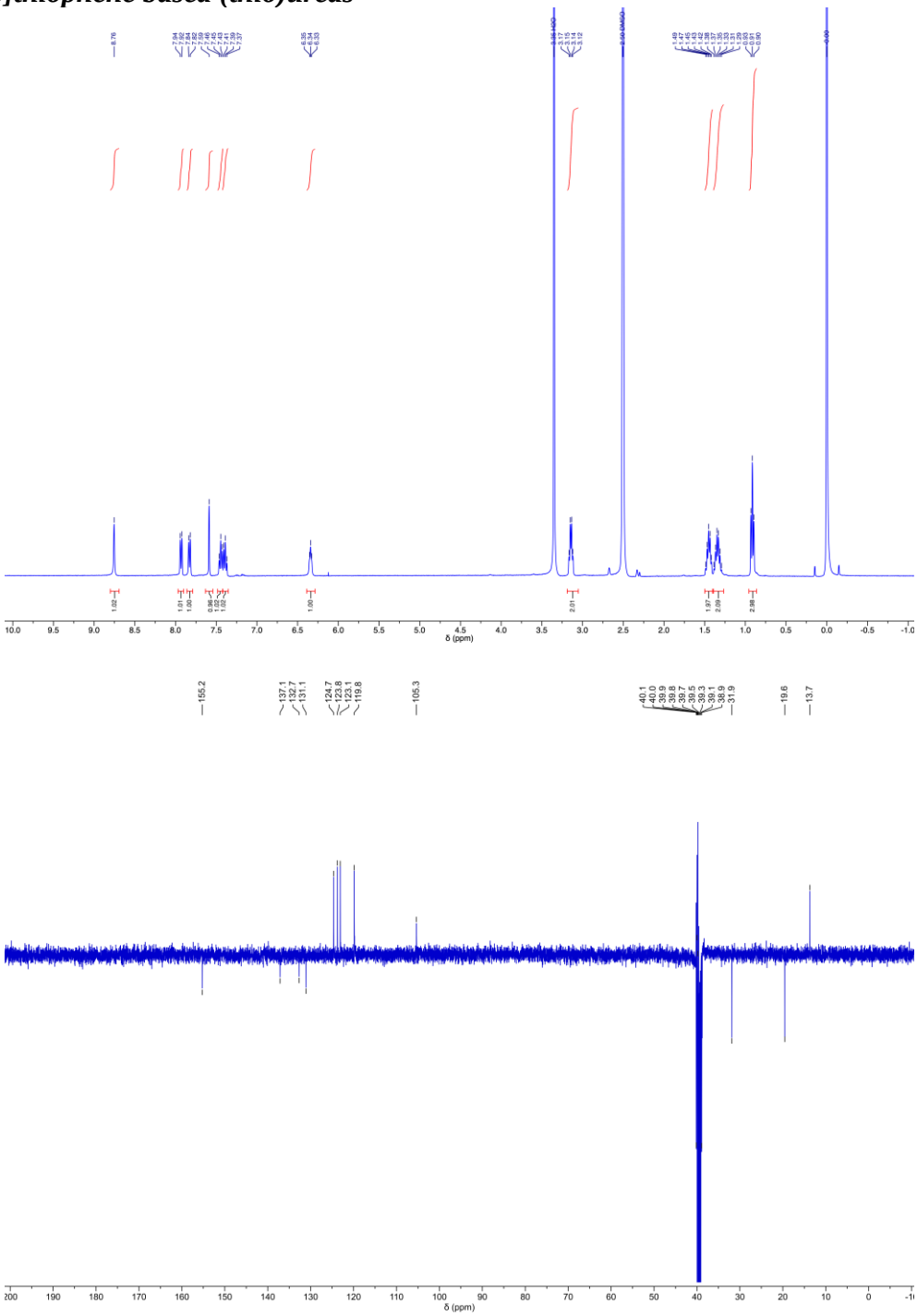

Figure S5. ^{1}H NMR (top) and ^{13}C APT NMR (bottom) spectra of **1** in DMSO-d_6 at 293 K.

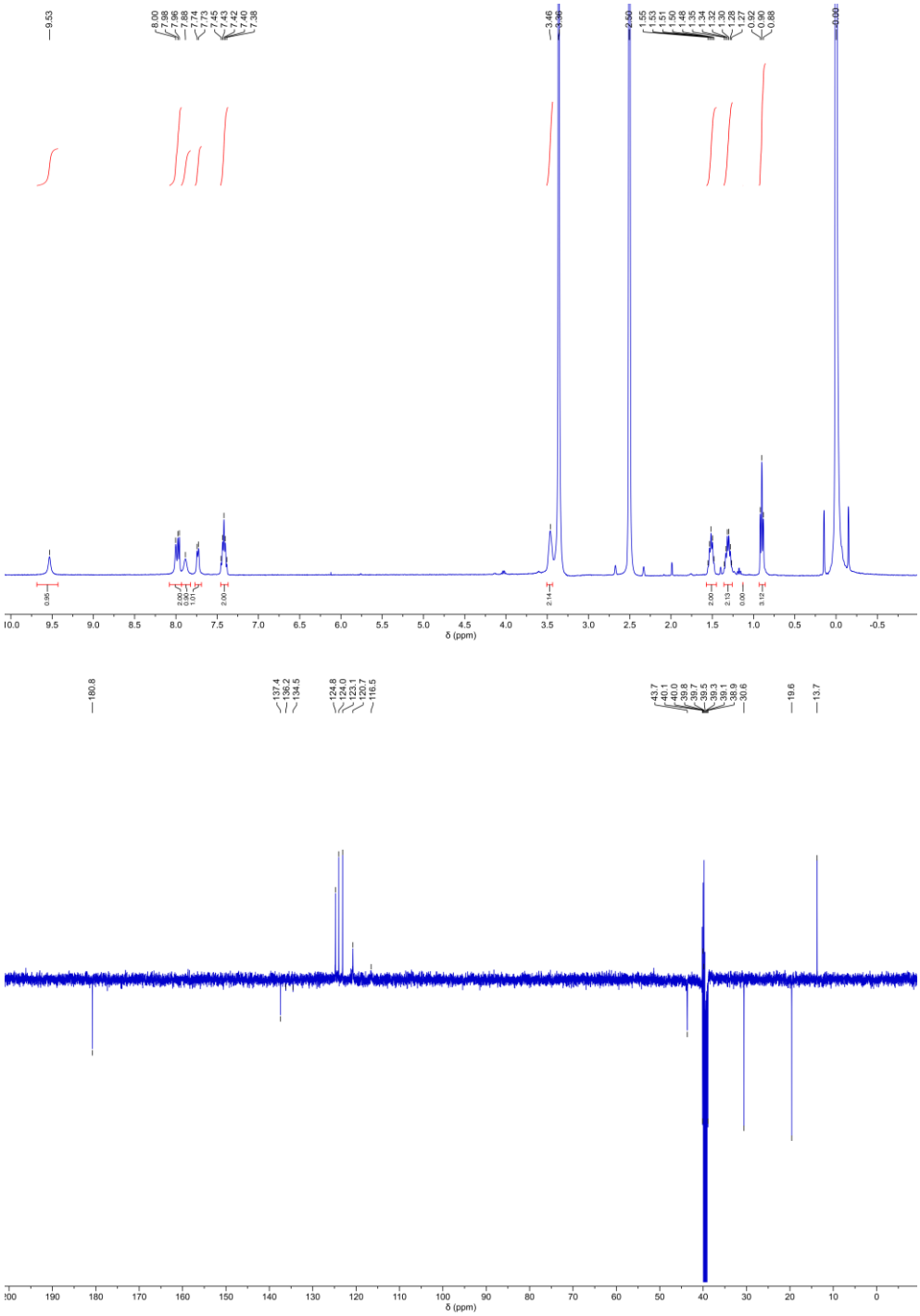

Figure S6. ^{1}H NMR (top) and ^{13}C APT NMR (bottom) spectra of **2** in DMSO-d_6 at 293 K.

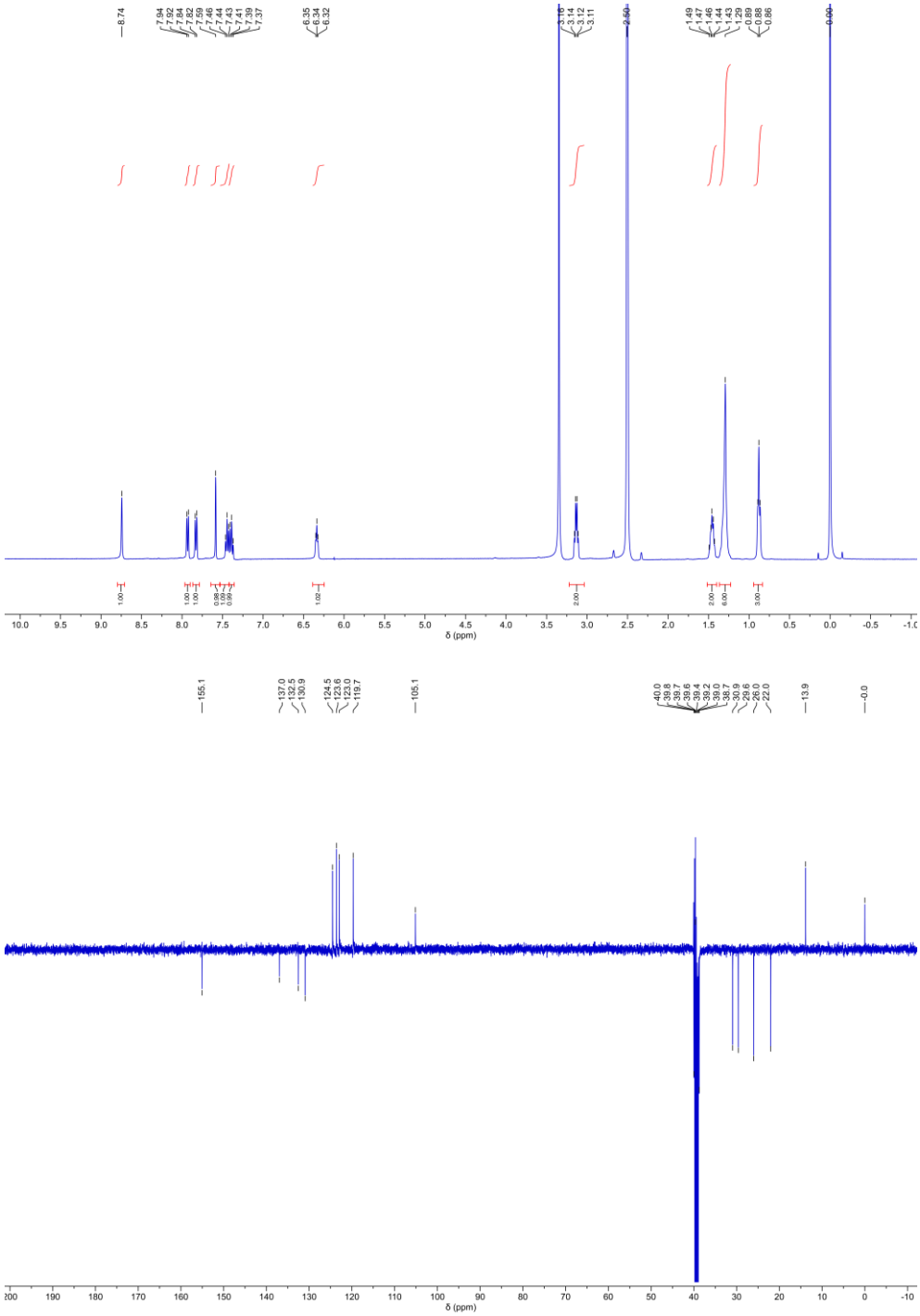

Figure S7. ^{1}H NMR (top) and ^{13}C APT NMR (bottom) spectra of **3** in DMSO-d_6 at 293 K.

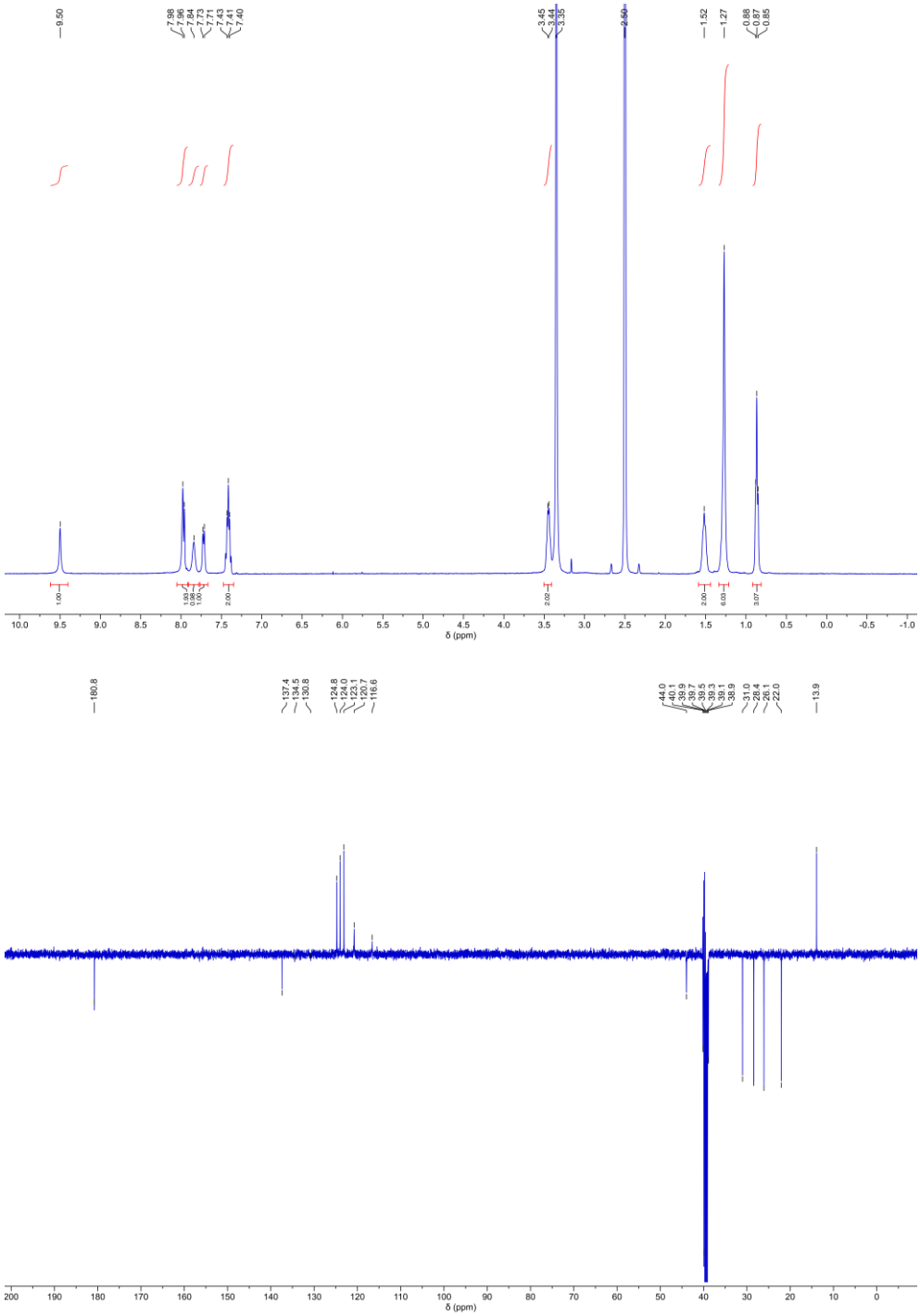

Figure S8. ^{1}H NMR (top) and ^{13}C APT NMR (bottom) spectra of **4** in DMSO-d_6 at 293 K.

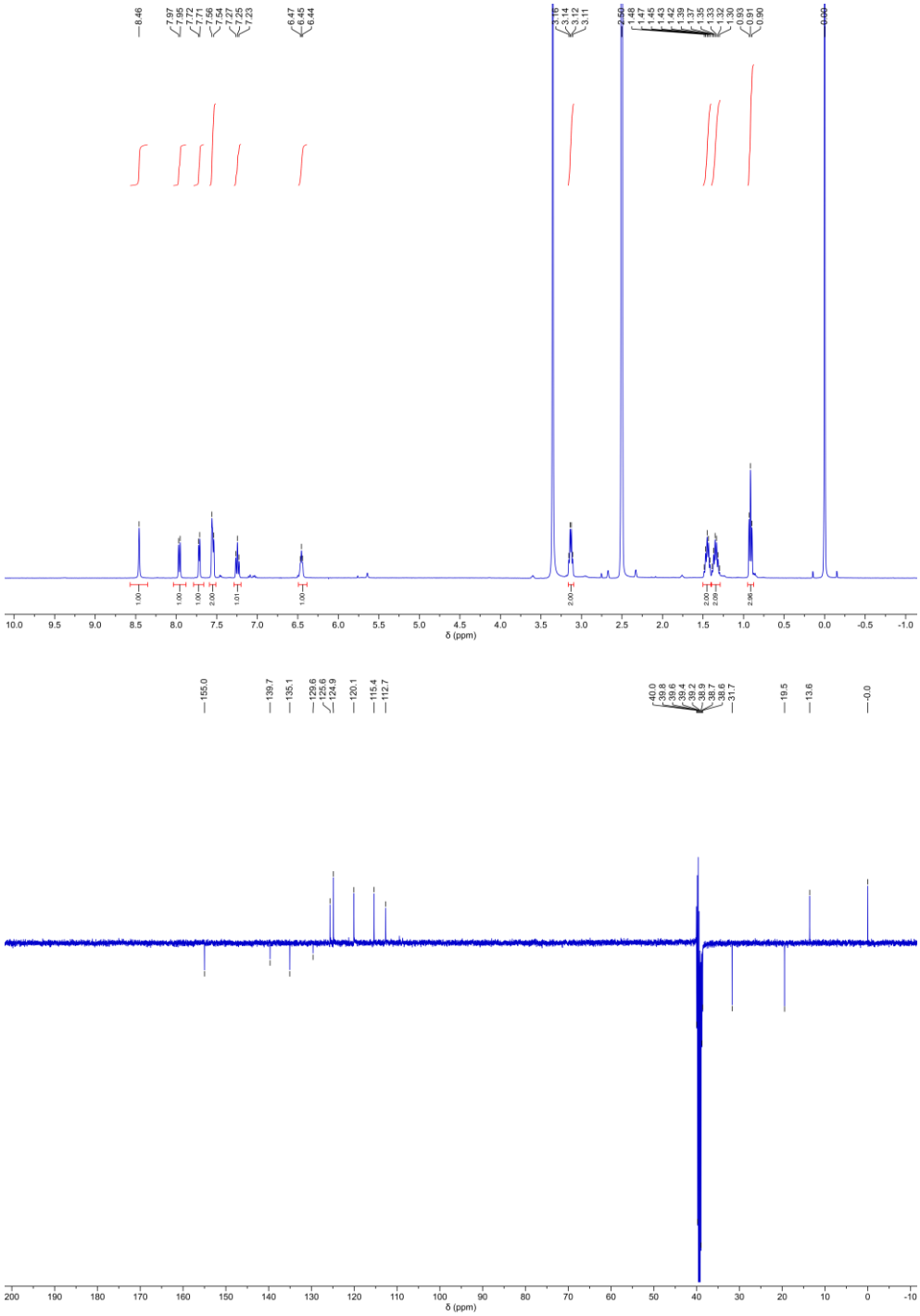

Figure S9. ^{1}H NMR (top) and ^{13}C APT NMR (bottom) spectra of **5** in DMSO-d_6 at 293 K.

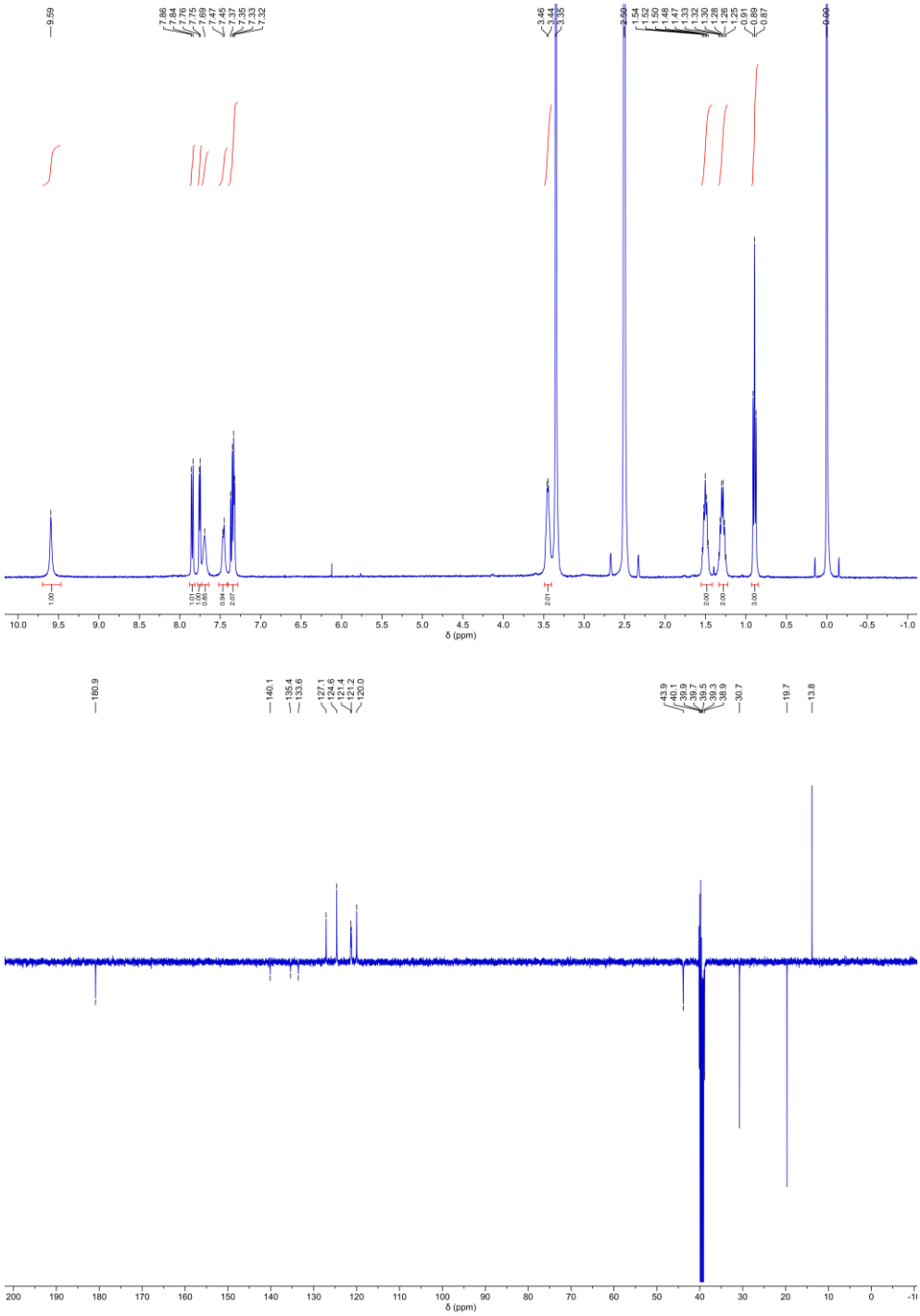

Figure S10. ^{1}H NMR (top) and ^{13}C APT NMR (bottom) spectra of **6** in DMSO-d_6 at 293 K.

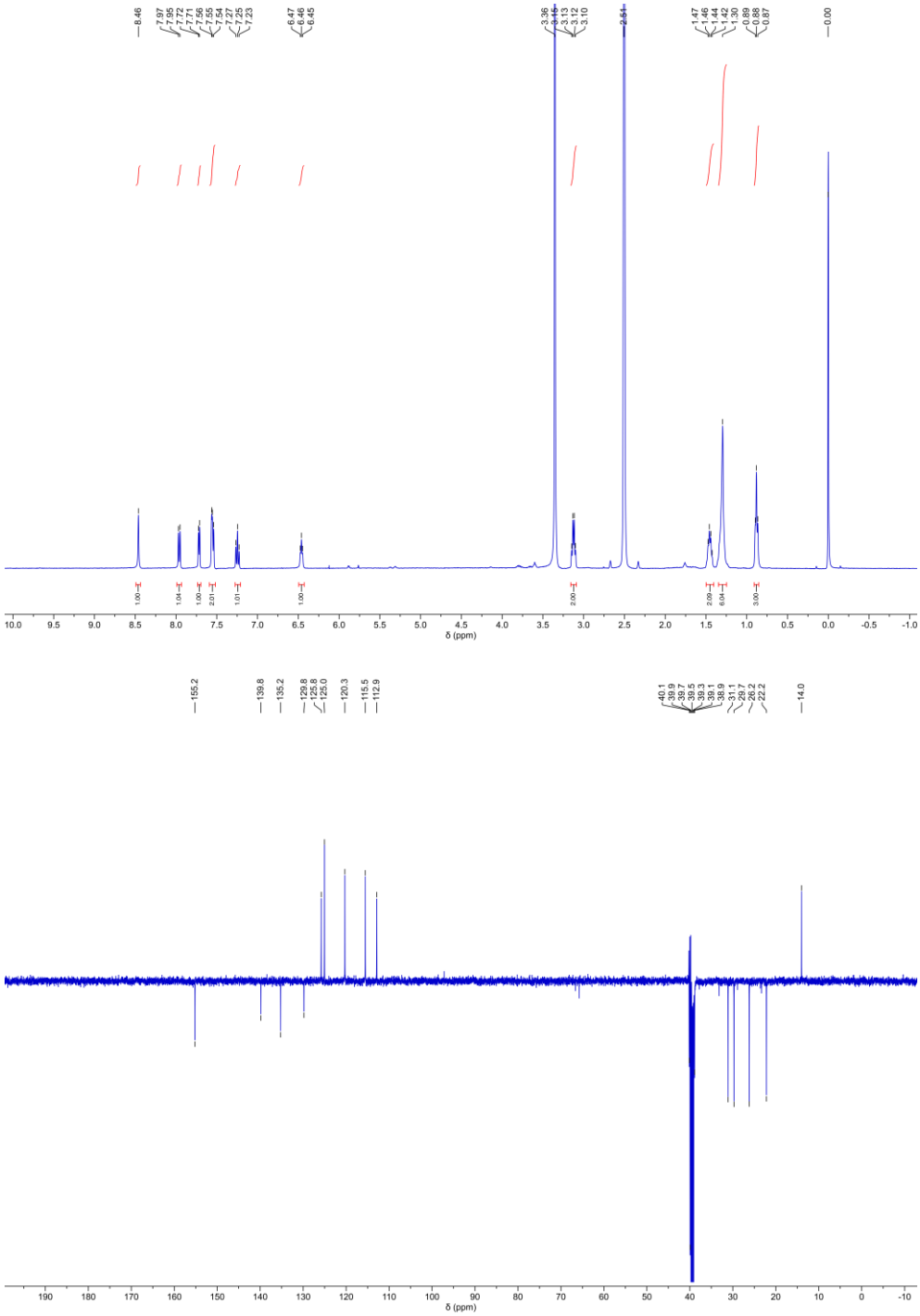

Figure S11. ^{1}H NMR (top) and ^{13}C APT NMR (bottom) spectra of **7** in DMSO-*d*$_6$ at 293 K.

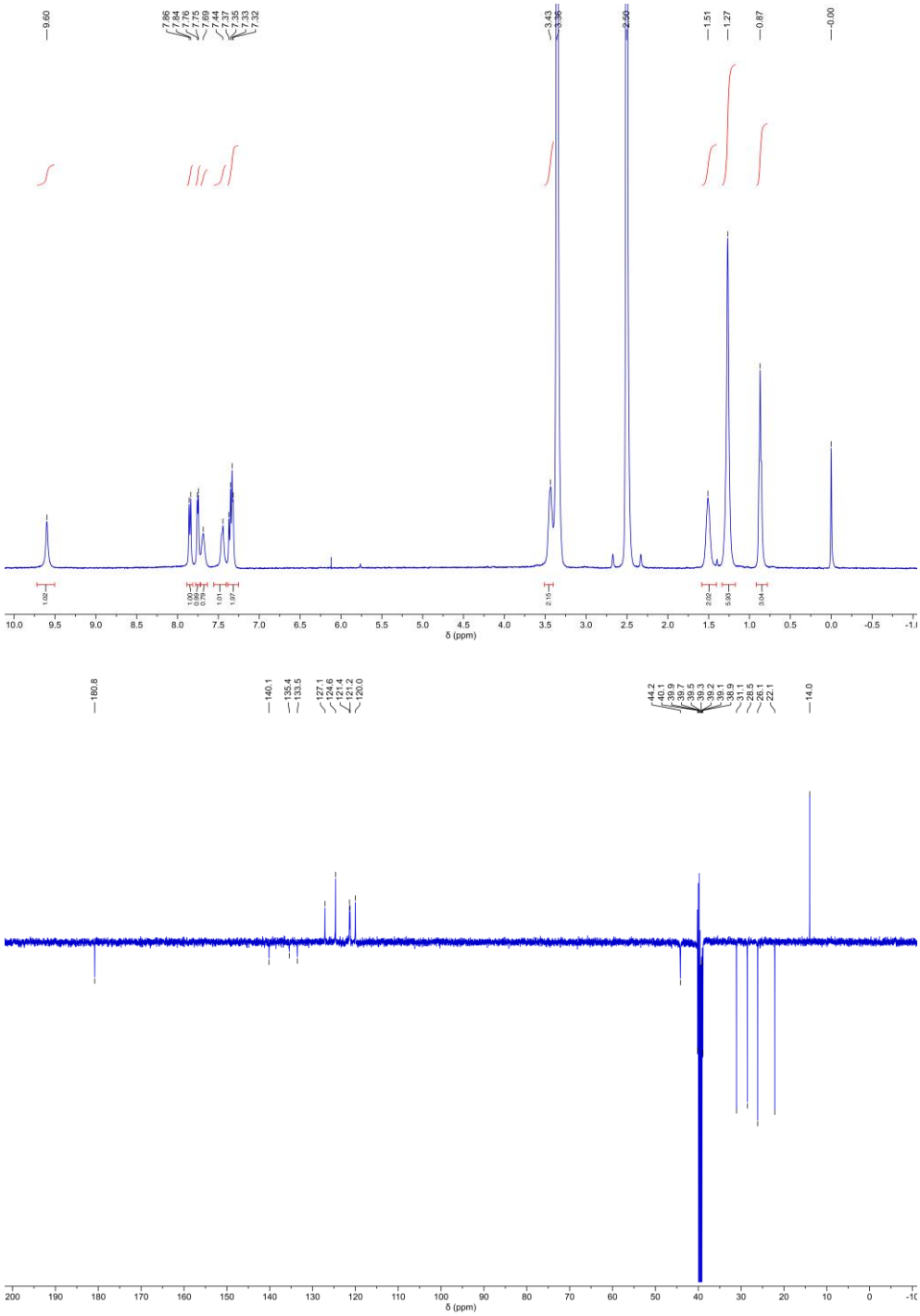

Figure S12. ^{1}H NMR (top) and ^{13}C APT NMR (bottom) spectra of **8** in DMSO-*d*$_6$ at 293 K.

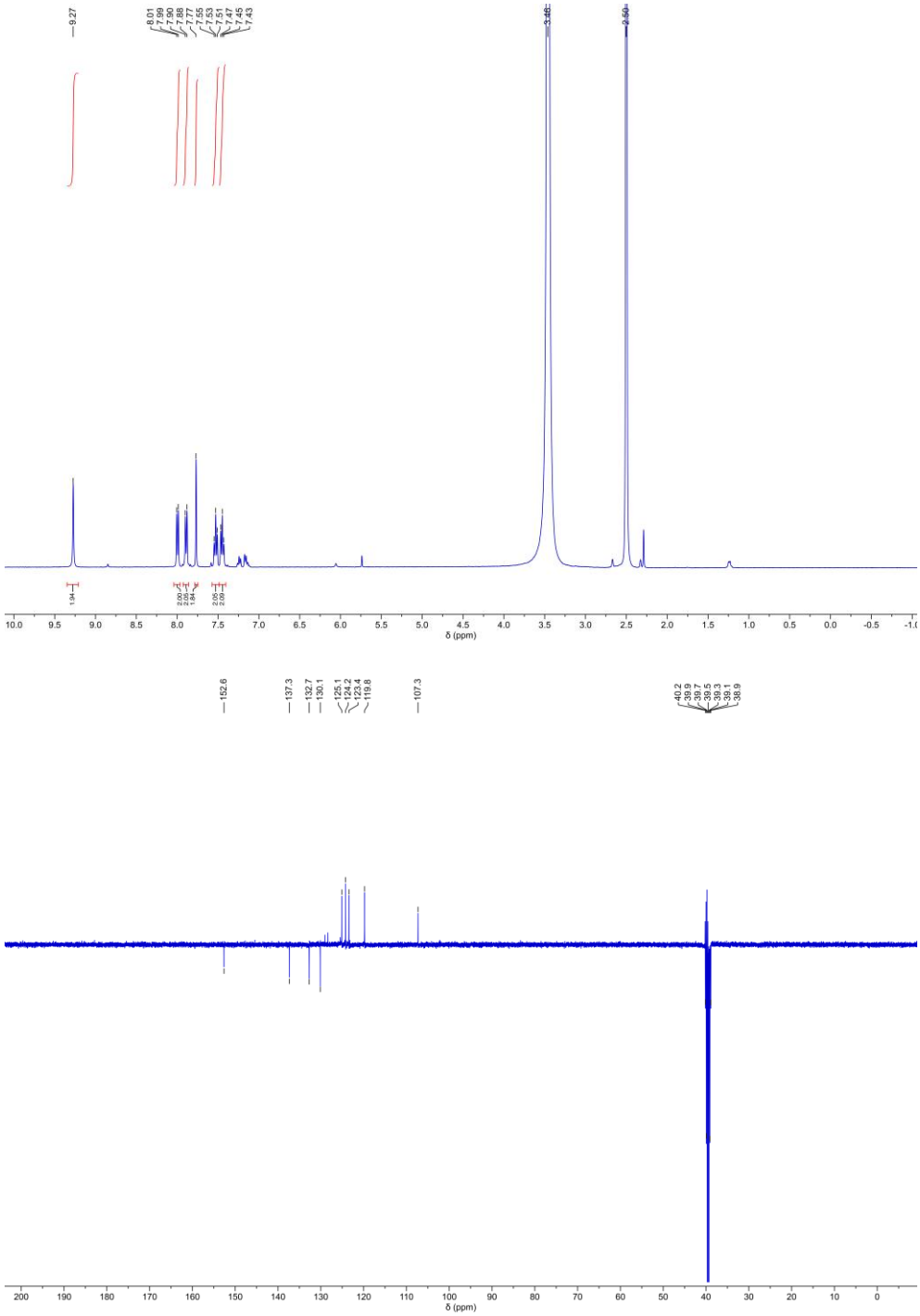

Figure S13. ^{1}H NMR (top) and ^{13}C APT NMR (bottom) spectra of **9** in DMSO-*d*$_6$ at 293 K.

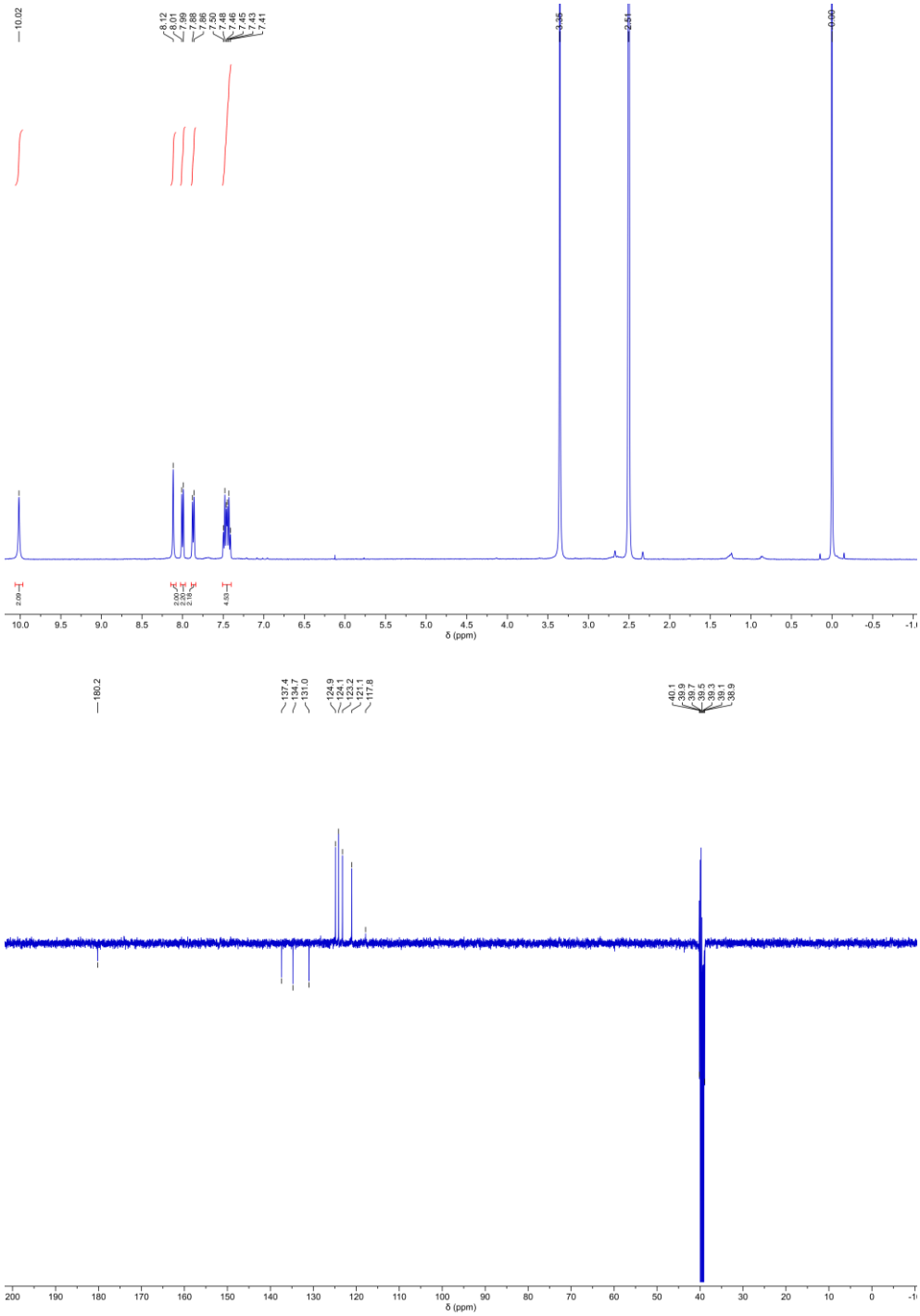

Figure S14. ^{1}H NMR (top) and ^{13}C APT NMR (bottom) spectra of **10** in DMSO-d_6 at 293 K.

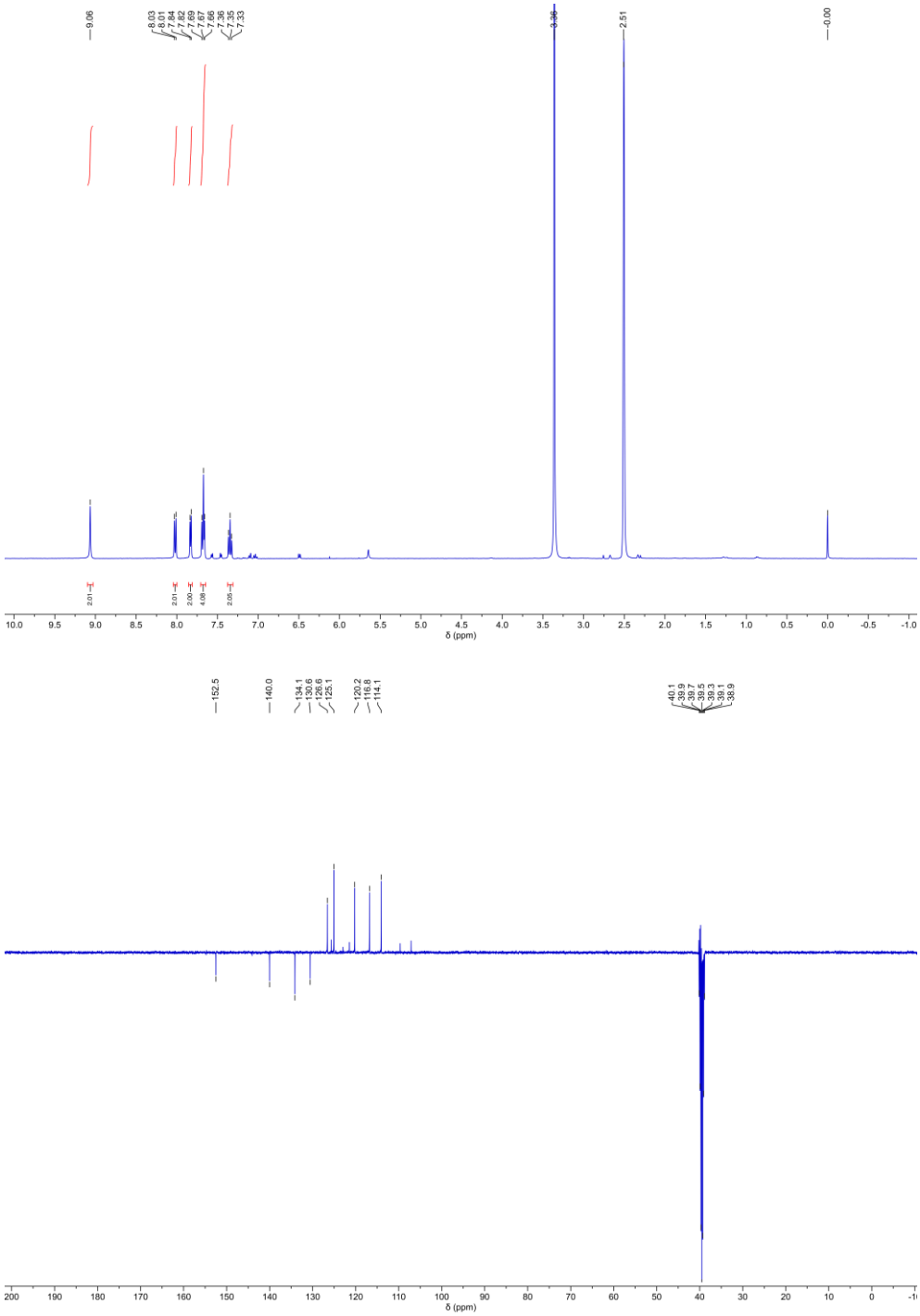

Figure S15. ^{1}H NMR (top) and ^{13}C APT NMR (bottom) spectra of **11** in DMSO-d_6 at 293 K.

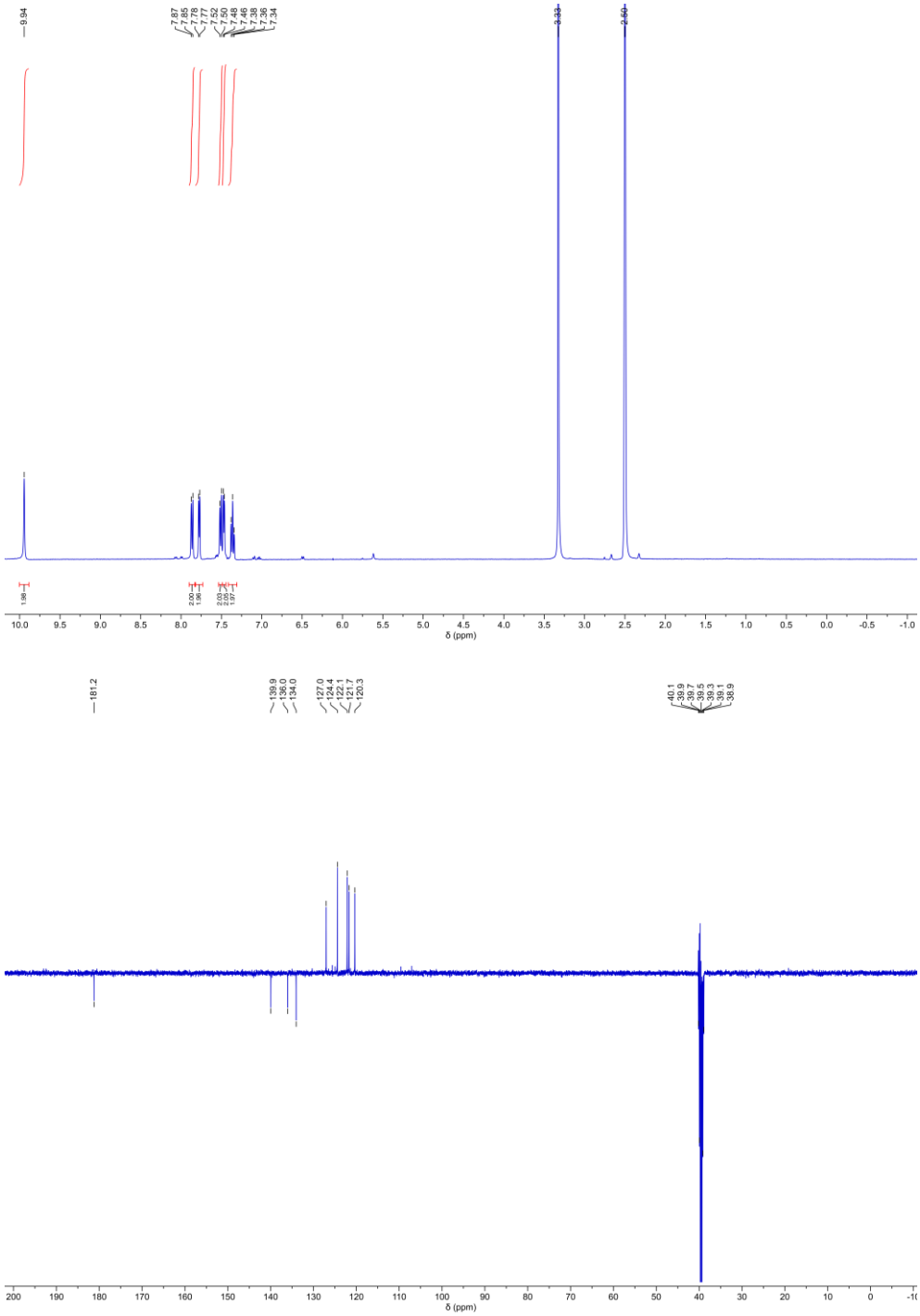

Figure S16. ^{1}H NMR (top) and ^{13}C APT NMR (bottom) spectra of **12** in DMSO-d_6 at 293 K.

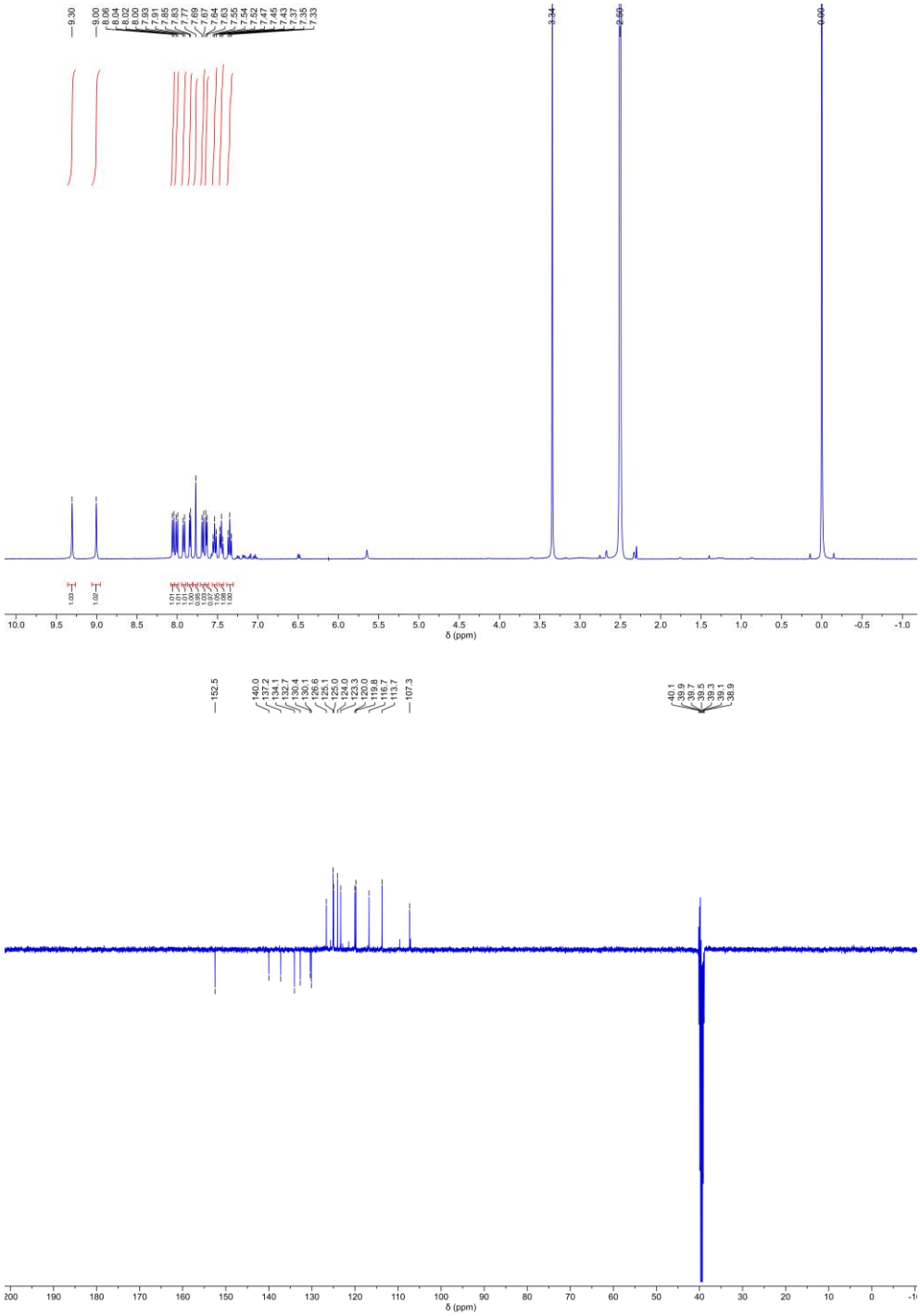

Figure S17. ^{1}H NMR (top) and ^{13}C APT NMR (bottom) spectra of **13** in DMSO-d_6 at 293 K.

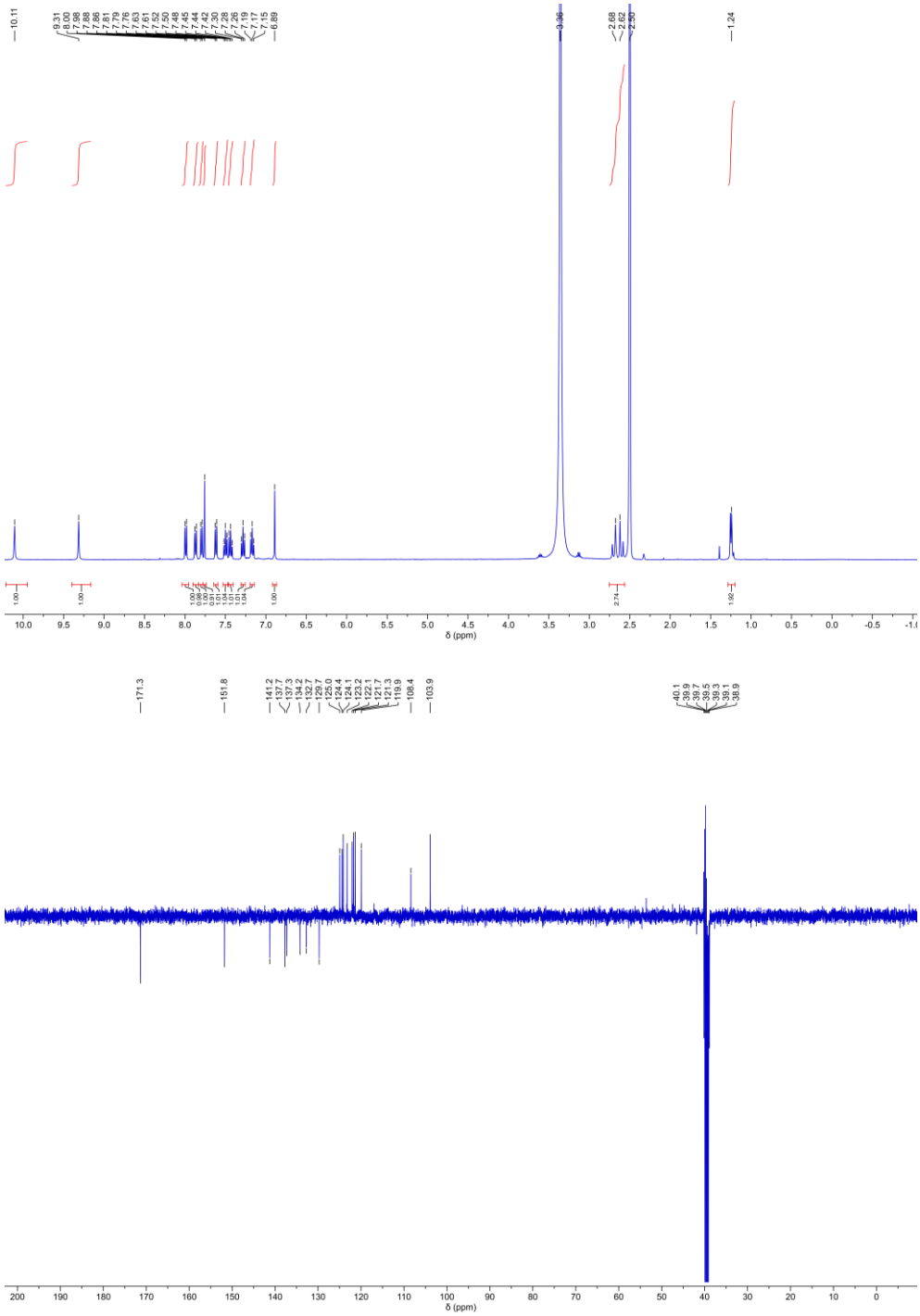

Figure S18. ^{1}H NMR (top) and ^{13}C APT NMR (bottom) spectra of **14** in DMSO-d_6 at 293 K.

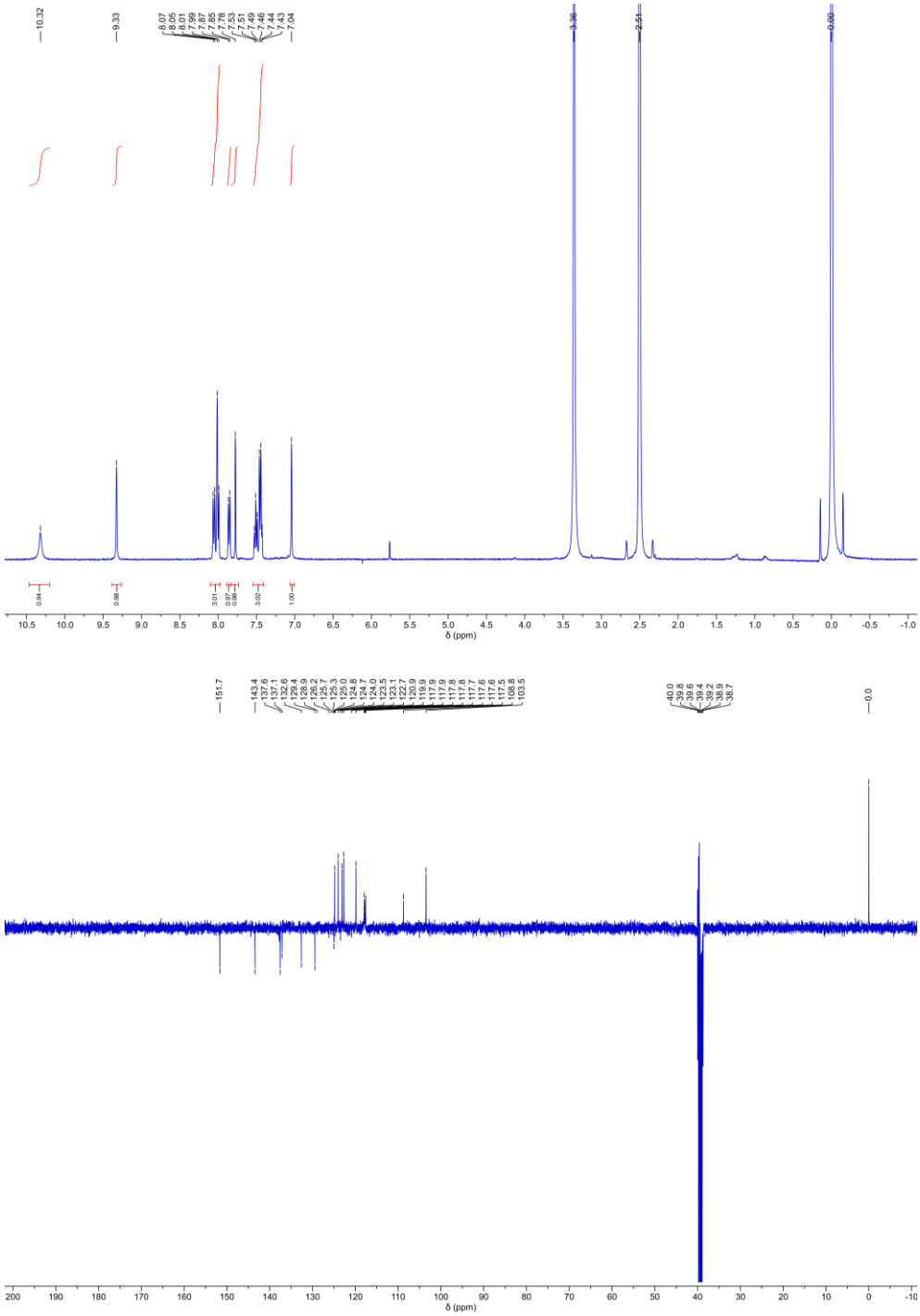

Figure S19. ^{1}H NMR (top) and ^{13}C APT NMR (bottom) spectra of **15** in DMSO-d_6 at 293 K.

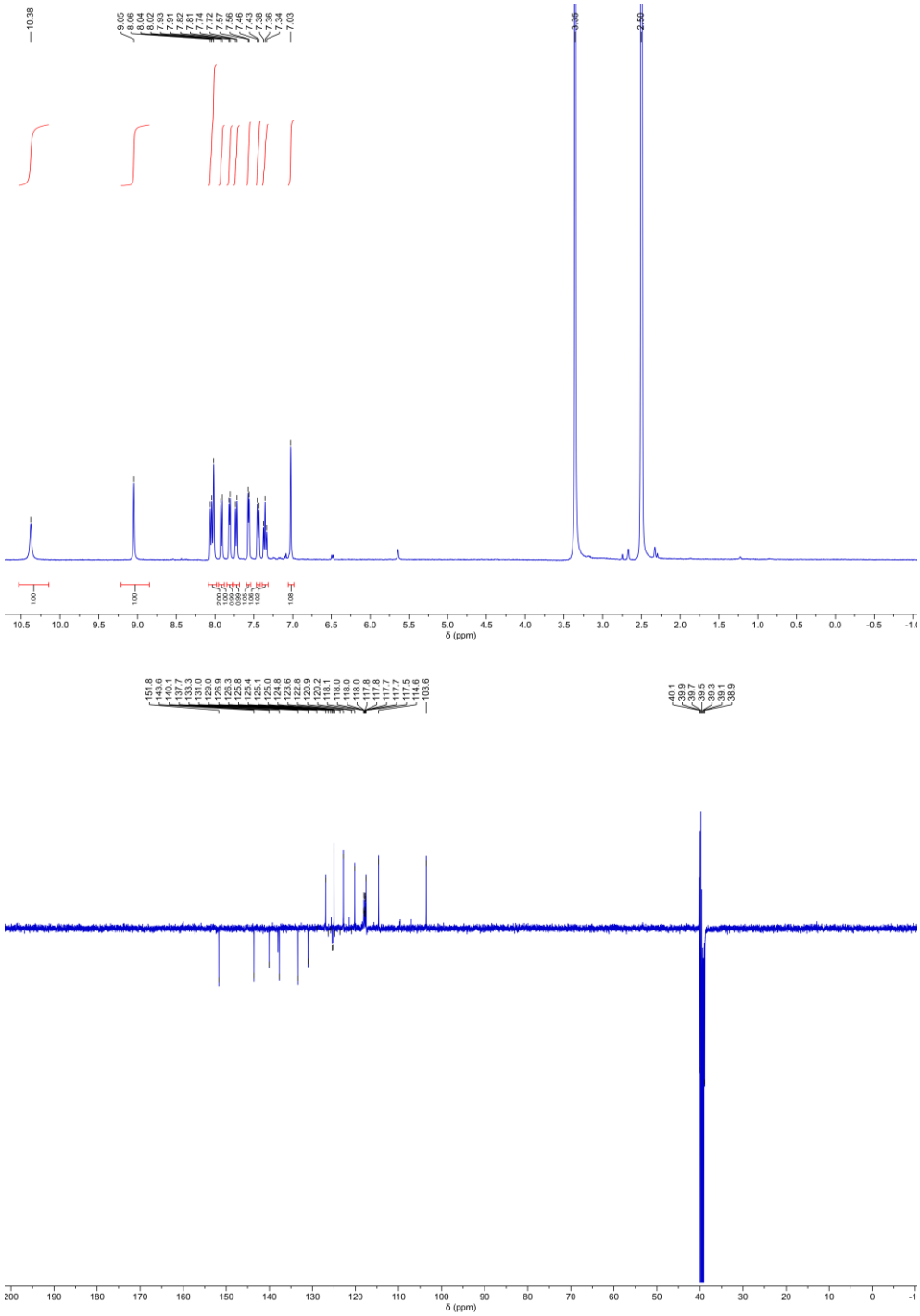

Figure S20. ^{1}H NMR (top) and ^{13}C APT NMR (bottom) spectra of **16** in DMSO-d_6 at 293 K.

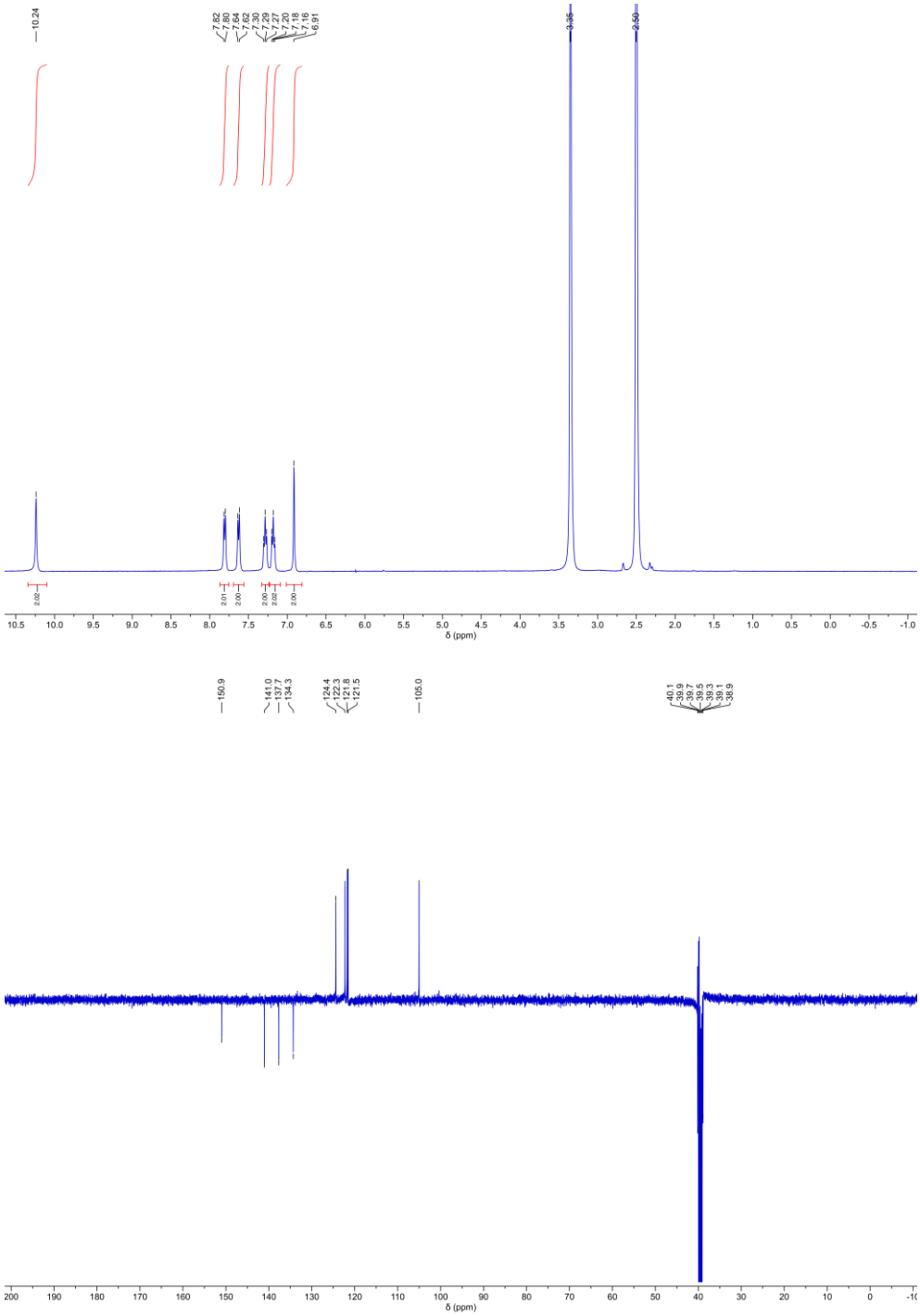

Figure S21. ^{1}H NMR (top) and ^{13}C APT NMR (bottom) spectra of **17** in DMSO-d_6 at 293 K.

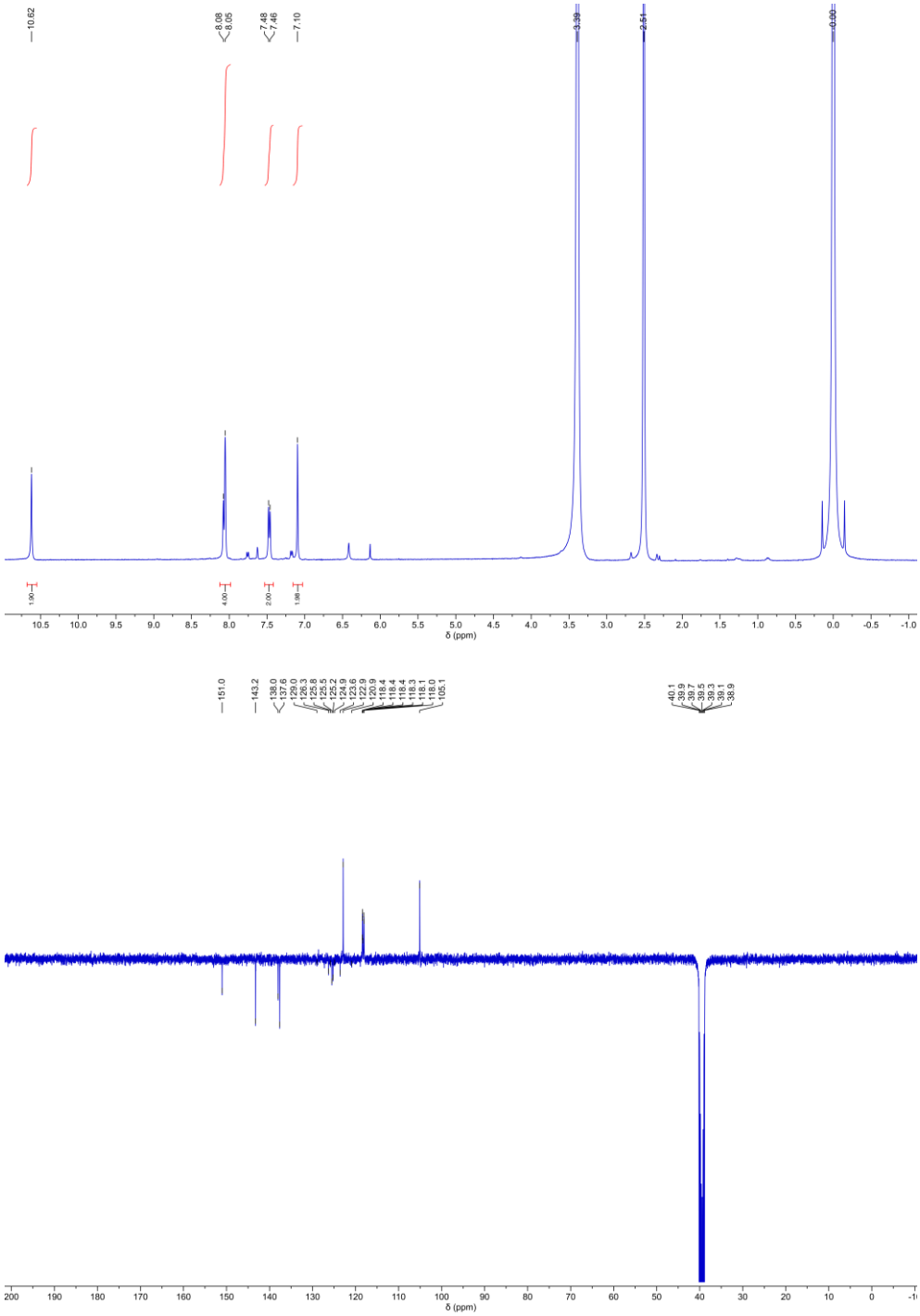

Figure S22. ^{1}H NMR (top) and ^{13}C APT NMR (bottom) spectra of **18** in DMSO-d_6 at 293 K.

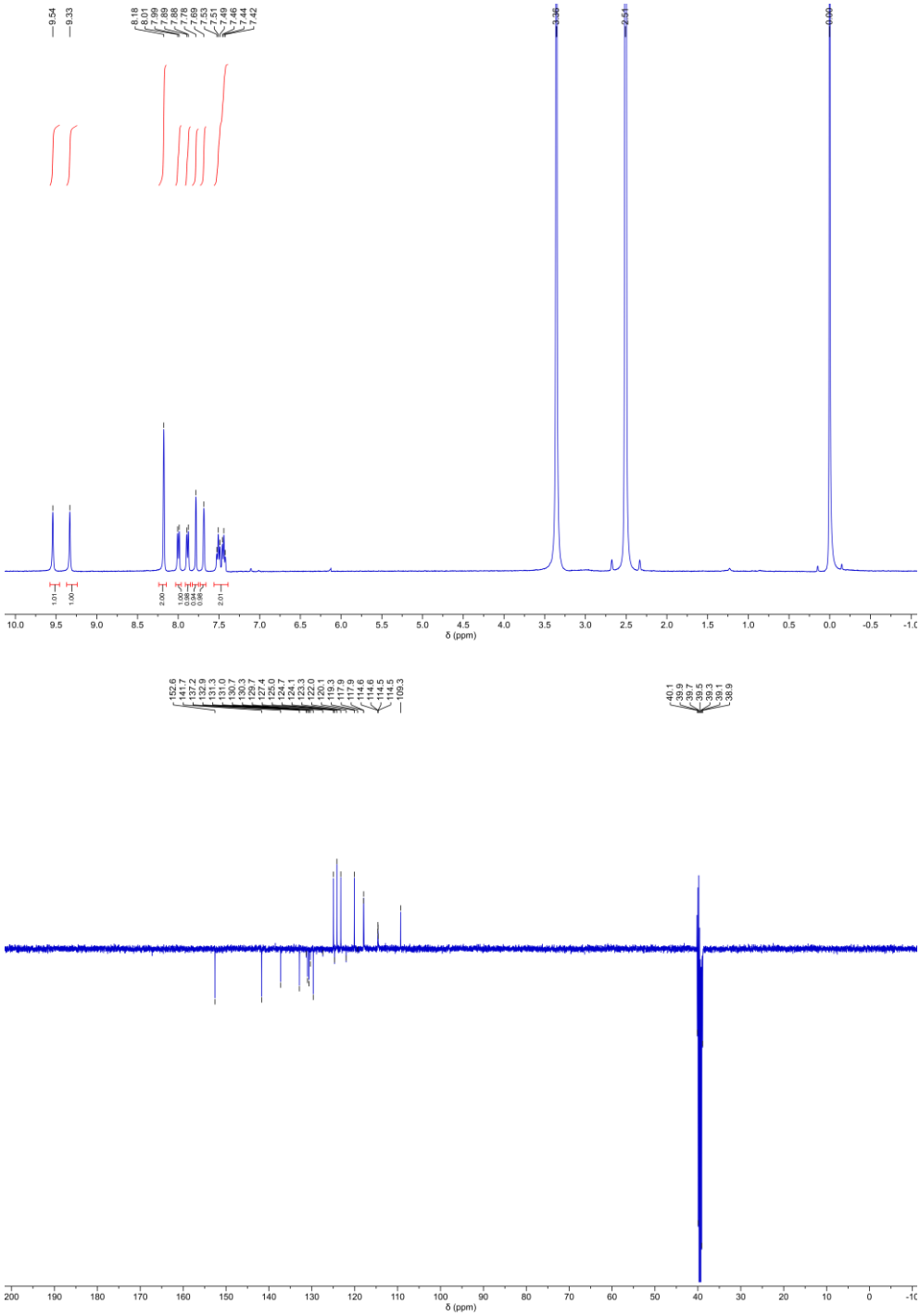

Figure S23. ^{1}H NMR (top) and ^{13}C APT NMR (bottom) spectra of **19** in DMSO-d_6 at 293 K.

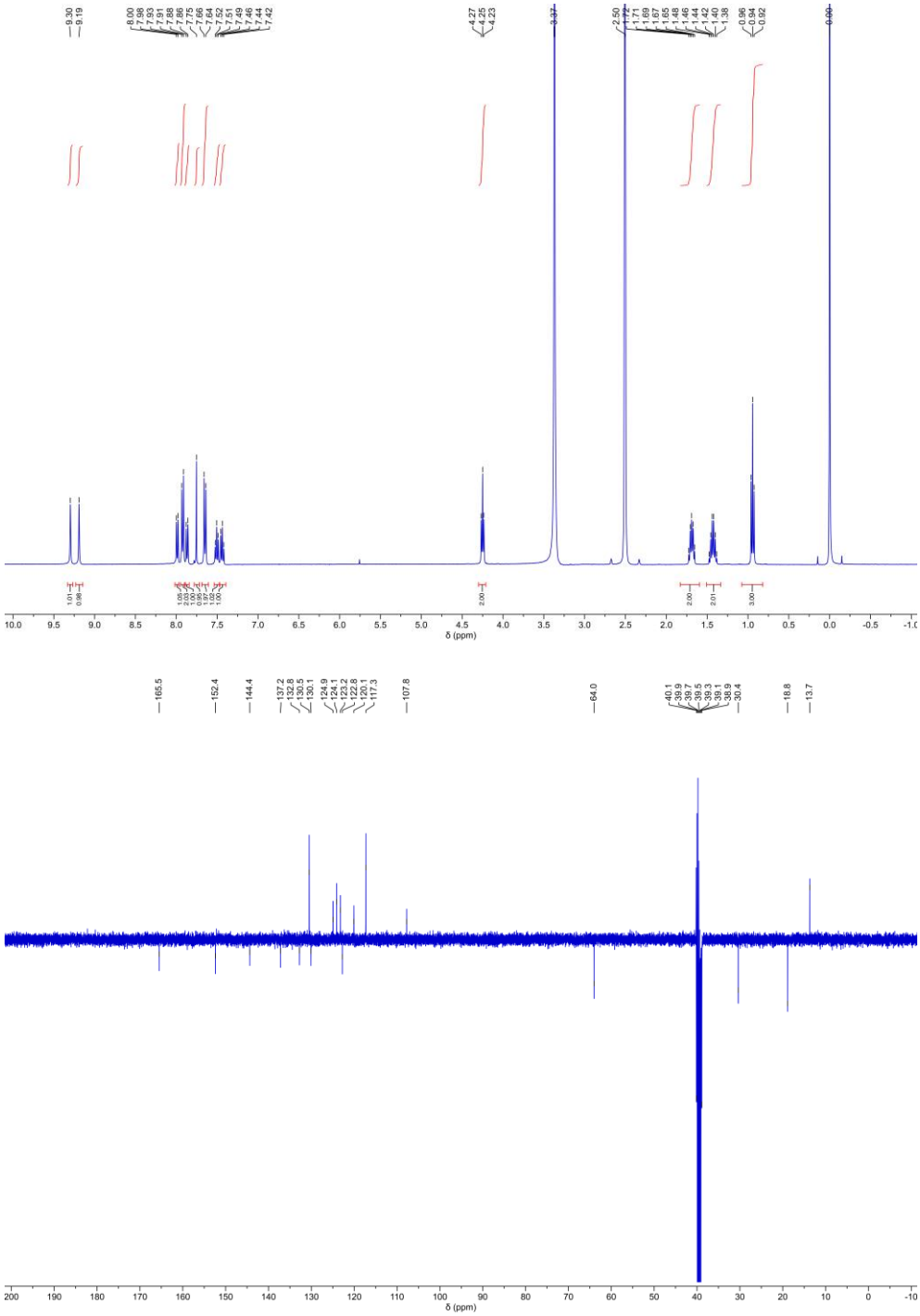

Figure S24. ^{1}H NMR (top) and ^{13}C APT NMR (bottom) spectra of **20** in DMSO-d_6 at 293 K.

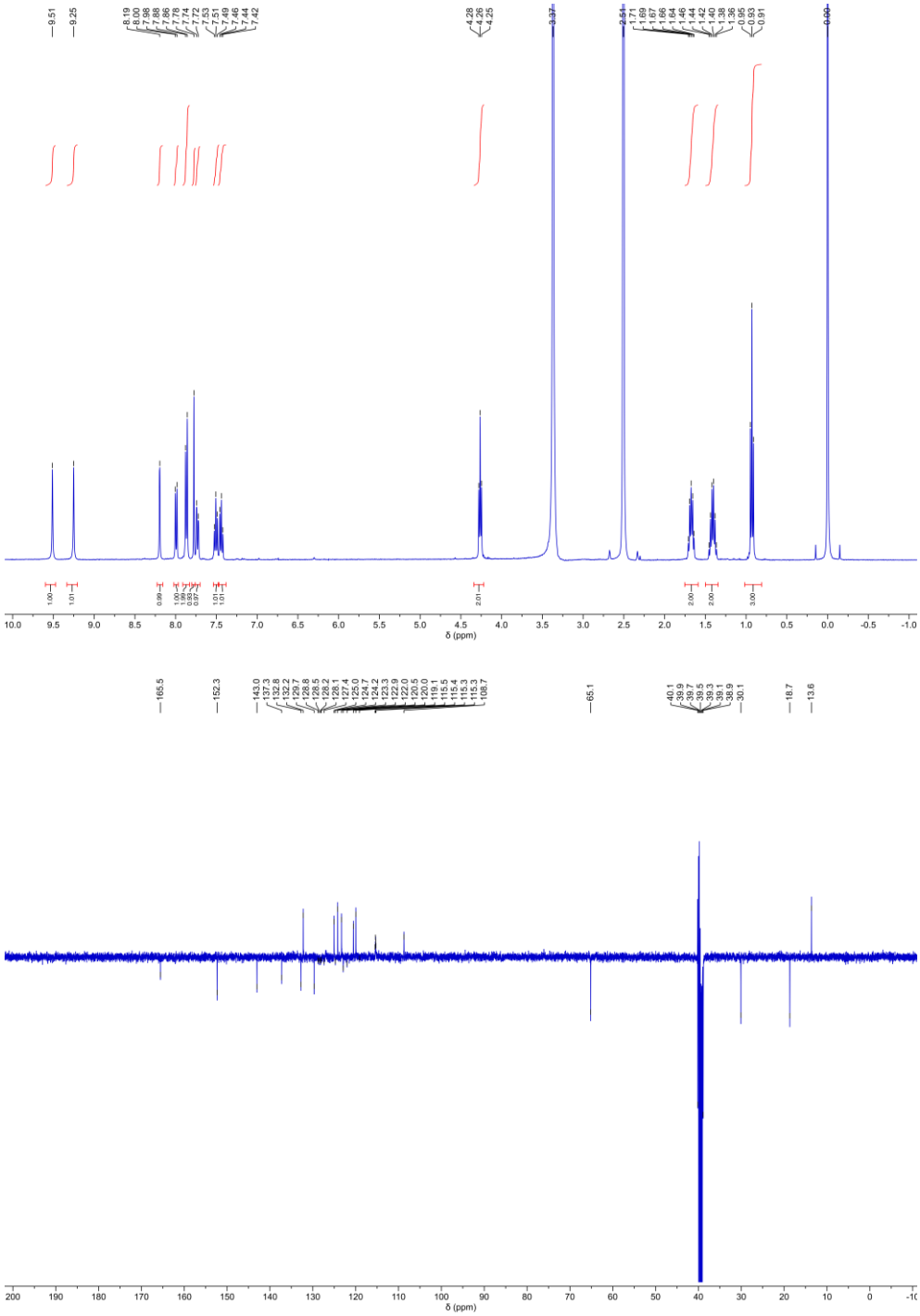

Figure S25. ^{1}H NMR (top) and ^{13}C APT NMR (bottom) spectra of **21** in DMSO-d_6 at 293 K.

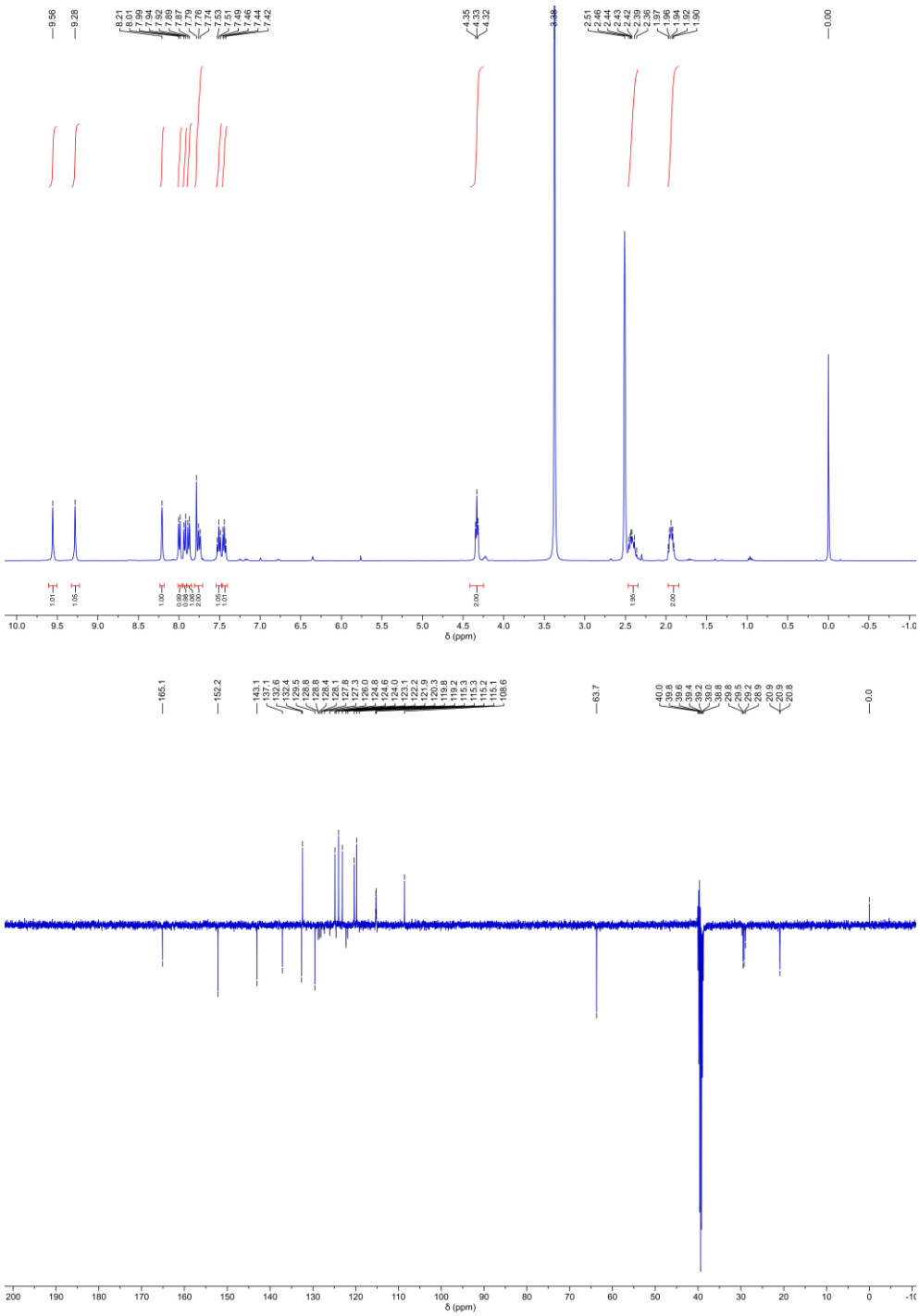

Figure S26. ^{1}H NMR (top) and ^{13}C APT NMR (bottom) spectra of **22** in DMSO-d_6 at 293 K.

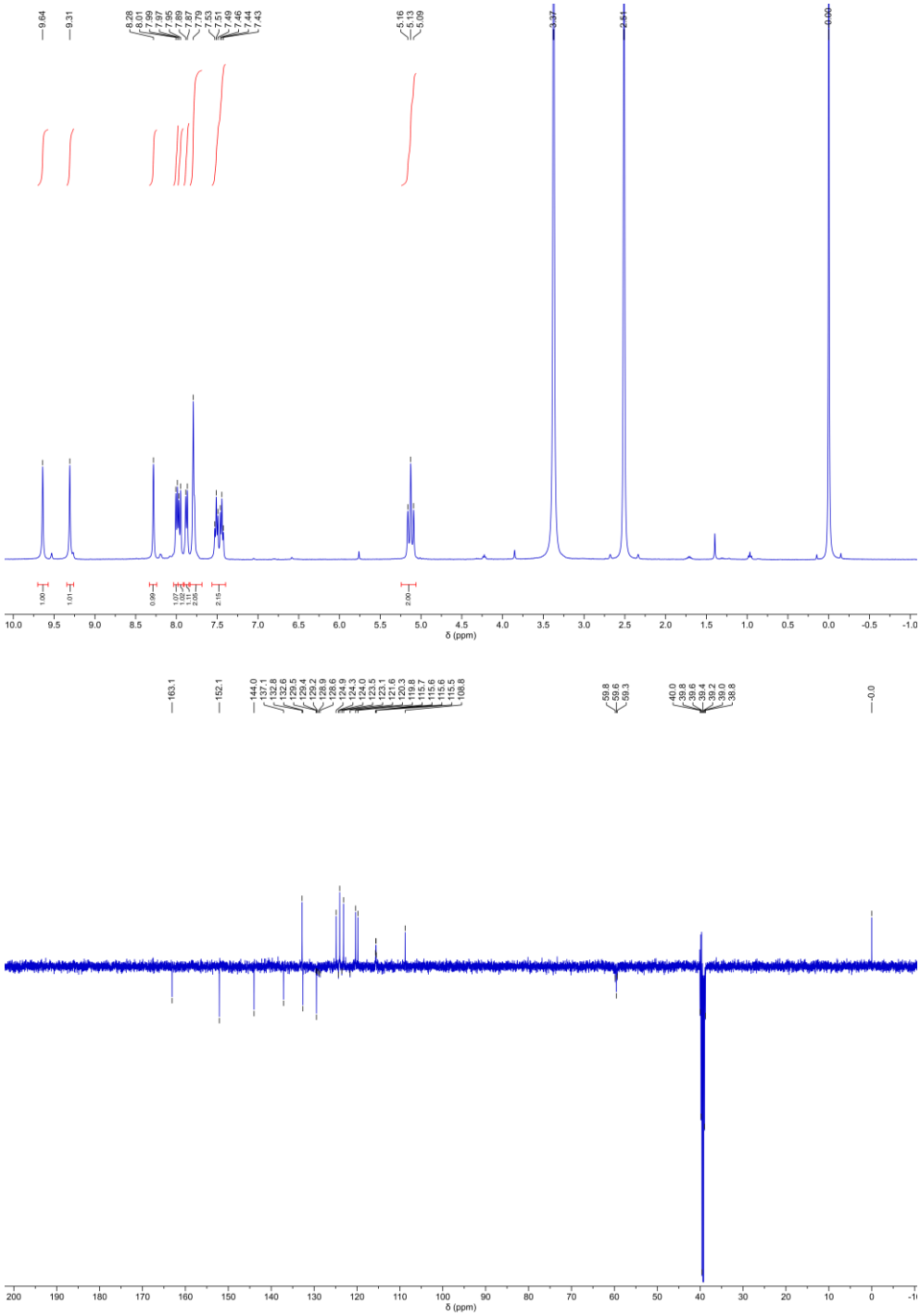

Figure S27. ^{1}H NMR (top) and ^{13}C APT NMR (bottom) spectra of **23** in DMSO-d_6 at 293 K.

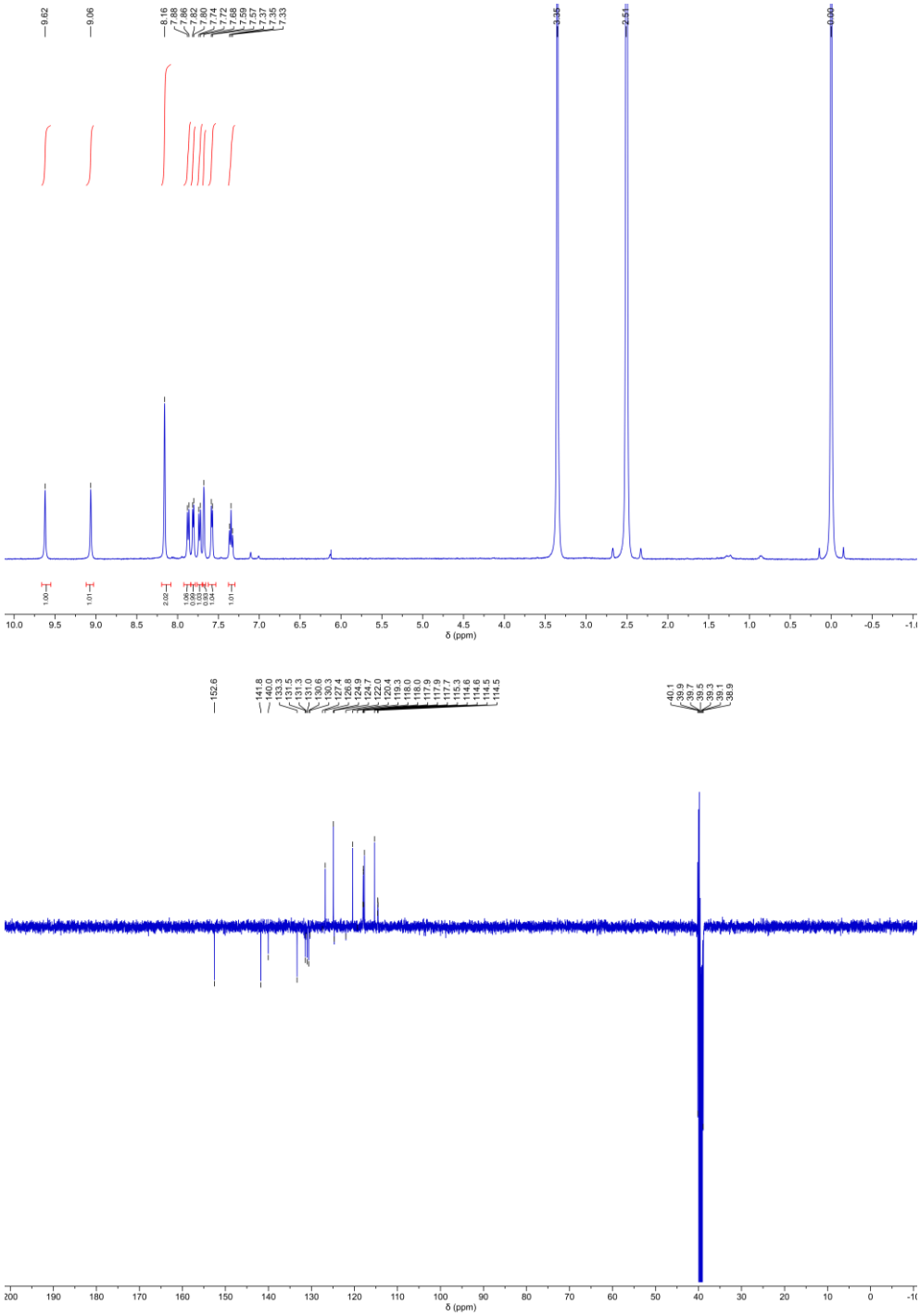

Figure S28. ^{1}H NMR (top) and ^{13}C APT NMR (bottom) of **24** in DMSO-d_6 at 293 K.

^{1}H NMR Titrations

Titration's protocol

^{1}H NMR titrations were performed on a Bruker Avance 400 spectrometer, in DMSO-d_6/0.5% H_2O, using TMS as internal reference, at 293 K.

The chloride was added as *n*-tetrabutylammonium salt (Bu_4NCl), which was dried under high vacuum before use. Afterwards, typically 97.24 mg of Bu_4NCl were dissolved in 2 mL of DMSO-d_6/0.5% H_2O, affording a solution with 0.175 M. The (thio)urea-based benzo[*b*]thiophene receptors, also previously dried under vacuum, were dissolved in a certain volume of DMSO-d_6/0.5% H_2O, to afford initial solutions with concentrations between 4.1 mM and 12.7 mM for **16** and **18**, respectively. Subsequently, a given number of aliquots of 550 μL of a receptor solution was transferred to different NMR tubes, to which increasing volumes of a Bu_4NCl solution were independently added. Furthermore, an initial ^{1}H NMR spectrum of the receptor was recorded prior to the addition of the salt, as reference. Upon addition of the salt, the (thio)urea protons, NH_7 and/or NH_9, exhibited significant downfield shifts and were followed throughout the NMR titrations, until the variations of these protons' chemical shifts were found to be insignificant, indicating the end point of the titration.

Chemical shifts of N_7-H and N_9-H protons, acquired throughout the ^{1}H NMR titration of each (thio)urea, receptor were processed together by non-linear multivariate regression analysis using the Bindfit program,[4] leading to the ^{1}H NMR binding constants listed in the Table 1 (main text).

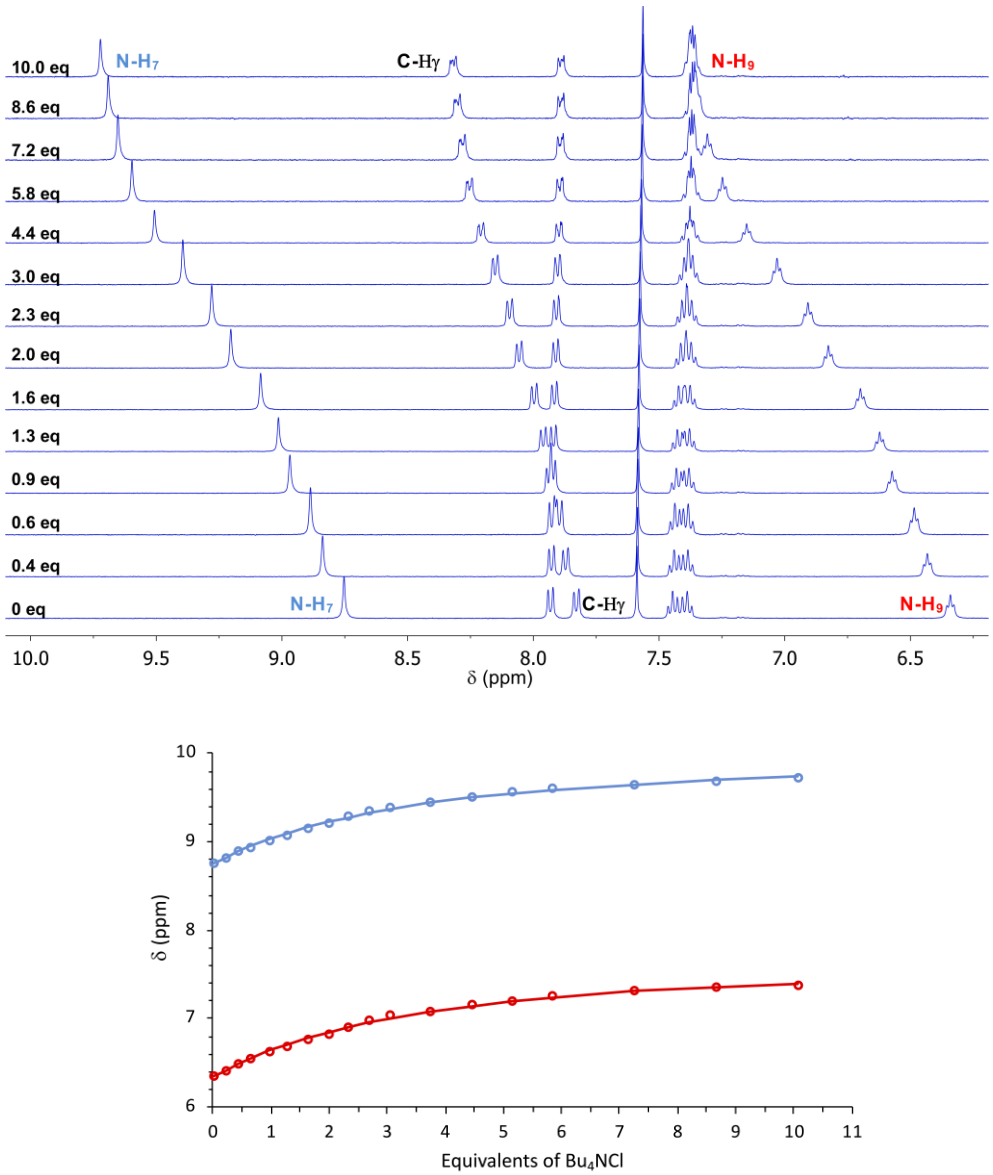

Figure S29. ^{1}H NMR titration of **1** (10.0 mM) with Bu_4NCl in DMSO-d_6/0.5% H_2O (400.13 MHz, 293 K): Top - stacked spectra showing the variations in chemical shifts of N_7-H, N_9-H and C-H_γ along the titration; Bottom - binding isotherms constructed with δ of N_7-H (∘) and N_9-H (∘) together with their curves fitted (36 points) to 1:1 binding model (solid lines).

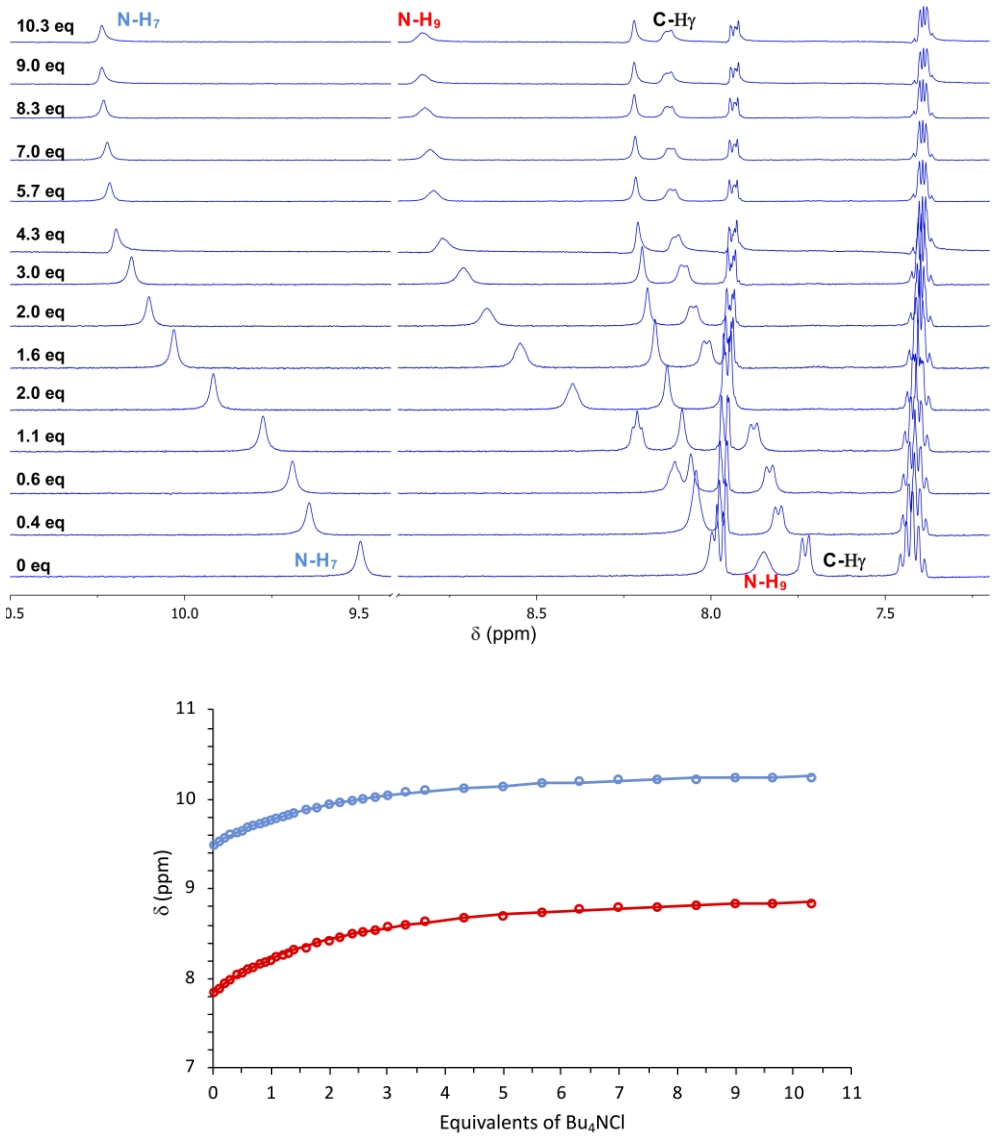

Figure S30. ^{1}H NMR titration of **2** (10.3 mM) with Bu_4NCl in DMSO-d_6/0.5% H_2O (400.13 MHz, 293 K): Top - stacked spectra showing the variations in chemical shifts of N_7-H, N_9-H and C-H_γ along the titration; Bottom - binding isotherms constructed with δ of N_7-H (∘) and N_9-H (∘) together with their curves fitted (70 points) to 1:1 binding model (solid lines).

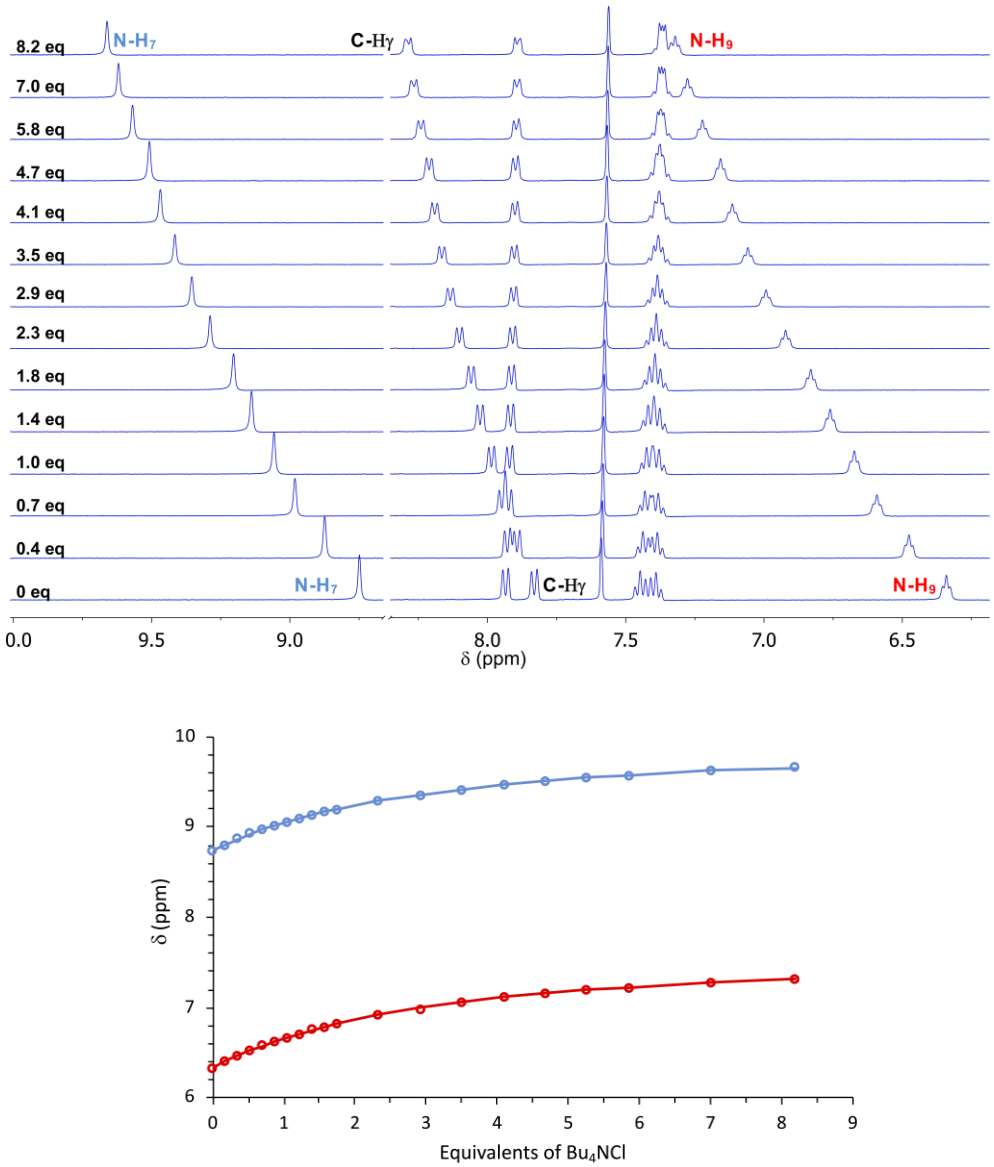

Figure S31. ^{1}H NMR titration of **3** (11.4 mM) with Bu_4NCl in DMSO-d_6/0.5% H_2O (400.13 MHz, 293 K): Top - stacked spectra showing the variations in chemical shifts of N_7-H, N_9-H and C-H_γ along the titration; Bottom - binding isotherms constructed with δ of N_7-H (○) and N_9-H (○) together with their curves fitted (40 points) to 1:1 binding model (solid lines).

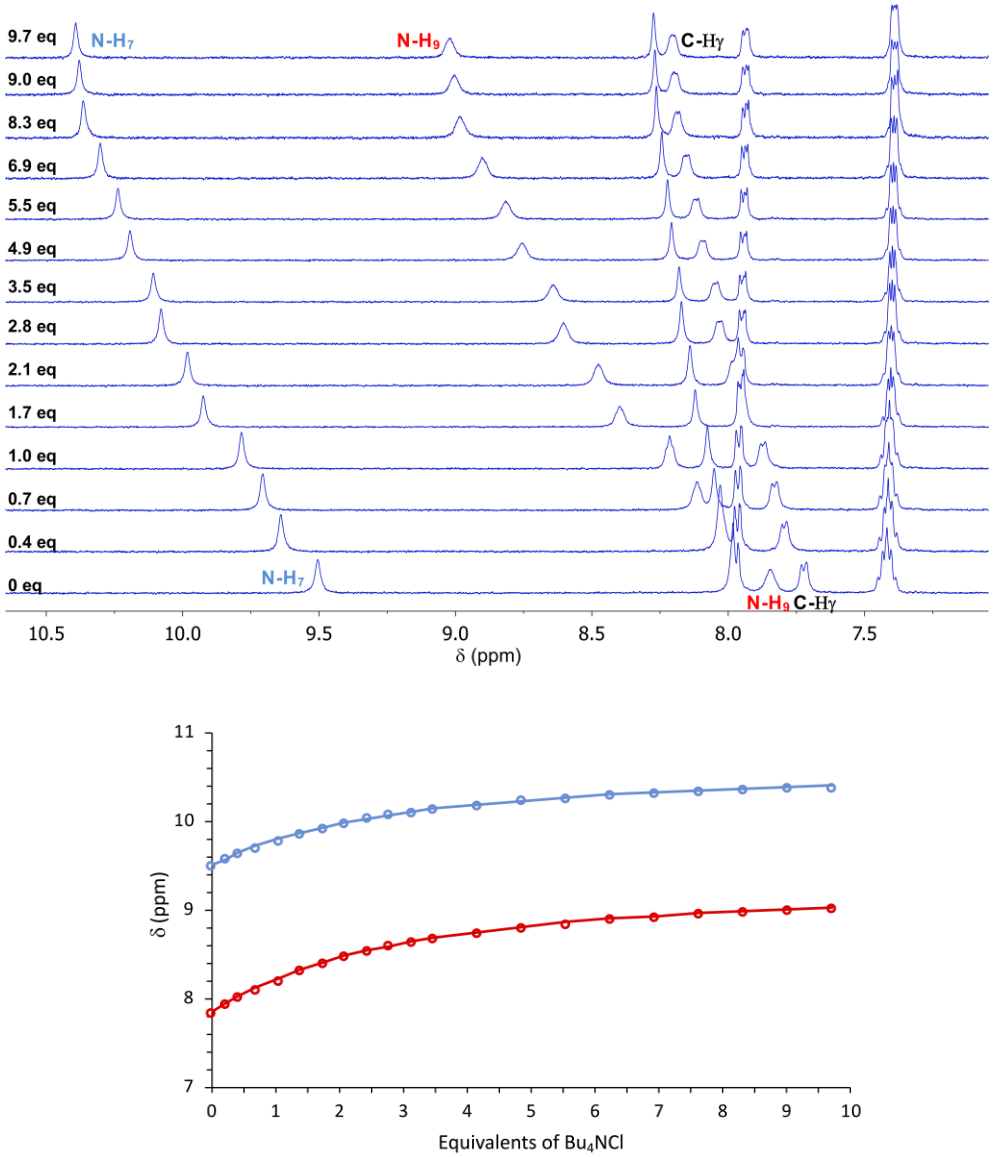

Figure S32. ^{1}H NMR titration of **4** (10.1 mM) with Bu_4NCl in DMSO-d_6/0.5% H_2O (400.13 MHz, 293 K): Top - stacked spectra showing the variations in chemical shifts of N_7-H, N_9-H and C-H_γ along the titration; Bottom - binding isotherms constructed with δ of N_7-H (○) and N_9-H (○) together with their curves fitted (42 points) to 1:1 binding model (solid lines).

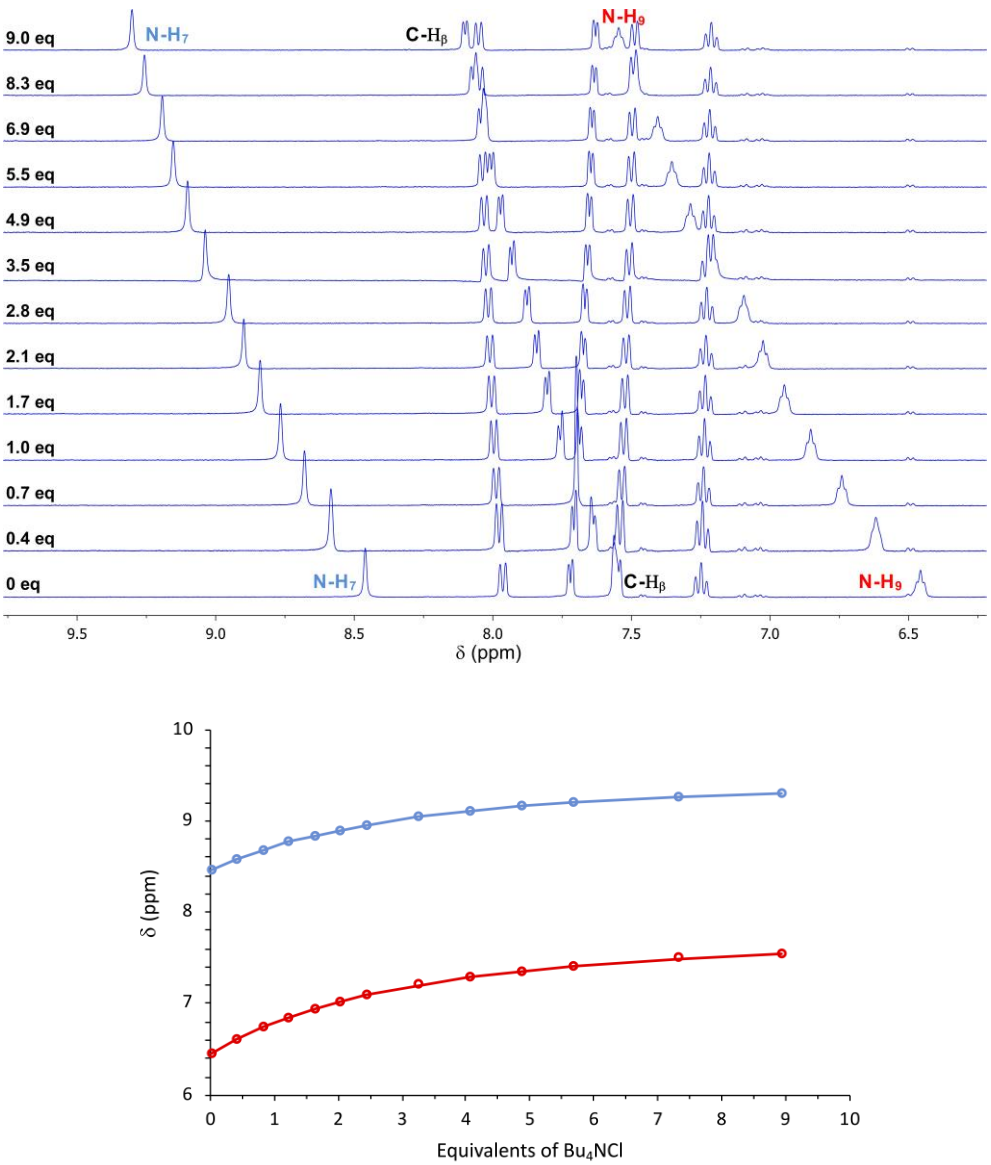

Figure S33. ^{1}H NMR titration of **5** (11.4 mM) with Bu_4NCl in DMSO-d_6/0.5% H_2O (400.13 MHz, 293 K): Top - stacked spectra showing the variations in chemical shifts of N_7-H, N_9-H and C-H$_\beta$ along the titration; Bottom - binding isotherms constructed with δ of N_7-H (∘) and N_9-H (∘) together with their curves fitted (26 points) to 1:1 binding model (solid lines).

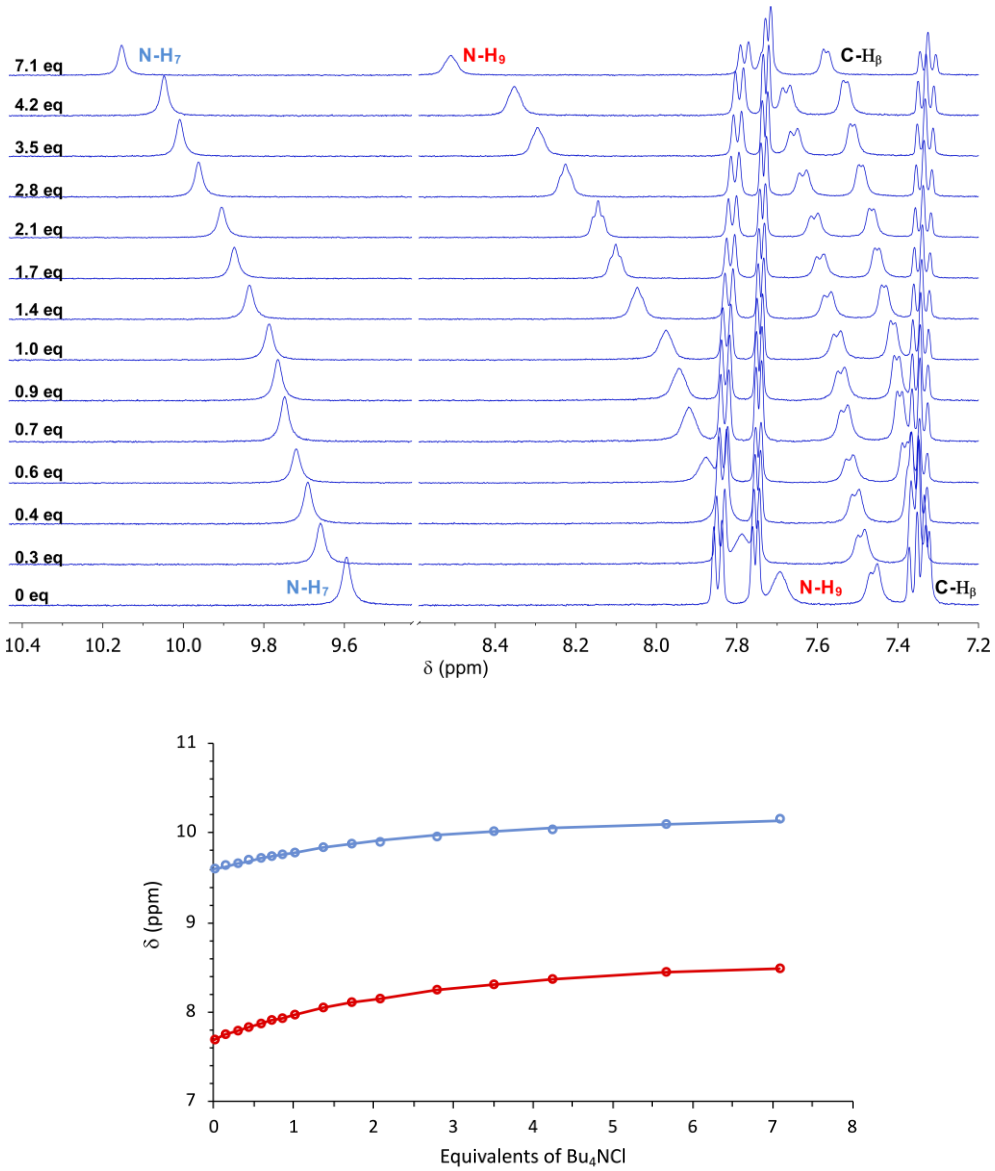

Figure S34. ^{1}H NMR titration of **6** (10.7 mM) with Bu_4NCl in DMSO-d_6/0.5% H_2O (400.13 MHz, 293 K): Top - stacked spectra showing the variations in chemical shifts of N_7-H, N_9-H and C-H_β along the titration; Bottom - binding isotherms constructed with δ of N_7-H (○) and N_9-H (○) together with their curves fitted (32 points) to 1:1 binding model (solid lines).

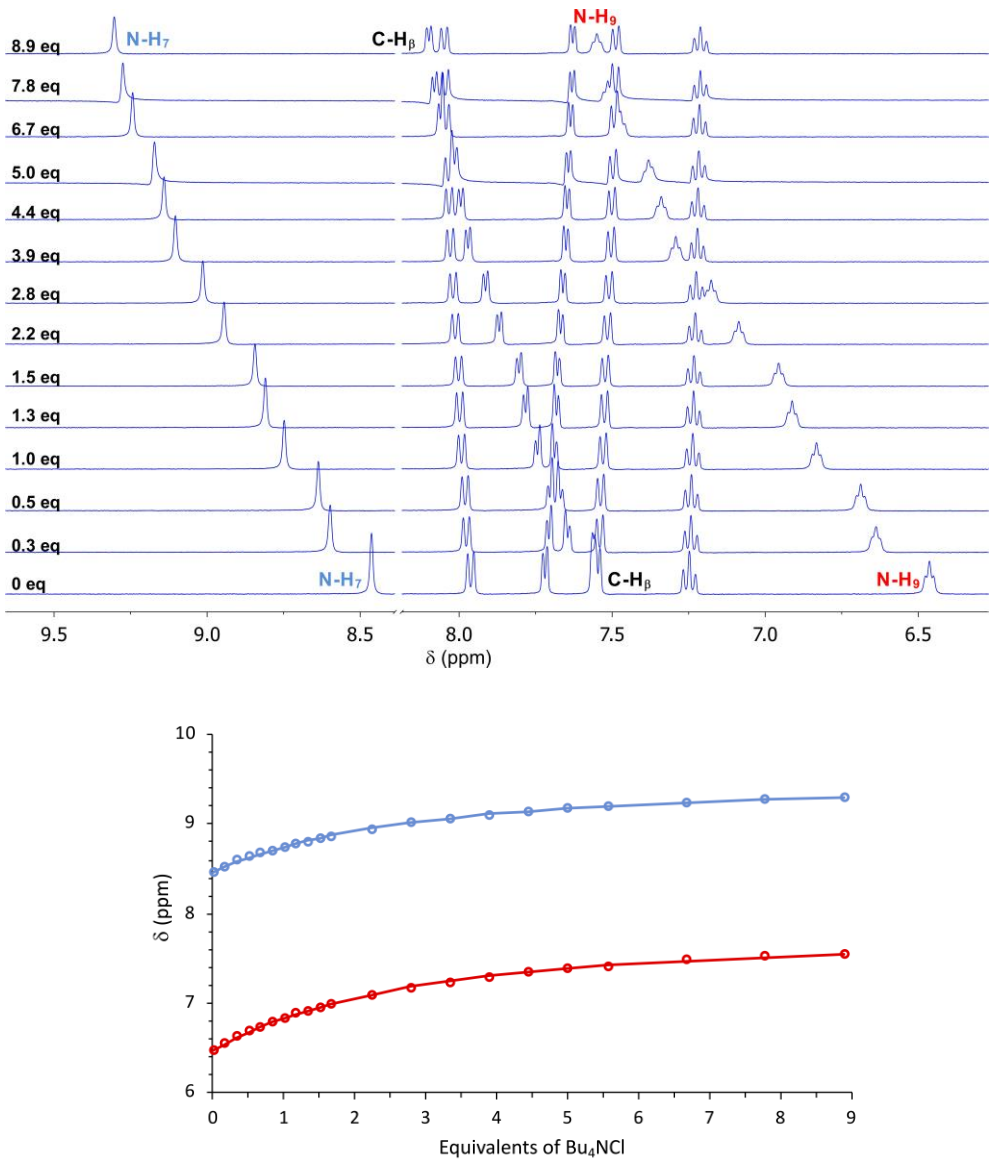

Figure S35. ^{1}H NMR titration of **7** (12.1 mM) with Bu_4NCl in DMSO-d_6/0.5% H_2O (400.13 MHz, 293 K): Top - stacked spectra showing the variations in chemical shifts of N_7-H, N_9-H and C-H$_\beta$ along the titration; Bottom - binding isotherms constructed with δ of N_7-H (∘) and N_9-H (∘) together with their curves fitted (42 points) to 1:1 binding model (solid lines).

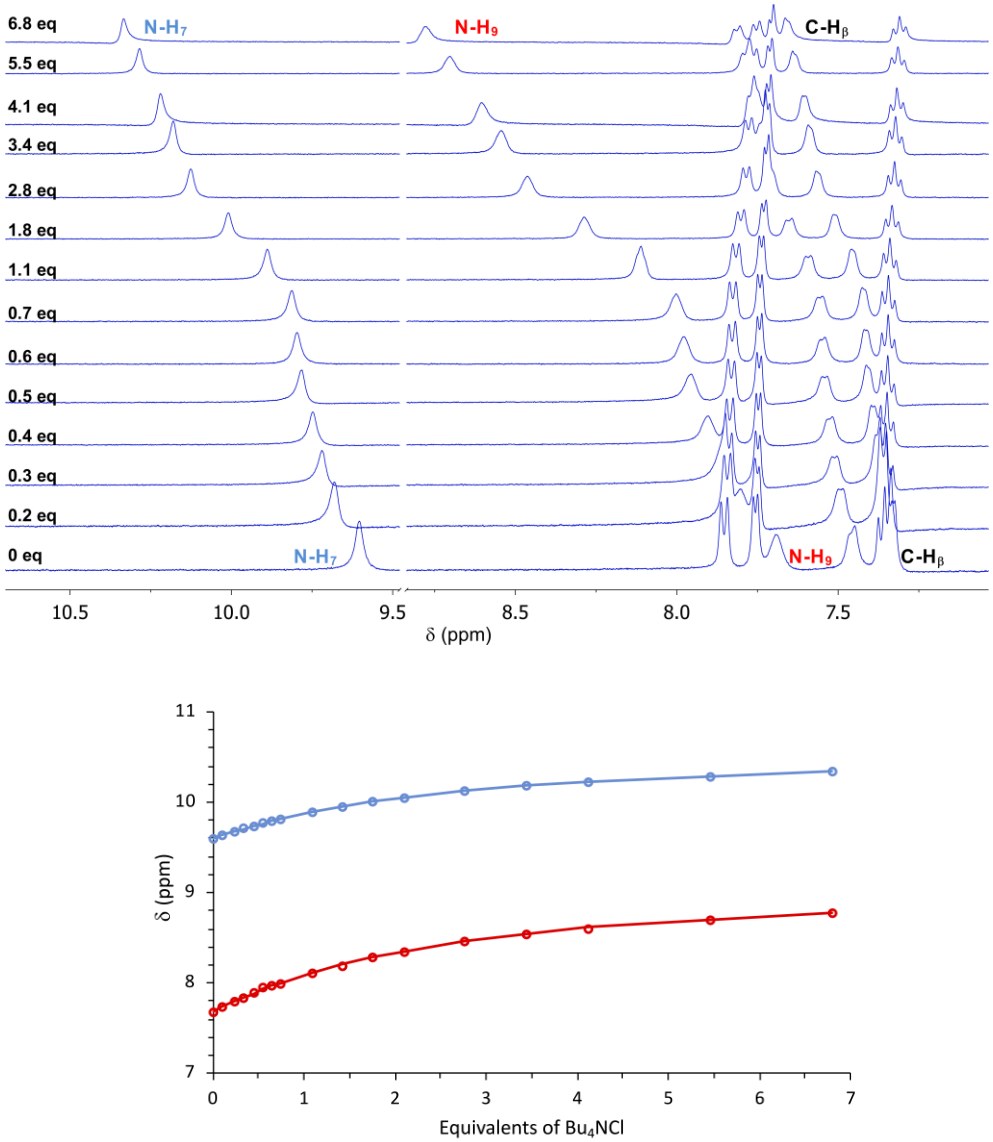

Figure S36. ^{1}H NMR titration of **8** (11.4 mM) with Bu_4NCl in DMSO-d_6/0.5% H_2O (400.13 MHz, 293 K): Top - stacked spectra showing the variations in chemical shifts of N_7-H, N_9-H and C-Hβ along the titration; Bottom - binding isotherms constructed with δ of N_7-H (∘) and N_9-H (∘) together with their curves fitted (34 points) to 1:1 binding model (solid lines).

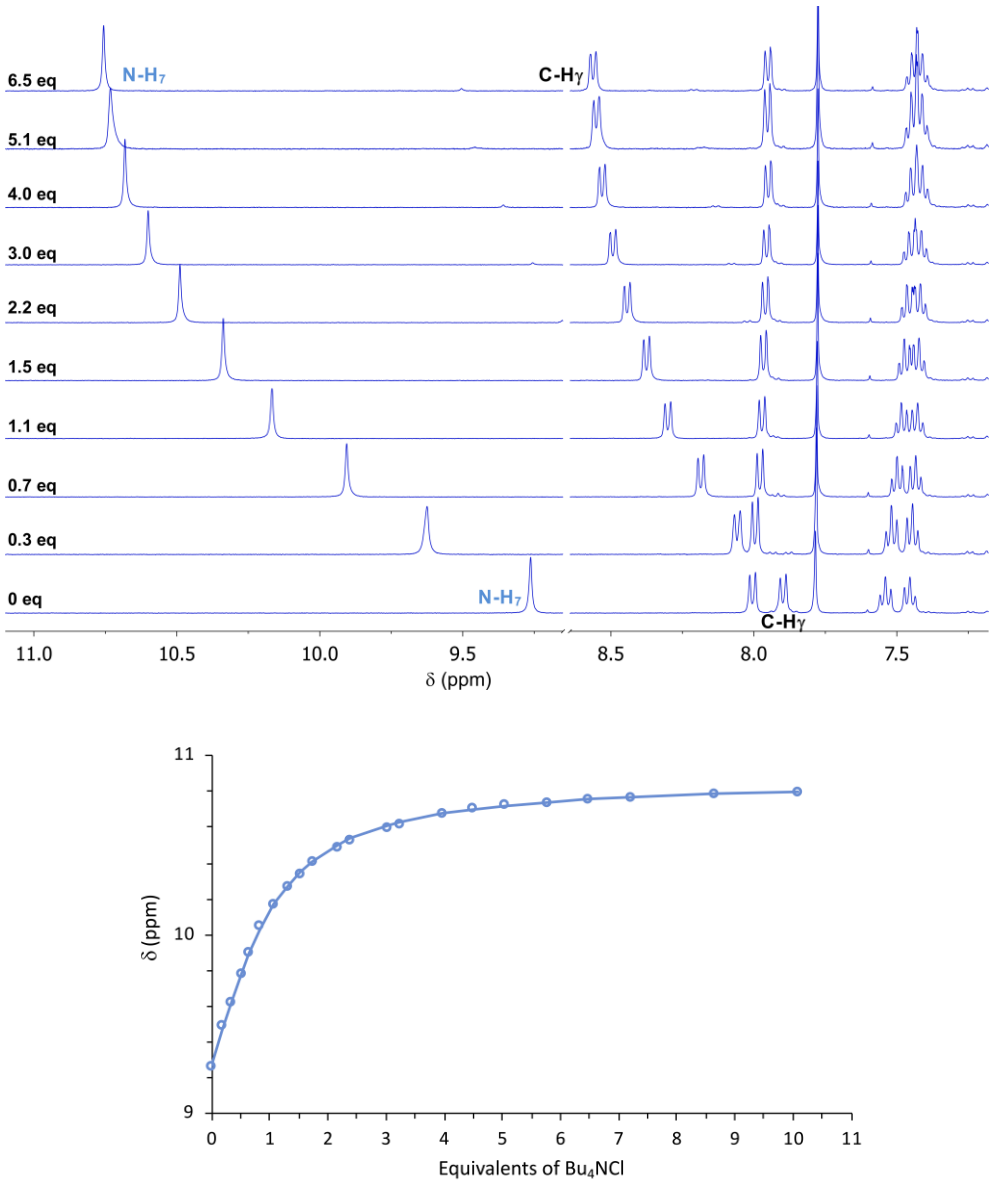

Figure S37. ^{1}H NMR titration of **9** (9.9 mM) with Bu_4NCl in DMSO-d_6/0.5% H_2O (400.13 MHz, 293 K): Top - stacked spectra showing the variations in chemical shifts of N_7-H, N_9-H and C-H_γ along the titration; Bottom - binding isotherms constructed with δ of N_7-H (∘) together with its curve fitted (22 points) to 1:1 binding mode (solid line).

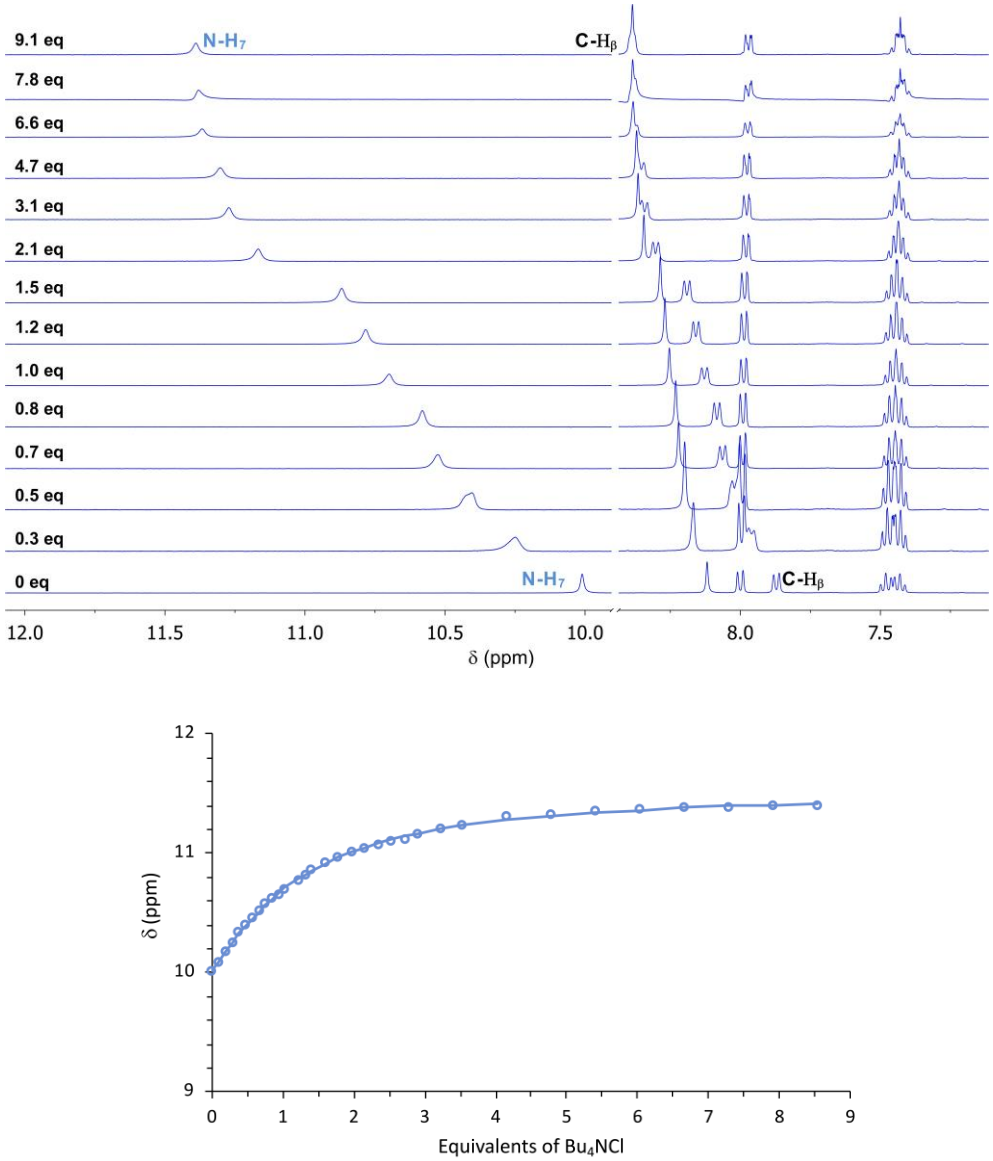

Figure S38. ^{1}H NMR titration of **10** (11.0 mM) with Bu_4NCl in DMSO-d_6/0.5% H_2O (400.13 MHz, 293 K): Top - stacked spectra showing the variations in chemical shifts of N_7-H, N_9-H and C-H_7 along the titration; Bottom - binding isotherms constructed with δ of N_7-H (∘) together with its curve fitted (33 points) to 1:1 binding model (solid line).

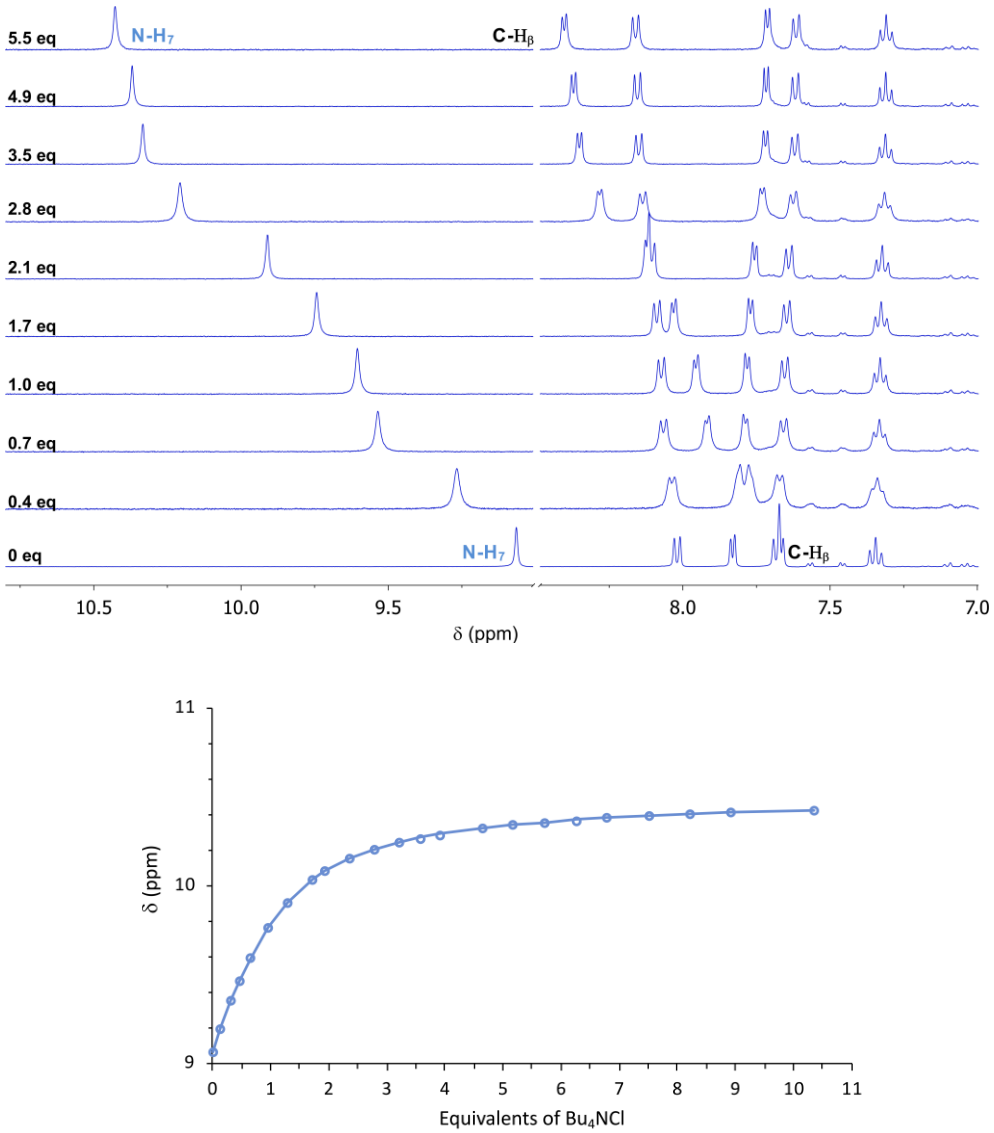

Figure S39. ^{1}H NMR titration of **11** (9.5 mM) with Bu_4NCl in DMSO-d_6/0.5% H_2O (400.13 MHz, 293 K): Top - stacked spectra showing the variations in chemical shifts of N_7-H, N_9-H and C-H_β along the titration; Bottom - binding isotherms constructed with δ of N_7-H (∘) together with its curve fitted (23 points) to 1:1 binding model (solid line).

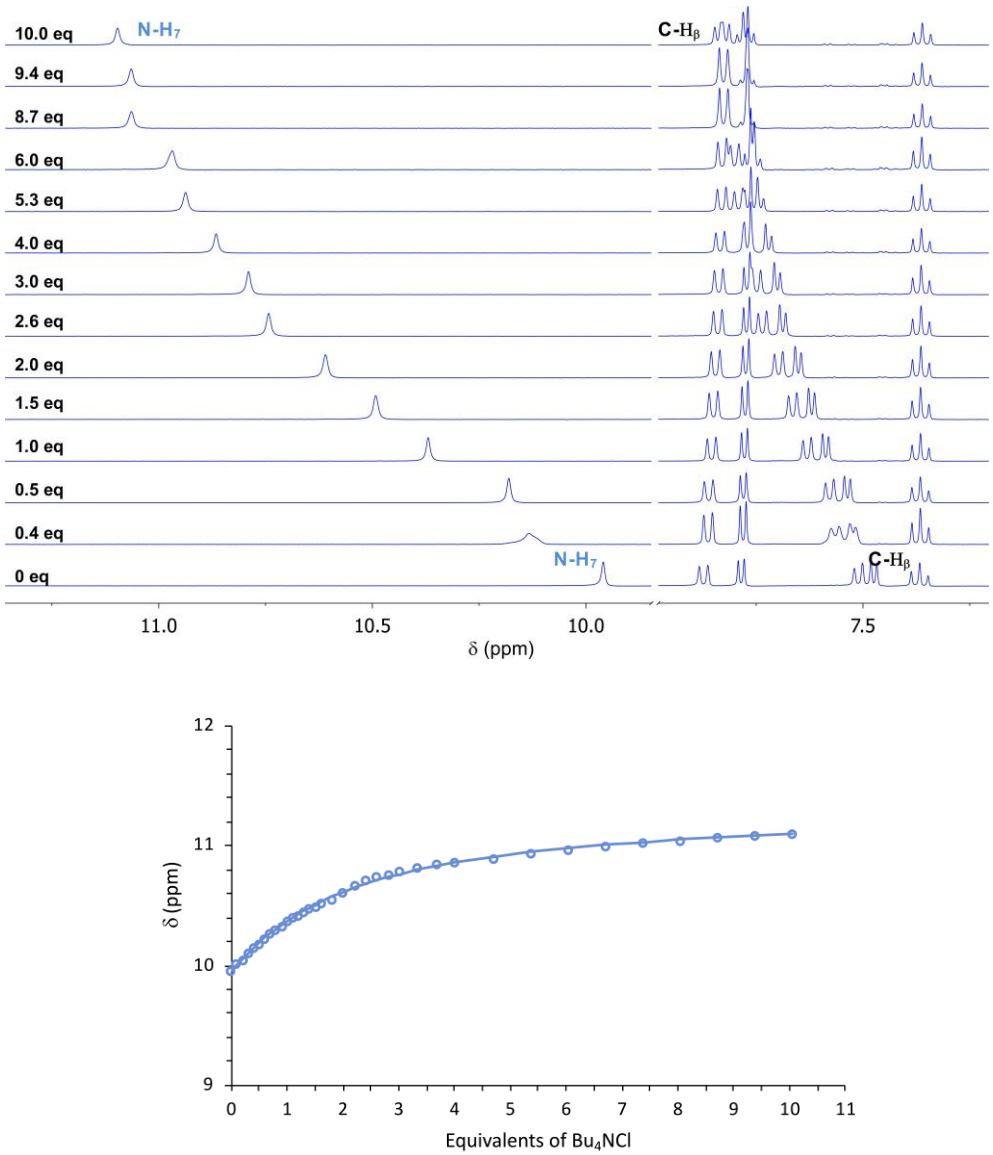

Figure S40. ^{1}H NMR titration of **12** (10.3 mM) with Bu_4NCl in DMSO-d_6/0.5% H_2O (400.13 MHz, 293 K): Top - stacked spectra showing the variations in chemical shifts of N_7-H, N_9-H and C-H_β along the titration; Bottom - binding isotherms constructed with δ of N_7-H (∘) together with its curve fitted (36 points) to 1:1 binding model (solid line).

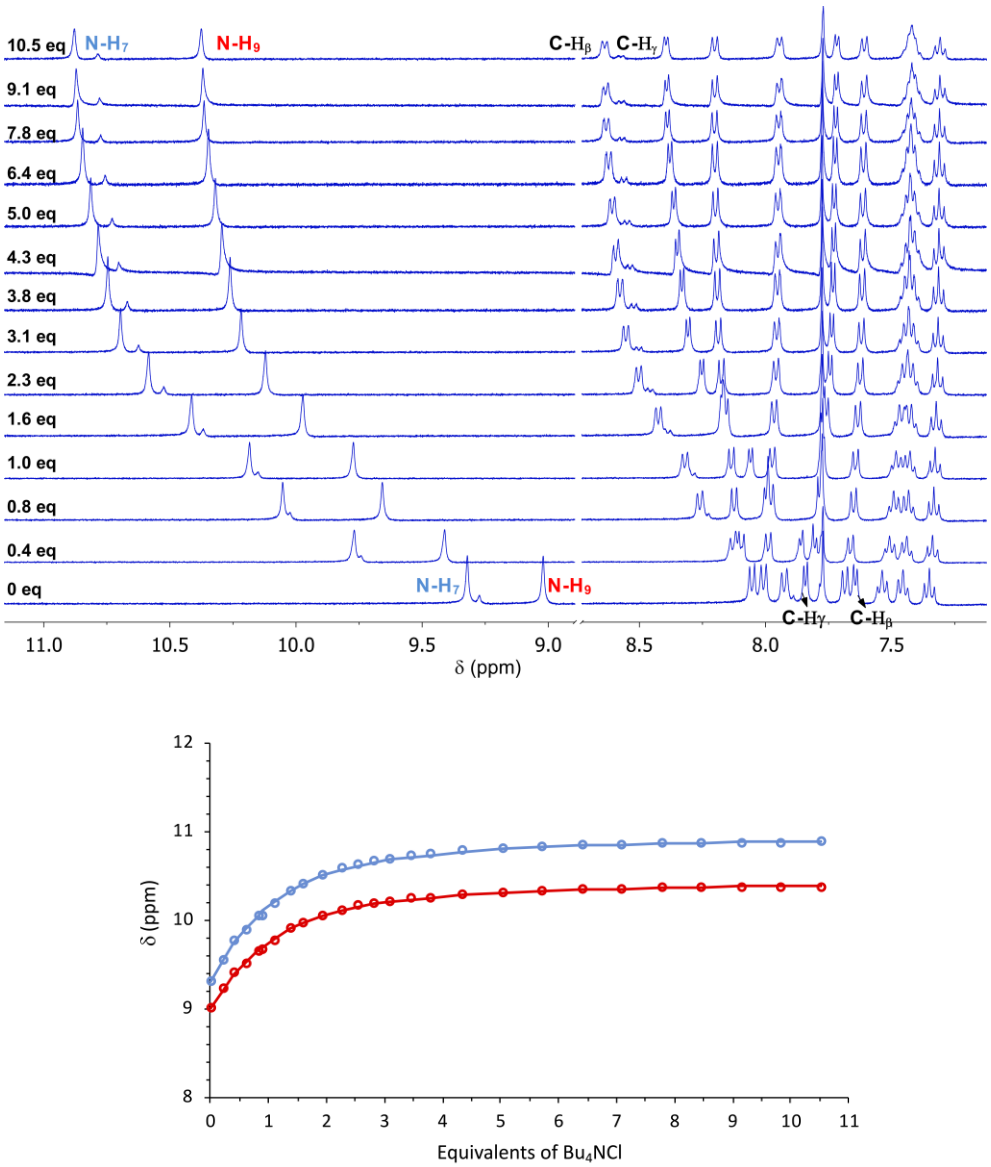

Figure S41. ^{1}H NMR titration of **13** (10.2 mM) with Bu_4NCl in DMSO-d_6/0.5% H_2O (400.13 MHz, 293 K): Top - stacked spectra showing the variations in chemical shifts of N_7-H, N_9-H, C-H$_\beta$ and C-H$_\gamma$ along the titration; Bottom - binding isotherms constructed with δ of N_7-H (∘) and N_9-H (∘) together with their curves fitted (52 points) to 1:1 binding model (solid lines).

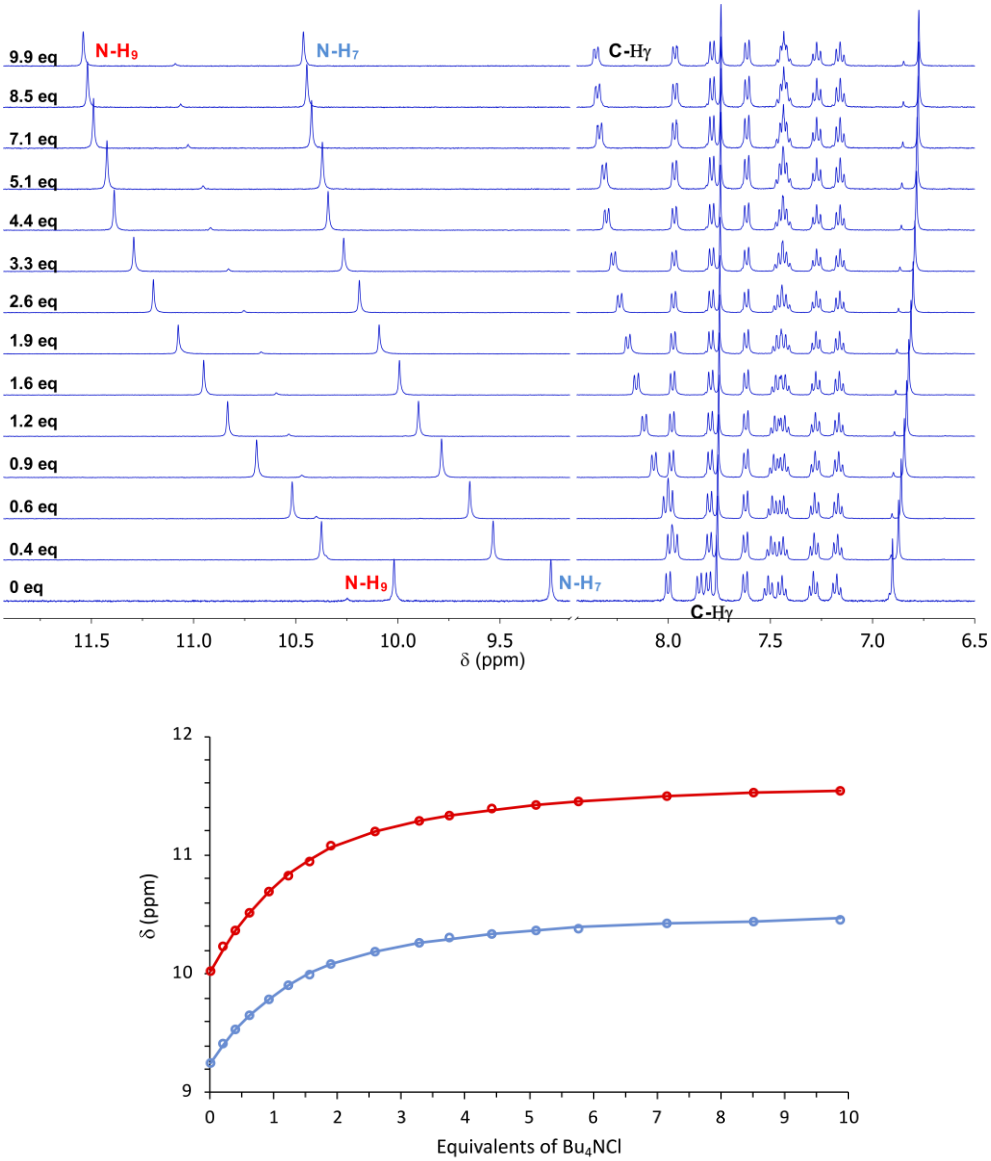

Figure S42. ^{1}H NMR titration of **14** (10.3 mM) with Bu_4NCl in DMSO-d_6/0.5% H_2O (400.13 MHz, 293 K): Top - stacked spectra showing the variations in chemical shifts of N_7-H, N_9-H and C-H_γ along the titration; Bottom - binding isotherms constructed with δ of N_7-H (∘) and N_9-H (∘) together with their curves fitted (34 points) to 1:1 binding model (solid lines).

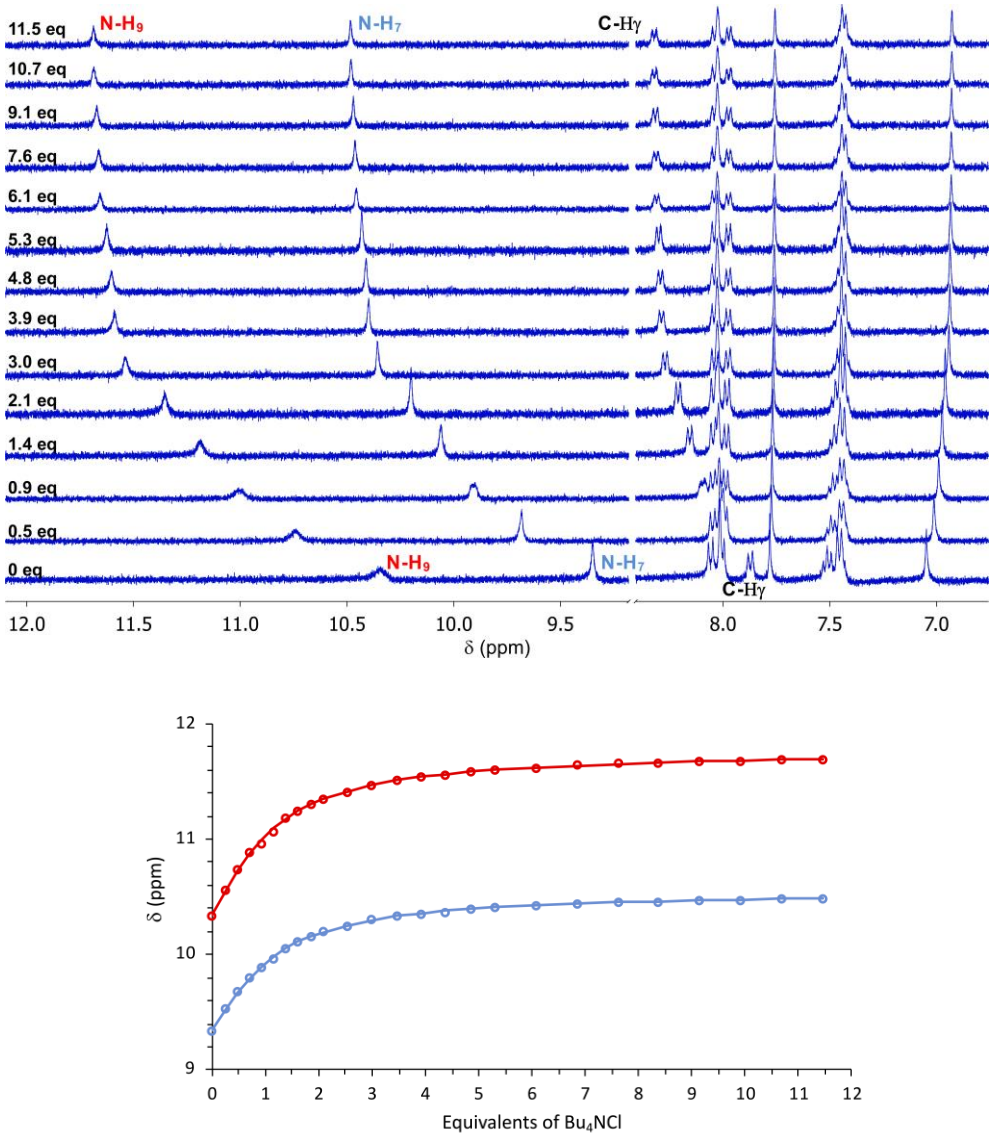

Figure S43. ^{1}H NMR titration of **15** (9.3 mM) with Bu_4NCl in DMSO-d_6/0.5% H_2O (400.13 MHz, 293 K): Top - stacked spectra showing the variations in chemical shifts of N_7-H, N_9-H, and C-H_γ along the titration; Bottom - binding isotherms constructed with δ of N_7-H (∘) and N_9-H (∘) together with their curves fitted (50 points) to 1:1 binding model (solid lines).

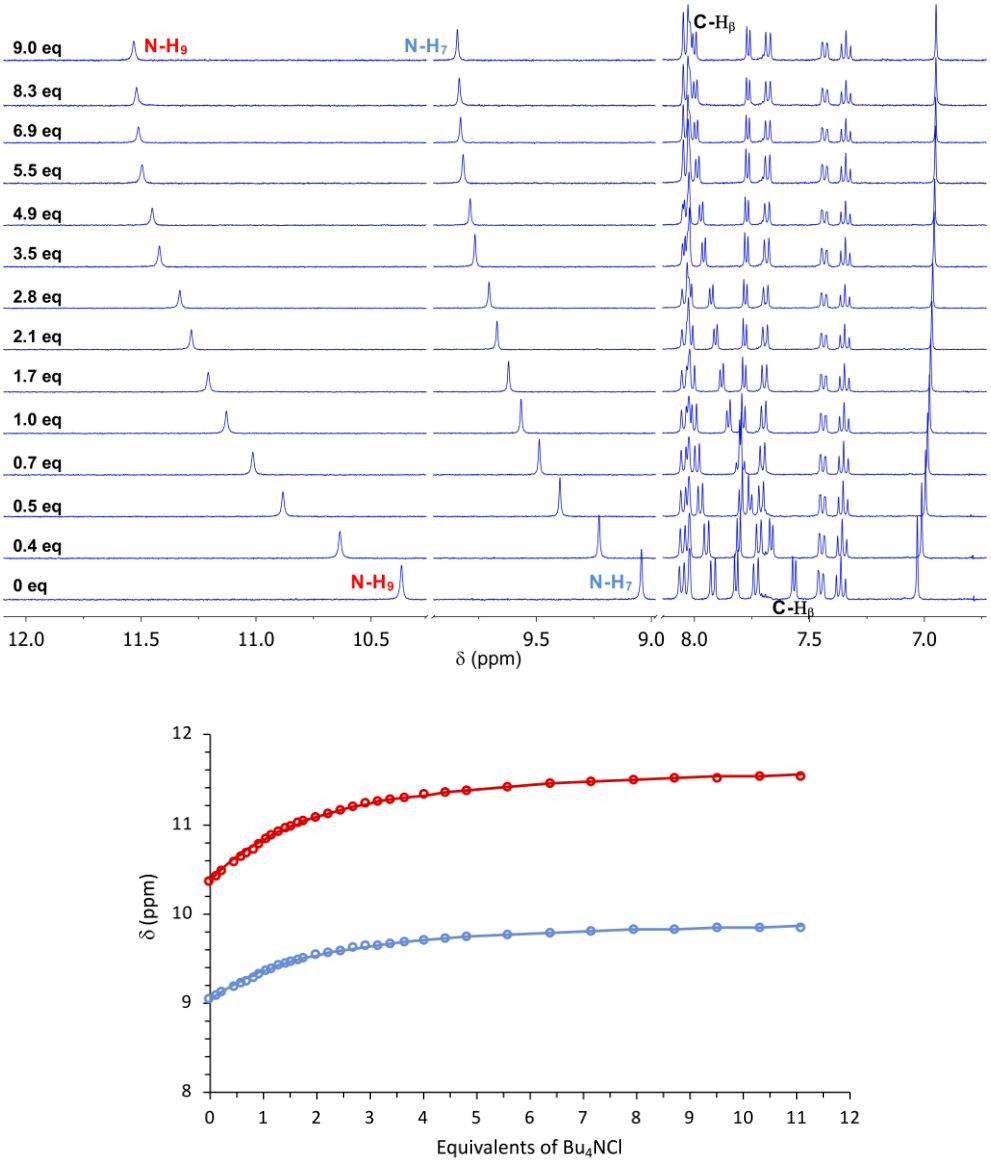

Figure S44. ^{1}H NMR titration of **16** (4.1 mM) with Bu_4NCl in DMSO-d_6/0.5% H_2O (400.13 MHz, 293 K): Top - stacked spectra showing the variations in chemical shifts of N_7-H, N_9-H and C-H_b along the titration; Bottom - binding isotherms constructed with δ of N_7-H (∘) and N_9-H (∘) together with their curves fitted (68 points) to 1:1 binding model (solid lines).

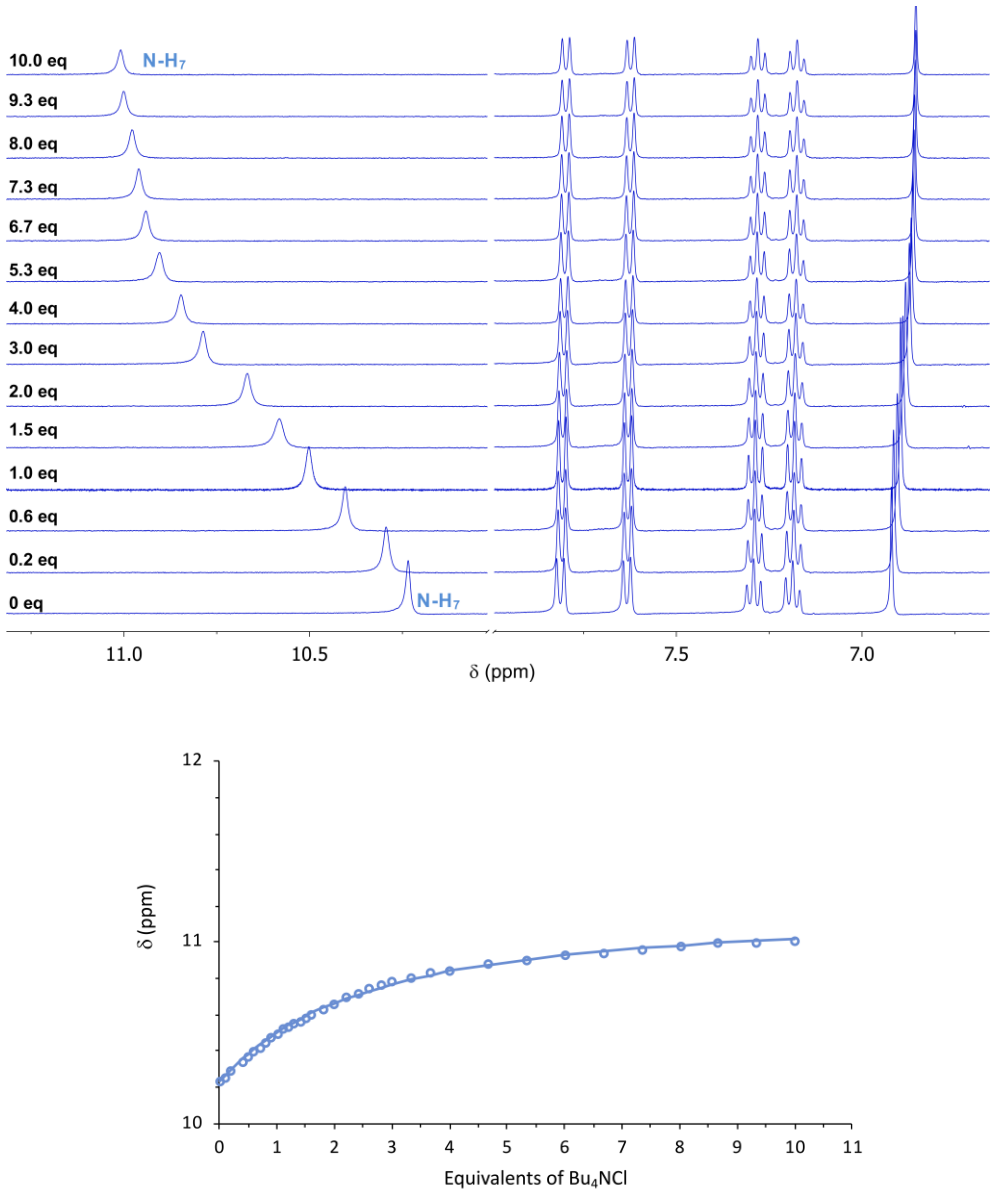

Figure S45. ^{1}H NMR titration of **17** (8.6 mM) with Bu_4NCl in DMSO-d_6/0.5% H_2O (400.13 MHz, 293 K): Top - stacked spectra showing the variations in chemical shifts of N_7-H and N_9-H along the titration; Bottom - binding isotherms constructed with δ of N_7-H (∘) together with its curve fitted (35 points) to 1:1 binding model (solid line).

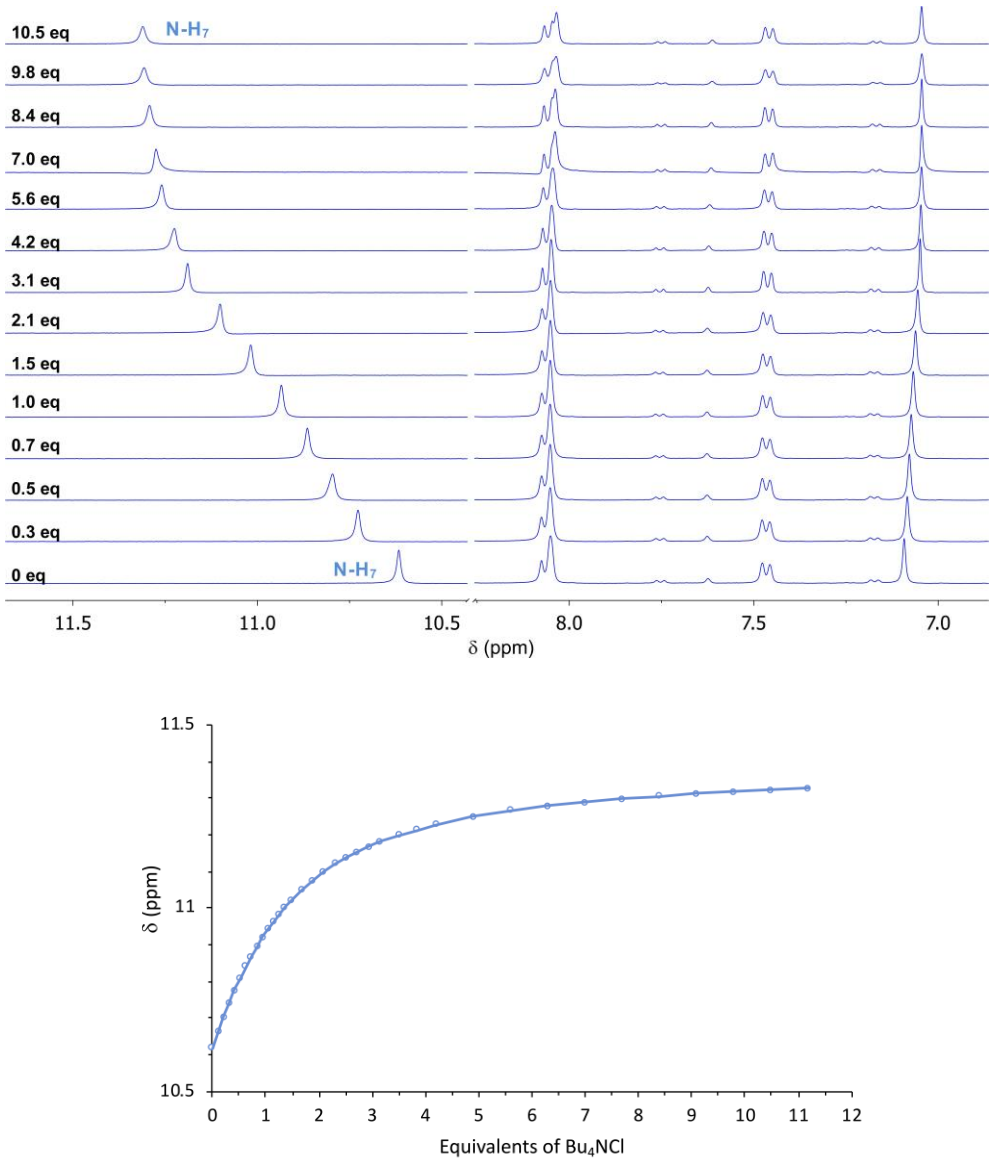

Figure S46. ^{1}H NMR titration of **18** (12.7 mM) with Bu_4NCl in DMSO-d_6/0.5% H_2O (400.13 MHz, 293 K): Top - stacked spectra showing the variations in chemical shifts of N_7-H and N_9-H along the titration; Bottom - binding isotherms constructed with δ of N_7-H (○) together with its curve fitted (36 points) to 1:1 binding model (solid line).

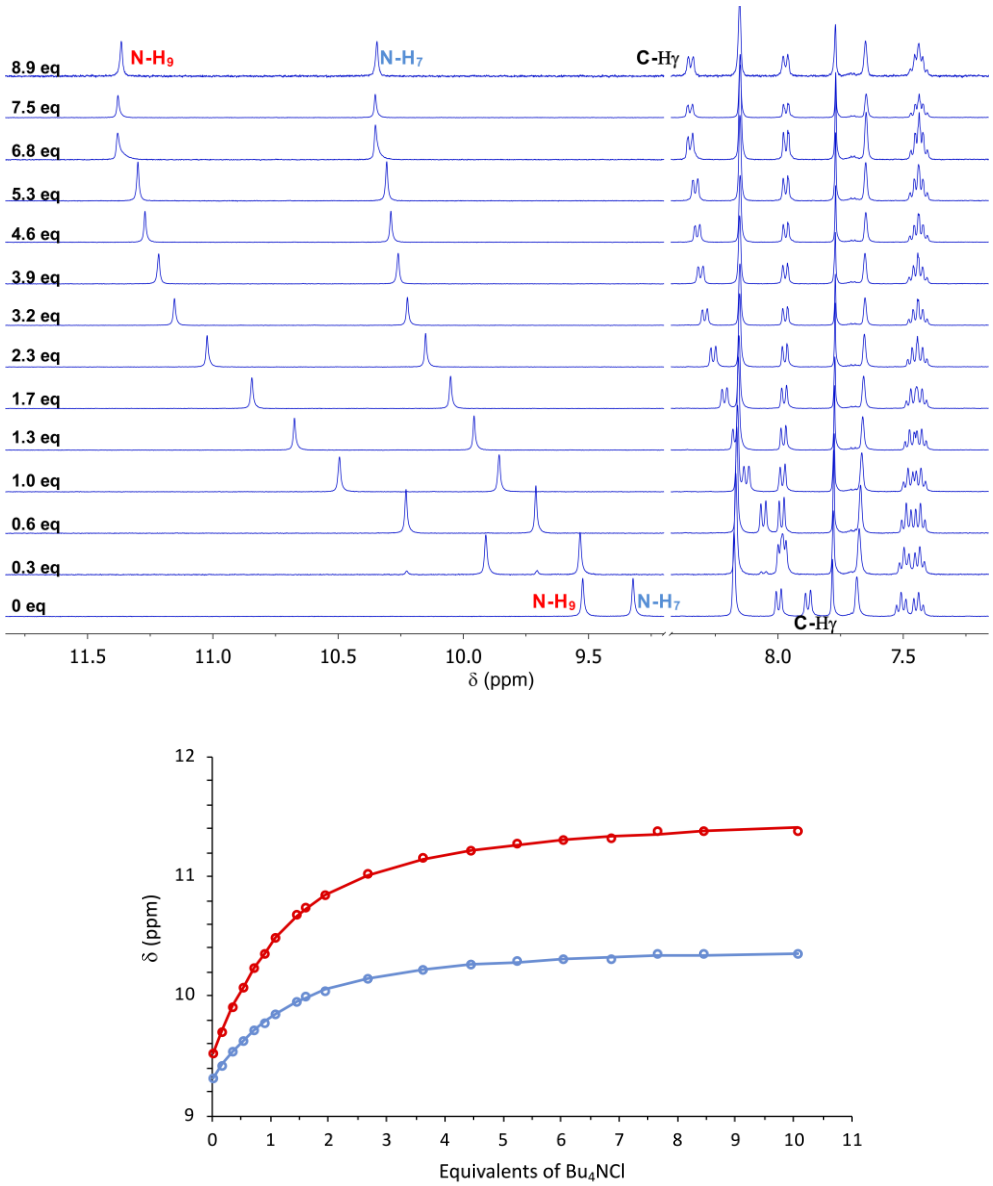

Figure S47. ^{1}H NMR titration of **19** (8.9 mM) with Bu_4NCl in DMSO-d_6/0.5% H_2O (400.13 MHz, 293 K): Top - stacked spectra showing the variations in chemical shifts of N_7-H, N_9-H and C-H_γ along the titration; Bottom - binding isotherms constructed with δ of N_7-H (○) and N_9-H (○) together with their curves fitted (38 points) to 1:1 binding model (solid lines).

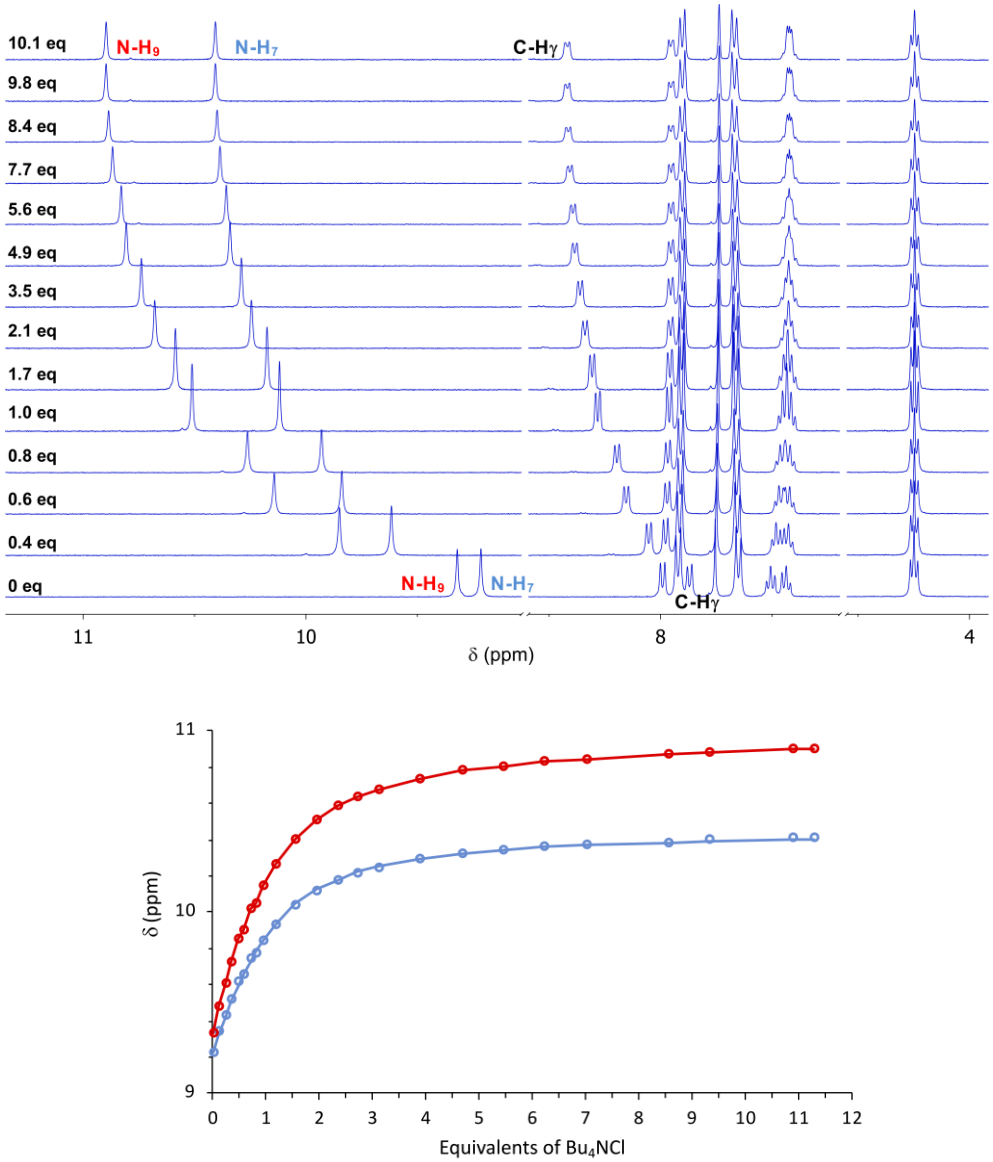

Figure S48. ^{1}H NMR titration of **20** (10.1 mM) with Bu_4NCl in DMSO-d_6/0.5% H_2O (400.13 MHz, 293 K): Top - stacked spectra showing the variations in chemical shifts of N_7-H, N_9-H and C-H_γ along the titration; Bottom - binding isotherms constructed with δ of N_7-H (∘) and N_9-H (∘) together with their curves fitted (48 points) to 1:1 binding model (solid lines).

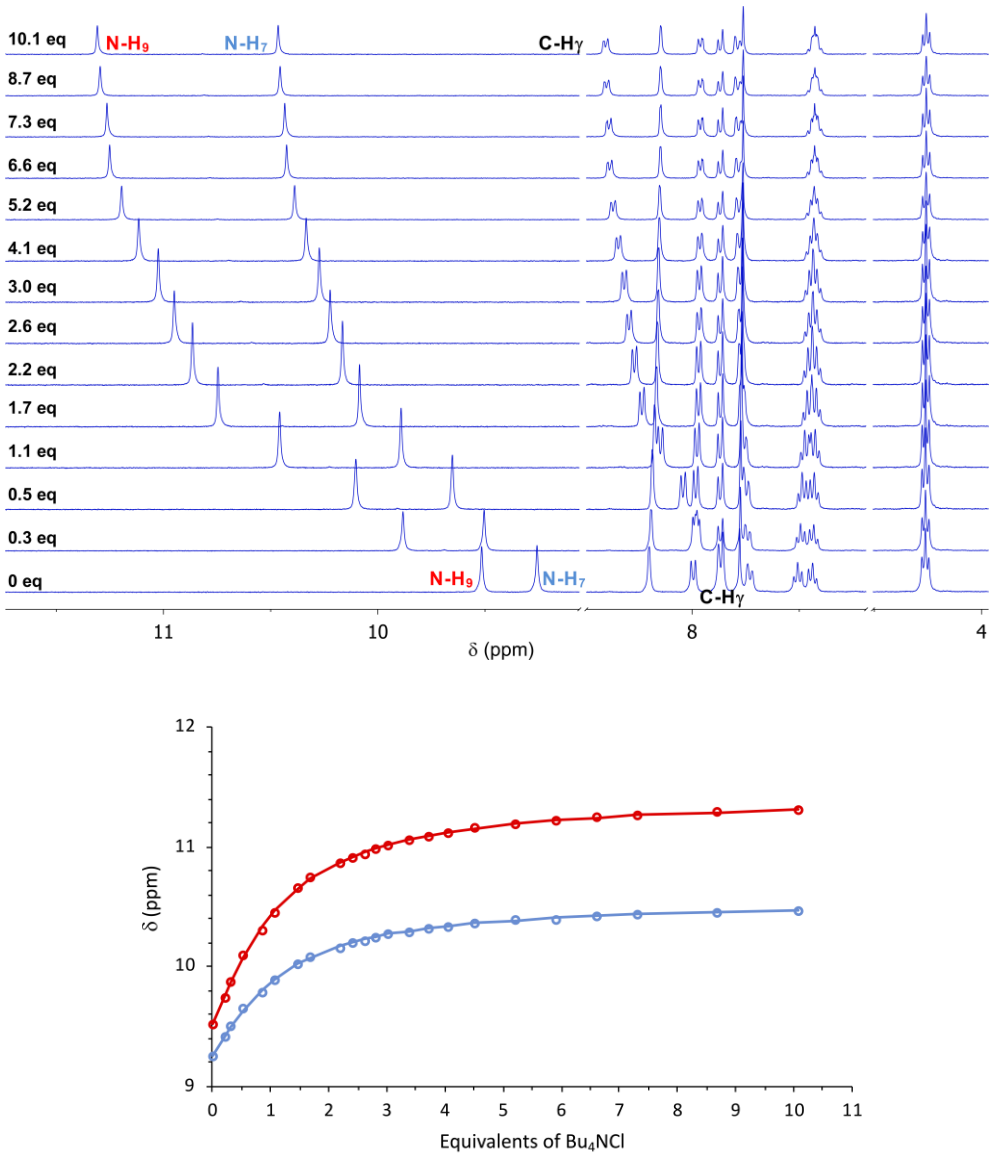

Figure S49. ^{1}H NMR titration of **21** (10.1 mM) with Bu_4NCl in DMSO-d_6/0.5% H_2O (400.13 MHz, 293 K): Top - stacked spectra showing the variations in chemical shifts of N_7-H, N_9-H and C-H_γ along the titration; Bottom - binding isotherms constructed with δ of N_7-H (○) and N_9-H (○) together with their curves fitted (46 points) to 1:1 binding model (solid lines).

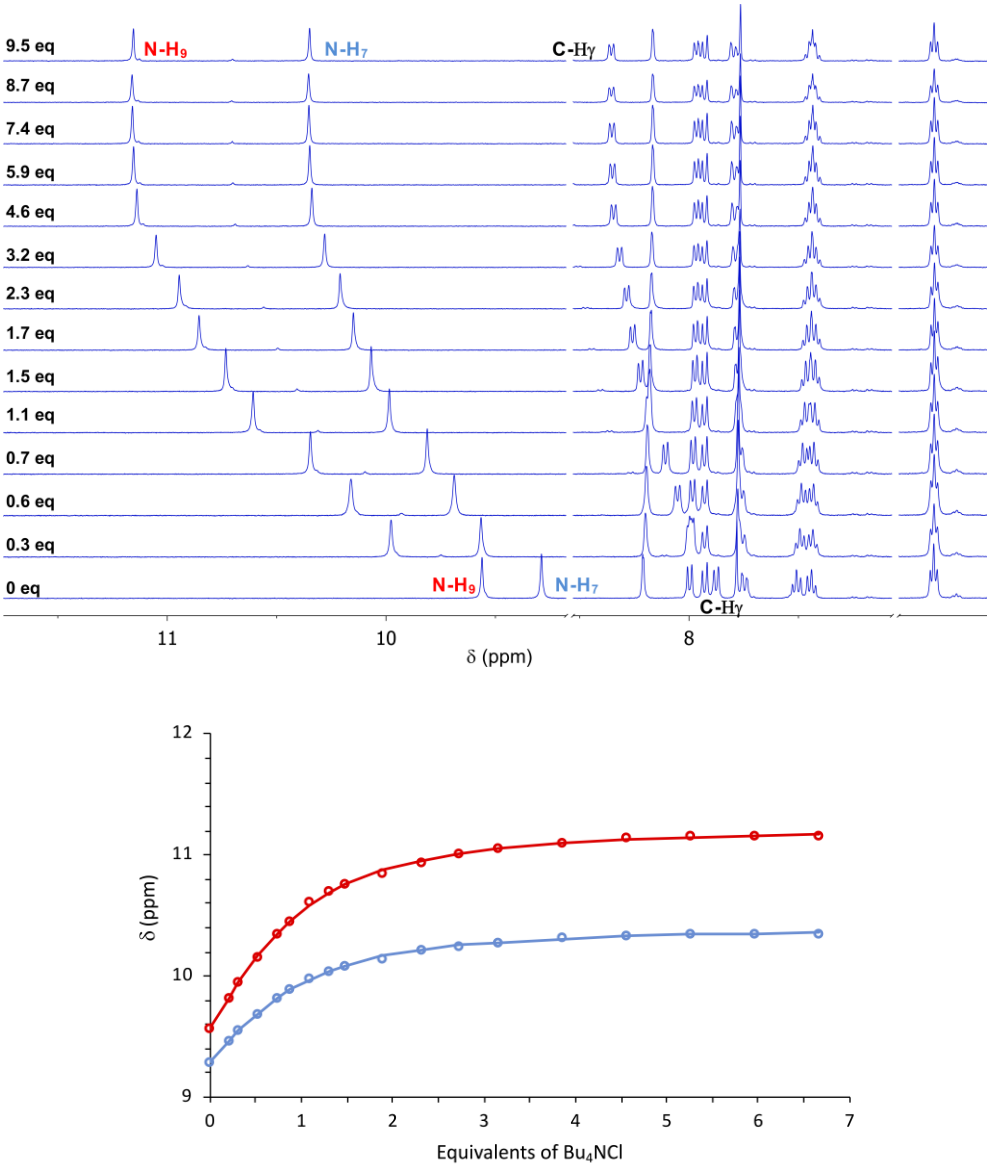

Figure S50. ^{1}H NMR titration of **22** (10.0 mM) with Bu_4NCl in DMSO-d_6/0.5% H_2O (400.13 MHz, 293 K): Top - stacked spectra showing the variations in chemical shifts of N_7-H, N_9-H and C-H_γ along the titration; Bottom - binding isotherms constructed with δ of N_7-H (○) and N_9-H (○) together with their curves fitted (36 points) to 1:1 binding model (solid lines).

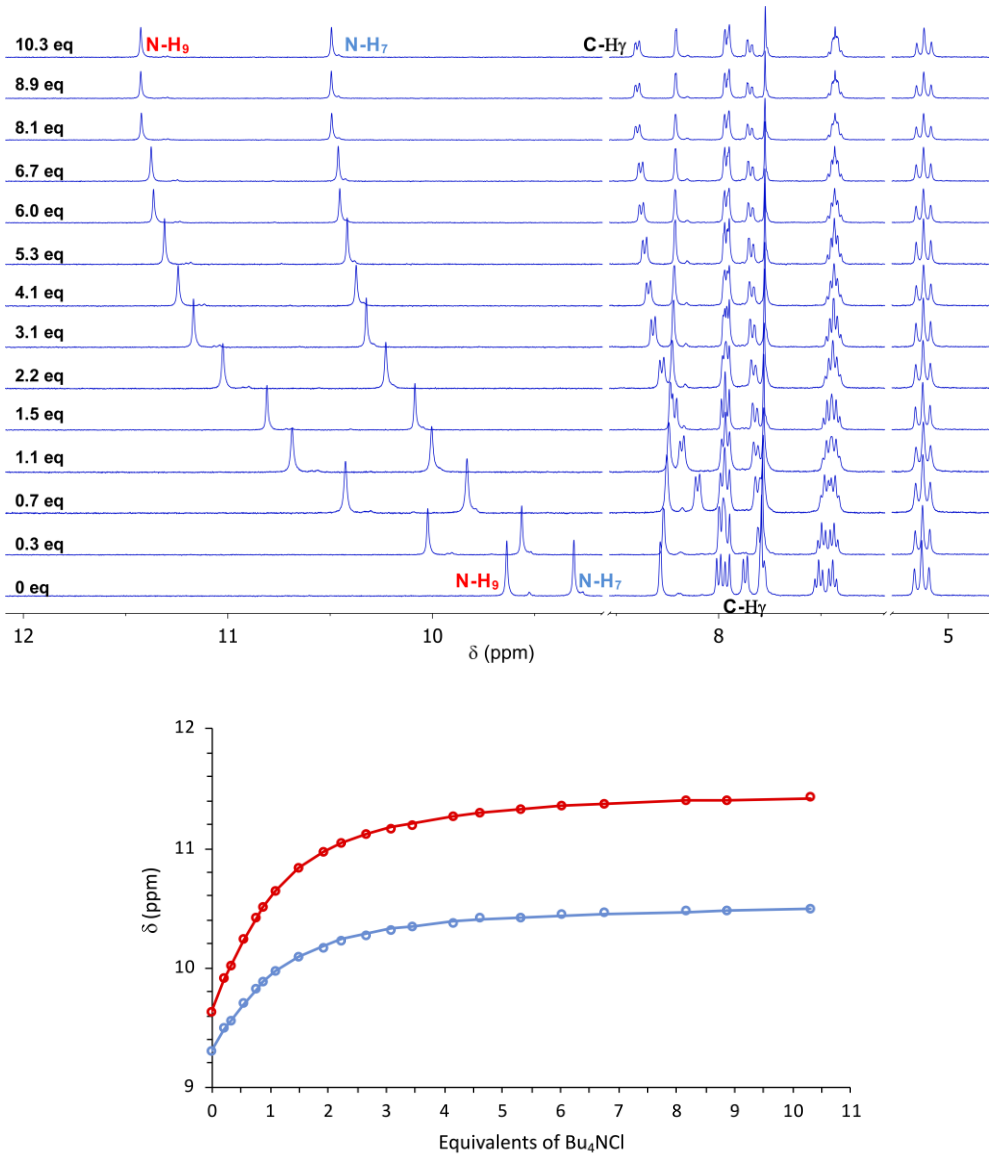

Figure S51. ^{1}H NMR titration of **23** (10.0 mM) with Bu_4NCl in DMSO-d_6/0.5% H_2O (400.13 MHz, 293 K): Top - stacked spectra showing the variations in chemical shifts of N_7-H, N_9-H and C-H_γ along the titration; Bottom - binding isotherms constructed with δ of N_7-H (○) and N_9-H (○) together with their curves fitted (42 points) to 1:1 binding model (solid lines).

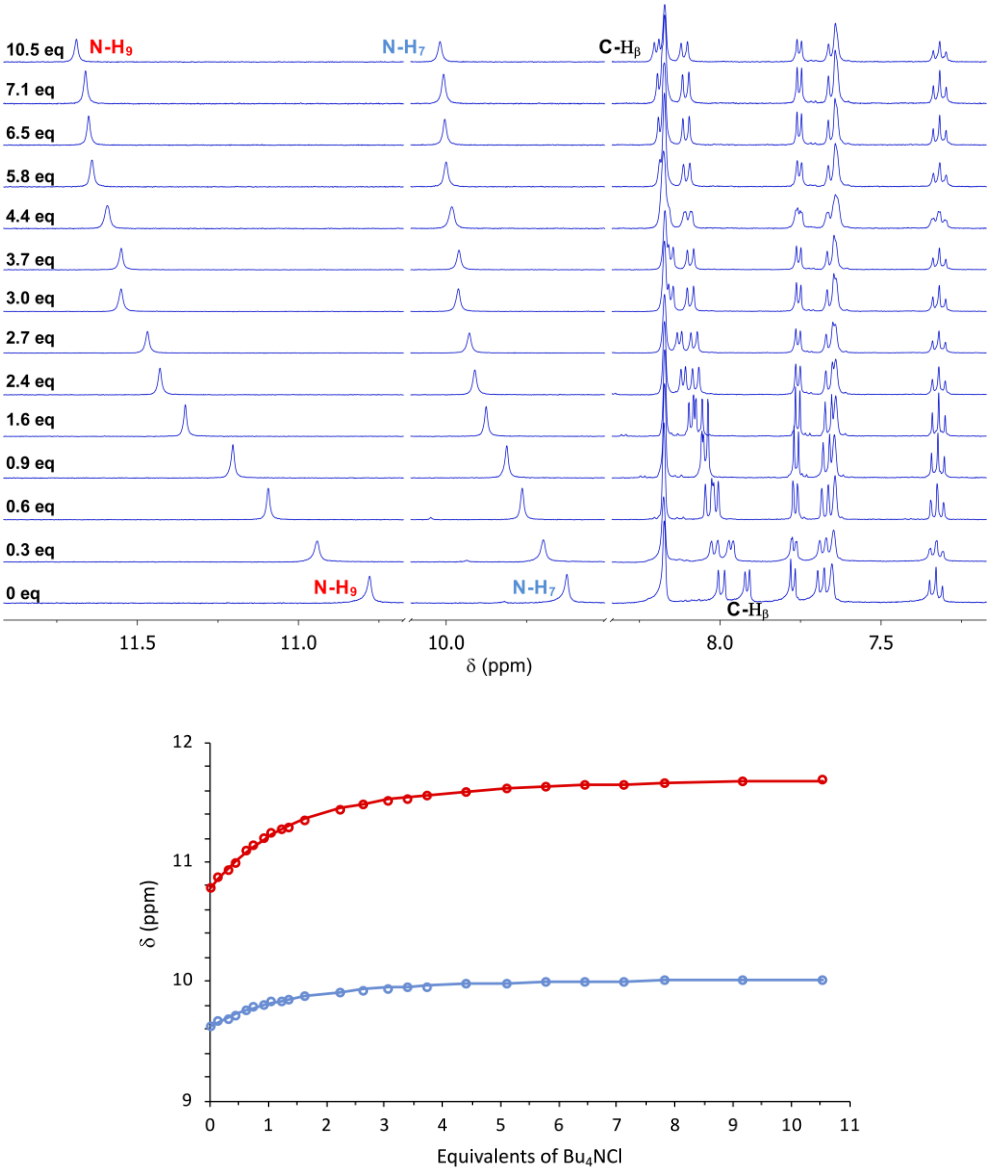

Figure S52. ^{1}H NMR titration of **24** (10.0 mM) with Bu_4NCl in DMSO-d_6/0.5% H_2O (400.13 MHz, 293 K): Top - stacked spectra showing the variations in chemical shifts of N_7-H, N_9-H and C-Hβ along the titration; Bottom - binding isotherms constructed with δ of N_7-H (○) and N_9-H (○) together with their curves fitted (48 points) to 1:1 binding model (solid lines).

Quantum studies

Additional details and Methods

All DFT calculations were carried out with the Gaussian 09 software,[5] These calculations include the geometry optimisations of the free mono-(thio)urea derivatives and their chloride complexes and the assessment of the distribution of electrostatic potential.

As explained in the main text, DFT calculations on chloride complexes of **1-24** were carried out in a single binding scenario by atomic manipulation of the crystal structures reported in this work. The chloride complexes were DFT optimised with the PBE0 functional coupled with Grimme's D3 dispersion correction,[6] and the 6-311+++G(3df,3pd) basis set,[7] obtained from the Basis Set Exchange database.[8] The solvent effects were account through the conductor-like polarisable continuum model (CPCM) formalism.[9] The structures of the free receptors were generated from the DFT structures of the complexes and subsequently were optimised at the same level of theory. All optimised geometries have been characterised as local minima by the absence of imaginary frequencies and are available for download as XYZ coordinate files.

The distribution of the electrostatic potential (V_S) on the molecular surface of each mono-(thio)urea small receptor was computed from previously optimised structures of its chloride complex, after removal of the anion, at the same level of theory. Afterwards, V_S was evaluated on the 0.001 electrons Bohr^{-3} contour of ρ. The electrostatic potential surface ranges, including the most positive and most negative values ($V_{S,max}$ and $V_{S,min}$, respectively), were ascertained using Multiwfn.[10]

The strength of the hydrogen bonding interactions between the receptors **1-24** and chloride was evaluated through the Quantum Theory of Atoms in Molecules (QTAIM)[11] and the Natural Bond Orbital (NBO) analysis.[12] The QTAIM analysis yielded the electron density (ρ), its Laplacian derivative ($\nabla^2\rho$) and the potential energy density ($\mathcal{V}$) for all hydrogen bonding interactions, together with their energy (EHB), estimated from $\mathcal{V}$ as $E_{HB} = ½\mathcal{V}$.[13] All $\nabla^2\rho$ calculated values are positive, indicating a depletion of the electron distribution consistent with the formation of the hydrogen bonding interactions. In the NBO analysis, the N-H···Cl$^-$ and C-H···Cl$^-$ hydrogen bonds were assessed as interactions between the lone pair orbitals of the chloride (n_{Cl^-}) and the antibonding orbitals from the N-H or C-H binding units (σ^*_{N-H} or σ^*_{C-H}) in **1-24**: $n_{Cl^-} \rightarrow \sigma^*_{N-H}$ and $n_{Cl^-} \rightarrow \sigma^*_{C-H}$, affording the E^2 stabilisation energies, related with the electron delocalisation from the lone pair orbitals to the antibonding ones.[12a, 14]

The images of computed structures as well as the representations of the electrostatic potential distributions onto the molecular surfaces were made with Pymol 2.5.[15]

Supplementary DFT Figures

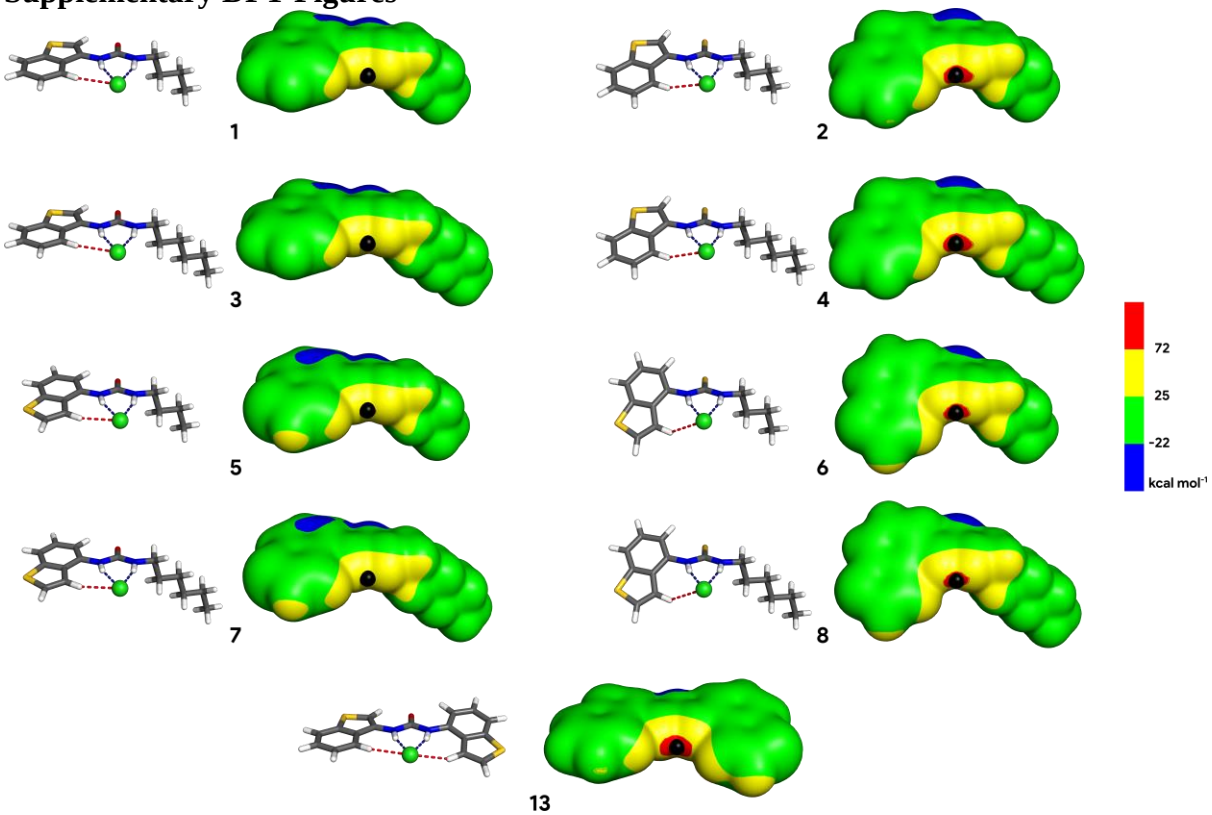

Figure S53. DFT optimised structures of the chloride associations of β- (**1-4**), γ- (**5-8**) and β,γ- (**13**) benzo[*b*]thiophene derivatives, with the anion being recognised by two N-H···Cl^- hydrogen bonds from the (thio)urea binding unit (blue dashed lines), aided by one or two C-H···Cl^- interactions from the β- or γ-benzo[*b*]thiophene fragments (red dashed lines). Each DFT optimised structure is accompanied by the respective distribution of electrostatic potential mapped onto the molecular surface of the receptor, at 0.001 *e*$Bohr^{-1}$ contour.

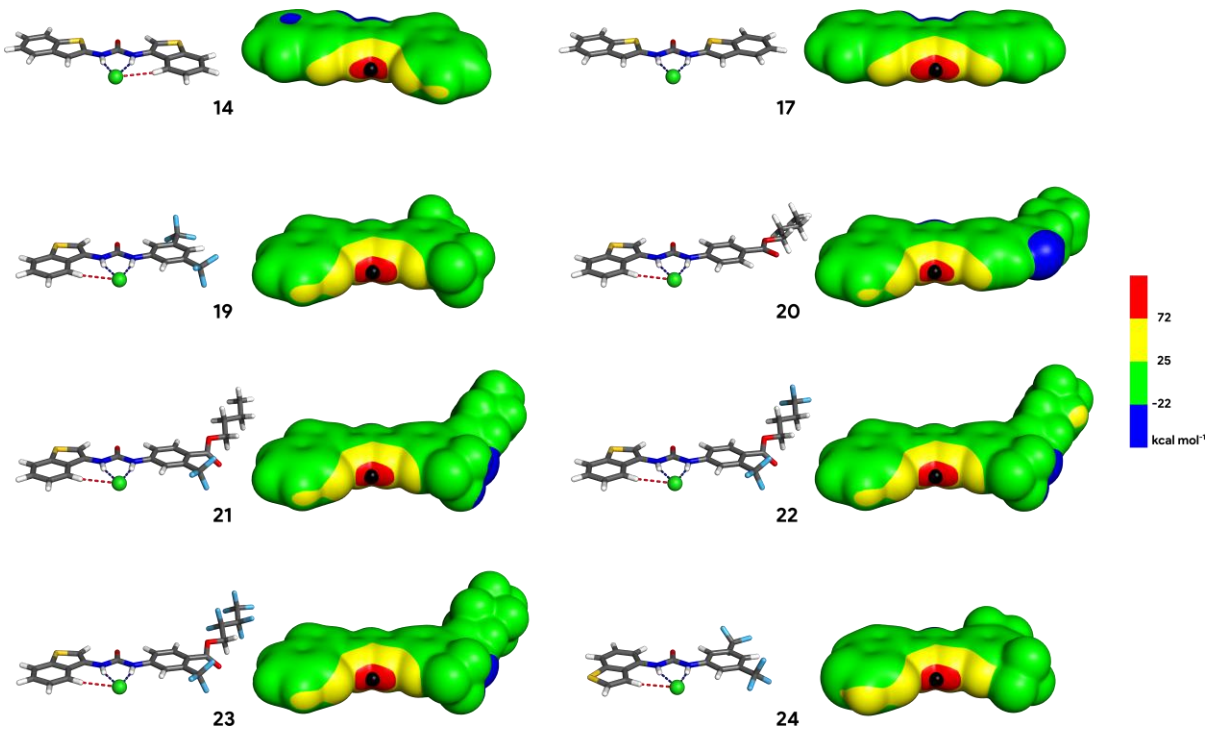

Figure S54. DFT optimised structures of the chloride associations of α,β- (**14**), α,α- (**17**), β- (**19-23**), and γ- (**24**) benzo[*b*]thiophene derivatives, together with the V_S of the corresponding receptors. Remaining details as given in Figure S53.

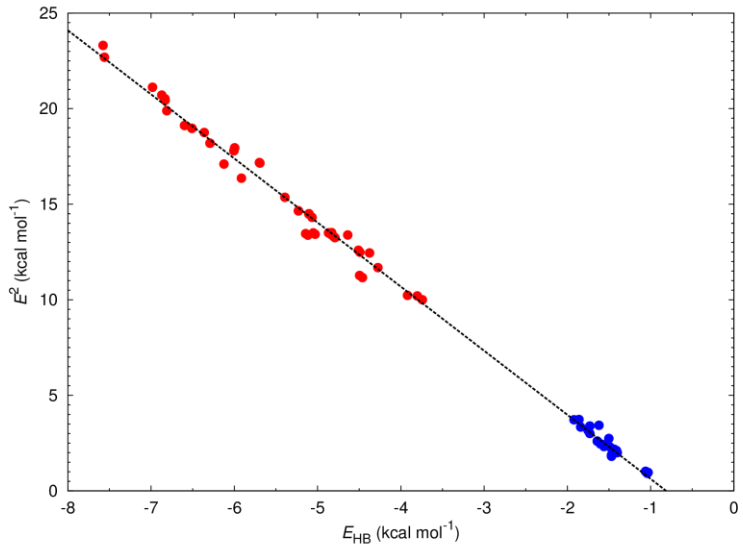

Figure S55. E^2 *vs*. E_{HB} for the N-H···Cl$^-$ (•) and C-H···Cl$^-$ (•) interactions, with an $R^2 > 0.99$ for the whole dataset, $R^2 > 0.98$ for the 96 N-H···Cl$^-$ interactions and $R^2 > 0.92$ for the 54 C-H···Cl$^-$ ones.

Supplementary DFT Tables

Captions for supplementary tables on the "Tables_S1_S2_S3_S4.xlsx" file:

Table S1. Dimensions of the N-H···Cl$^-$ and C-H···Cl$^-$ dimensions in the chloride associations of **1**-**24**, together with the ξ torsional angles.

Table S2. Average and range of N-H···Cl$^-$ and C-H···Cl$^-$ dimensions, together with the average and range of ξ torsional angles (see Scheme 3, main text), grouped by binding unit (urea or thiourea) and by its decorating motif.

Table S3. E_{HB} and E^2 values (kcal mol^{-1}) assessed for the individual N-H···Cl$^-$ and C-H···Cl$^-$ interactions in the chloride complexes of **1**-**24**.

Table S4. Average and range of E_{HB} and E^2 values (kcal mol^{-1}) assessed for the N-H···Cl$^-$ and C-H···Cl$^-$ interactions in the chloride complexes of **1**-**24**, grouped by binding unit (urea or thiourea) and by its decorating motif.

Table S5. Uncorrected electronic binding energies ($\Delta\varepsilon_{sol}$), Zero Point Corrections (ΔZPE),[a] thermal corrected binding energies (ΔE),[b] binding enthalpies (ΔH),[c] binding entropies term contribution ($T\Delta S$),[d] binding free energies (ΔG^D),[e] and standard state corrected binding free energies (ΔG^{SS})[f] (in kcal mol^{-1}) estimated from the DFT optimised structures of the chloride complexes of **1**-**24**, using the CPCM DMSO solvent model calculations.

Receptor	$\Delta\varepsilon_{sol}$	ΔZPE	ΔE	ΔH	$T\Delta S$	ΔG	ΔG^{SS}
1	-10.43	0.45	-9.66	-10.25	-7.15	-3.10	-4.99
2	-11.01	0.49	-10.20	-10.80	-7.32	-3.48	-5.37
3	-10.44	0.43	-9.69	-10.29	-7.24	-3.05	-4.94
4	-10.99	0.44	-10.20	-10.80	-7.04	-3.76	-5.65
5	-10.51	0.44	-9.78	-10.38	-7.77	-2.61	-4.50
6	-10.62	0.48	-9.83	-10.42	-7.20	-3.22	-5.11
7	-10.55	0.48	-9.17	-9.76	-5.13	-4.63	-6.52
8	-10.62	0.52	-9.81	-10.40	-7.29	-3.11	-5.00
9	-13.27	0.49	-12.58	-13.18	-7.05	-6.12	-8.01
10	-12.30	0.79	-11.33	-11.92	-8.30	-3.62	-5.51
11	-12.96	0.49	-12.24	-12.83	-8.12	-4.72	-6.61
12	-11.97	0.68	-11.09	-11.68	-7.82	-3.87	-5.76
13	-13.14	0.41	-12.45	-13.04	-7.72	-5.32	-7.21
14	-13.14	0.35	-12.54	-13.13	-7.75	-5.37	-7.26
15	-13.40	0.14	-12.93	-13.52	-7.10	-6.42	-8.31
16	-13.44	0.14	-12.94	-13.54	-7.07	-6.47	-8.36
17	-12.86	0.13	-12.44	-13.03	-7.20	-5.84	-7.73
18	-13.40	0.10	-13.01	-13.60	-8.22	-5.38	-7.27
19	-13.42	0.18	-12.90	-13.49	-7.88	-5.61	-7.50
20	-12.91	0.40	-12.24	-12.84	-8.03	-4.80	-6.69
21	-13.39	0.31	-12.75	-13.34	-7.30	-6.04	-7.93
22	-13.42	0.24	-12.86	-13.45	-7.49	-5.96	-7.85
23	-13.59	0.26	-13.00	-13.60	-7.44	-6.16	-8.05
24	-13.41	0.19	-12.85	-13.44	-7.40	-6.04	-7.93

[a] ΔZPE is included in the ΔE, ΔH and ΔG terms; [b] $\Delta E = \Delta\varepsilon_{sol} + \Delta E_{Tot}$, where ΔE_{Tot} accounts for the differences in the internal energy due to translational, rotational, vibrational and electronic motions; [c] $\Delta H = \Delta E + \Delta nRT$, where n is -1 for a 1:1 host-guest systems, R is the ideal gas constant and T is the temperature (298.15 K); [d] $\Delta S = \Delta S_{translational} + \Delta S_{rotational} + \Delta S_{vibrational}$; [e] $\Delta G = \Delta H - T\Delta S$; [f] ΔG^{SS} is the free energy (ΔG^D) including a –1.89 kcal mol^{-1} correction which corresponds to the conversion from the standard state at 1 atm (1 mol per 24.46 L at 298.15 K) to 1 M (1 mol/L at 298.15 K).[16]

Crystallographic studies

Data collection and structure refinement

Single crystals of three free receptors, **5**, **11** and **22**, four DMSO associations of **19**, **24**, **16** and **20**, and four chloride complexes of **9**, **14**, **15** and **21**, were obtained from DMSO solutions obtained upon ^{1}H NMR titrations of these small-molecules with tetrabutylammonium. X-ray diffraction data were collected at low temperature (150 K) on a Bruker D8 QUEST diffractometer with a photon 100 CMOS detector, using monochromated Mo-Kα radiation (λ = 0.71073 Å). The structures were solved by intrinsic phasing with SHELXT[17] and refined by least-squares methods using SHELXL,[18] within the Olex2 crystallographic package.[19] All non-hydrogen atoms were refined with anisotropic thermal displacements while the hydrogen atoms were placed in calculated positions and refined using the riding model.

Despite the low quality of the X-ray diffraction data of **19**·DMSO, indicated by the gauged R_{int} value of 0.1226 (Table S7), its crystal structure was unambiguously determined. The difference Fourier maps showed that one of DMSO solvent molecules in the asymmetric unit was disordered. This molecule was refined with the sulfur and the methyl groups occupying two alternative positions with occupancy factors of 1-*x* and *x*, being *x* equal to 0.575(6). In the crystal structure of **20**·DMSO, the solvent molecule was also refined applying an equivalent disorder model, with *x* value of 0.652(1).

The single crystals of **21**·Cl·TBA also showed a poor-quality for X-ray structure determination. In line, the selected crystal for data collection displayed a diffraction pattern composed of low intensity reflections with a sen(θ)/λ up to 0.557 Å^{-1}, slightly below the recommended value (sen(θ_{max})/λ = 0.575 Å^{-1}), and a high R_{int} value of 0.1629. Despite the low-quality of the X-ray data, the structure was unequivocally determined without disorder and with acceptable *R* values (see Table S8).

In the crystal structure of **15**$_2$·Cl·TBA an alkyl chain of the TBA counter-ion and a -CF_3 substituent of the receptor were found disordered. The alkyl chain was refined in two alternative positions with equal occupancy factors of 0.5. The -CF_3 substituent was also refined with each fluorine atom occupying two alternative tetrahedral sites with occupancy factors set to 0.25 and 0.75. Moreover, distance restraints (DFIX for the C-F bonds and SAID for the C-F bonds and F···F distances) and anisotropic thermal displacement restraints (ISOR) were applied in the refinement of this substituent. However, the high values of the anisotropic parameters calculated for each fluorine atom suggested a more complex disorder model and further attempts to improve the -CF_3 disorder model were unsuccessful.

The thermal ellipsoids were made with Mercury,[20] while the crystal packing diagrams were made with Pymol.[15]

The crystal data together with pertinent data collection and refinement details, along with the Cambridge Crystallographic Data Centre (CCDC) deposit numbers, are summarised in Table S6 for free receptors **5**, **11**, and **22**, in Table S7 for DMSO associations of **16**, **19**, **20**, and **24**, and in Table S8 for chloride complexes of **9**, **14**, **15**, and **21**.

Table S6. Crystal data and structure refinement details for free receptors

Compound	**5**	**11**	**22**
CCDC Deposition Number	2120023	2120027	2120025
Empirical formula	$C_{13}H_{16}N_2OS$	$C_{17}H_{12}N_2OS_2$	$C_{21}H_{16}F_6N_2O_3S$
Formula weight	248.34	324.41	490.42
Crystal size/mm^3	0.160 × 0.100 × 0.020	0.180 × 0.100 × 0.030	0.180 × 0.120 × 0.010
Crystal system	monoclinic	monoclinic	monoclinic
Space group	$P2_1/c$	$C2/c$	$P2_1/c$
a/Å	9.7310(7)	24.2459(18)	19.4220(8)
b/Å	8.1438(6)	4.5454(3)	7.9240(3)
c/Å	16.5793(12)	12.9168(9)	13.4721(6)
α/°	(90)	(90)	(90)
β/°	104.951(3)	97.998(2)	103.664(2)
γ/°	(90)	(90)	(90)
Volume/Å^3	1269.39(16)	1409.68(17)	2014.67(15)
Z	4	4	4
ρ_{calc} g/cm^3	1.299	1.529	1.617
μ/mm^{-1}	0.240	0.380	0.244
F(000)	528.0	672.0	1000.0
2θ range for data collection/°	5.086 to 50.758	6.37 to 61.098	5.576 to 55.986
Index ranges	$-11 \le h \le 11$, $-9 \le k \le 9$, $-19 \le l \le 19$	$-34 \le h \le 34$, $-6 \le k \le 6$, $-18 \le l \le 18$	$-25 \le h \le 25$, $-10 \le k \le 10$, $-17 \le l \le 17$
Reflections collected	14162	21612	78765
Independent reflections, R_{int}, R_{sigma}	2321, 0.0742, 0.0478	2169, 0.0709, 0.0337	4791, 0.0309, 0.0120
Data/restraints/parameters	2321/0/155	2169/0/101	4791/0/298
Final R indexes [$I \geq 2\sigma(I)$], R_1, wR_2	0.0459, 0.1200	0.0405, 0.1008	0.0412, 0.1068
Final R indexes [all data], R_1, wR_2	0.0677, 0.1400	0.0476, 0.1060	0.0452, 0.1100
Largest diff. peak/hole /eÅ^{-3}	0.32/-0.30	0.40/-0.30	0.67/-0.67

Table S7. Crystal data and structure refinement details for mono-urea associations with dimethyl sulfoxide.

Compound	**16**·DMSO	**19**·DMSO	**20**·DMSO	**24**·DMSO
CCDC Deposition Number	2120028	2120020	2120019	2120022
Empirical formula	$C_{20}H_{17}F_3N_2O_2S_3$	$C_{19}H_{16}F_6N_2O_2S_2$	$C_{22}H_{26}N_2O_4S_2$	$C_{19}H_{16}F_6N_2O_2S_2$
Formula weight	470.53	482.46	446.57	482.46
Crystal size/mm^3	0.200 × 0.100 × 0.010	0.300 × 0.180 × 0.020	0.180 × 0.080 × 0.020	0.200 × 0.060 × 0.040
Crystal system	monoclinic	triclinic	monoclinic	monoclinic
Space group	$P2_1/n$	$P\bar{1}$	$P2_1/n$	$P2_1/n$
a/Å	14.0348(9)	9.563(6)	11.6491(7)	9.5027(6)
b/Å	8.9460(6)	14.457(8)	15.6763(8)	7.6506(5)
c/Å	17.4837(10)	15.780(9)	13.3173(7)	28.0513(17)
α/°	(90)	84.87(2)	(90)	(90)
β/°	111.279(2)	85.747(18)	112.574(2)	95.558(2)
γ/°	(90)	78.59(2)	(90)	(90)
Volume/Å^3	2045.5(2)	2126(2)	2245.6(2)	2029.8(2)
Z	4	4	4	4
ρ_{calc}g/cm^3	1.528	1.507	1.321	1.579
μ/mm^{-1}	0.410	0.321	0.268	0.336
F(000)	968.0	984.0	944.0	984.0
2θ range for data collection/°	3.208 to 54.386	4.352 to 51.198	4.21 to 54.43	4.412 to 52.976
Index ranges	$-17 \le h \le 18$, $-11 \le k \le 11$, $-22 \le l \le 22$	$-11 \le h \le 11$, $-16 \le k \le 17$, $-19 \le l \le 19$	$-14 \le h \le 14$, $-20 \le k \le 20$, $-17 \le l \le 17$	$-11 \le h \le 11$, $-9 \le k \le 9$, $-35 \le l \le 35$
Reflections collected	53256	48849	93888	38399
Independent reflections, R_{int}, R_{sigma}	4540, 0.0457, 0.0249	7921, 0.1226, 0.0781	4987, 0.0321, 0.0114	4184, 0.0416, 0.0209
Data/restraints/parameters	4540/0/273	7921/12/593	4987/0/284	4184/0/282
Final R indexes [$I \geq 2\sigma(I)$], R_1, wR_2	0.0384, 0.0925	0.1011, 0.2715	0.0385, 0.0959	0.0422, 0.0987
Final R indexes [all data], R_1, wR_2	0.0552, 0.1022	0.1295, 0.2948	0.0454, 0.1025	0.0540, 0.1056
Largest diff. peak/hole /eÅ^{-3}	0.82/-0.62	0.80/-0.42	0.50/-0.42	0.58/-0.58

Table S8. Crystal data and structure refinement details for chloride associations.

Compound	**9**·Cl·TBA	**14**·Cl·TBA	**15**$_2$·Cl·TBA	**21**·Cl·TBA
CCDC Deposition Number	2120018	2120024	2120029	2120021
Empirical formula	$C_{33}H_{48}ClN_3OS_2$	$C_{33}H_{48}ClN_3OS_2$	$C_{52}H_{58}ClF_6N_5O_2S_4$	$C_{37}H_{55}ClF_3N_3O_3S$
Formula weight	602.31	602.31	1062.72	714.35
Crystal size/mm^3	0.32 × 0.20 × 0.10	0.220 × 0.080 × 0.020	0.22 × 0.10 × 0.002	0.100 × 0.080 × 0.010
Crystal system	monoclinic	orthorhombic	triclinic	monoclinic
Space group	$P2_1/c$	$P2_12_12_1$	$P\bar{1}$	$P2_1/n$
a/Å	8.3411(3)	8.2884(7)	12.6628(9)	11.2847(12)
b/Å	22.5958(9)	18.0404(15)	14.0933(9)	28.302(3)
c/Å	17.9310(7)	21.5174(15)	16.5930(12)	12.3152(14)
α/°	(90)	(90)	105.085(3)	(90)
β/°	101.716(2)	(90)	93.470(3)	102.183(4)
γ/°	(90)	(90)	110.692(3)	(90)
Volume/Å^3	3309.1(2)	3217.4(4)	2636.3(3)	3844.6(8)
Z	4	4	2	4
ρ_{calc}g/cm^3	1.209	1.243	1.339	1.234
μ/mm^{-1}	0.271	0.279	0.297	0.206
F(000)	1296.0	1296.0	1112.0	1528.0
2θ range for data collection/°	3.604 to 52.792	4.516 to 54.28	4.32 to 50.902	3.676 to 46.688
Index ranges	$-10 \le h \le 9$, $-28 \le k \le 28$, $-22 \le l \le 17$	$-10 \le h \le 10$, $-23 \le k \le 23$, $-27 \le l \le 26$	$-15 \le h \le 15$, $-17 \le k \le 17$, $-20 \le l \le 20$	$-12 \le h \le 12$, $-31 \le k \le 31$, $-13 \le l \le 13$
Reflections collected	37997	79809	99965	84519
Independent reflections, R_{int}, R_{sigma}	6786, 0.0660,0.0630	7108, 0.0325, 0.0161	9720, 0.0593, 0.0271	5572, 0.1629,0.0550
Data/restraints/parameters	6786/0/365	7108/0/366	9720/60/691	5572/0/439
Final R indexes [$I \geq 2\sigma(I)$], R_1, wR_2	0.0461, 0.0940	0.0294, 0.0822	0.0393, 0.0913	0.0498, 0.1219
Final R indexes [all data], R_1, wR_2	0.0821, 0.1036	0.0307, 0.0832	0.0590, 0.1014	0.0920, 0.1440
Largest diff. peak/hole /eÅ^{-3}	0.33/-0.31	0.59/-0.31	0.31/-0.44	0.59/-0.27

Crystal packing features

The free receptors **5** and **11** are self-assembled into one-dimensional chains, as depicted in Figure S56 and Figure S57, respectively, through convergent hydrogen bonds between the carbonyl groups and urea binding units of neighbouring molecules with N···O distances of 2.840(2) and 3.048(2) Å and N-H···O angles of 161 and 148° for **5** and 2.820(2) Å and 150° for **11**. Moreover, benzo[*b*]thiophene rings from adjacent molecules adopt a parallel spatial disposition with $C_{6,centroid}\cdots C_{6,centroid}$ distances between adjacent benzo[*b*]thiophene rings of 4.55 Å.

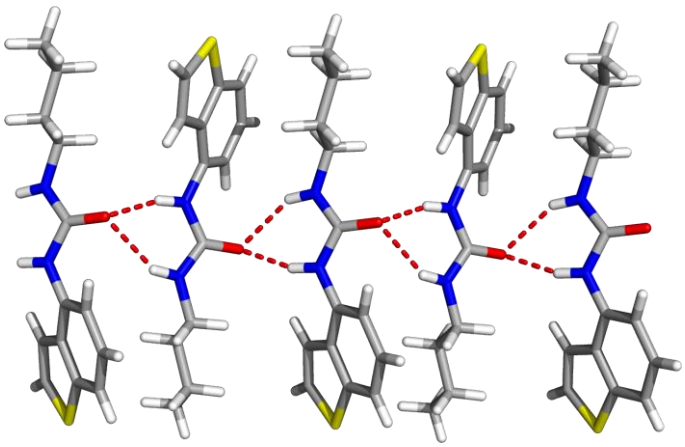

Figure S56. One-dimensional chains of N-H···O=C hydrogen bonds (red dashed lines) between molecules of **5** exhibiting two-fold screw axis symmetry running along the *b* direction.

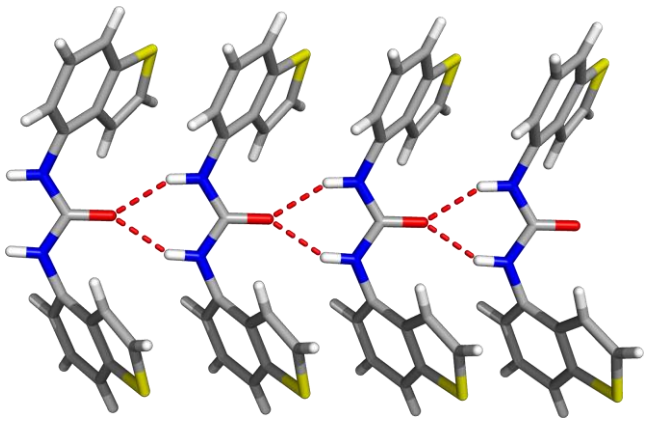

Figure S57. One-dimensional chains of N-H···O=C hydrogen bonds (red dashed lines) between molecules of **11** exhibiting two-fold axis symmetry with the γ-benzo[*b*]thiophene rings from adjacent molecules adopting a parallel disposition.

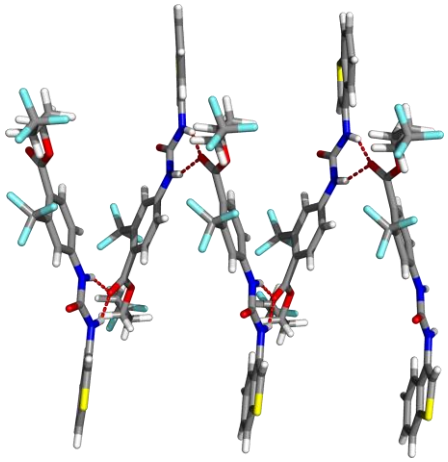

Figure S58. One-dimensional chains of N-H···O=C hydrogen bonds (red dashed lines) between molecules of **22** displaying a two-fold screw axis symmetry.

Anion efflux studies

General

POPC (1-palmitoyl-2-oleoyl-*sn*-glycero-3-phosphocholine) was stored at –20°C as a solution in chloroform (1 g POPC in 35 mL chloroform) and was supplied by Corden Pharma Switzerland LLC. Triton X-100 was used as detergent and was supplied by Sigma-Aldrich. Chloride concentrations during transport experiments were determined using an Accumet chloride selective electrode. The electrode was calibrated against sodium chloride solutions of known concentrations prior to each experiment in accordance with the supplier's manual.

General procedure for LUV preparation

Unilamellar vesicles were prepared following literature procedures from Jowett and Gale.[21] A lipid film of POPC (1-palmitoyl-2-oleoyl-*sn*-glycero-3-phosphocholine) was prepared from a chloroform solution evaporated under reduced pressure and dried under high vacuum for 8 or more hours. The lipid film was rehydrated by vortexing with an aqueous metal chloride (MCl) salt solution until the lipids were removed from the sides. The suspension was subjected to nine freeze-thaw cycles by freezing in a liquid nitrogen bath and thawing in room temperature water bath. The lipid suspension was allowed to rest at room temperature for 30 mins and was subsequently extruded 25 times through a 200 nm polycarbonate membrane (Nucleopore™) using an extruder set (Avanti Polar Lipids Inc). The resulting unilamellar vesicles were dialysed (Spectra/Por® 2 Membrane MWCO 12-14 kD) against the external solution to remove unencapsulated MCl salts. The internal and external solutions vary from each experiment and are given in the figure captions.

Cl^-/NO_3^- exchange assay

POPC LUVs were prepared as mentioned in the general procedure. The LUVS were loaded with 487 mM NaCl, buffered to pH 7.2 with 5 mM phosphate salts and suspended in the external medium consisting of 487 mM $NaNO_3$ solution buffered to pH 7.2 with 5 mM sodium phosphate salts (500 mM total ionic strength for both external and internal solutions). The lipid concentration per sample was 1 mM. The transporter was added as a solution of DMSO (5 mM, 10 μL) at 1 mol% w.r.t. lipid to start the experiment and the efflux of chloride was monitored by a chloride selective electrode. After 300 s the vesicles were lysed using a solution of Triton X-100 (11 w%) in H_2O:DMSO (7:1 v/v) (50 μL) and the 100% chloride efflux reading was taken after 420 s. The electrode voltages were converted to chloride concentration using a standard calibration, the final 700 s value was used as 100% chloride efflux and the initial 0 s value was set to 0% chloride efflux. The data points were converted to percentages and plotted as a function of transporter concentration (mol%, transporter : lipid molar percent), and fit to the Hill equation using Origin2021:

$$y = y_0 + (y_1 - y_0)\frac{x^n}{k^n + x^n} = V_{max}\frac{x^n}{k^n + x^n} = 100\%\frac{x^n}{(\mathrm{EC}_{50})^n + x^n}$$

where y is the chloride efflux at 270 s (%) and x is the carrier concentration (mol% carrier to lipid). V_{max}, k and n are the parameters to be fitted. V_{max} is the maximum efflux possible (often fixed to 100% (hence $y_0 = 0$ and $y_1 = 100$), as this is physically the maximum chloride efflux possible), n is the Hill coefficient and k is the carrier concentration needed to reach $V_{max}/2$ (when V_{max} is fixed to 100%, k equals EC_{50}). EC_{50}values at 270 s are defined as the carrier concentration (mol% w.r.t. lipid) needed to obtain 50% chloride efflux after 270 s.

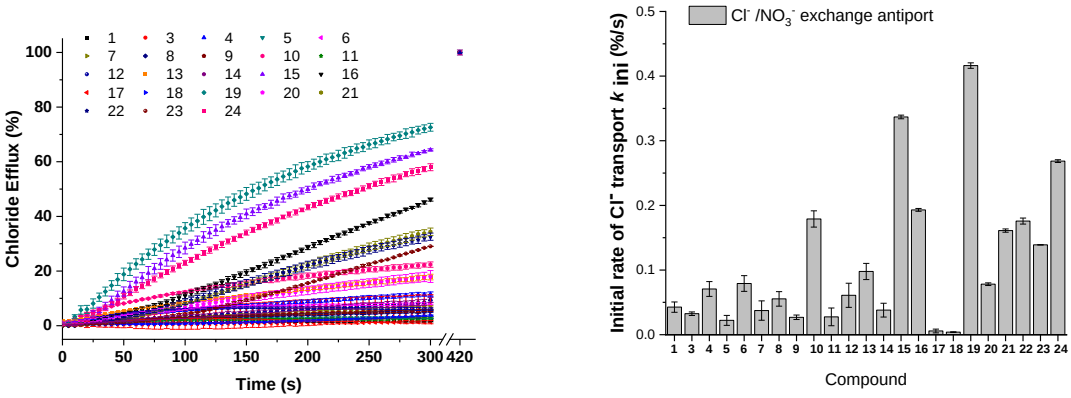

Figure S59. Overview of the anion transport ability of thiophene compounds in LUVs. (a) Cl^-/NO_3^- exchange plots demonstrating chloride efflux at 270 s mediated by compounds **1-24** (1 mol%) in POPC LUVs (200 nm mean diameter) loaded with NaCl (487 nm) and suspended in $NaNO_3$ (487 nm), buffered to pH 7.2 with sodium phosphate salts (5.0 mM). Transporters were added at 0 s. Each data point represents the average of three or four repeated measurements with standard deviations indicated through error bars. (b) Initial rates of chloride efflux mediated by transporters **1-24** (1 mol%) calculated by exponential or linear fitting.

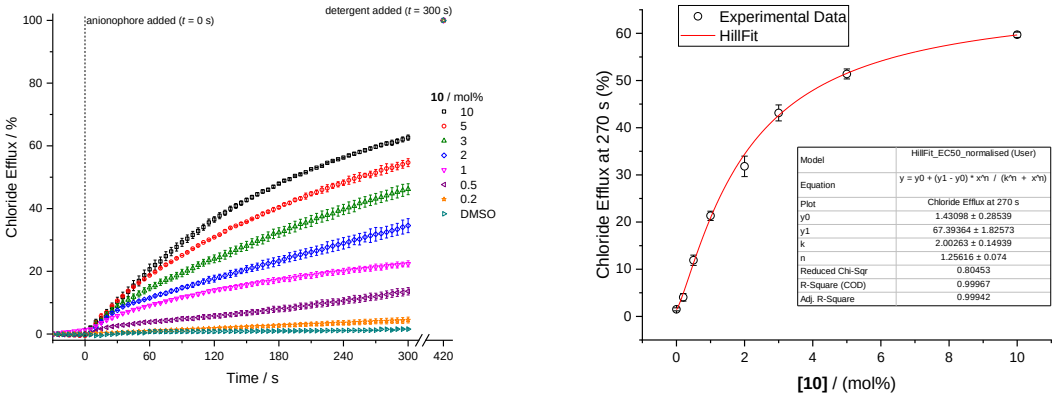

Figure S60. Hill analyses of chloride efflux through Cl^-/NO_3^-exchange at 270 s mediated by compound **10** in POPC LUVs (200 nm mean diameter) loaded with NaCl (487 nm) and suspended in $NaNO_3^-$ (487 nm), buffered to pH 7.2 with sodium phosphate salts (5.0 mM). Transporters were added at 0 s; concentrations are shown as carrier:lipid molar percentage. At 300s detergent was added to lyse the vesicles and calibrate the ISE to 100% chloride efflux. DMSO was used as a control (0 mol%). Each data point represents the average of three or four repeated measurements.

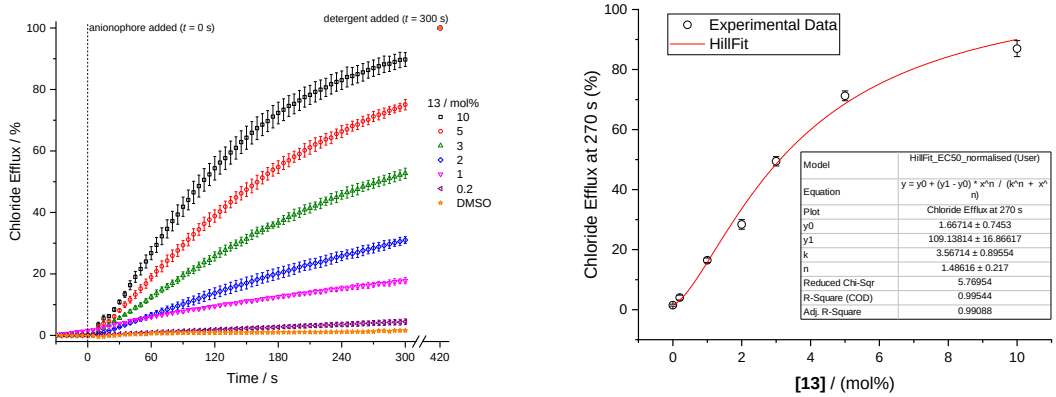

Figure S61. Hill analyses of chloride efflux through Cl^-/NO_3^- exchange at 270 s mediated by compound **13** in POPC LUVs. Remaining details as given in Figure S60.

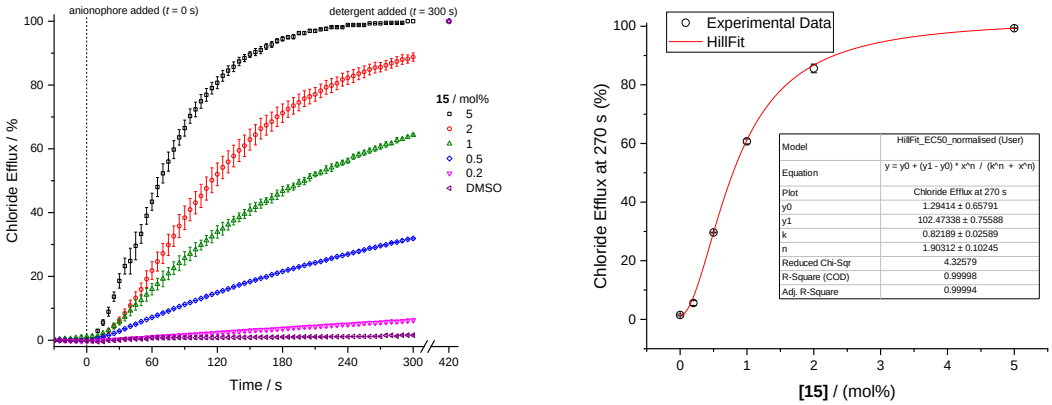

Figure S62. Hill analyses of chloride efflux through Cl^-/NO_3^- exchange at 270 s mediated by compound **15** in POPC LUVs. Remaining details as given in Figure S60.

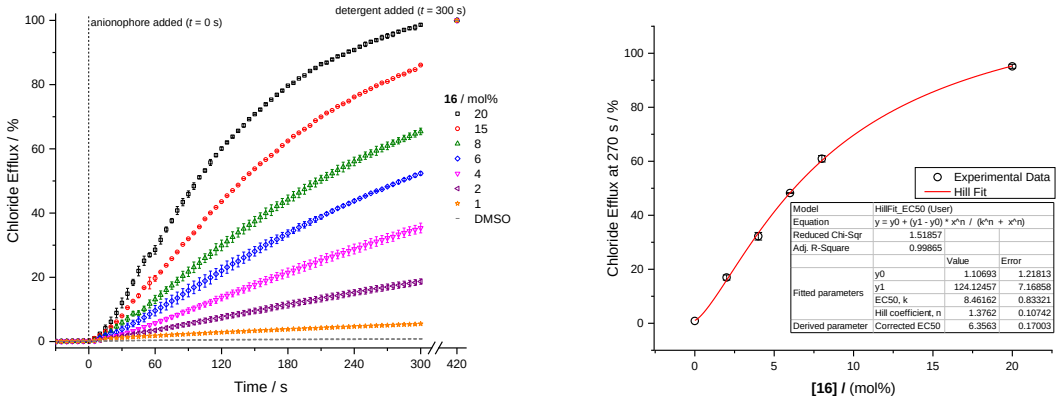

Figure S63. Hill analyses of chloride efflux through Cl^-/NO_3^- exchange at 270 s mediated by compound **16** in POPC LUVs. Remaining details as given in Figure S60.

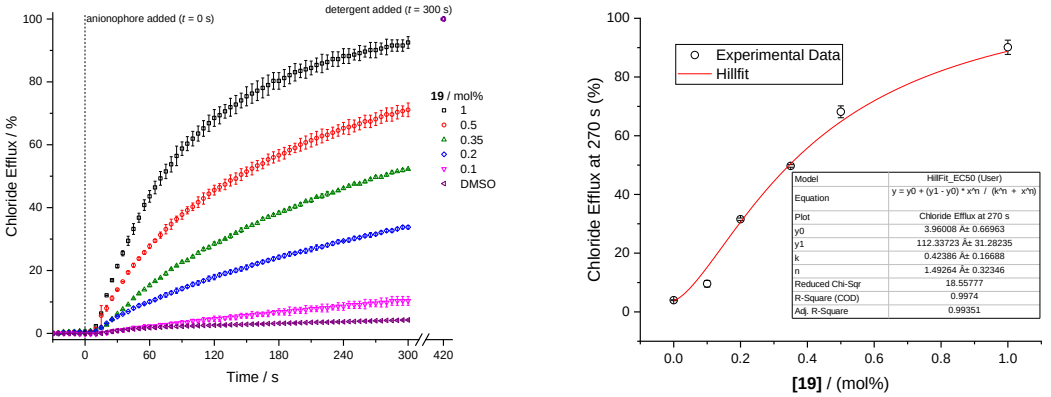

Figure S64. Hill analyses of chloride efflux through Cl^-/NO_3^- exchange at 270 s mediated by compound **19** in POPC LUVs. Remaining details as given in Figure S60.

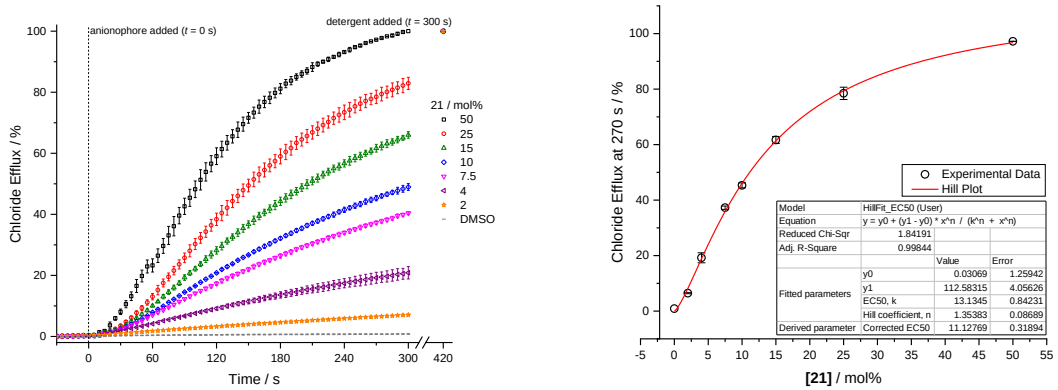

Figure S65. Hill analyses of chloride efflux through Cl^-/NO_3^- exchange at 270 s mediated by compound **21** in POPC LUVs. Remaining details as given in Figure S60.

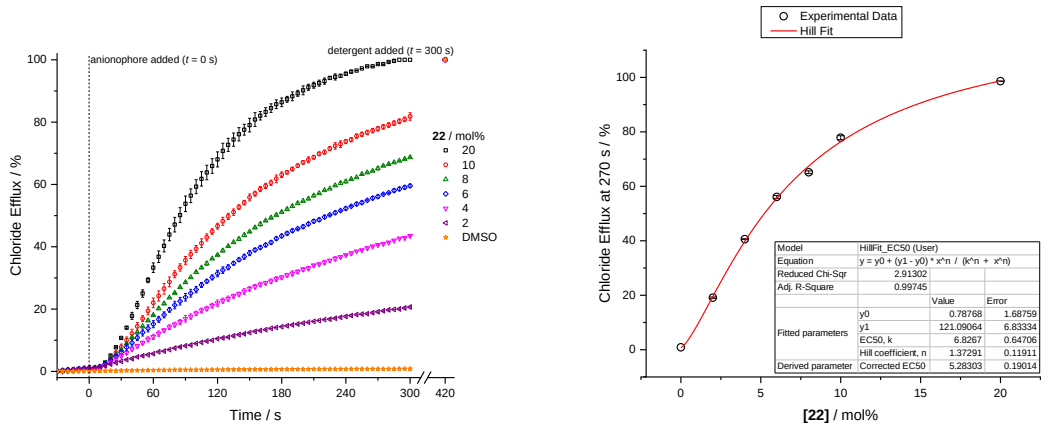

Figure S66. Hill analyses of chloride efflux through Cl^-/NO_3^- exchange at 270 s mediated by compound **22** in POPC LUVs. Remaining details as given in Figure S60.

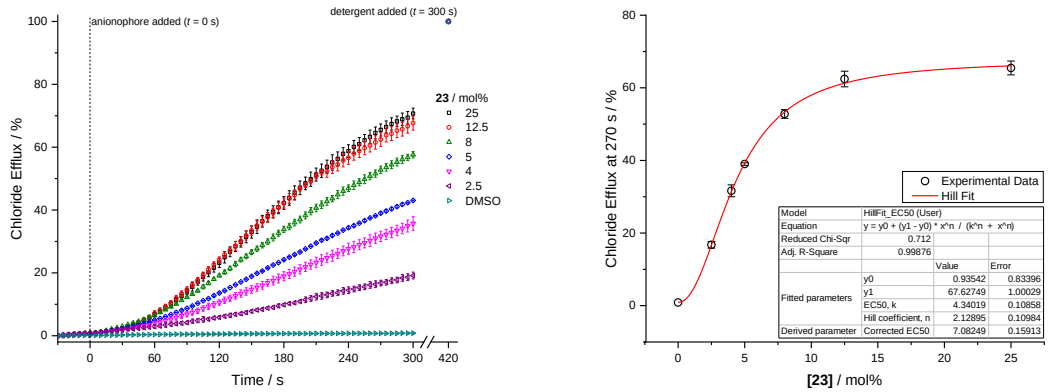

Figure S67. Hill analyses of chloride efflux through Cl^-/NO_3^- exchange at 270 s mediated by compound **23** in POPC LUVs. Remaining details as given in Figure S60.

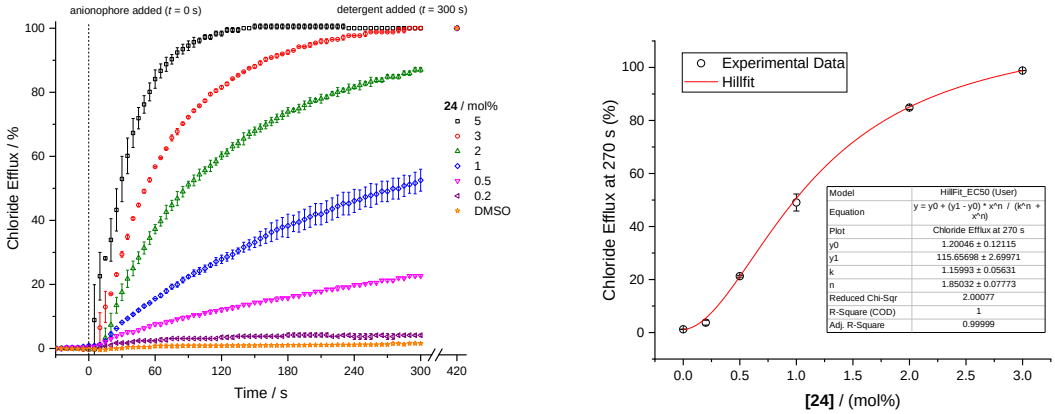

Figure S68. Hill analyses of chloride efflux through Cl^-/NO_3^- exchange at 270 s mediated by compound **24** in POPC LUVs. Remaining details as given in Figure S60.

Electrogenic vs electroneutral Cl^- transport

POPC LUVs were prepared as mentioned in the general procedure. The LUVs were loaded with 300 mM KCl buffered to pH 7.2 with 5 mM phosphate buffer and suspended in an external solution of 300 mM of KGlu buffered to pH 7.2 with 5 mM phosphate buffer. The lipids were diluted to a 1 mM concentration to be used per sample. Two DMSO solutions of ionophores valinomycin and monensin were prepared (0.1 mol%, transporter:lipid molar concentration). Either the valinomycin or the monensin solution was added (10 µL) to the test solution 30 s before the start of the experiment. The transporter was added as a solution of DMSO (5 mM, 10 µL) to initiate the start of the experiment, efflux of chloride out of the vesicles was monitored by a chloride selective electrode. After 300 s the vesicles were lysed using a solution of Triton X-100 (11 w%) in H_2O:DMSO (7:1 v/v) (50 µL) and then 100% chloride efflux reading was taken after 420 s. The electrode voltages were converted to chloride concentration using a standard calibration, the final 700 s value was used as 100% chloride efflux and the initial 0 s value was set to 0% chloride efflux. The data points were converted to percentages and plotted as a function of transporter concentration (mol%, transporter:lipid molar concentration).

k_{ini} values were calculated by fitting the obtained chloride efflux with the asymptotic function $y = a - bc^x$ using Origin2021b, where y is the chloride efflux (%), x is time (s) and k_{ini} is then given by $k_{ini} = -b\ln(c)$ (obtained in % s^{-1}), or by fitting the initial linear range of the obtained chloride efflux to $y = a + bx$, where y is the chloride efflux (%), x is time (s) and k_{ini} is given by the slope b. In case of a sigmoidal time dependence, the first two or three data points were omitted from the fit. To obtain standard deviations on the initial rate of transport, the fits were performed for each individual repeat and subsequently averaged.

Table S9. Overview of the initial rate of chloride transport (k_{ini}) reported from Cl^-/NO_3^- exchange and complementary cationophore coupling assays.

k_{ini}	Cl^-/NO_3^- (% s^{-1})[a]	Electrogenic Cl^- (% s^{-1})[b]	Electroneutral H^+/Cl^- (% s^{-1})[c]	Ratio[d]
Blank[e]	0.003	0.001	0.015	-
10	0.179	0.187	0.127	0.68
13	0.098	0.204	0.051	0.25
15	0.337	0.467	0.353	0.76
19	0.416	1.964	1.515	0.77
24	0.269	2.217	2.171	0.98

[a)] Initial rate of chloride efflux for the Cl^-/NO_3^- exchange assay described above (1 mol% transporter: lipid molar concentration); [b)] Initial rate of chloride efflux for 1 mol% carrier to lipid in the presence of 0.1 mol% valinomycin, for

electrogenic Cl^- transport calculated as described above; [c] Initial rate of chloride efflux for 1 mol% carrier to lipid in the presence of 0.1 mol% monensin, for electrogenic Cl^- transport calculated as described above; [d] Ratio of electrogenic: electroneutral transport ratio < 1 indicates an affinity to electrogenic over electroneutral transport; [e] DMSO only, 0.1 mol% valinomycin only, or 0.1 mol% monensin.

Table S10. Overview of the initial rate of chloride transport (k_{ini}) reported from Cl^-/NO_3^- exchange and complementary cationophore coupling assays.

k_{ini}	Cl^-/NO_3^- (% s^{-1})[a]	Electrogenic Cl^- (% s^{-1})[b]	Electroneutral H^+/Cl^- (% s^{-1})[c]	Ratio[d]
Blank[e]	0.003	0.001	0.015	-
14	0.02	0.06	0.071	1.19
16	1.636	2.751	2.116	0.77
18	0.033	0.058	0.066	1.13
20	0.027	0.049	0.058	1.17
21	0.094	0.962	0.444	0.46
22	0.051	1.461	0.603	0.41
23	0.029	0.325	0.275	0.85

[a] Initial rate of chloride efflux for the Cl^-/NO_3^- exchange assay described above (20 mol% transporter: lipid molar concentration); [b] Initial rate of chloride efflux for 20 mol% carrier to lipid in the presence of 0.1 mol% valinomycin, for electrogenic Cl^- transport calculated as described above; [c] Initial rate of chloride efflux for 20 mol% carrier to lipid in the presence of 0.1 mol% monensin, for electrogenic Cl^- transport calculated as described above; [d] Ratio of electrogenic: electroneutral transport ratio < 1 indicates an affinity to electrogenic over electroneutral transport; [e] DMSO only, 0.1 mol% valinomycin only, or 0.1 mol% monensin.

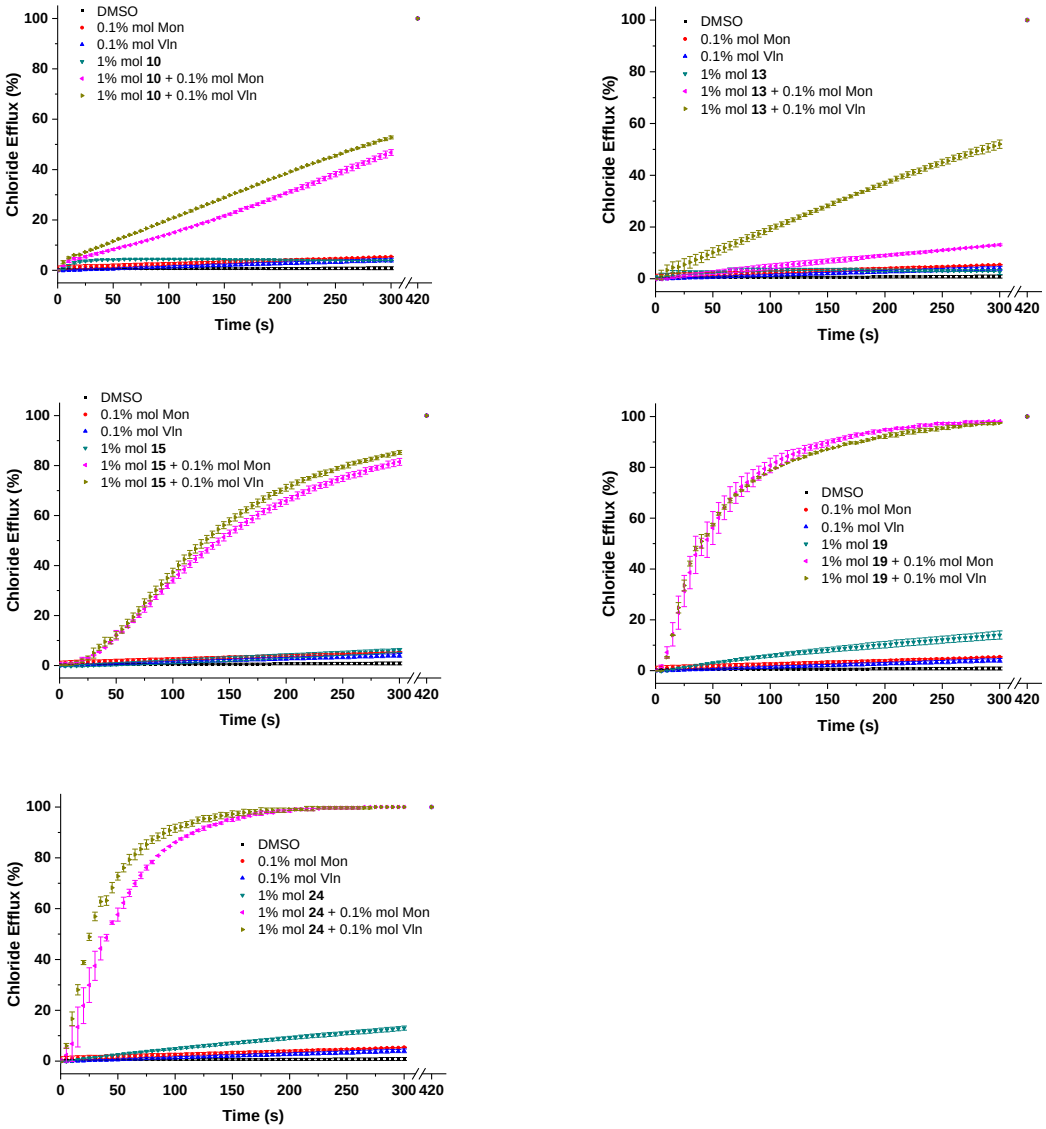

Figure S69. Electrogenic or electroneutral transport evaluated from the complementary-cationophore assay (1 mol%, transporter:lipid molar concentration) in the presence of monensin and valinomycin (0.1 mol% w.r.t. lipid). LUVs were loaded with 300 mM KCl buffered to pH 7.2 with 5 mM phosphate buffer and suspended in an external solution of 300 mM of KGlu buffered to pH 7.2 with 5 mM phosphate buffer. Either the valinomycin or the monensin solution was added (10 µL) to the test solution 30 s before the start of the experiment. The transporter was added as a solution of DMSO at t=0. At the end of the experiment, detergent was added to lyse the vesicles and calibrate the ISE to 100% chloride efflux. Concentrations are shown as carrier:lipid molar percentage. DMSO was used as a control (0 mol%). Each data point represents the average of three or four repeated measurements.

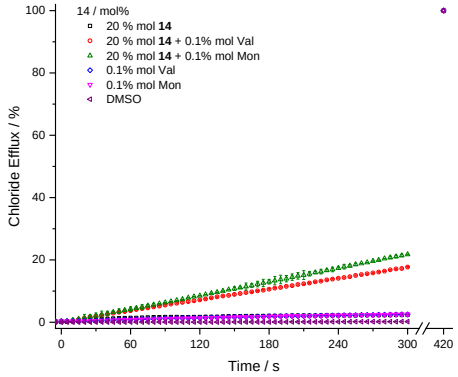

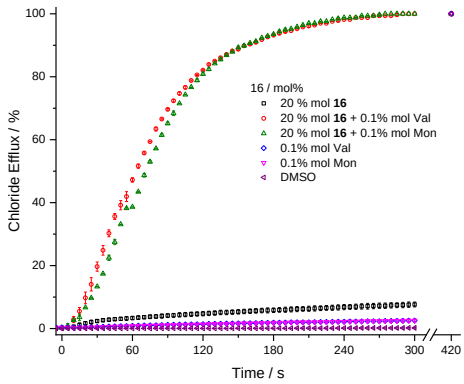

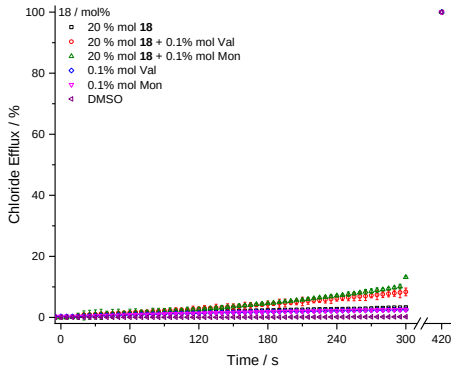

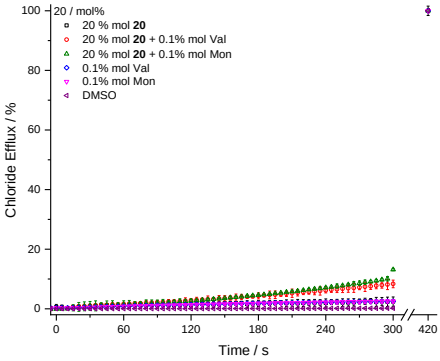

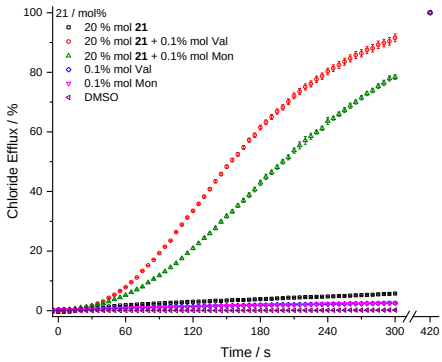

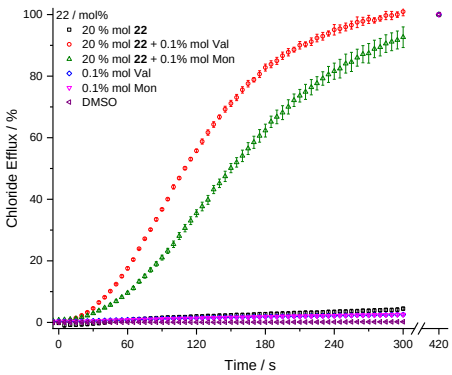

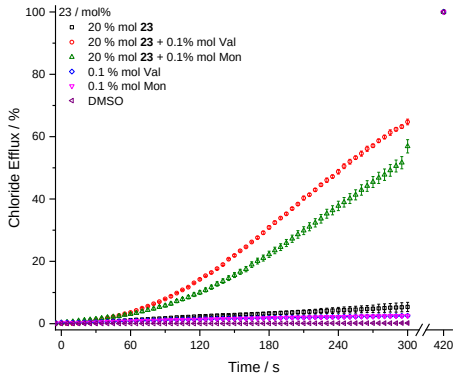

Figure S70. Electrogenic or electroneutral transport evaluated from the complementary-cationophore assay (20 mol%, transporter:lipid molar concentration) in the presence of monensin and valinomycin (0.1 mol% w.r.t. lipid). Remaining details as given in Figure S69.

NMDG-Cl Assay

POPC LUVs were prepared as mentioned in the general procedure. A lipid film of POPC (1-palmitoyl-2-oleoyl-*sn*-glycero-3-phosphocholine) was prepared from a chloroform solution evaporated under reduced pressure and dried under high vacuum for 8 or more hours. The lipid film was rehydrated by vortexing with an aqueous HPTS (1 mM) and NMDG-Cl (100 mM) buffered to pH 7 with HEPES (10 mM) until the lipids were removed from the sides. The suspension was subjected to nine freeze-thaw cycles by freezing in a liquid nitrogen bath and thawing in room temperature water bath. The lipid suspension was allowed to rest at room temperature for 30 mins and was subsequently extruded 25 times through a 200 nm polycarbonate membrane (Nucleopore™) using an extruder set (Avanti Polar Lipids Inc). Unencapsulated salts were removed through size exclusion chromatography using a Sephadex G-25 column and an external solution containing no HPTS. The LUVs were diluted with the external solution to a standard volume to formulate a known concentration of lipids. The pre-treated lipids were prepared adding BSA (1 mol%, w.r.t. lipid) to the lipid solution and leaving to mix by agitation for 2 hours. The lipid stock was diluted with the external buffer to a standard reaction vessel (2.5 mL) to afford a test solution with a lipid concentration of 0.1 mM. The transporter was added as a solution of DMSO (5 μL). Additions of oleic acid (2 mol%, w.r.t. lipid) and gramicidin (0.1 mol% w.r.t. lipid) were added as a DMSO solutions (5 μL) prior to the addition of the transporter. The experiment was started upon the addition of a base pulse to initiate chloride efflux in the form of NMDG-OH (5 μL, 0.5 M). After 200 s, the vesicles were lysed using a detergent (50 μL of Triton X-100 (11 w%) in H_2O:DMSO (7:1 v/v)) and after 300 s the final reading was taken as 100% chloride efflux for calibration. The fractional fluorescence intensity (I_f) was calculated using:

$$I_f = \frac{R_t - R_0}{R_d - R_0}$$

where R_t is the fluorescence ratio at time t, R_0 is the fluorescence ratio at time 0 and R_d is the fluorescence ratio at the end of the experiment, after the addition of detergent. The HPTS assay was performed as above at varying concentrations. Transporter concentration (mol%, w.r.t. lipid concentration) was plotted as a function against fluorescence ratios at 200 s and fitted to the Hill equation using Origin2021b:

$$y = y_0 + (y_{max} - y_0)\frac{x^n}{K + x^n}$$

where y is the I_f at 200 s, y_0 is I_f recorded for the blank DMSO run, y_{max} is the maximum I_f at 200 s, x is the transporter concentration, and k and n are the parameters to be fitted. n is the Hill coefficient and K is the EC_{50}. Through H^+/Cl^- symport (or Cl^-/OH^- antiport) the rate of pH dissipation will change the fluorescent intensity. The three conditions monitor the different mechanisms of chloride transport. The addition of oleic acid, to examine the Cl^-/H^+ cotransport through fatty acid flip-flop. The pre-treatment of BSA, to monitor H^+/Cl^- symport (or Cl^-/OH^- antiport). The addition of gramicidin, to examine Cl^- uniport. For each receptor, the concentration dependent Hill analyses are shown below.

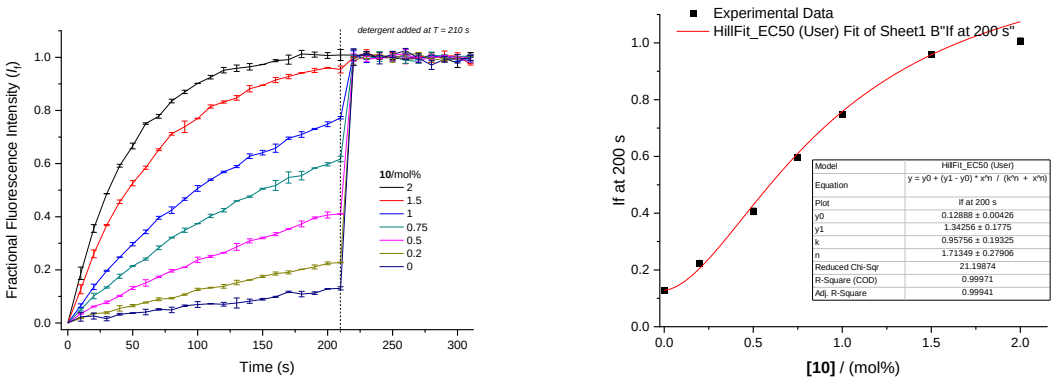

Figure S71. Hill analysis of H^+/Cl^- symport (or Cl^-/OH^- antiport) facilitated by a combination of oleic acid and **10** in the NMDG-Cl assay.

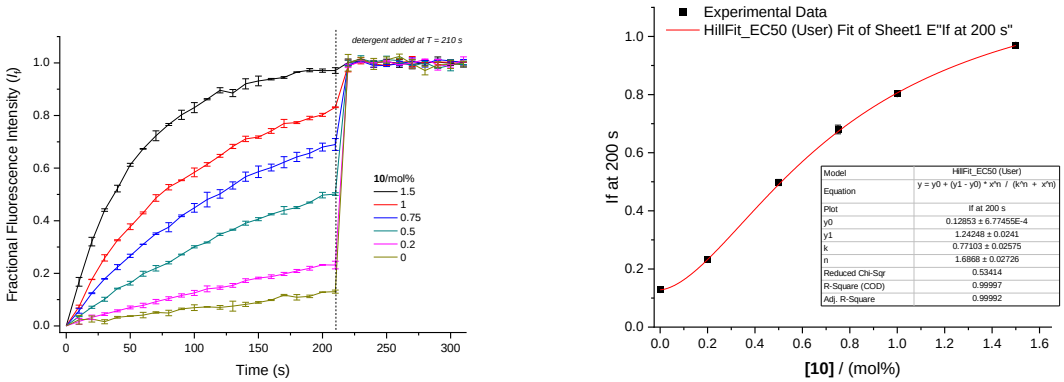

Figure S72. Hill analysis of Cl^- uniport facilitated by a combination of gramicidin and **10** in the NMDG-Cl assay.

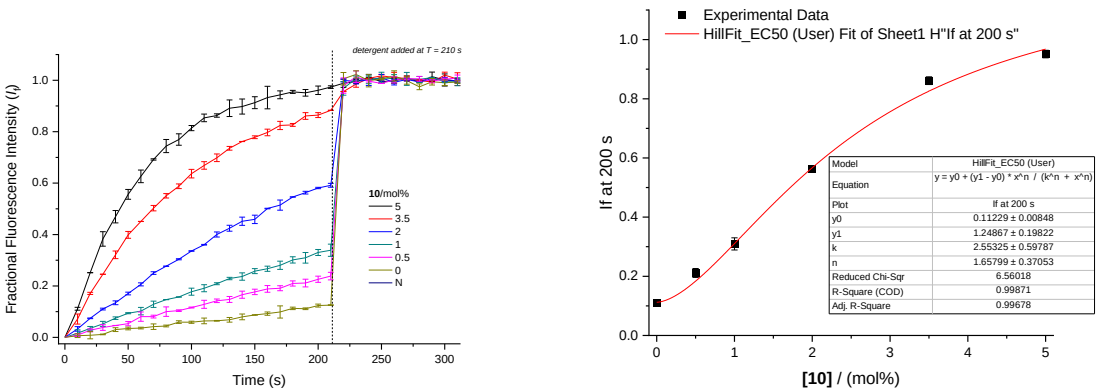

Figure S73. Hill analysis of H^+/Cl^- symport (or Cl^-/OH^- antiport) facilitated by **10** and pre-treated BSA LUVs in the NMDG-Cl assay.

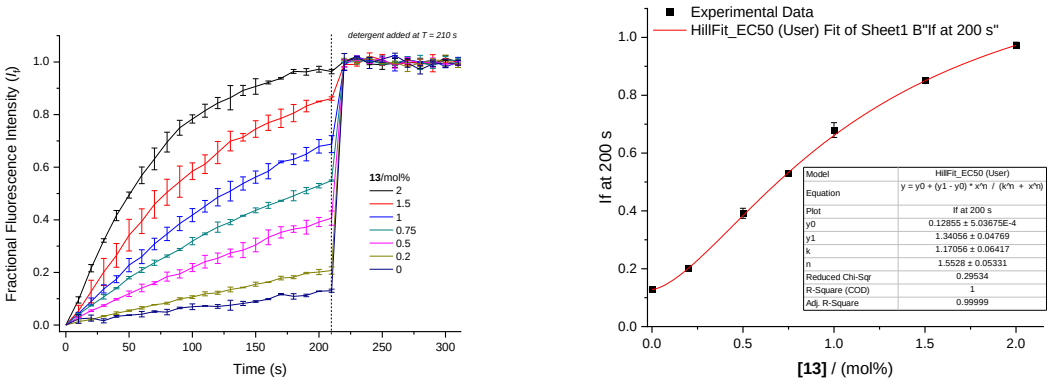

Figure S74. Hill analysis of H^+/Cl^- symport (or Cl^-/OH^- antiport) facilitated by a combination of oleic acid and **13** in the NMDG-Cl assay.

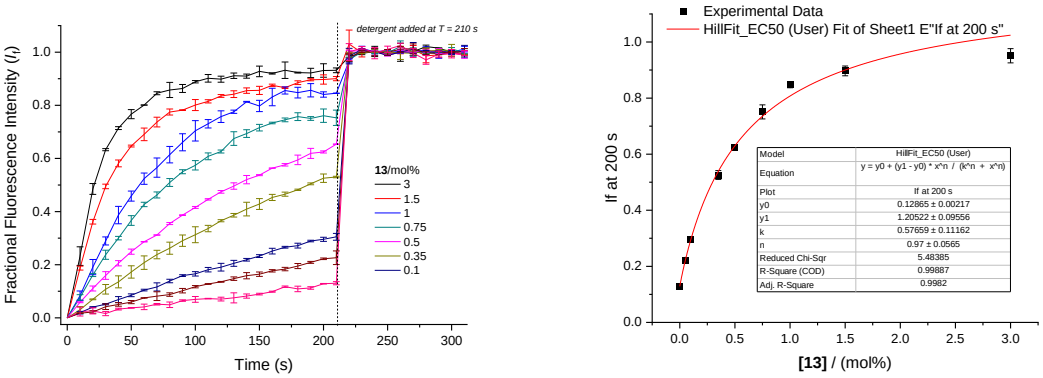

Figure S75. Hill analysis of Cl^- uniport facilitated by a combination of gramicidin and **13** in the NMDG-Cl assay.

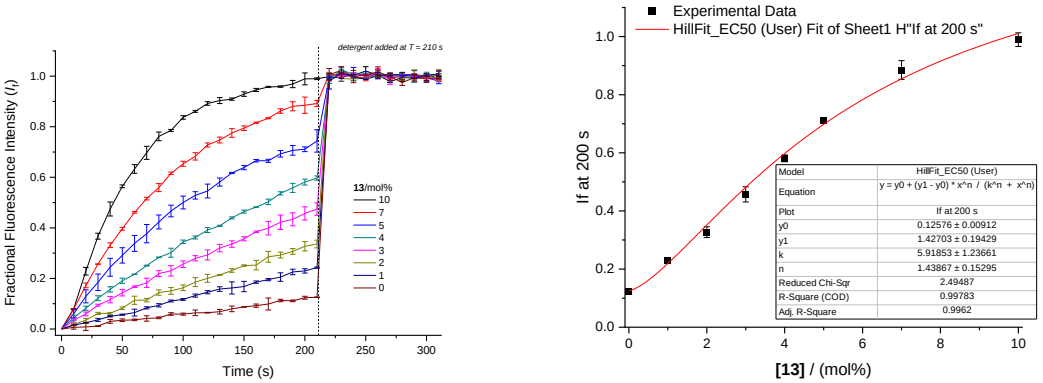

Figure S76. Hill analysis of H^+/Cl^- symport (or Cl^-/OH^- antiport) facilitated by **13** and pre-treated BSA LUVs in the NMDG-Cl assay.

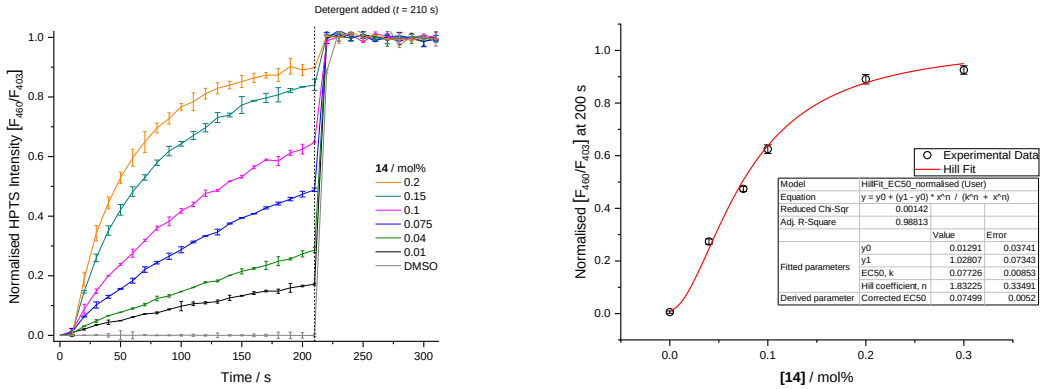

Figure S77. Hill analysis of H^+/Cl^- symport (or Cl^-/OH^- antiport) facilitated by a combination of oleic acid and **14** in the NMDG-Cl assay.

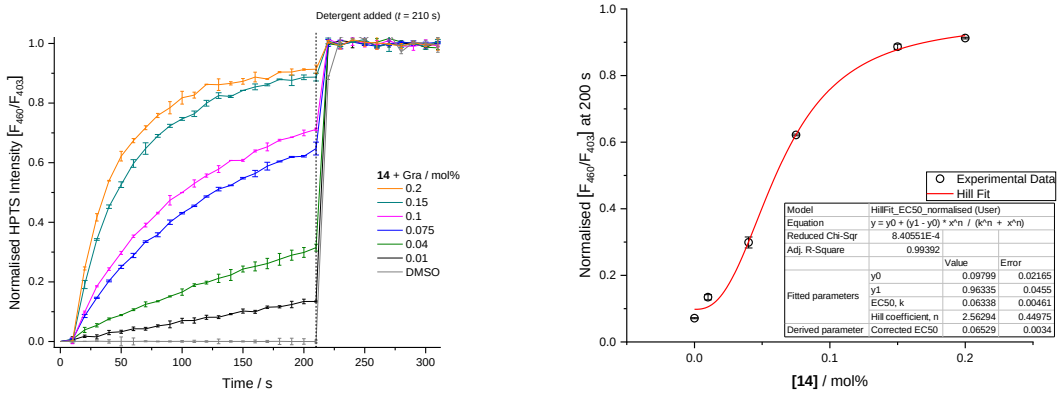

Figure S78. Hill analysis of Cl^- uniport facilitated by a combination of gramicidin and **14** in the NMDG-Cl assay.

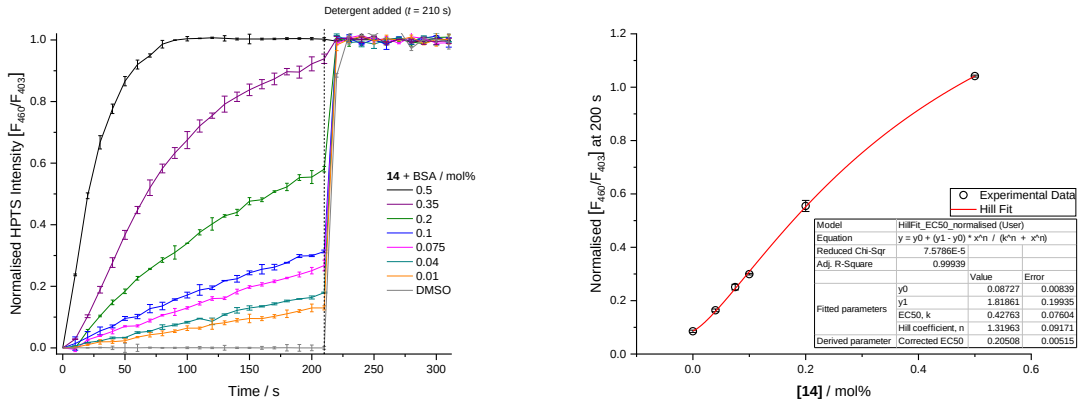

Figure S79. Hill analysis of H^+/Cl^- symport (or Cl^-/OH^- antiport) facilitated by **14** and pre-treated BSA LUVs in the NMDG-Cl assay.

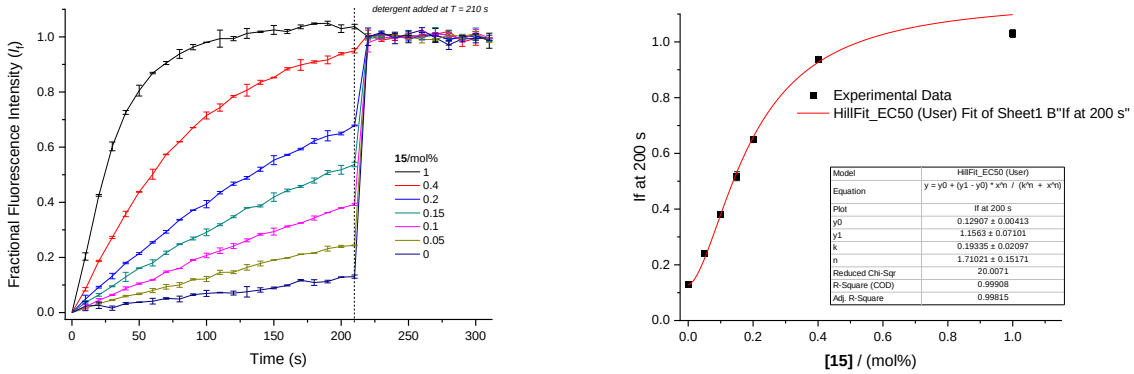

Figure S80. Hill analysis of H^+/Cl^- symport (or Cl^-/OH^- antiport) facilitated by a combination of oleic acid and **15** in the NMDG-Cl assay.

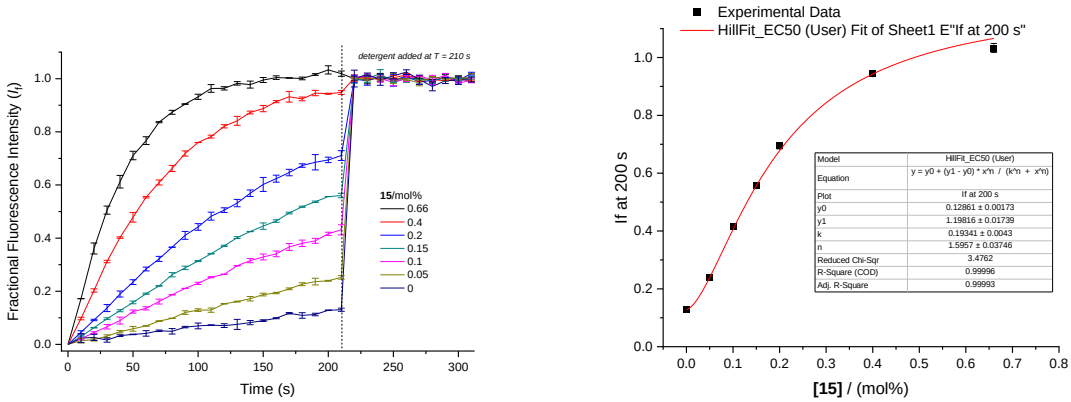

Figure S81. Hill analysis of Cl^- uniport facilitated by a combination of gramicidin and **15** in the NMDG-Cl assay.

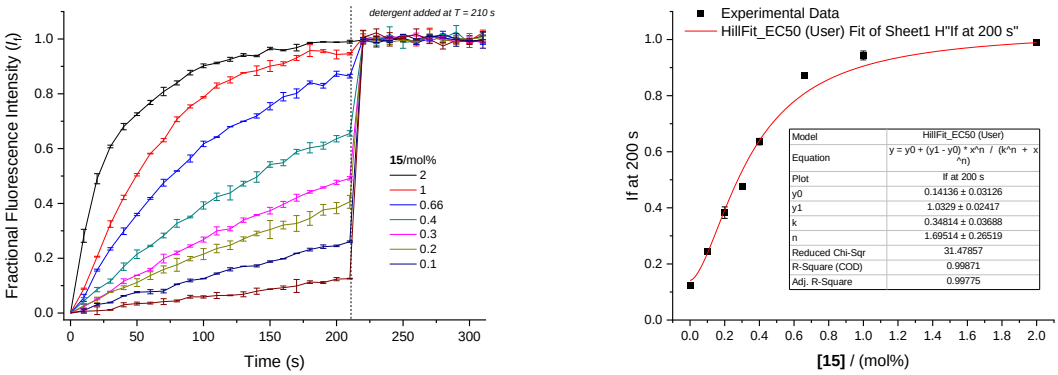

Figure S82. Hill analysis of H^+/Cl^- symport (or Cl^-/OH^- antiport) facilitated by **15** and pre-treated BSA LUVs in the NMDG-Cl assay.

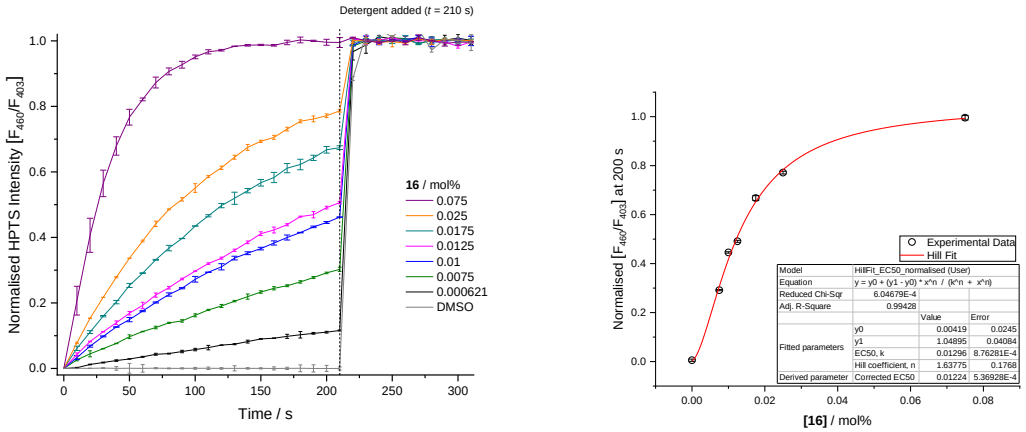

Figure S83. Hill analysis of H^+/Cl^- symport (or Cl^-/OH^- antiport) facilitated by a combination of oleic acid and **16** in the NMDG-Cl assay.

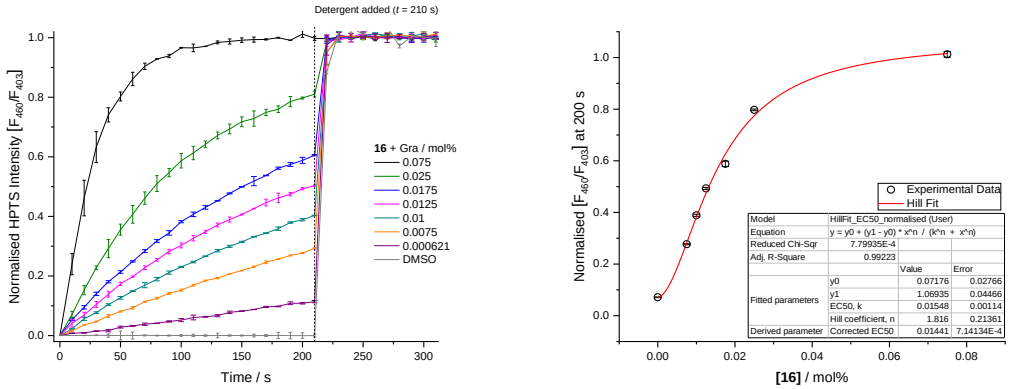

Figure S84. Hill analysis of Cl^- uniport facilitated by a combination of gramicidin and **16** in the NMDG-Cl assay.

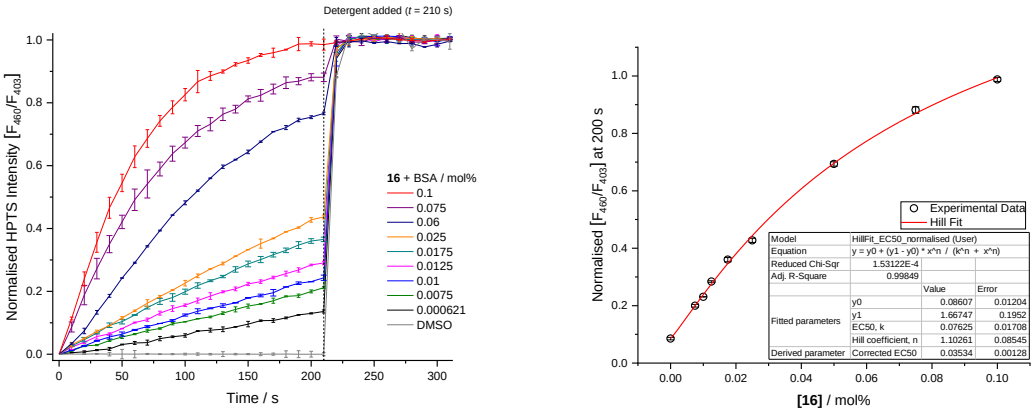

Figure S85. Hill analysis of H^+/Cl^- symport (or Cl^-/OH^- antiport) facilitated by **16** and pre-treated BSA LUVs in the NMDG-Cl assay.

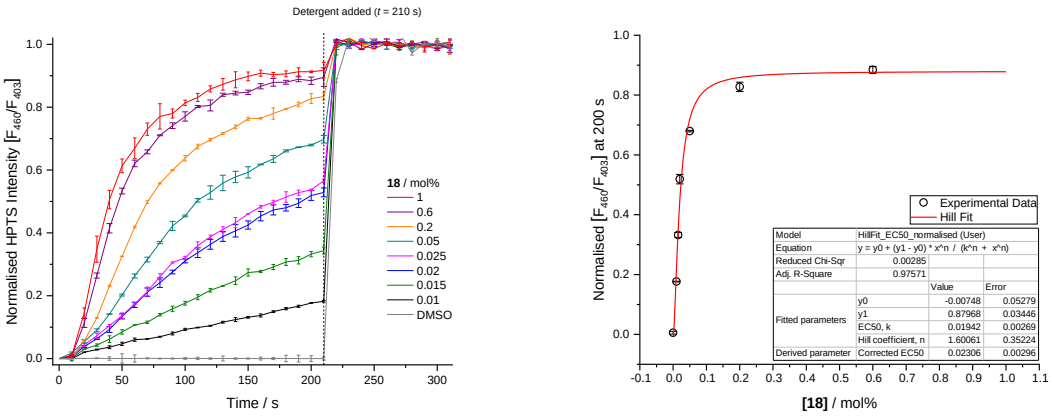

Figure S86. Hill analysis of H^+/Cl^- symport (or Cl^-/OH^- antiport) facilitated by a combination of oleic acid and **18** in the NMDG-Cl assay.

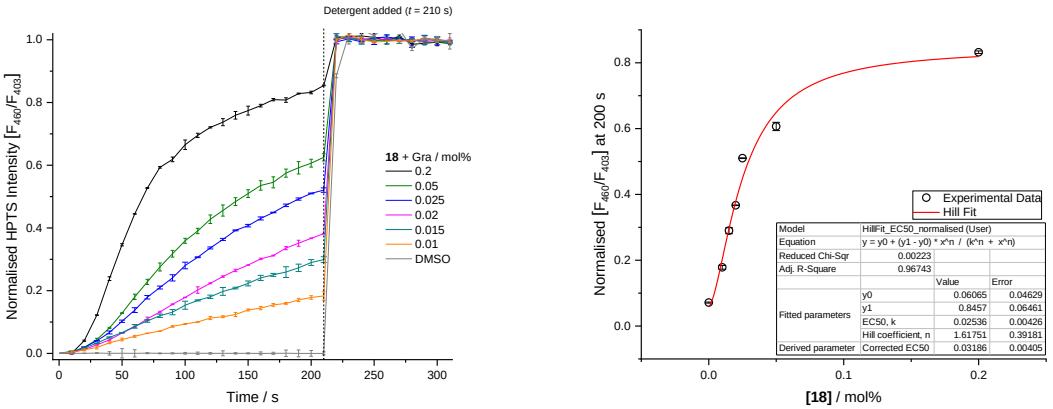

Figure S87. Hill analysis of Cl^- uniport facilitated by a combination of gramicidin and **18** in the NMDG-Cl assay.

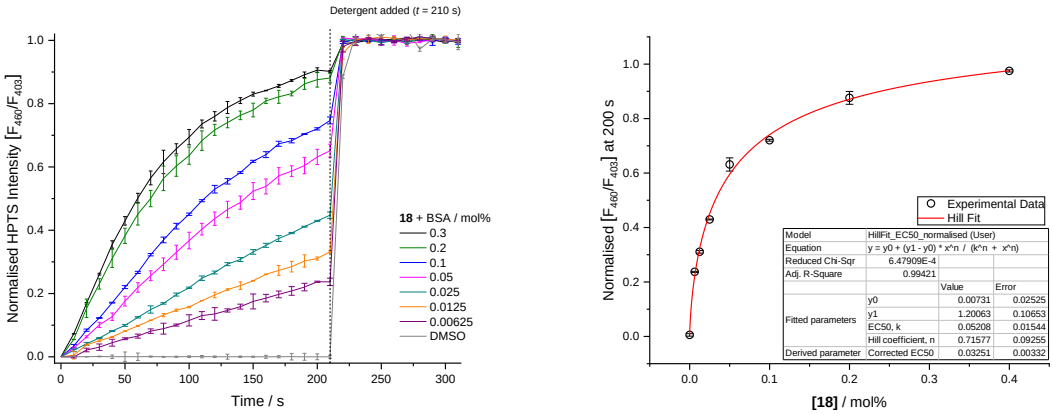

Figure S88. Hill analysis of H^+/Cl^- symport (or Cl^-/OH^- antiport) facilitated by **18** and pre-treated BSA LUVs in the NMDG-Cl assay.

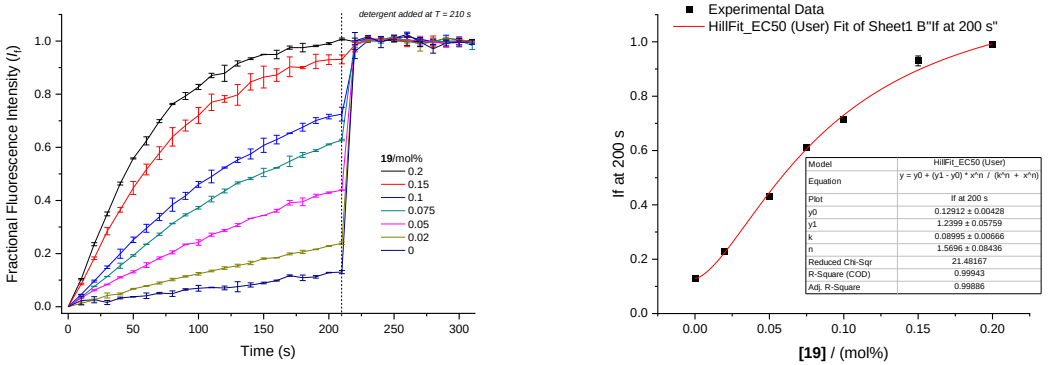

Figure S89. Hill analysis of H^+/Cl^- symport (or Cl^-/OH^- antiport) facilitated by a combination of oleic acid and **19** in the NMDG-Cl assay.

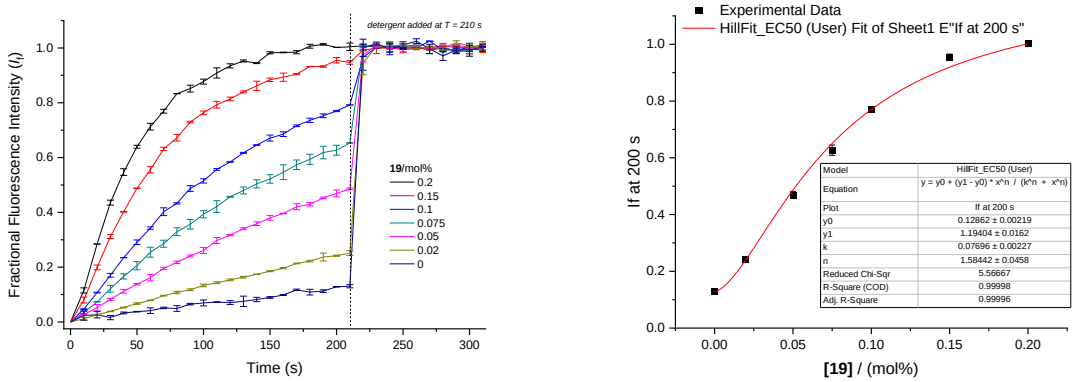

Figure S90. Hill analysis of Cl^- uniport facilitated by a combination of gramicidin and **19** in the NMDG-Cl assay.

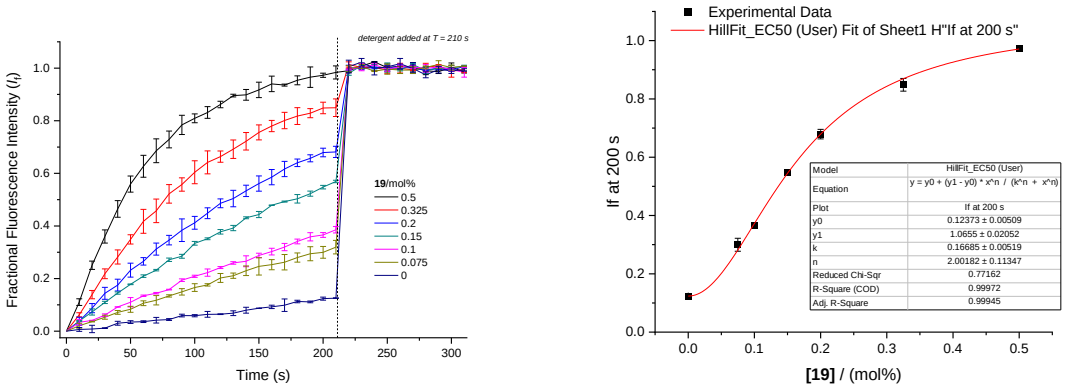

Figure S91. Hill analysis of H^+/Cl^- symport (or Cl^-/OH^- antiport) facilitated by **19** and pre-treated BSA LUVs in the NMDG-Cl assay.

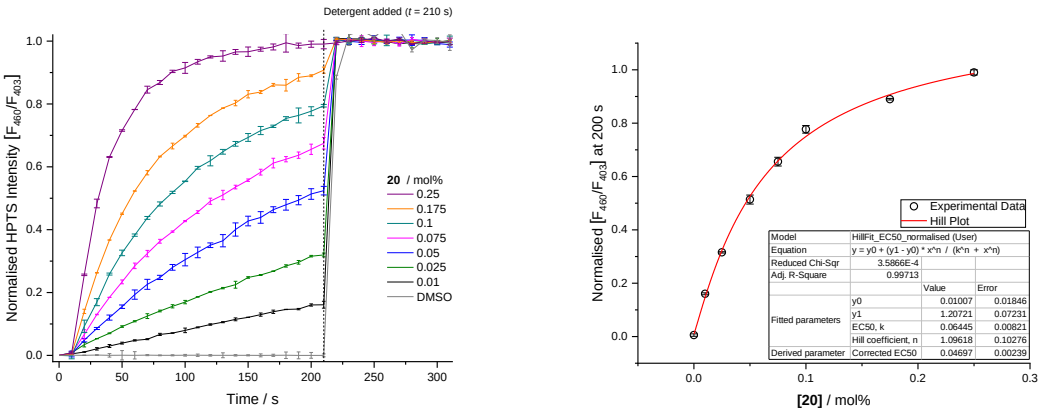

Figure S92. Hill analysis of H^+/Cl^- symport (or Cl^-/OH^- antiport) facilitated by a combination of oleic acid and **20** in the NMDG-Cl assay.

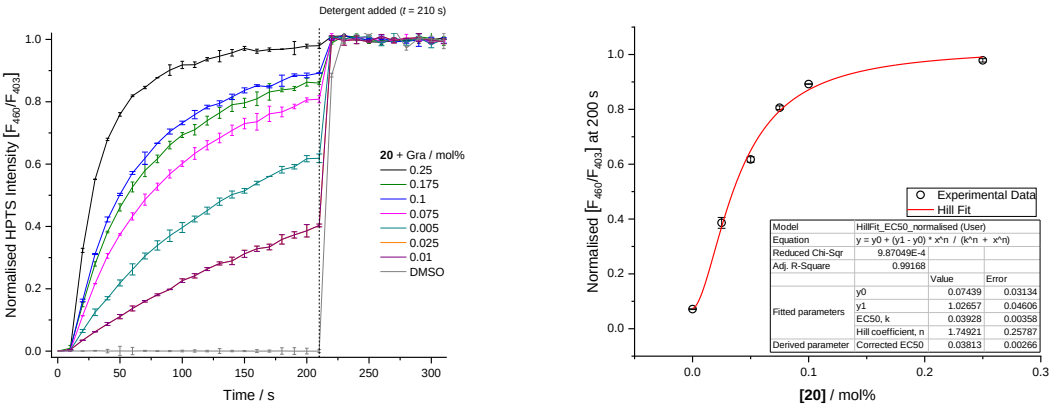

Figure S93. Hill analysis of Cl^- uniport facilitated by a combination of gramicidin and **20** in the NMDG-Cl assay.

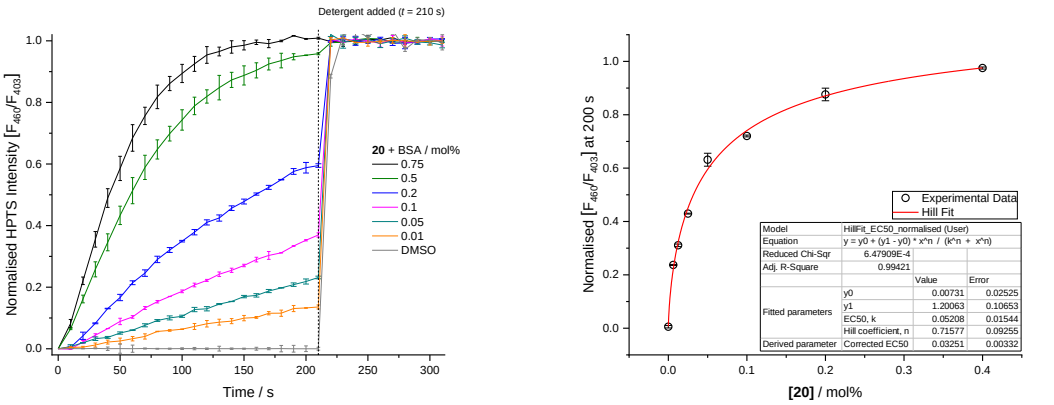

Figure S94. Hill analysis of H^+/Cl^- symport (or Cl^-/OH^- antiport) facilitated by **20** and pre-treated BSA LUVs in the NMDG-Cl assay.

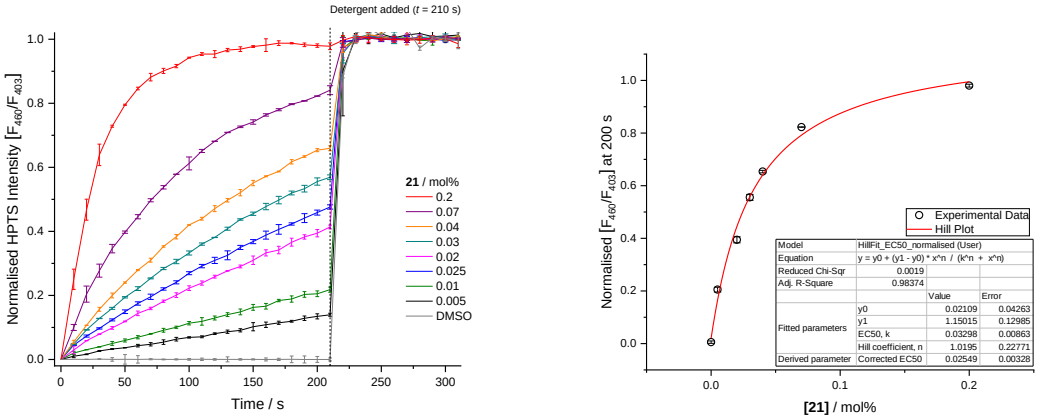

Figure S95. Hill analysis of H^+/Cl^- symport (or Cl^-/OH^- antiport) facilitated by a combination of oleic acid and **21** in the NMDG-Cl assay.

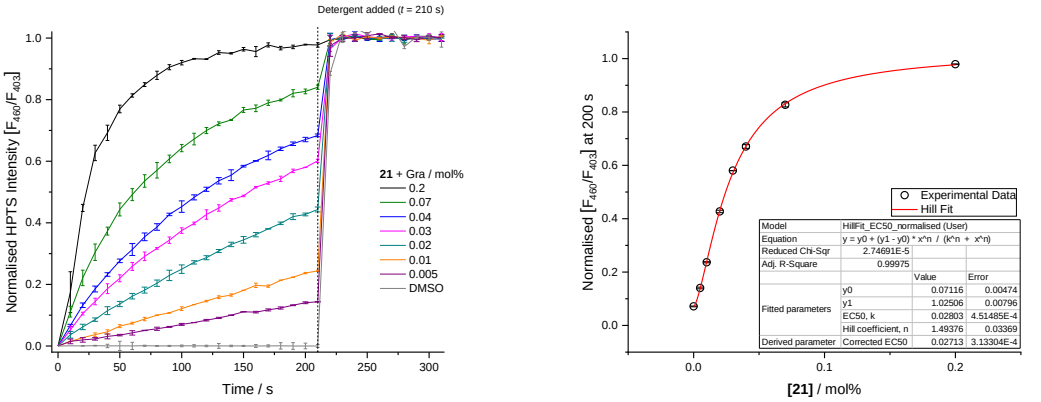

Figure S96. Hill analysis of Cl^- uniport facilitated by a combination of gramicidin and **21** in the NMDG-Cl assay.

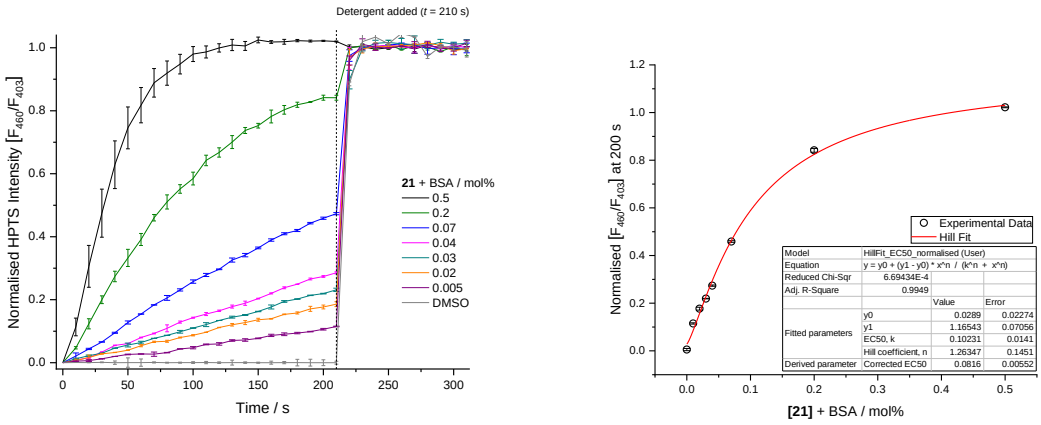

Figure S97. Hill analysis of H^+/Cl^- symport (or Cl^-/OH^- antiport) facilitated by **21** and pre-treated BSA LUVs in the NMDG-Cl assay.

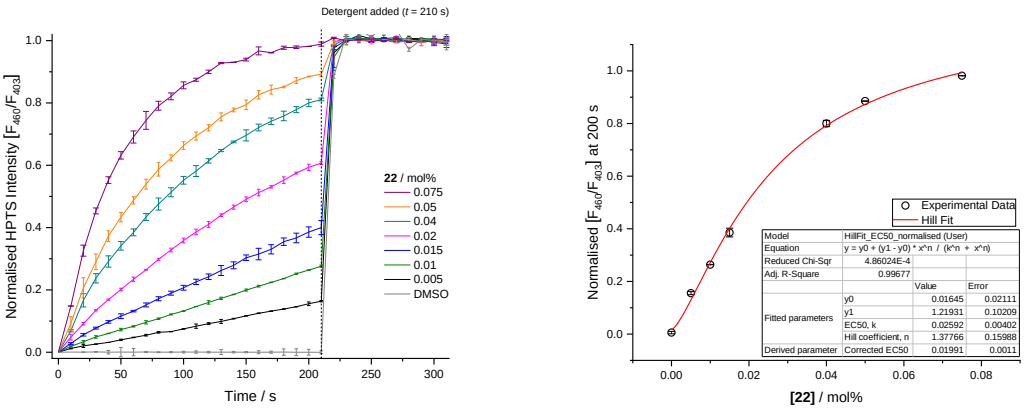

Figure S98. Hill analysis of H^+/Cl^- symport (or Cl^-/OH^- antiport) facilitated by a combination of oleic acid and **22** in the NMDG-Cl assay.

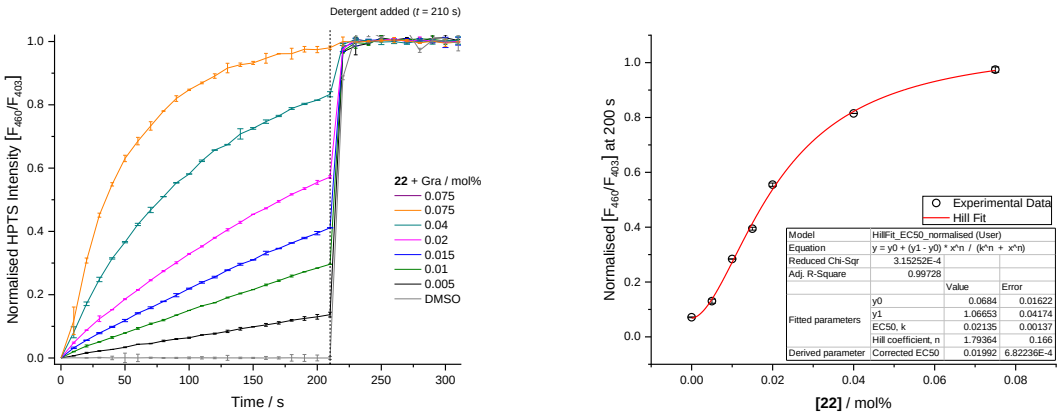

Figure S99. Hill analysis of Cl^- uniport facilitated by a combination of gramicidin and **22** in the NMDG-Cl assay.

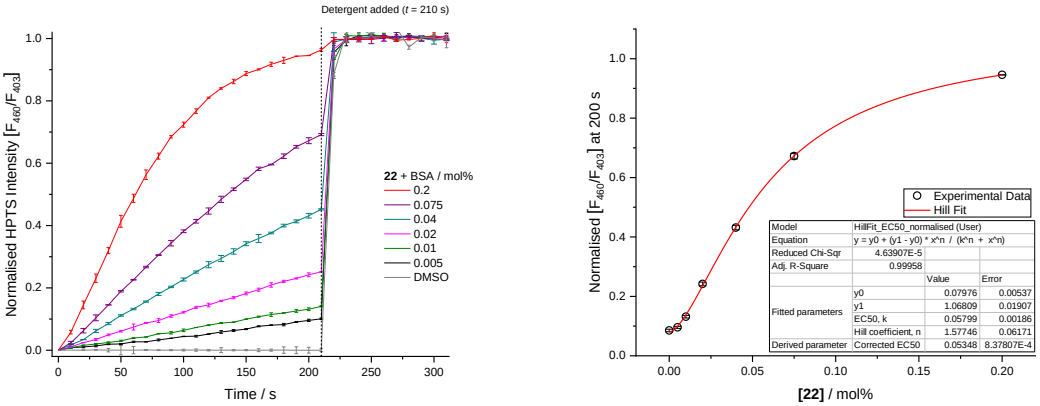

Figure S100. Hill analysis of H^+/Cl^- symport (or Cl^-/OH^- antiport) facilitated by **22** and pre-treated BSA LUVs in the NMDG-Cl assay.

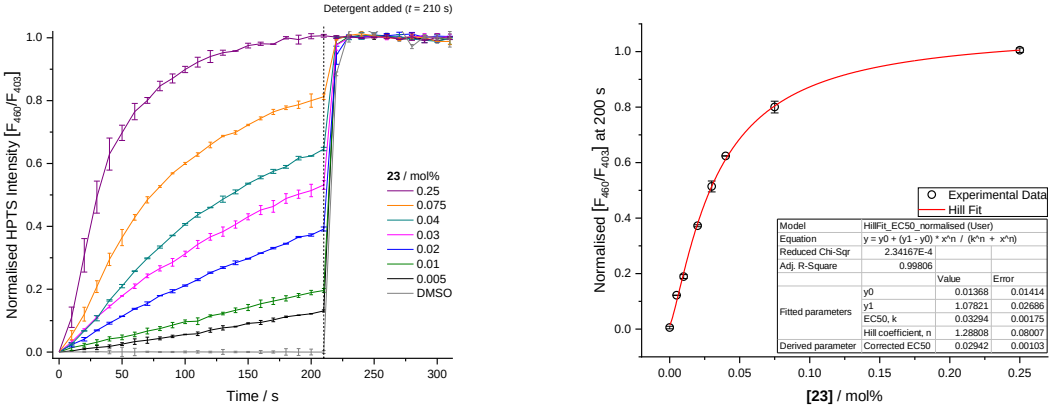

Figure S101. Hill analysis of H^+/Cl^- symport (or Cl^-/OH^- antiport) facilitated by a combination of oleic acid and **23** in the NMDG-Cl assay.

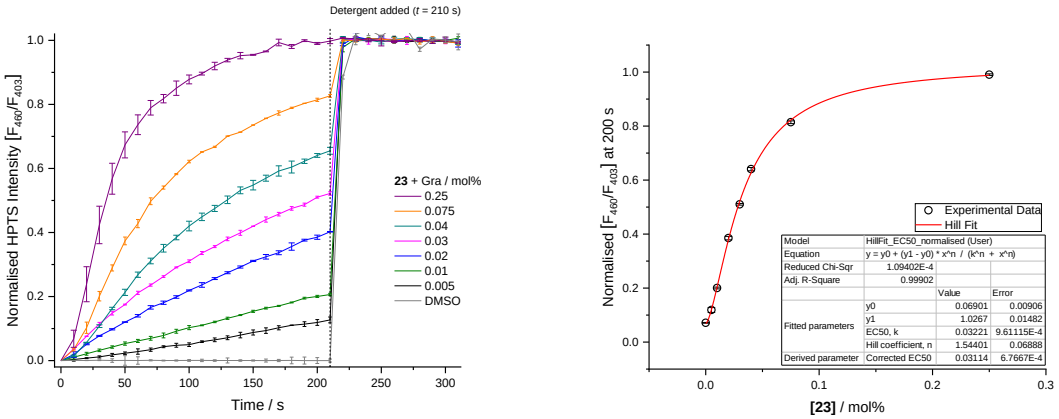

Figure S102. Hill analysis of Cl^- uniport facilitated by a combination of gramicidin and **23** in the NMDG-Cl assay.

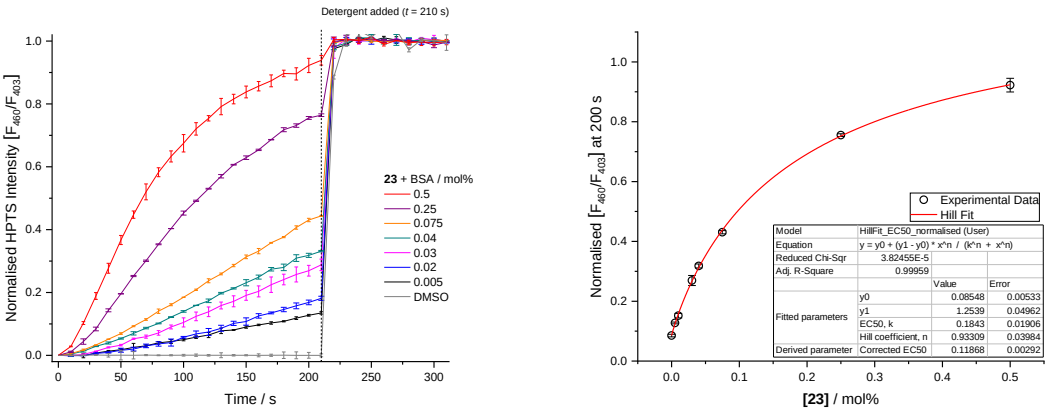

Figure S103. Hill analysis of H^+/Cl^- symport (or Cl^-/OH^- antiport) facilitated by **23** and pre-treated BSA LUVs in the NMDG-Cl assay.

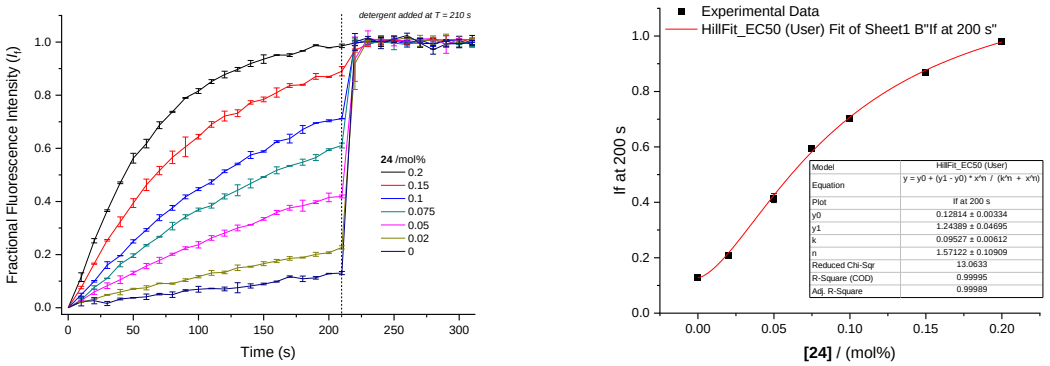

Figure S104. Hill analysis of H^+/Cl^- symport (or Cl^-/OH^- antiport) facilitated by a combination of oleic acid and **24** in the NMDG-Cl assay.

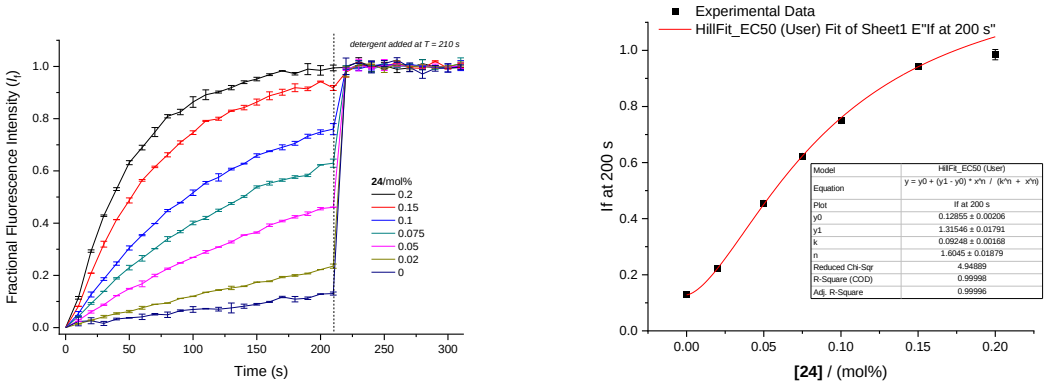

Figure S105. Hill analysis of Cl^- uniport facilitated by a combination of gramicidin and **24** in the NMDG-Cl assay.

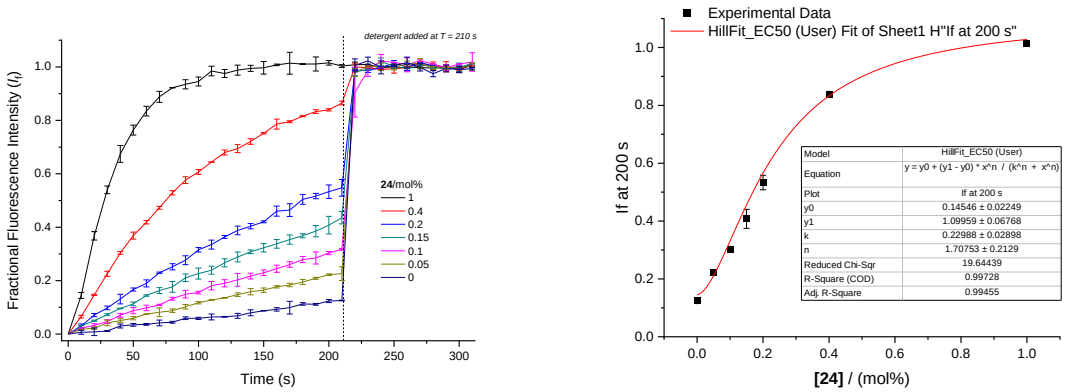

Figure S106. Hill analysis of H^+/Cl^- symport (or Cl^-/OH^- antiport) facilitated by **24** and pre-treated BSA LUVs in the NMDG-Cl assay.

MD simulations in POPC bilayers

Additional details and Methods

Molecular Dynamics (MD) simulations of the DFT optimised chloride complexes of **1**, **9**, **15**, **16**, **18**, **19**, **23**, and **24** were carried out in POPC bilayer models. MD simulations were performed using AMBER18.[22] The benzo[*b*]thiophene urea-based compounds were described with GAFF2 and RESP atomic charges,[23] while Lipid17 was employed for the 128 lipids.[24] The 18 Na^+ and 18 Cl^- ions, affording a *ca*. 0.15 M concentration, were described using 12-6 Lennard Jones parameters[25] compatible with the 6500 TIP3P water model molecules.[26]

The RESP charges for **1**, **19**, **24**, **9**, **15**, **16**, **18** and **23** were obtained as follows: The free receptors were optimised at the HF/6-31G* level with Gaussian 09.[5] A single point calculation ensued to generate the electrostatic potential (ESP) at the same theory level, using the Merz-Singh-Kollman scheme with 4 concentric layers per atom and 6 density points in each layer (IOp(6/33=2, 6/41=4, 6/42=6)).[27] After a two-stage RESP fitting of the ESP data, the atomic charges were obtained.

The chloride complexes of each receptor were inserted in a previously equilibrated POPC bilayer membrane model, as described above, with Packmol,[28] either in the water phase (scenario *A*) or between the phospholipid tails (scenario *B*). Subsequently, two independent runs were carried in these two alternative starting scenarios for each chloride complex (2 × 2 runs), using the following simulation protocol: the initial configuration of each system underwent 20000 steps of MM energy minimisation with a 500 kcal mol^{-1} $Å^{-2}$ positional restraint on the chloride complex and lipid molecules (10000 steps of steepest descent algorithm plus 10000 steps of conjugated gradient algorithm). Afterwards, these restraints were removed, and the entire system was relaxed for another 20000 steps, with the same algorithms. The system was then equilibrated by heating it to 303 K in an NVT ensemble for 100 ps with a 10 kcal mol^{-1} $Å^{-2}$ positional restraint on the chloride complex and lipid molecules, followed by a 5 ns run using an NPT ensemble with a 5 kcal mol^{-1} $Å^{-2}$ restraint on the chloride complex. This positional restraint was removed, and the simulation continued for 200 ns. Long-range electrostatic interactions were described with the Particle Mesh Ewald (PME) algorithm[29] using a real-space cut-off at 10 Å). The cut-off for the Lennard-Jones interactions was also set at 10 Å. The temperature of the system was maintained at 303 K, using the Langevin thermostat,[30] with a collision frequency γ of 1.0 ps^{-1}. The pressure was controlled by the Berendsen barostat[31] at 1 atm and compressibility of 44.6×10^{-6} bar^{-1}, with a relaxation time of 1.0 ps. The covalent bonds to hydrogen atoms were constrained using the SHAKE algorithm,[32] allowing the use of a 2 fs time step. The MD simulation trajectory frames were saved every 10.0 ps and were post-processed and analysed with cpptraj.[33]

The starting configurations required for the umbrella sampling (US) simulations of the **15**, **18** and **19** free receptors and chloride complexes were obtained from the unrestrained MD simulations. Configurations were selected with a spacing of *ca.* 1 Å between centres of mass (COM), completing a total of 41 evenly spaced starting points (from 0 to +40 Å along the *z* coordinate). Subsequently, the US simulations were carried out using as starting scenario each selected configuration and applying a distance restraint of 5 kcal·mol^{-1}·$Å^{-2}$ along the *z* coordinate, between the COM of the heavy atoms of the receptor, and the COM of the phosphorous atoms of the lipid headgroups and the terminal carbon atoms of the lipid tails. Where applicable, the chloride complexes throughout the US simulations were also maintained using a distance restraint of 3.5 Å with a harmonic force constant of 5 kcal·mol^{-1}·$Å^{-2}$. Each independent US window was properly minimised and heated to 303 K prior to the production phase, in the same conditions as the passive diffusion MD simulations, apart from the distance restraints. Although the production stage was composed of 100 to 140 ns, only the last 50 ns were considered as sampling time. This sampling period was achieved by monitoring the evolution of the convergence and equilibration of the PMF profiles, with the assessment of the

data in sequential intervals of 10 ns, until it the curves were continuously overlapping (see Figure S117).
The variational free energy profile (vFEP) method[34] was used to reconstruct the free energy profiles from the US simulations of **15**, **18** and **19** free receptors and their chloride complexes. The profile bootstrap errors were calculated from 100 random data sets of equal size (see Figure S118).

Supplementary MD simulations Figures

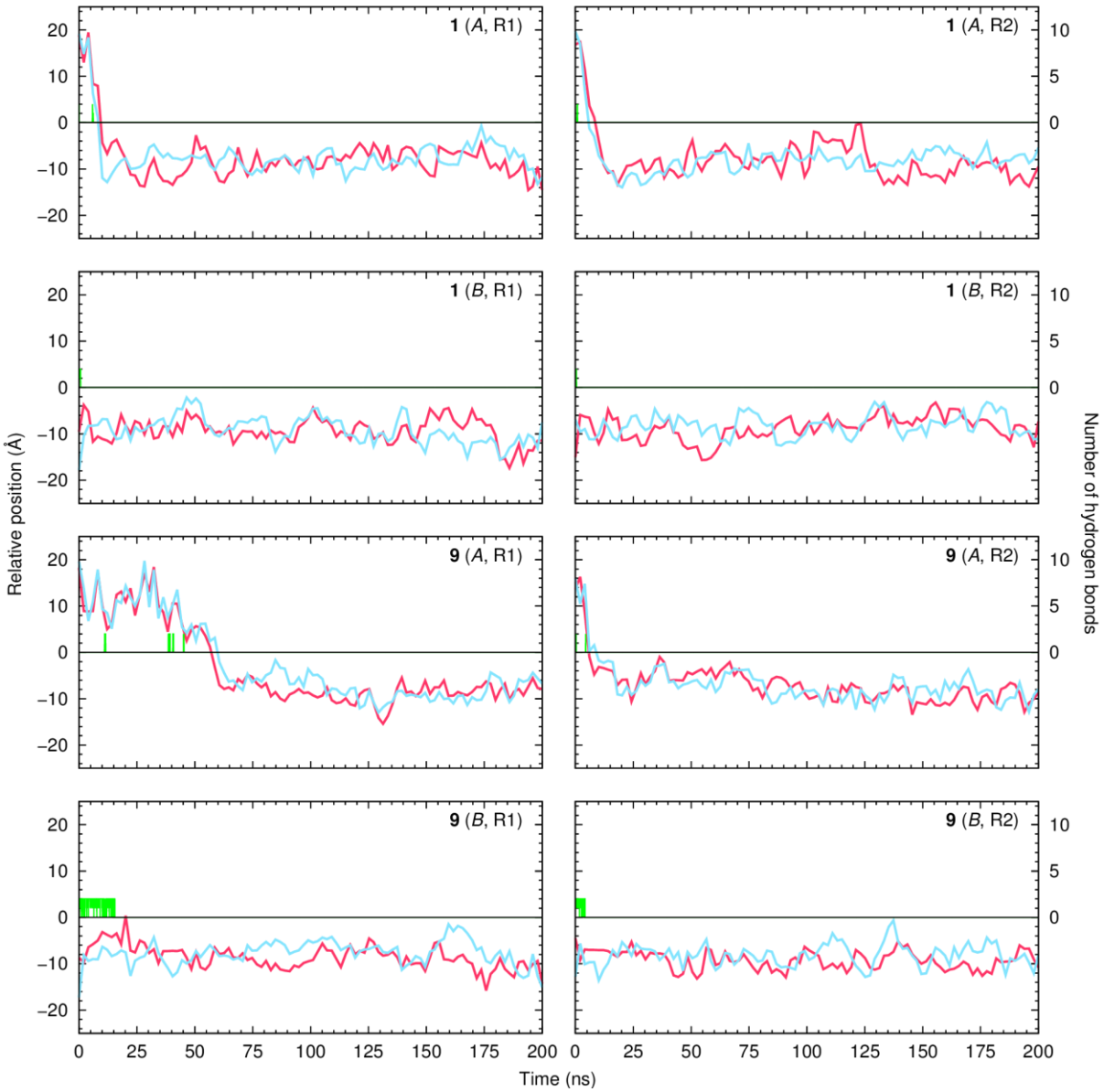

Figure S107. Evolution of the $c_1\cdots P_{int}$ and $c_2\cdots P_{int}$ relative distances (magenta and cyan lines, respectively. See Scheme 4A, main text) in the MD runs of **1** and **9**, starting in scenarios *A* or *B*. The evolution of the total number of N-H···Cl^- hydrogen bonds is also plotted as a green line. The water/lipid interface is represented as a black line at z = 0 Å. Distance data were smoothed using Bézier curves.

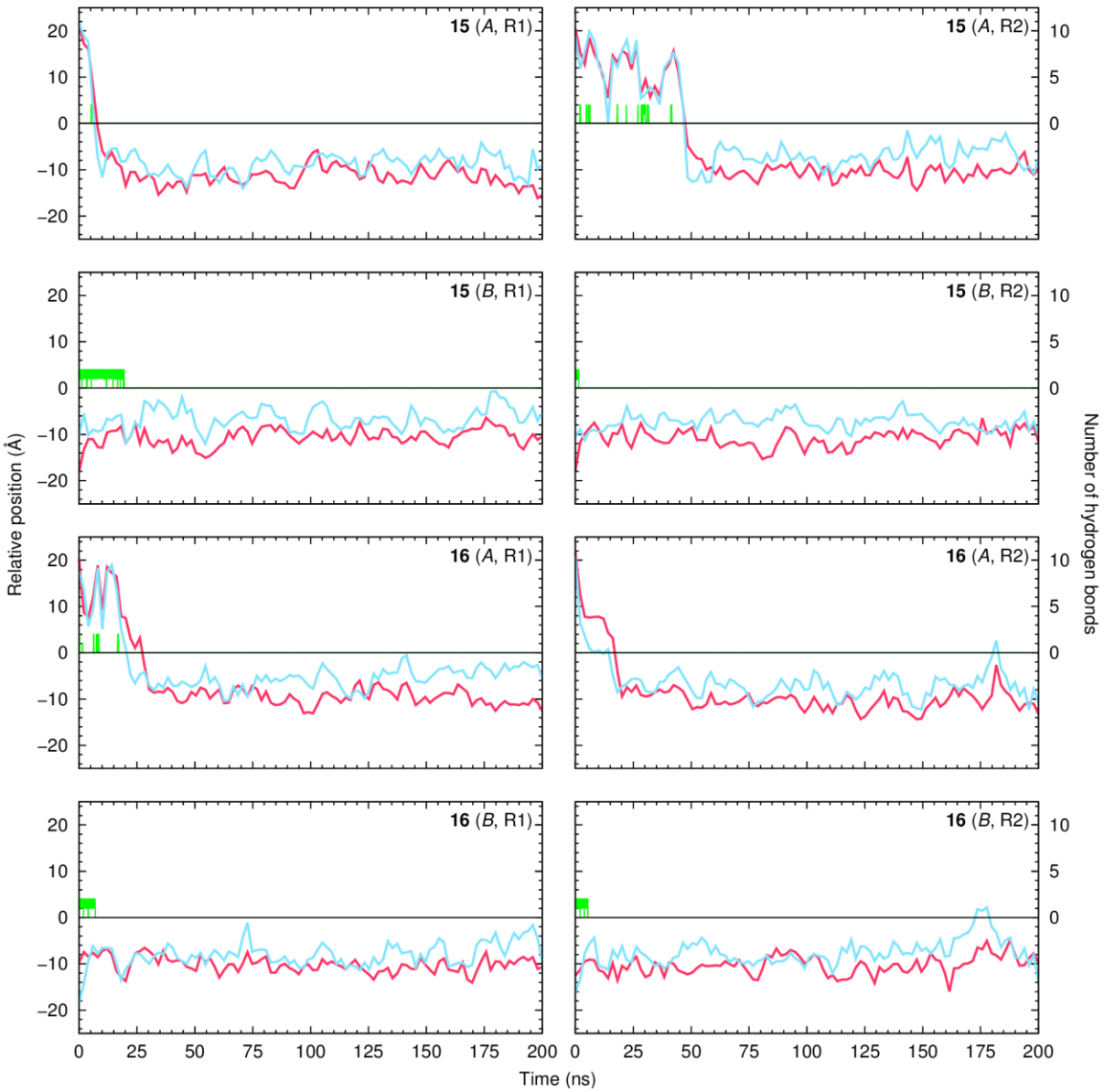

Figure S108. Evolution of the $c_1 \cdots P_{int}$ and $c_2 \cdots P_{int}$ relative distances (magenta and cyan lines, respectively. See Scheme 4A, main text) in the MD runs of **15** and **16**, starting in scenarios *A* or *B*. The evolution of the total number of N-H···Cl^- hydrogen bonds is also plotted as a green line. The water/lipid interface is represented as a black line at z = 0 Å. Distance data were smoothed using Bézier curves.

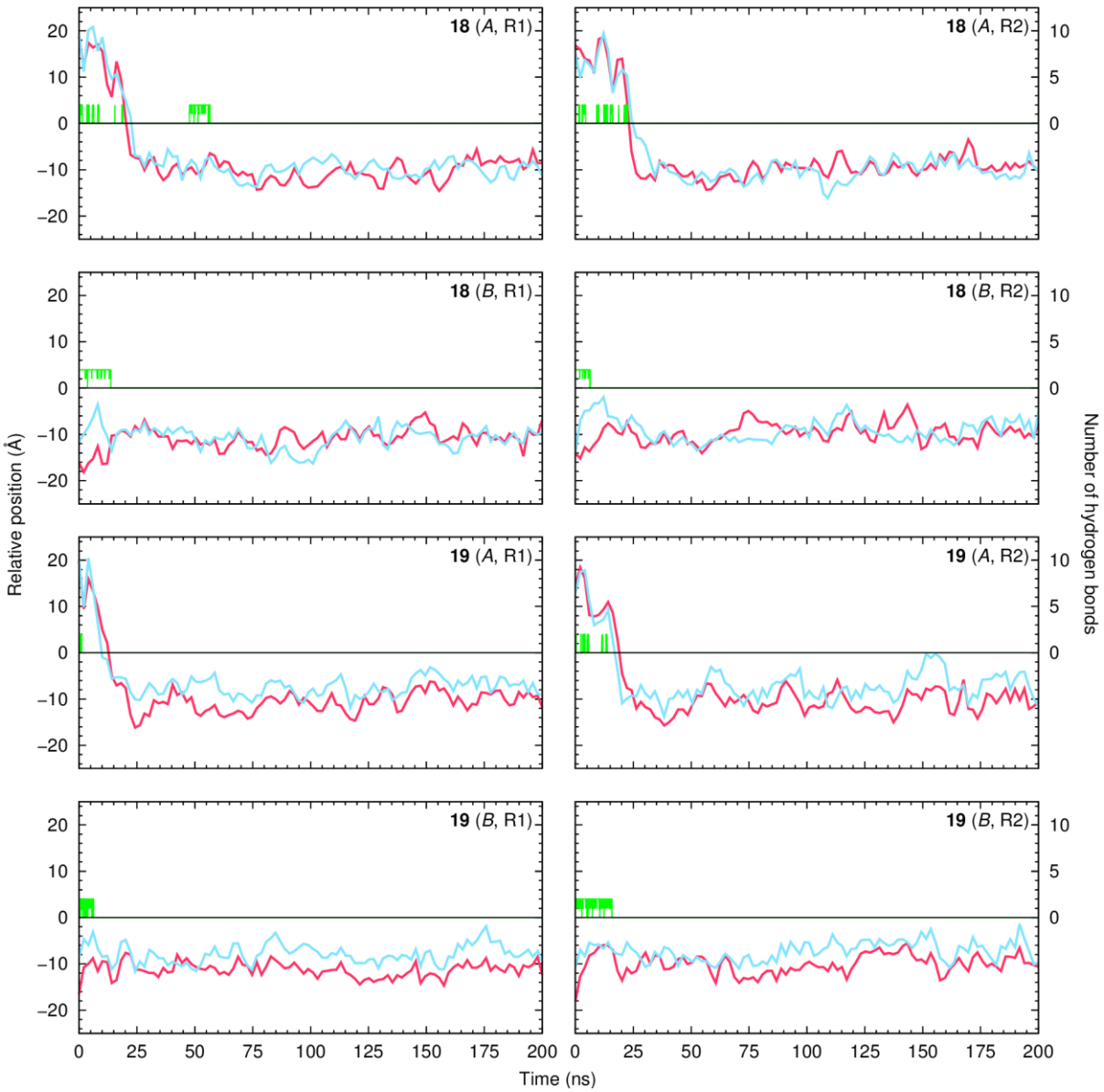

Figure S109. Evolution of the $c_1 \cdots P_{int}$ and $c_2 \cdots P_{int}$ relative distances (magenta and cyan lines, respectively. See Scheme 4A, main text) in the MD runs of **18** and **19**, starting in scenarios *A* or *B*. The evolution of the total number of N-H···Cl^- hydrogen bonds is also plotted as a green line. The water/lipid interface is represented as a black line at z = 0 Å. Distance data were smoothed using Bézier curves.

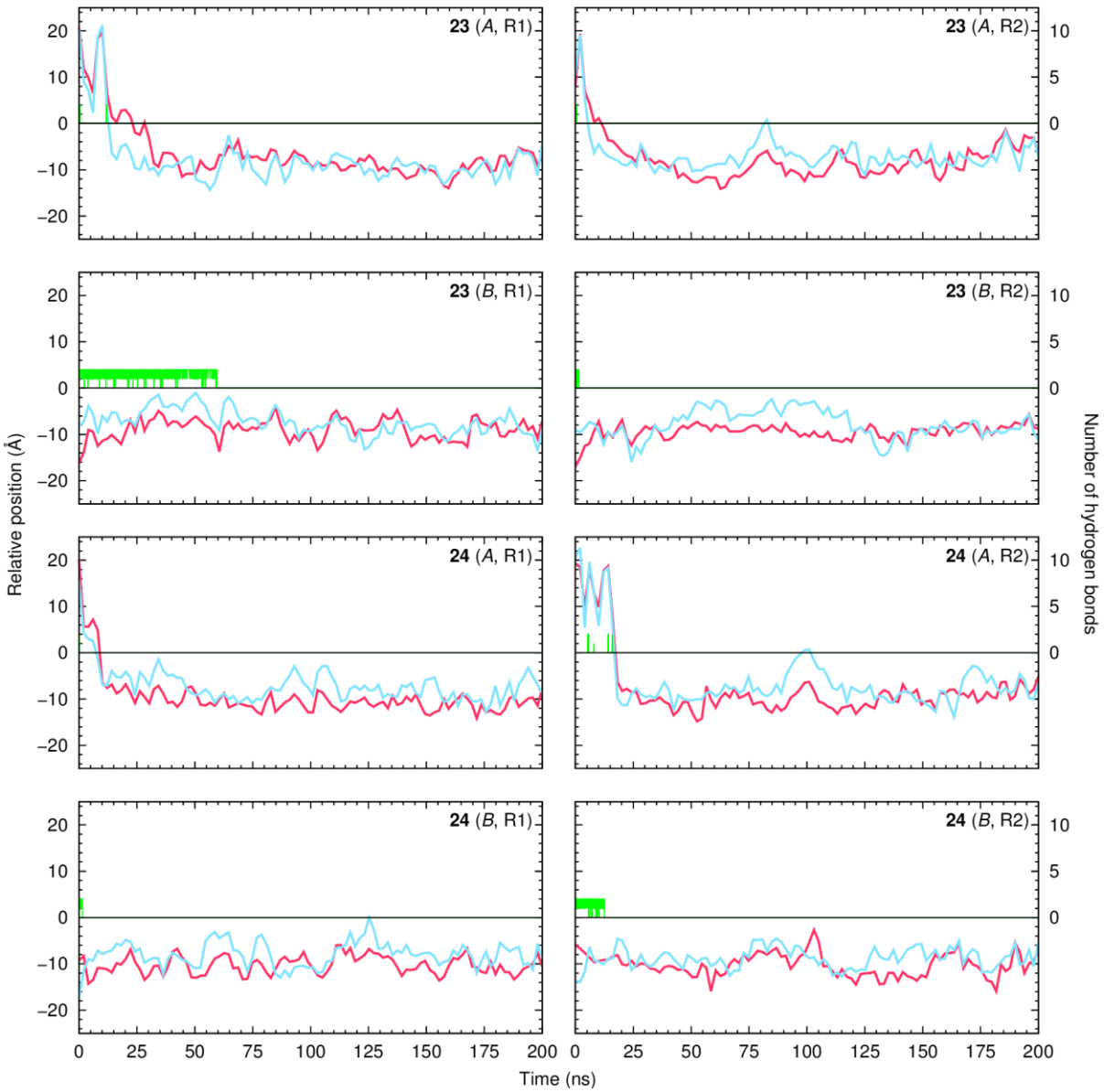

Figure S110. Evolution of the $c_1 \cdots P_{int}$ and $c_2 \cdots P_{int}$ relative distances (magenta and cyan lines, respectively. See Scheme 4A, main text) in the MD runs of **23** and **24**, starting in scenarios *A* or *B*. The evolution of the total number of N-H···Cl^- hydrogen bonds is also plotted as a green line. The water/lipid interface is represented as a black line at z = 0 Å. Distance data were smoothed using Bézier curves.

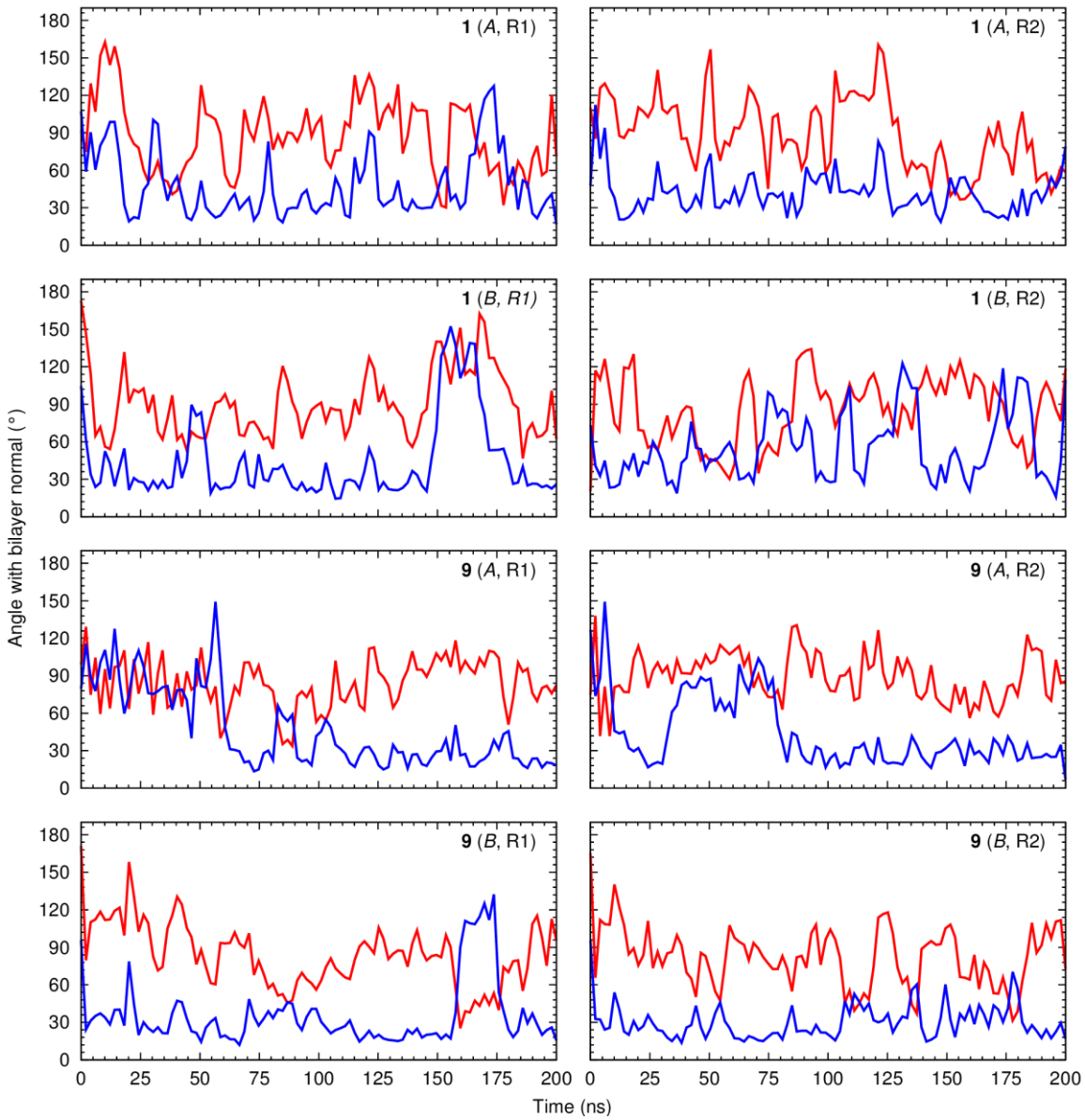

Figure S111. Evolution of the ω and ε angles (red and blue lines, respectively. See Scheme 4B, main text) in the MD runs of **1** and **9**, starting in scenarios *A* or *B*. Data were smoothed using Bézier curves.

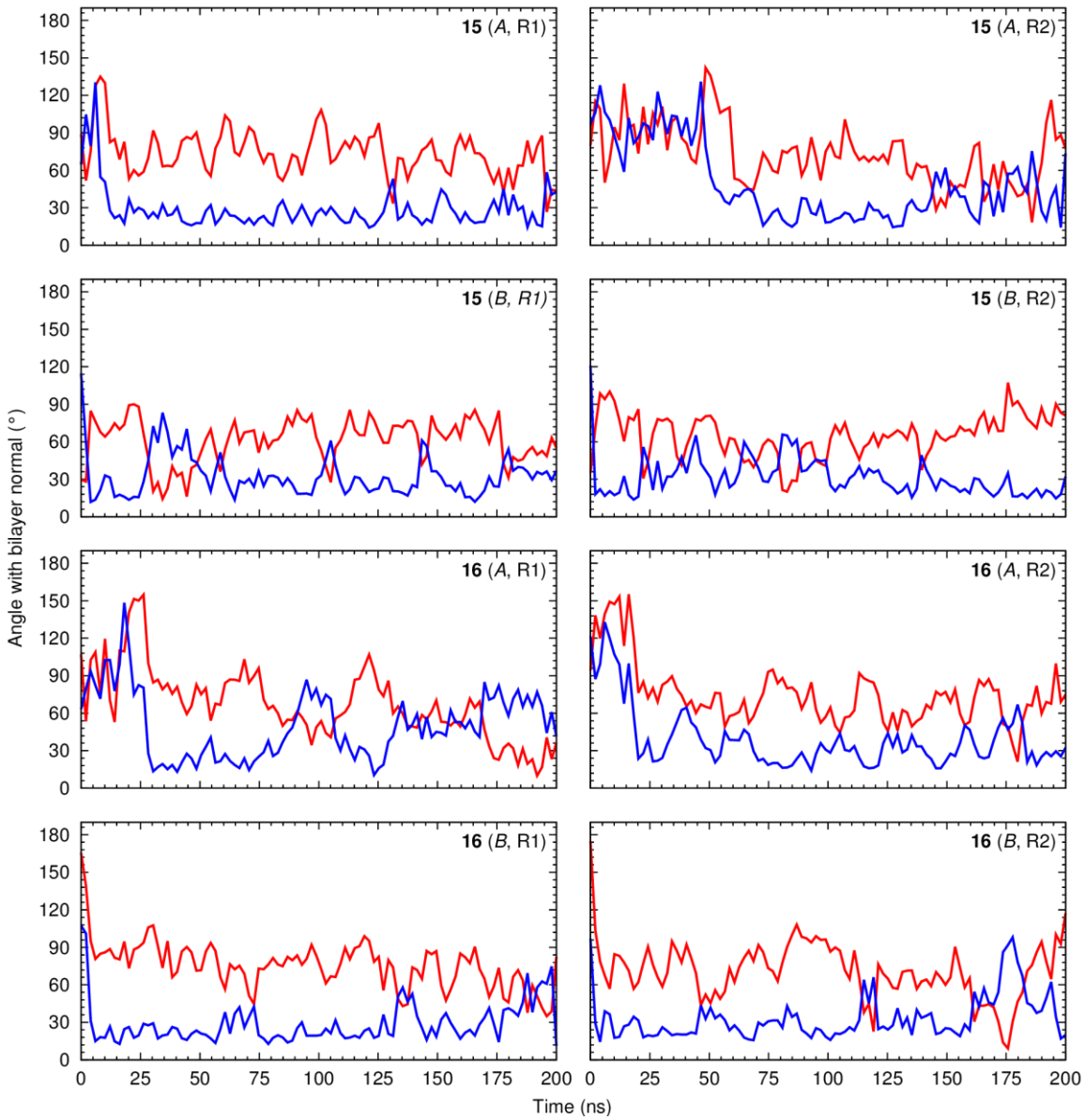

Figure S112. Evolution of the ω and ε angles (red and blue lines, respectively. See Scheme 4B, main text) in the MD runs of **15** and **16**, starting in scenarios *A* or *B*. Data were smoothed using Bézier curves.

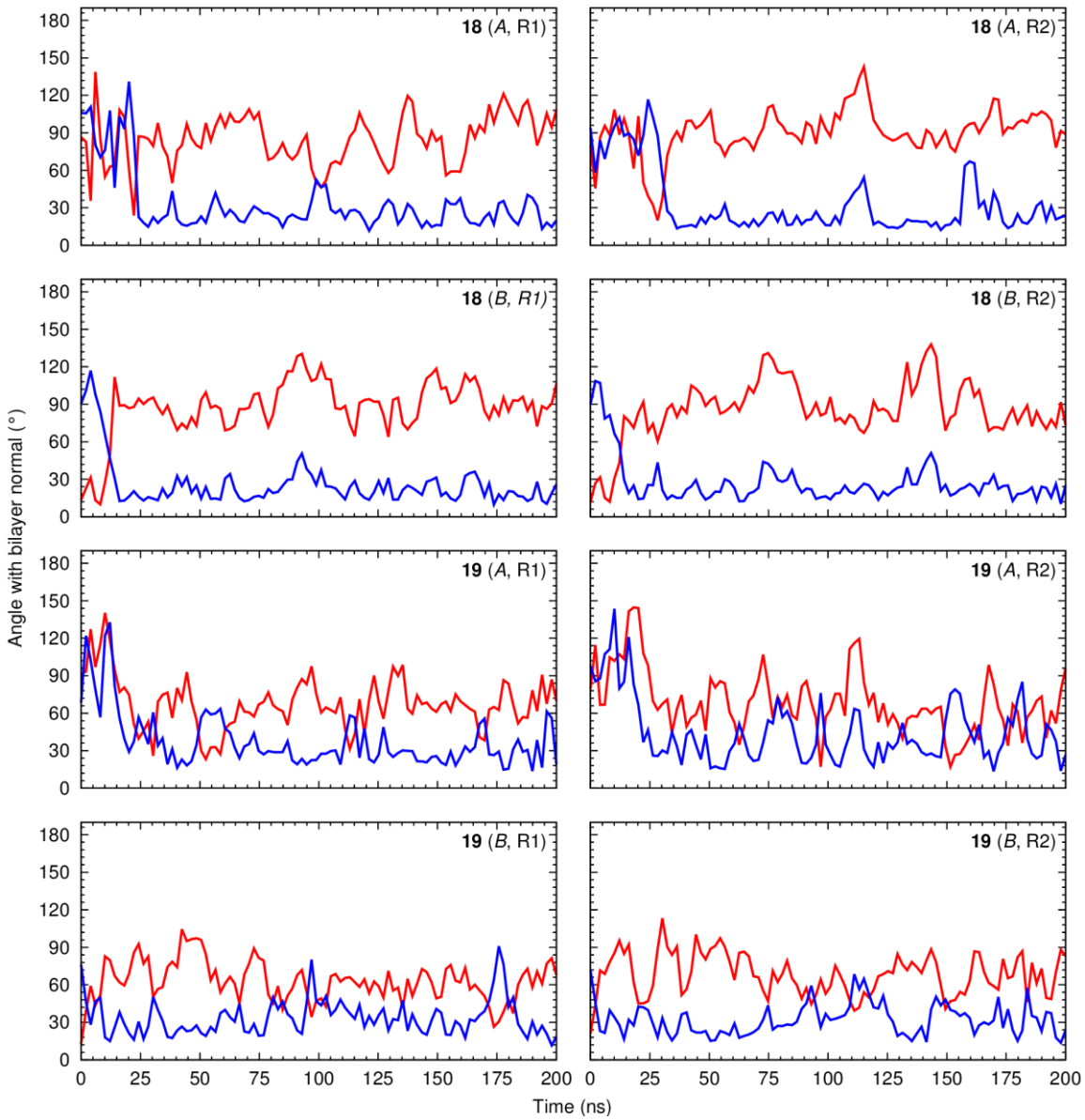

Figure S113. Evolution of the ω and ε angles (red and blue lines, respectively. See Scheme 4B, main text) in the MD runs of **18** and **19**, starting in scenarios *A* or *B*. Data were smoothed using Bézier curves.

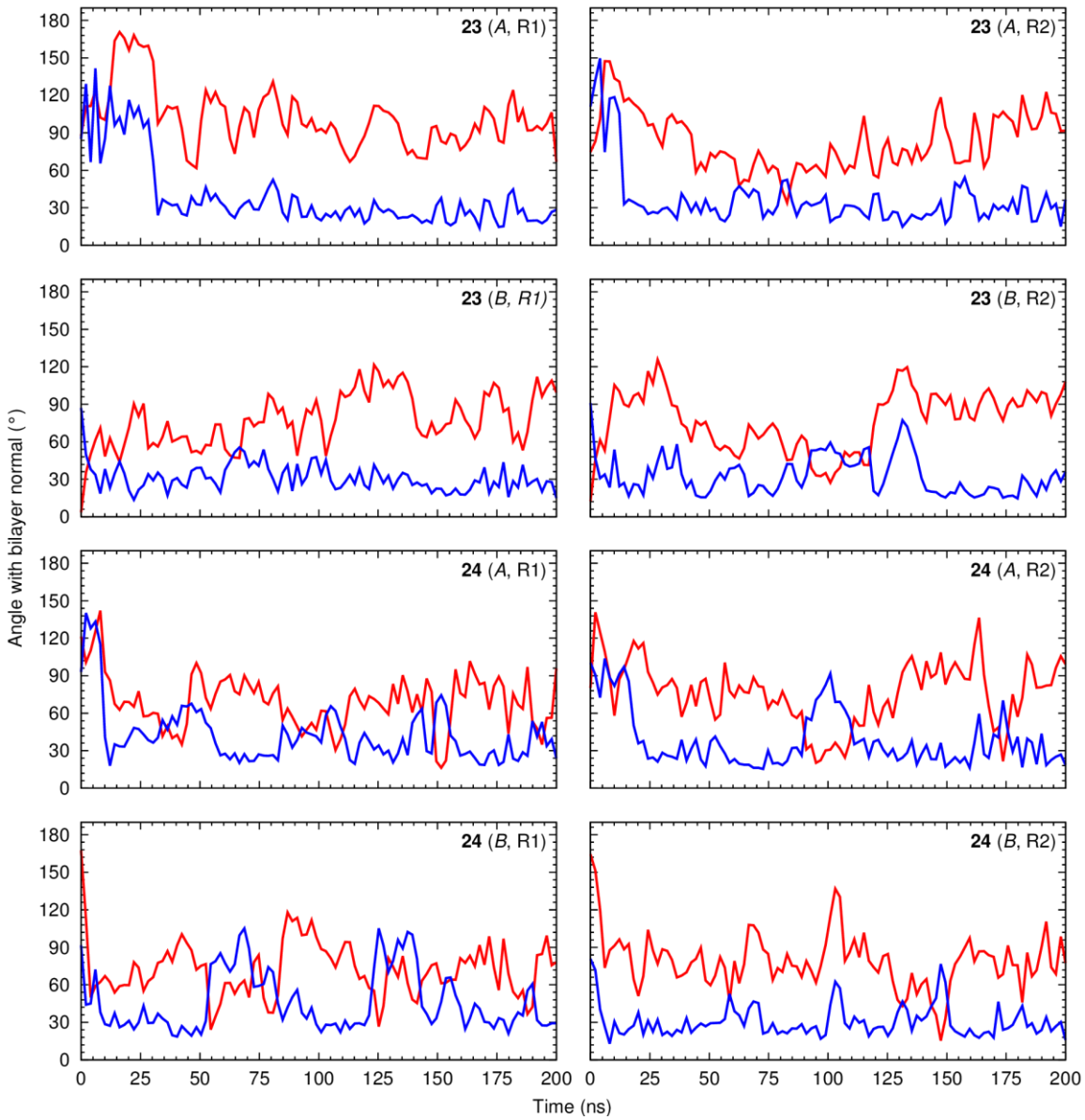

Figure S114. Evolution of the ω and ε angles (red and blue lines, respectively. See Scheme 4B, main text) in the MD runs of **23** and **24**, starting in scenarios *A* or *B*. Data were smoothed using Bézier curves.

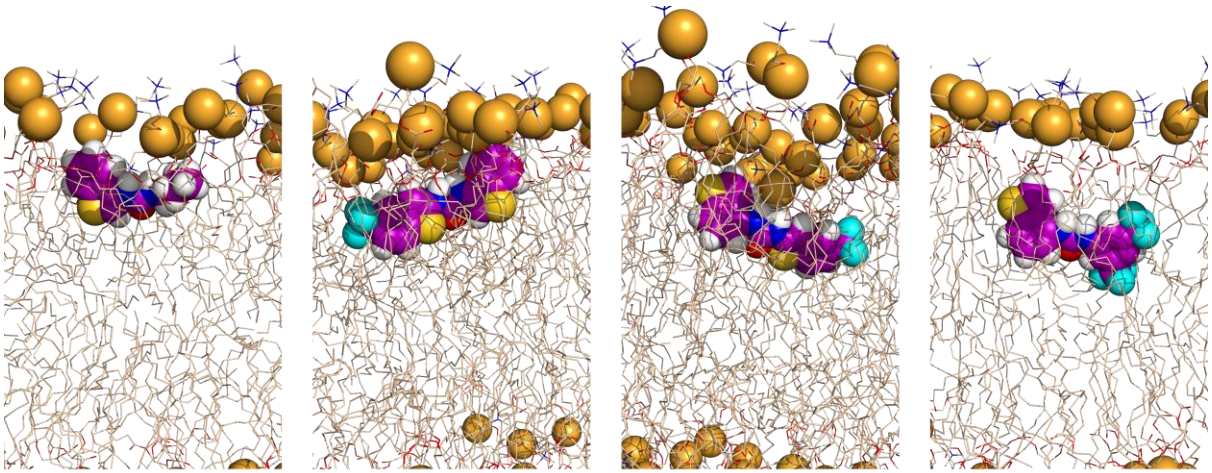

Figure S115. Snapshots of MD runs with transporters **1**, **15**, **16**, and **24**, illustrating their orientations at the water/lipid interface. Water molecules, phospholipid aliphatic protons, and ions were omitted for clarity.

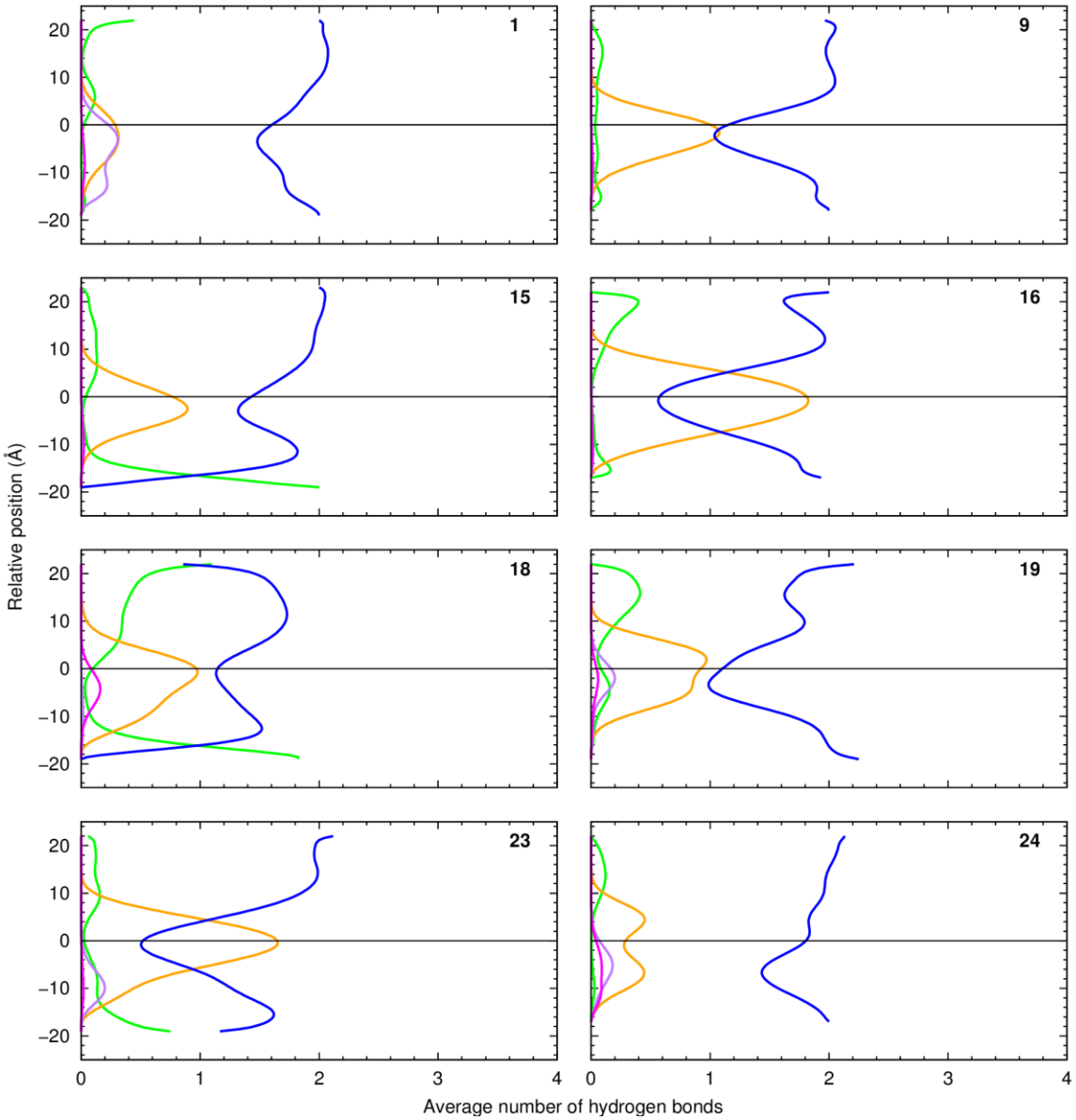

Figure S116. Average number of urea hydrogen bonds vs the relative position of the centre of mass of **1**, **9**, **15**, **16**, **18**, **19**, **23** and **24**. The following colour scheme is used for the interactions with the chloride ions (green), water molecules (blue), POPC head groups (orange), and ester groups (magenta for the *sn*-1 chains and purple for the *sn*-2 chains). The water/lipid interface is represented as a black line at z = 0 Å. Data were smoothed using Bézier curves.

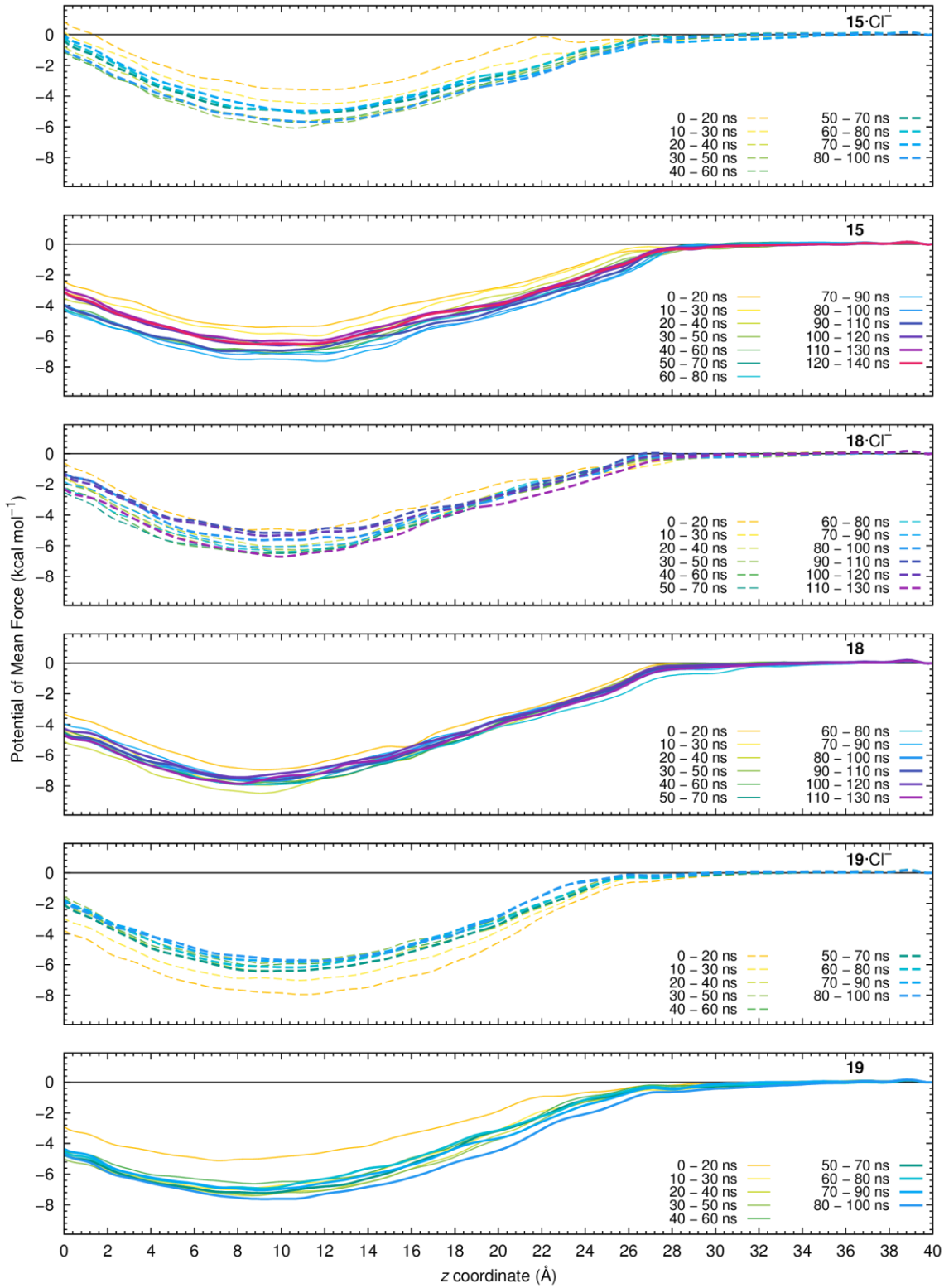

Figure S117. The equilibration and convergence of the umbrella sampling simulation windows were assessed in 20 ns intervals (coloured according to time interval), taken through the trajectory and used to calculate the PMF of free (solid lines) and anion associated **15**, **18** and **19** (dashed lines).

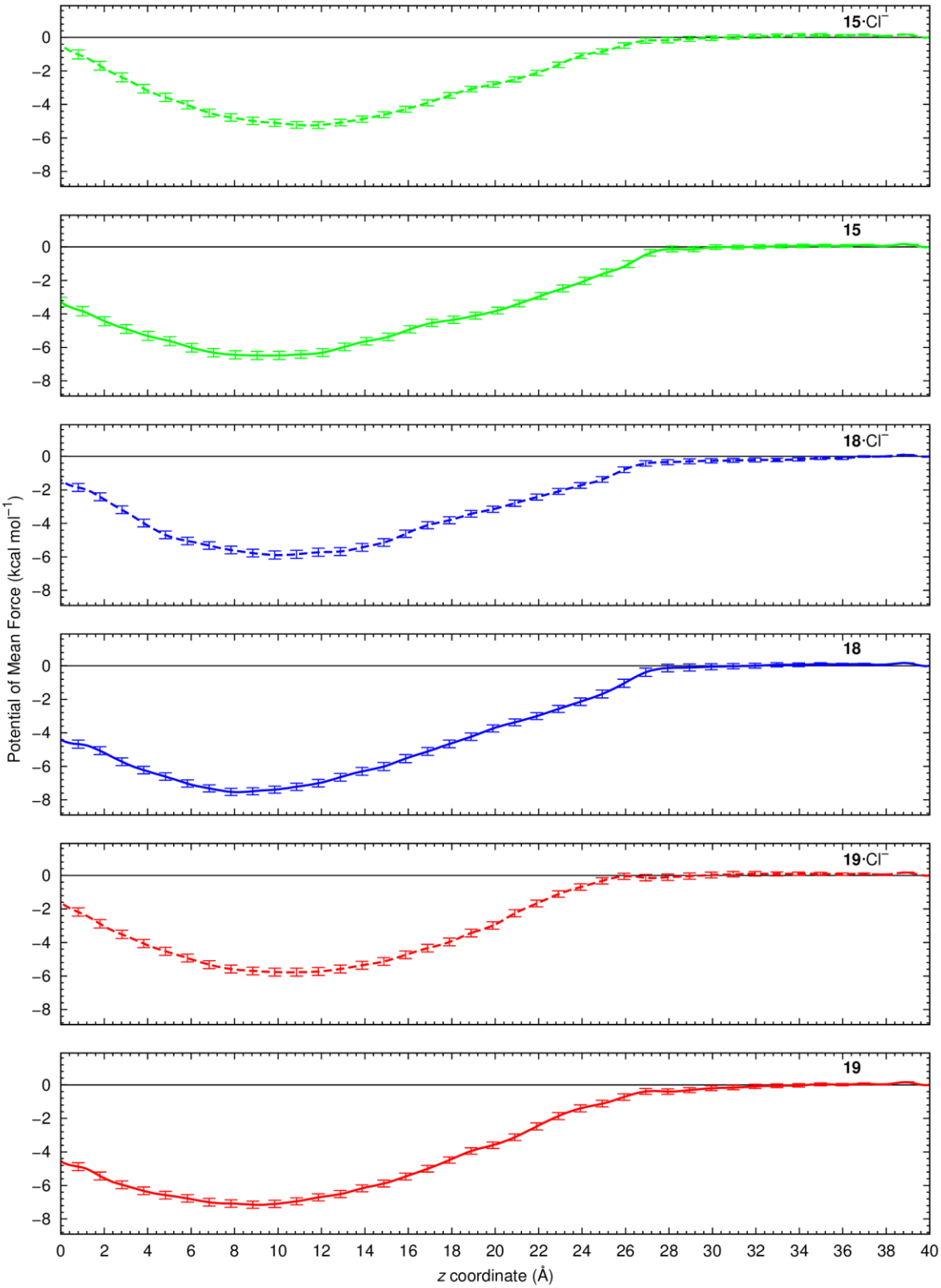

Figure S118. PMF as a function of transporters' distance to the membrane centre of mass (z = 0 Å), for free **15**, **18** and **19** (solid green, blue and red lines, respectively) and their Cl^- complexes (dashed green, blue and red lines, in this order). The error bars correspond to the bootstrap errors calculated from 100 random data sets with the same size and are upscaled 2 times.

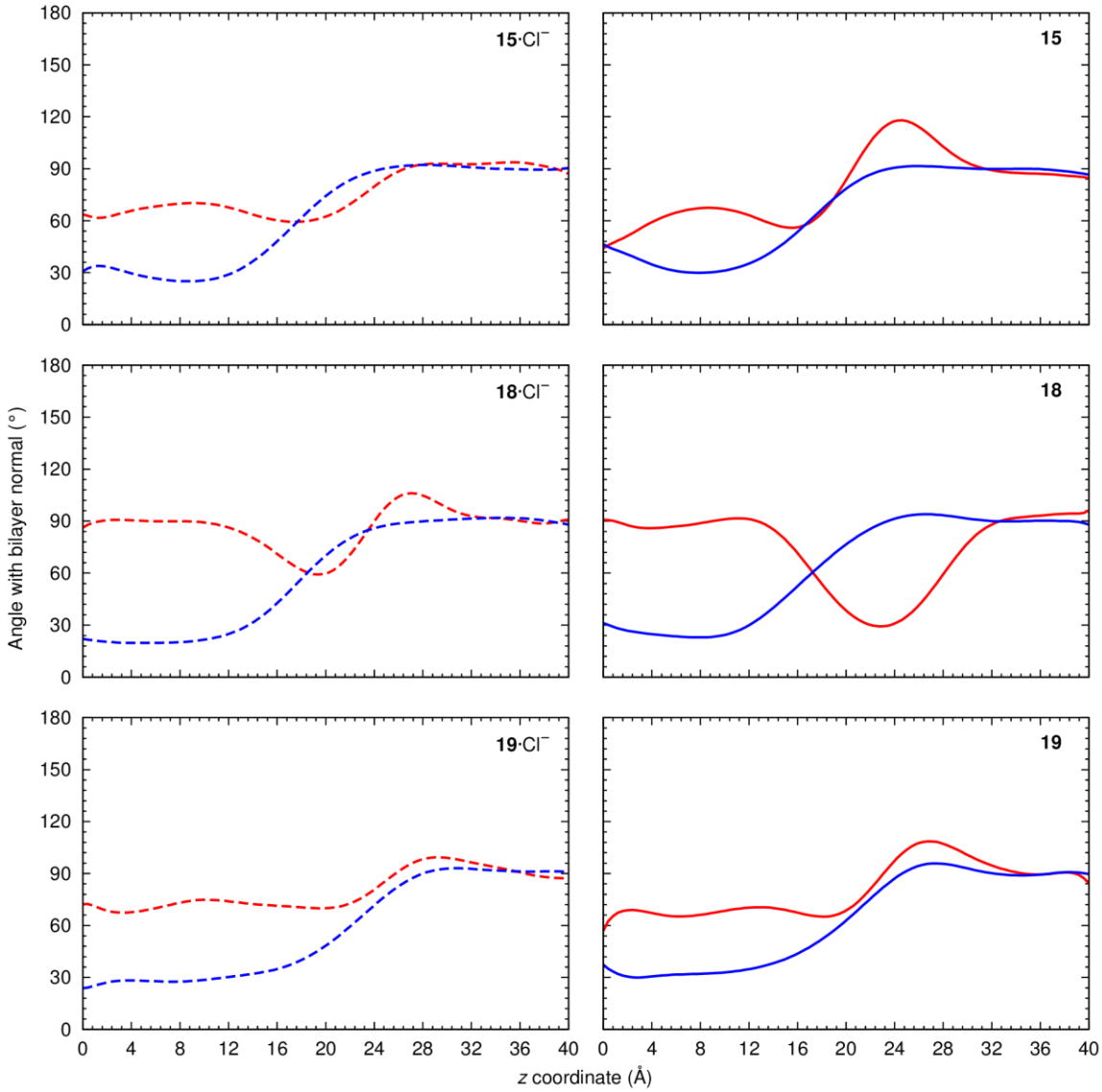

Figure S119. Average ω and ε angles (red and blue lines, respectively. See Scheme 4B, main text) in the US MD simulations of **15**, **18**, and **19** free receptors (solid lines) or chloride complexes (dashed lines). Data were smoothed using Bézier curves.

Supplementary MD simulations Tables

Table S11. PMF energetic data at z = 0 Å, together with PMF minima energy values and z positions.

Transporter	Situation	PMF at z = 0 Å (kcal mol^{-1})	PMF minima (kcal mol^{-1})	PMF minima (Å)
15	Free	-3.3	-6.5	9.65
	Cl^- complex	-0.4	-5.3	11.46
18	Free	-4.4	-7.5	-8.04
	Cl^- complex	-1.4	-5.9	10.05
19	Free	-4.6	-7.2	9.05
	Cl^- complex	-1.6	-5.8	10.45

References

[1] W. L. F. Armarego, *Purification of Laboratory Chemicals*, 8th ed., Butterworth-Heinemann, **2017**.

[2] P. Vieira, M. Q. Miranda, I. Marques, S. Carvalho, L. J. Chen, E. N. W. Howe, C. Zhen, C. Y. Leung, M. J. Spooner, B. Morgado, E. S. O. A. B. da Cruz, C. Moiteiro, P. A. Gale, V. Felix, *Chem. Eur. J.* **2020**, *26*, 888-899.

[3] T. W. Bevan, J. Francis-Taylor, H. Wong, P. T. Northcote, J. E. Harvey, *Tetrahedron* **2018**, *74*, 2942-2955.

[4] (a) http://supramolecular.org; (b) D. Brynn Hibbert, P. Thordarson, *Chem. Commun.* **2016**, *52*, 12792-12805; (c) C. Frassineti, S. Ghelli, P. Gans, A. Sabatini, M. S. Moruzzi, A. Vacca, *Anal. Biochem.* **1995**, *231*, 374-382.

[5] *Gaussian 09, Revision D.01*, M. J. Frisch, G. W. Trucks, H. B. Schlegel, G. E. Scuseria, M. A. Robb, J. R. Cheeseman, G. Scalmani, V. Barone, B. Mennucci, G. A. Petersson, H. Nakatsuji, M. Caricato, X. Li, H. P. Hratchian, A. F. Izmaylov, J. Bloino, G. Zheng, J. L. Sonnenberg, M. Hada, M. Ehara, K. Toyota, R. Fukuda, J. Hasegawa, M. Ishida, T. Nakajima, Y. Honda, O. Kitao, H. Nakai, T. Vreven, J. A. Montgomery, Jr., J. E. Peralta, F. Ogliaro, M. Bearpark, J. J. Heyd, E. Brothers, K. N. Kudin, V. N. Staroverov, T. Keith, R. Kobayashi, J. Normand, K. Raghavachari, A. Rendell, J. C. Burant, S. S. Iyengar, J. Tomasi, M. Cossi, N. Rega, J. M. Millam, M. Klene, J. E. Knox, J. B. Cross, V. Bakken, C. Adamo, J. Jaramillo, R. Gomperts, R. E. Stratmann, O. Yazyev, A. J. Austin, R. Cammi, C. Pomelli, J. W. Ochterski, R. L. Martin, K. Morokuma, V. G. Zakrzewski, G. A. Voth, P. Salvador, J. J. Dannenberg, S. Dapprich, A. D. Daniels, O. Farkas, J. B. Foresman, J. V. Ortiz, J. Cioslowski, and D. J. Fox, Gaussian, Inc., Wallingford CT, **2013**.

[6] S. Grimme, J. Antony, S. Ehrlich, H. Krieg, *J. Chem. Phys.* **2010**, *132*, 154104.

[7] (a) R. Krishnan, J. S. Binkley, R. Seeger, J. A. Pople, *J. Chem. Phys.* **1980**, *72*, 650-654; (b) A. D. McLean, G. S. Chandler, *J. Chem. Phys.* **1980**, *72*, 5639-5648; (c) M. M. Francl, W. J. Pietro, W. J. Hehre, J. S. Binkley, M. S. Gordon, D. J. DeFrees, J. A. Pople, *J. Chem. Phys.* **1982**, *77*, 3654-3665; (d) T. Clark, J. Chandrasekhar, G. W. Spitznagel, P. V. R. Schleyer, *J. Comput. Chem.* **1983**, *4*, 294-301; (e) M. J. Frisch, J. A. Pople, J. S. Binkley, *J. Chem. Phys.* **1984**, *80*, 3265-3269; (f) G. W. Spitznagel, T. Clark, P. von Ragué Schleyer, W. J. Hehre, *J. Comput. Chem.* **1987**, *8*, 1109-1116.

[8] (a) D. Feller, *J. Comput. Chem.* **1996**, *17*, 1571-1586; (b) K. L. Schuchardt, B. T. Didier, T. Elsethagen, L. Sun, V. Gurumoorthi, J. Chase, J. Li, T. L. Windus, *J. Chem. Inf. Model.* **2007**, *47*, 1045-1052; (c) B. P. Pritchard, D. Altarawy, B. Didier, T. D. Gibson, T. L. Windus, *Journal of Chemical Information and Modeling* **2019**, *59*, 4814-4820.

[9] (a) V. Barone, M. Cossi, *The Journal of Physical Chemistry A* **1998**, *102*, 1995-2001; (b) M. Cossi, N. Rega, G. Scalmani, V. Barone, *J. Comput. Chem.* **2003**, *24*, 669-681.

[10] (a) T. Lu, F. Chen, *J. Comput. Chem.* **2012**, *33*, 580-592; (b) T. Lu, F. Chen, *J. Mol. Graph. Model.* **2012**, *38*, 314-323.

[11] (a) R. F. W. Bader, *Chem. Rev.* **1991**, *91*, 893-928; (b) R. F. W. Bader, *Atoms in Molecules: A Quantum Theory*, Oxford University Press, **1991**; (c) T. Lu, F. Chen, *Acta Chim. Sinica* **2011**, *69*, 2393-2406.

[12] (a) F. Weinhold, C. R. Landis, *Chem. Educ. Res. Pract.* **2001**, *2*, 91-104; (b) E. D. Glendening, C. R. Landis, F. Weinhold, *J. Comput. Chem.* **2013**, *34*, 1429-1437.

[13] E. Espinosa, E. Molins, C. Lecomte, *Chem. Phys. Lett.* **1998**, *285*, 170-173.

[14] F. Weinhold, C. R. Landis, *Valency and Bonding*, Cambridge University Press, Cambridge, **2009**.

[15] The PyMOL Molecular Graphics System, Version 2.5 Schrödinger, LLC..

[16] C. P. Kelly, C. J. Cramer, D. G. Truhlar, *J Phys Chem B* **2007**, *111*, 408-422.

[17] G. M. Sheldrick, *Acta Crystallogr A Found Adv* **2015**, *71*, 3-8.

[18] G. M. Sheldrick, *Acta Crystallogr C Struct Chem* **2015**, *71*, 3-8.

[19] O. V. Dolomanov, L. J. Bourhis, R. J. Gildea, J. A. K. Howard, H. Puschmann, *J. Appl. Crystallogr.* **2009**, *42*, 339-341.

[20] (a) R. Taylor, C. F. Macrae, *Acta crystallographica. Section B, Structural science* **2001**, *57*, 815-827; (b) I. J. Bruno, J. C. Cole, P. R. Edgington, M. Kessler, C. F. Macrae, P. McCabe, J.

Pearson, R. Taylor, *Acta crystallographica. Section B, Structural science* **2002**, *58*, 389-397; (c) C. F. Macrae, P. R. Edgington, P. McCabe, E. Pidcock, G. P. Shields, R. Taylor, M. Towler, J. van De Streek, *J. Appl. Crystallogr.* **2006**, *39*, 453-457; (d) C. F. Macrae, I. J. Bruno, J. A. Chisholm, P. R. Edgington, P. McCabe, E. Pidcock, L. Rodriguez-Monge, R. Taylor, J. van de Streek, P. A. Wood, *J. Appl. Crystallogr.* **2008**, *41*, 466-470.

[21] L. A. Jowett, P. A. Gale, *Supramolecular Chemistry* **2019**, *31*, 297-312.

[22] (a) R. Salomon-Ferrer, A. W. Gotz, D. Poole, S. Le Grand, R. C. Walker, *J. Chem. Theory Comput.* **2013**, *9*, 3878-3888; (b) S. Le Grand, A. W. Götz, R. C. Walker, *Comput. Phys. Commun.* **2013**, *184*, 374-380; (c) D.A. Case, S.R. Brozell, D.S. Cerutti, T.E. Cheatham, III, V.W.D. Cruzeiro, T.A. Darden, R.E. Duke, D. Ghoreishi, H. Gohlke, A.W. Goetz, D. Greene, R Harris, N. Homeyer, S. Izadi, A. Kovalenko, T.S. Lee, S. LeGrand, P. Li, C. Lin, J. Liu, T. Luchko, R. Luo, D.J. Mermelstein, K.M. Merz, Y. Miao, G. Monard, H. Nguyen, I. Omelyan, A. Onufriev, F. Pan, R. Qi, D.R. Roe, A. Roitberg, C. Sagui, S. Schott-Verdugo, J. Shen, C.L. Simmerling, J. Smith, J. Swails, R.C. Walker, J. Wang, H. Wei, R.M. Wolf, X. Wu, L. Xiao, D.M. York and P.A. Kollman (**2018**), *AMBER 2018*, University of California, San Francisco.

[23] C. I. Bayly, P. Cieplak, W. Cornell, P. A. Kollman, *J Phys Chem-Us* **2002**, *97*, 10269-10280.

[24] I. R. Gould, S. A.A., C. J. Dickson, B. D. Madej, R. C. Walker, *Manuscript in preparation* **2018**.

[25] P. Li, L. F. Song, K. M. Merz, Jr., *J. Chem. Theory Comput.* **2015**, *11*, 1645-1657.

[26] W. L. Jorgensen, J. Chandrasekhar, J. D. Madura, R. W. Impey, M. L. Klein, *J. Chem. Phys.* **1983**, *79*, 926-935.

[27] (a) J. Wang, R. M. Wolf, J. W. Caldwell, P. A. Kollman, D. A. Case, *J. Comput. Chem.* **2004**, *25*, 1157-1174; (b) J. Wang, R. M. Wolf, J. W. Caldwell, P. A. Kollman, D. A. Case, *J. Comput. Chem.* **2005**, *26*, 114.

[28] (a) L. Martínez, R. Andrade, E. G. Birgin, J. M. Martínez, *Vol. 2010*, http://www.ime.unicamp.br/~martinez/packmol/, Campinas - SP, **2008**; (b) L. Martinez, R. Andrade, E. G. Birgin, J. M. Martinez, *J. Comput. Chem.* **2009**, *30*, 2157-2164.

[29] T. Darden, D. York, L. Pedersen, *J. Chem. Phys.* **1993**, *98*, 10089-10092.

[30] R. J. Loncharich, B. R. Brooks, R. W. Pastor, *Biopolymers* **1992**, *32*, 523-535.

[31] H. J. C. Berendsen, J. P. M. Postma, W. F. Vangunsteren, A. Dinola, J. R. Haak, *J. Chem. Phys.* **1984**, *81*, 3684-3690.

[32] J.-P. Ryckaert, G. Ciccotti, H. J. C. Berendsen, *J. Comput. Phys.* **1977**, *23*, 327-341.

[33] D. R. Roe, T. E. Cheatham, 3rd, *J. Chem. Theory Comput.* **2013**, *9*, 3084-3095.

[34] T. S. Lee, B. K. Radak, A. Pabis, D. M. York, *J. Chem. Theory Comput.* **2013**, *9*, 153-164.